Universidade de São Paulo
Instituto de Física

Propriedades fora do equilíbrio do plasma de quarks e glúons fortemente acoplado

Renato Anselmo Judica Critelli

Tese apresentada ao Instituto de Física da Universidade de São Paulo como requisito para o título de Doutor em Ciências.

Comissão examinadora:

Prof. Dr. Jorge José Leite Noronha Junior (Orientador) (IF-USP)
Profa. Dra. Betti Hartmann (IFSC-USP)
Prof. Dr. Eduardo Souza Fraga (IF-UFRJ)
Prof. Dr. Jun Takahashi (IFGW-UNICAMP)
Prof. Dr. Matthew Luzum (IF-USP)

São Paulo
2019

FICHA CATALOGRÁFICA
Preparada pelo Serviço de Biblioteca e Informação
do Instituto de Física da Universidade de São Paulo

Critelli, Renato Anselmo Judica

Propriedades fora do equilíbrio do plasma de quarks e glúons fortemente acoplado / Far from equilibrium properties of the strongly coupled quark-gluon plasma. São Paulo, 2019.

Tese (Doutorado) – Universidade de São Paulo. Instituto de Física. Depto. Física Experimental.

Orientador: Prof. Dr. Jorge José Leite Noronha Júnior
Área de Concentração: Física

Unitermos: 1. Holografia; 2. Colisões de íons pesados relativisticos; 3. Física teórica; 4. Física nuclear.

USP/IF/SBI-042/2019

University of São Paulo
Institute of Physics

Far-from-equilibrium properties of the strongly coupled quark-gluon plasma

Renato Anselmo Judica Critelli

Thesis presented to the Institute of Physics from University of São Paulo as a requisite to the title of Doctor of Science.

Examining committee:

Prof. Dr. Jorge José Leite Noronha Junior (Advisor) (IF-USP)
Prof. Dr. Betti Hartmann (IFSC-USP)
Prof. Dr. Eduardo Souza Fraga (IF-UFRJ)
Prof. Dr. Jun Takahashi (IFGW-UNICAMP)
Prof. Dr. Matthew Luzum (IF-USP)

São Paulo
2019

Agradecimentos

Apesar de a escrita de uma tese ser um trabalho solitário, gostaria de agradecer algumas pessoas que tornaram possível a realização do meu doutorado, o qual me deu o privilégio de estudar temas tão interessantes e variados das ciências naturais.

Gostaria de agradecer ao meu orientador, Jorge Noronha, por ter me aceito como seu aluno e por dividir comigo seu tempo e entusiasmo com física. As lições que aprendi vão muito além do campo da física, seu profissionalismo e vontade de fazer trabalhos de qualidade serão levados comigo.

Aos colaboradores que tive durante esses anos, Stefano, Maicon, Israel, Jaki, e Claudia, meu muito obrigado. Ao meu colaborador e camarada Rômulo, agradecimentos mais do que especiais.

Gostaria de agradecer o pessoal do grupo de hádrons da USP, o GRHAFITE, por manterem um ambiente amigável e de constante aprendizagem. Agradeço aos professores, Fernando, Manuel, Marina, Kanchan, Alberto, Renato, e também os colegas, Davi, Pedro, Luiz, Leonardo, Rafael, Diego, Samuel, Jorgivan, Maurício, Hugo, Tiago, e tantos outros que passaram por lá. Gostaria também de agradecer o camarada Anderson, por estar presente desde o começo desta jornada.

Agradeço também a comissão julgadora, composta pelos professores Betti Hartmann, Eduardo Fraga, Jun Takahashi, e Matthew Luzum, por comentários e sugestões dados durante minha defesa.

À Fernanda, por tornar meu mundo mais colorido, pelo carinho, amor, e apoio em momentos difíceis, meu muito obrigado.

À minha família, pai, mãe, irmão, e tia, meu muito obrigado por todo o amor e apoio incondicional, mesmo no começo desta jornada, quando o estudo de física parecia algo intangível.

Por último, gostaria de agradecer à Fundação de Amparo à Pesquisa do Estado de São Paulo (FAPESP) pelo fomento financeiro dado ao meu projeto de pesquisa (projeto № 2016/09263-2).

"I do not know what I may appear to the world, but to myself I seem to have been only like a boy playing on the sea-shore, and diverting myself in now and then finding a smoother pebble or a prettier shell than ordinary, whilst the great ocean of truth lay all undiscovered before me."

Sir Isaac Newton

Resumo

Critelli, R. **Propriedades fora do equilíbrio do plasma de quarks e glúons fortemente acoplado.** Tese (Doutorado) - Instituto de Física, Universidade de São Paulo, São Paulo, 2019.

A cromodinâmica quântica (QCD) é a teoria fundamental que rege as interações fortes, cujas partículas elementares são os quarks e glúons. Em termos de escala de energia, a QCD é caracterizada pela liberdade assintótica (quarks e glúons aproximadamente livres) e confinamento de cor (quarks e gluons confinados dentro de hádrons), sendo o primeiro tratado de maneira perturbativa e o último sendo um fenômeno intrinsicamente não-perturbativo. À temperatura finita, conforme se aumenta a temperatura, a matéria hadrônica sofre uma transição de fase do tipo crossover indo de um gás de hádrons ao plasma de quarks e glúons (QGP). Na vizinhança do crossover, onde os hádrons estão "derretendo" para formar o QGP, a QCD se encontra em uma região não perturbativa e portanto o QGP nessa região é fortemente acoplado, dificultando estudos analíticos. A chamada dualidade AdS/CFT, também conhecida como holografia, aparece para oferecer uma oportunidade única para o estudo do QGP ao prover um mapa entre teorias fortemente acopladas (muito difícil de serem resolvidas) e uma teoria de gravitação clássica.

Na frente experimental, o estudo do QGP é feito em aceleradores de partículas colidindo íons pesados ultrarelativísticos. Nestes experimentos, o QGP criado sofre rápida expansão, com uma intrincada interação entre escalas duras e moles de energia, do estado inicial ao estado final. Tal cenário evidencia a necessidade de formular uma teoria para o QGP que inclua propriedades fora do equilíbrio. Afortunadamente, a dualidade holográfica encaixa-se bem para essa tarefa. Resolvendo-se as equações de Einstein dependentes do tempo, um problema da área da relatividade geral numérica, é possível estudar fenômenos fora do equilíbrio de plasmas fortemente acoplados.

Ademais, o diagrama de fase da QCD no plano (T, μ_B), onde T é a temperatura e μ_B o potencial químico bariônico, permanece amplamente desconhecido devido a sua natureza não-perturbativa. Em particular, é conjecturada a existência de um ponto crítico delimitando o crossover de uma transição de fase de primeira ordem. Motivados por tais

fatos, esta tese utiliza a dualidade holográfica para analisar o papel do ponto crítico na dinâmica fora do equilíbrio. Por exemplo, é apresentado aqui um estudo de como o ponto crítico afeta o tempo que leva para um plasma não-Abeliano fortemente acoplado adquirir comportamento hidrodinâmico partindo de um estado completamente fora do equilíbrio.

Palavras-chave: Holografia, dualidade gauge-gravidade, plasma não-Abeliano, dinâmica fora do equilíbrio, fenômenos críticos.

Abstract

Critelli, R. **Far-from-equilibrium properties of the strongly coupled quark-gluon plasma.** Thesis (PhD) - Institute of Physics, University of São Paulo, São Paulo, 2019.

Quantum Chromodynamics (QCD) is the fundamental theory that governs the strong interaction, whose fundamental particles are quarks and gluons. In terms of energy scales, QCD is characterized by asymptotic freedom (approximately free quarks and gluons) and color confinement (quarks and gluons confined inside hadrons), where the former can be treated perturbatively and the latter is an intrinsic non-perturbative phenomenon. At finite temperature, hadronic matter undergoes a crossover phase transition from a gas of hadrons to the quark-gluon plasma (QGP) as the temperature increases. Near the crossover, where hadrons "melt" to release quarks and gluons, QCD is in its non-perturbative regime and the QGP is strongly coupled, posing great challenges for analytical studies. The so-called AdS/CFT duality, also known as holography, comes to offer a unique opportunity to study the QGP by providing a map between strongly coupled theories (which are generally very hard to solve) and a classical theory of gravity.

On the experimental front, the study of the QGP is carried out in particle accelerators by colliding ultrarelativistic heavy ions. In these experiments, the QGP created undergoes rapid expansion and there is a very intricate interplay between soft and hard scales, from initial conditions to final the stream of particles. This scenario makes it evident that one must understand the QGP also out of equilibrium. Fortunately, holography is well suited for this task. By solving the time dependent Einstein's equations, using general techniques previously employed in numerical general relativity, one can study non-equilibrium phenomena of strongly coupled plasmas.

Furthermore, the QCD phase diagram on the (T, μ_B) plane, where T is the temperature and μ_B the baryon chemical potential, remains largely unknown due to its non-perturbative aspects. In particular, it is conjectured the existence of a critical point delimiting the crossover region from the first order phase transition. Motivated by these facts, this thesis employs holography to analyze the role of the critical point on far-from-equilibrium dynamics. For instance, it is investigated how the critical point affects the

time that it takes for a strongly coupled plasma to display hydrodynamic behavior starting from a far-from-equilibrium initial state.

Keywords: Holography, gauge-gravity duality, non-Abelian plasmas, far-from-equilibrium dynamics, critical phenomena.

List of Publications

This thesis is based on the papers:

1. R. Critelli, R. Rougemont and J. Noronha, *Holographic Bjorken flow of a hot and dense fluid in the vicinity of a critical point*. [arXiv:1805.00882 [hep-th]]. Accepted for publication in Phys. Rev. D.

2. R. Critelli, R. Rougemont and J. Noronha, "*Homogeneous isotropization and equilibration of a strongly coupled plasma with a critical point*". JHEP **12** (2017) 029, [arXiv:1709.03131 [hep-th]].

3. S. Finazzo, R. Rougemont, M. Zaniboni, R. Critelli and J. Noronha, "*Critical behavior of non-hydrodynamic quasinormal modes in a strongly coupled plasma*". JHEP **01** (2017) 137, [arXiv:1610.01519 [hep-th]].

Other related papers published during my PhD:

1. R. Rougemont, R. Critelli and J. Noronha, *Nonhydrodynamic quasinormal modes and equilibration of a baryon dense holographic QGP with a critical point*. Phys. Rev. **D98** (2018) no.3, 034028, [arXiv:1804.00189 [hep-ph]].

2. R. Critelli, J. Noronha-Hostler, I. Portillo, C. Ratti, R. Rougemont and J. Noronha, *Critical point in the phase diagram of primordial quark-gluon matter from black hole physics*. Phys. Rev. **D96** (2017) no.9, 096026, [arXiv:1706.00455 [hep-ph]].

3. R. Rougemont, R. Critelli, J. Noronha-Hostler, C. Ratti and J. Noronha, *Dynamical versus equilibrium properties of the QCD phase transition: A holographic perspective*. Phys. Rev. **D96** (2017) no.1, 014032, [arXiv:1704.05558 [hep-ph]].

4. R. Critelli, R. Rougemont, S. Finazzo and J. Noronha, "*Polyakov loop and heavy quark entropy in strong magnetic fields from holographic black hole engineering* ". Phys. Rev. **D94** (2016) no.12, 125019, [arXiv:1606.09484 [hep-ph]].

Contents

List of Figures

Chapter 1

Introduction

Interactions are hard to understand.

The phrase above synthesizes the struggles of theoretical physicists in the realm of quantum field theory (QFT). Nonetheless, even in more ordinary situations, interactions tend to add substantial complexity to different phenomena. For instance, the equation of state of a classical rarefied gas is approximated by the relation $pV = NRT$. However, if the gas is not so dilute, and the interactions between the molecules become relevant, one can derive corrections to this equation of state from the underlying microscopic theory via statistical physics methods [1]. It happens that such corrections, known as the *virial expansion*, are extremely hard to do in practice, and the complexity increases rapidly as one advances in the number of terms of this perturbative approach. Similarly, one may also use the Boltzmann transport equation [2], a non-linear integro-differential equation, to describe transport phenomena in many-body dilute systems from a microscopic point of view. This transport equation possessess the so-called collision term, which is a complicated integral in phase space which encompasses the interactions of the constituents of the gas[1]. Indeed, even from a purely mathematical point of view the Boltzmann equation is interesting, with a Fields Medal being given to Cédric Villani in 2010 for his work on this problem [4, 5].

Coming back to the QFT case, the situation is similar. After learning the free scalar field, the typical graduate student is introduced to its interactions (e.g. $\lambda\phi^4$) as a slight deformation of the free field theory. What is important here is that such approach is valid only if the coupling among the fields is small, i.e. the rules to compute the S-matrix in QFT are perturbative corrections of the free theory [6]. After the formal exposition to the interaction picture in QFT, the graduate student learns how to compute the S-matrix using the so-called *Feynman diagrams*, which represent a pictorial way to organize the

[1]The collision term can be so complicated that very often one uses an *ad-hoc* simplification that substitutes it by a relaxation-like term [3].

perturbative expansion in QFT. Nonetheless, even in this "simple" approach things are tough, especially if one wants to increase the order of the perturbative series and/or the number of interacting particles. For instance, in a non-Abelian gauge theory, a simple 2-to-6 boson interaction at the leading order needs more than 10^6 (one million) Feynman diagrams [7]. As a consequence, people tried to figure out how to simplify the evaluation of Feynman diagrams and, as a consequence, there is now a whole field (scattering amplitudes) dedicated to solve these diagrams in a smarter way [8]. Moreover, with the recent progress made in the mathematical structure of quantum amplitudes, such as the fact that amplitudes of highly symmetric theories[2] have an analogous description in terms of high simplified geometrical patterns, it became feasible to infer the properties of fundamental aspects of spacetime by studying quantum scattering [9, 10].

Regarding the formal mathematics behind quantum field theories, things become even more puzzling. The oddity is that, according to Haag's theorem [11, 12], the interaction picture that is used to derive scattering amplitudes in QFT is not well defined. This illustrates that the mathematics of QFT is still poorly understood, and there is room for new mathematics to play an important role in QFT. Nonetheless, despite the lack of rigorous mathematical proofs in field theories, physicists stick with the set of rules derived for QFT's due to its tremendous success; for instance, in the context of quantum electrodynamics (QED), the anomalous magnetic moment of the electron can be calculated within a precision of 12 digits [13–15].

While one can follow the standard perturbative QFT rules to calculate processes when interactions among the particles are weak, i.e. when the coupling constant is small, the scenario is different when the coupling is large. In fact, we do not have a general recipe in such a case. To circumvent this problem, one has three alternatives:

1. Build a new weakly coupled effective theory that encompasses the important aspects of the strongly coupled theory. This lies within the framework of effective field theories (EFT), which provide general guidance to construct quantum field theories even beyond the standard model [16].

2. Solve numerically the path integral in supercomputers [17]. This approach, known as lattice QFT is being more explored now since it requires powerful supercomputers to do the calculations. More comments on this will be made when we talk about lattice QCD [18] below.

3. Resort to a weak/strong duality [19]. The philosophy here is to find an equivalent description of a strongly coupled theory in terms of a weakly coupled one. In contrast

[2] As it is common in physics, when dealing with an extremely complex problem, it is better to start with simplified models also referred as "toy models".

with the first option, there are no general recipes to find dualities.

Now, one may wonder in what situation one may encounter a strongly coupled field theory. There are at least two major areas that involve the study of strongly coupled QFT's: (a) in the context of condensed matter, we have for instance the so-called strange metals, which correspond to an emergent strongly interacting phase that appears in some materials [20]; (b) in the context of nuclear physics one has the famous example of quantum chromodynamics (QCD) [21, 22], which is the fundamental theory of the strong interactions. In this thesis, we are interested in the latter, i.e. we want to further our knowledge of strongly coupled QCD matter. Thus, in what follows, I will briefly review the main features of the strong interactions and why it is still a challenge to understand them.

The fundamental interactions of nature are organized in the so-called Standard Model [23], the current theory responsible to describe the basic building blocks of our universe - with the exception of gravity[3], dark matter and dark energy. Furthermore, all fundamental interactions are based on gauge theories and, in terms of group theory, the Standard Model is organized as

$$SU(3) \times SU(2) \times U(1), \tag{1.1}$$

where, in general, $SU(N)$ denotes the *special unitary group of rank N*. The $SU(2) \times U(1)$ part is the electroweak sector, whilst the $SU(3)$ factor denotes the strong interactions, the aim of this thesis. The strong interactions are responsible for nearly 98% of the visible matter in the known universe [24][4], and they describe the complex and intricate interactions between quarks and gluons.

The Lagrangian density of QCD, which defines the set of rules of how the strong interactions behave in Nature, is a four dimensional Lorentz invariant and local SU(3) gauge theory whose explicit expression is [21, 22]

$$\mathcal{L} = -\frac{1}{4} G^a_{\mu\nu} G^{a\mu\nu} + \sum_f^{N_f} \bar{\psi}_f \left(\gamma^\mu D_\mu - m_f\right) \psi_f, \tag{1.2}$$

where ψ_f denotes Dirac quark fields with mass m_f, and γ^μ are the Dirac matrices. Above, N_f defines the number of quark flavors and, as far as we know, QCD has six flavors of quarks: up, down, strange, charm, bottom, and top[5]. The covariant derivative D_μ is given

[3] The "problem" with gravity is that this force is too weak compared to the others. For instance, compared to electromagnetism, gravity is about 10^{40} weaker. As a consequence, to probe the quantum nature of gravity would require access to an energy scale ($E_{Planck} \sim 10^{19}$ GeV) far beyond our current reach in particles accelerators.

[4] The other 2% is due to the Higgs mechanism [25–27] that gives mass to elementary particles such as electrons and quarks. Moreover, the "invisible" universe, i.e. the part that does not interact with photons, is constituted by the so-called dark matter and dark energy, whose microscopic origin are still unknown [28].

[5] The current masses of these flavors are, $m_u = 2.3$ MeV, $m_d = 4.8$ MeV, $m_s = 95$ MeV, $m_c = 1275$

by

$$D_\mu = \partial_\mu + igA^a_\mu t^a, \tag{1.3}$$

where g is the strong coupling constant, A^a_μ is the gluon field in the adjoint representation, and t^a represents the Gell-Mann matrices that span the Lie algebra of the SU(3) group. The quantity $G^a_{\mu\nu}$ is the non-Abelian Yang-Mills field strength, defined as

$$G^a_{\mu\nu} = \partial_\mu A_\nu + \partial_\nu A_\mu + g f^{abc} A^a A^b, \tag{1.4}$$

where f^{abc} are the structure constants of the $SU(3)$ group, i.e. $[t^a, t^b] = i f^{abc} t^c$.

With the Lagrangian (1.2) at hand, one is able to proceed with standard perturbative calculations as long as the coupling g remains small. To see the validity of this assumption, one has to look at the QCD beta function $\beta(\mu) = \partial g / \partial \ln \mu$ [6]. The beta function of a quantum field theory tells us how the coupling runs with the energy scale μ. For a non-Abelian SU(N_c) gauge theory with N_f flavors, at the *1-loop level*, the beta function is given by [6]

$$\beta(\mu) = -\left(\frac{11}{3}N_c - \frac{2N_f}{3}\right)\frac{g^3}{16\pi^2}. \tag{1.5}$$

Thus, if we use the values of QCD for the number of colors and flavors, i.e. $N_c = 3$ and $N_f = 6$, we conclude that the beta function (1.5) is always negative. Moreover, from the QCD beta function, it is possible to get an expression for g as a function of the energy scale

$$g(\mu) \sim \frac{1}{\ln \frac{\mu}{\Lambda_{QCD}}}, \tag{1.6}$$

where $\Lambda_{QCD} \approx 200$ MeV is the QCD intrinsic energy scale [6]. The physical interpretation of this result is straightforward: as the energy increases, the strength of interactions decreases. This result is the celebrated property of *asymptotic freedom* [21, 22], in the sense that quarks and gluons interact very weakly at sufficiently large energies. Furthermore, this property allows one to compute high energy QCD scatterings using perturbative methods and, as one can observe in e.g. Fig. 1.1, this has achieved great success.

However, for low energy processes QCD becomes a strongly coupled theory, a fact that can be suggested by looking at the enhancement of $\alpha_s(Q) = g^2(Q)/(4\pi)$ as Q decreases in Fig. 1.1. In this sense, the strong interaction is the only fundamental force that has this peculiar behavior. Such feature is responsible for the phenomenon of *color confinement*, that is, if one tries to pull apart a quark from the proton, it will be more favourable energetically for the vacuum to create a quark-antiquark pair and form a meson. As a consequence, color charged particles cannot be observed in experiments. Given the breakdown of perturbative QCD one cannot compute analytically, for instance, the spectrum

MeV, $m_b = 4180$ MeV, $m_t = 173$ GeV [29], respectively.

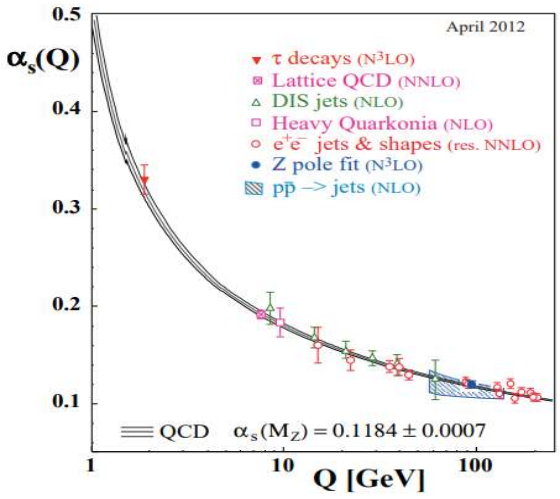

Figure 1.1: *The QCD coupling α_s as function of the energy scale Q. Figure adapted from Ref. [30].*

of hadrons, which can only be done using *ab initio* techniques such as Lattice QCD [24][6].

Lattice quantum field theories were proposed by Kenneth Wilson in 1974 [33] and were first implemented by Michael Creutz in 1980 in the case of SU(2) gauge theory [34]. Roughly speaking, the idea is to solve the path integral corresponding to the QCD generating functional in supercomputers. Evidently, such effort is highly non-trivial, but Lattice QCD managed to have great success over the years and it has become our main guide when experiments are absent. Nowadays, the fundamental issues of Lattice methods are the difficulties in handling out of equilibrium behavior [35] and finite density phenomena [36]. The subject of this thesis, which is the study of hot QCD matter out of equilibrium at finite chemical potential, deals precisely with those limitations of lattice techniques.

Although quarks and gluons are confined inside hadrons in vacuum, it is possible to deconfine them for a very short time in laboratory. The way to do this is by colliding two ultrarelativistic heavy nuclei against each other. In this way, as proposed more than thirty years ago [37], one can inject enough energy to probe the bulk properties of the vacuum, in this case, the quarks and gluons. In the very short period of time that quarks and gluons are deconfined, the *quark-gluon plasma* (QGP) [38–41] is formed. Additionally, the experimental data indicates that the QGP behaves more like a fluid than a colored plasma [42–44], in the sense that the ratio between the shear viscosity (η) and the entropy density (s) is closer to the non-perturbative regime of QCD than the corresponding perturbative regime [45, 46]. This "perfect fluidity" of the QGP was a great surprise for the community as it contradicted many early predictions that the QGP would be a gas of weakly interacting particles [47]. In Sec. 1.3 more details are given about how one can

[6]It is also possible to devise effective theory descriptions, such as QCD sum rules [31], which give estimates for the QCD spectrum which match some experimental data and lattice results [32].

describe the different stages of the QGP created in laboratory.

Furthermore, one could add to the seminal phrase "interactions are hard to understand" that *liquids* are difficult to understand as well. In order to describe a liquid, besides using equations of motion, one has to specify some *transport coefficients*, such as shear viscosity, bulk viscosity, conductivities and so on, and each type of liquid has different underlying microscopic physics from which these *emergent properties* are derived. Indeed, when comparing liquids to solids and gases, the famous physicist Viktor Weisskopf remarked how difficult it is to predict emergent properties from liquids found in even daily life such as water [48]. Imagine then how difficult it is to extract the emergent properties of the QGP (the hottest, tiniest, most perfect and vortical fluid [49]) from the QCD Lagrangian in the non-perturbative regime. To make it even more challenging to describe the time evolution of the QGP, there is also the fact that viscous relativistic hydrodynamics is far from being a trivial generalization of Navier-Stokes theory [50]. For instance, Landau and Lifshitz developed the relativistic version of Navier-Stokes theory in Ref. [51] (see also Eckart in [52]), whose resulting partial differential equations are parabolic and, as such, this theory is acausal (for more information, see Ref. [53]). Therefore, it is paramount to have a complete theoretical understanding of relativistic viscous hydrodynamics to unequivocally interpret heavy ion experimental data.

In the middle of the dearth of tools to describe dynamic properties of the QGP, a very unusual and unpredictable way to describe this system appeared in 1997. In this year, Maldacena conjectured the existence of a duality between a quantum field theory and a string theory [54]. This duality, commonly known as AdS/CFT (anti-de Sitter/Conformal field theory) correspondence, states that SU(N_c) $\mathcal{N} = 4$ super Yang-Mills (SYM) in the large number of colors ($N_c \to \infty$) and sufficently large coupling, has a dual description in terms of classical gravity in anti-de Sitter space [55]. Such duality sparked a revolution in high energy physics since it gave the opportunity to study strongly coupled non-Abelian QFT's from first principles by solving Einstein's equations of general relativity. One of the most startling results obtained from AdS/CFT is the ratio between the shear viscosity to entropy density [56],

$$\frac{\eta}{s} = \frac{\hbar}{4\pi k_B}, \tag{1.7}$$

where $\hbar$ is the Planck constant and k_B is the Boltzmann constant. The importance of the result (1.7) is that it is valid for a broad range of systems according to the AdS/CFT conjecture. As aforementioned, the estimates for the QGP η/s extracted from comparisons between phenomenological calculations to heavy ion experiments produce very small value, being remarkably compatible with (1.7). This agreement suggested a new way to study the dynamics of QGP [57].

One of the features that makes AdS/CFT very attractive is its ability to deal with

non-equilibrium phenomena, which is a very hard task to do in QFT [58]. For instance, in the context of strongly coupled theories, it is possible to study the formation and thermalization of the plasma through the time dependence of an asymptotically AdS_5 space-time that evolves according to general relativity [59]. This is precisely the main goal of this thesis: *to unveil the properties of a strongly coupled non-Abelian plasma in the far-from-equilibrium regime.* Evidently, as will be discussed in Chapter 2, AdS/CFT does not provide a holographic dual of QCD but it certainly gives fresh insight into this complex problem.

However, before we dwell into the details of the original research done in this thesis, in the rest of this Introduction a more detailed overview of the QGP is given to help motivate the work presented here. In Sec. 1.1 I present some well-established results concerning thermal QCD that come from lattice calculations. Sec. 1.2 explains how the QGP is created in laboratory and why this introduces several theoretical and experimental challenges that must be surpassed. Next, in Sec. 1.3 there is a more detailed explanation of how AdS/CFT is used to study the properties of the QGP, though the technical details are presented in Chapter 2. In Sec. 1.4 a detailed summary of each chapter of this thesis is given.

1.1 Strong interactions under extreme conditions

One question that may be posed is the following: what happens to hadrons under extreme conditions? Here, by extreme conditions we mean high temperature and/or high density. Clearly, to answer this question, one has to resort to a many-body QCD formulation that allows us to, at least, compute the equilibrium properties, i.e. the thermodynamics, of the system [60].

The first step to work with QFT at finite temperature is to go from Minkowski space to Euclidean space with periodic boundary conditions, that is, $t \to i\tau$ $(0 \leq \tau \leq \beta)$, where $\beta = 1/(k_B T)$, with T being the temperature. With this procedure, the action in the path integral formulation becomes a probability weight, and the path integral itself becomes a partition function. In the grand canonical ensemble, the partition function of QCD is a functional that depends on the temperature (T), flavor chemical potential (μ_f), and volume (V) [61],

$$Z[V,\mu,T] = \int \mathcal{D}A\mathcal{D}\psi\mathcal{D}\bar{\psi}\, e^{-S_g[A_\mu]} e^{-S_f[\psi,\bar{\psi},A_\mu]}, \tag{1.8}$$

where S_g and S_f are the Euclidean gluonic and fermionic actions, respectively. Their

explicit forms are

$$S_g[A_\mu] = \int^\beta d\tau \int_V d^3x \frac{1}{4} G^a_{\mu\nu}(x) G^{a\mu\nu}(x), \tag{1.9}$$

$$S_f[\psi, \bar{\psi}, A_\mu] = \int^\beta d\tau \int_V d^3x \sum_{f=1}^{N_f} \bar{\psi}_f(x) \left(\gamma^\mu D_\mu + m_f - \mu_f \gamma_0\right) \psi_f(x). \tag{1.10}$$

Moreover, in order to ensure Bose-Einstein statistics for bosons and Fermi-Dirac statistics for fermions, the fields must have periodic/anti-periodic boundary conditions, i.e. $A_\mu(\tau, \mathbf{x}) = A_\mu(\tau + \beta, \mathbf{x})$ and $\psi(\tau, \mathbf{x}) = -\psi(\tau + \beta, \mathbf{x})$.

Thus, once one is given equations (1.8), (1.9), and (1.10), in principle one could proceed to "solve" the theory and compute its observables, such as the free energy density (f) and pressure (p), which are given by

$$f = -\frac{k_B T}{V} \ln Z, \quad p = -f. \tag{1.11}$$

However, as extensively remarked before, this is not easy to do in practice and it is even worse in the non-perturbative regime due to lack of analytic approaches. At very high temperatures, where the coupling is small and perturbation theory is applicable, it is possible to perform calculations and obtain reasonable results. Moreover, at finite temperature, although the convergence of perturbation theory is poor[7], the hard-thermal-loop (HTLpt) program managed to achieve some interesting results [62]. On the other hand, as the temperature decreases and the coupling increases, we do not have an analytic method to compute the QCD partition function. Currently, the only way to overcome this limitation in *ab initio* calculations is to solve the path integral (1.8) in supercomputers using lattice QCD.

Following the standard paradigms of physical simulations in digital computers, in lattice QCD one has to discretize the QCD Lagrangian in a four-dimensional Euclidean space. Then, Monte-Carlo method is employed to integrate numerically the path integral. At the end, the infinite volume limit (i.e. the continuum limit), and the physical quark mass[8] limit are taken. In Fig. 1.2 recent lattice results for the Equation of State (EoS) near the confined/deconfined phase transition around $T \sim 150$ MeV are shown. It is important to notice that the phase transition between the gas of hadrons and the QGP is

[7] At finite temperature one needs to introduce the scales gT and g^2T, and perturbation theory is organized assuming $g^2T \ll gT \ll T$ [47].

[8] It is interesting to notice that the type of phase transition (i.e. 1st order, 2nd order, or crossover) between confined/deconfined quarks and gluons depends on the masses of the quarks. For instance, in the chiral limit, i.e. when the masses of the light quarks vanish, one has a first order phase transition, as one can see from the famous Columbia plot [63, 64].

a crossover, i.e. the thermodynamic variables vary smoothly in the transition[9]. Moreover, in a crossover, there is not a sharp definition for the critical temperature (T_c) since each observable may give a slight different result, which can be inferred from the inflection points of the observables. For this reason, it is common to use the term pseudo critical temperature in crossovers transitions. Lastly, the "HRG" acronym in Fig. 1.2 refers to the *Hadron Resonance Gas* [66], an effective weakly interacting QCD theory assumed to be valid low temperatures.

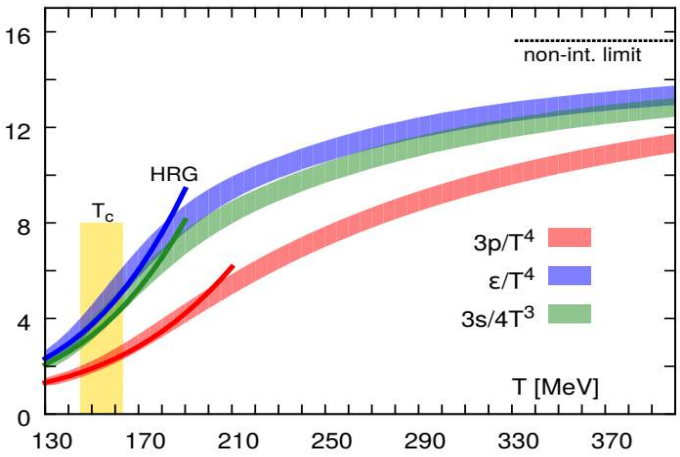

Figure 1.2: *The equation of state for the strong interactions at zero chemical potential. The plot shows simultaneously the result for the pressure (p), energy density (ε), and entropy density (s). Figure taken from Ref. [67].*

At this stage, for zero chemical potential, the general picture is the following. It is possible to study QCD analytically for very low temperatures ($T \lesssim 100$ MeV) using the HRG, and also at very high temperatures ($T \gtrsim 500$ MeV) via perturbative QCD. However, near the crossover, when the hadrons "melt" and the quarks and gluons become the important degrees of freedom, one does not have a clear effective theory to do the computations. It is in this regime that AdS/CFT enters since it offers tools to compute observables of strongly coupled theories that resemble QCD [68–70]. Naturally, there are other ways to try to study the non-perturbative QGP, such as the so-called Nambu-Jona-Lasinio (NJL) [71,72] model and its subsequent improvements [73]. Furthermore, it is nice to have lattice results near the crossover region because one can see the validity of a given model by looking at how it matches the lattice.

The current status of lattice QCD at finite chemical potential is much worse due to fundamental technical complications [36,74]. To understand this, let us first integrate out the fermions in Eq. (1.8) assuming only one flavor for the sake of simplicity ($\mu = \mu_f$)

[9]For some time in the 80's it was thought that the transiton was a first order phase transition, similar to what occurs in pure gauge theory [65].

[75, 76],

$$Z = \int dU e^{-S_g} \mathrm{det}M(\mu), \tag{1.12}$$

where $\mathrm{det}M(\mu)$ is the so-called fermionic determinant, given by

$$M(\mu) = \gamma^\mu D_\mu + m_f - \mu\gamma_0. \tag{1.13}$$

It turns out that due to the absence of γ_5-hermicity in the term containing μ, the determinant of $M(\mu)$ is a complex quantity, i.e,

$$[\mathrm{det}M(\mu)]^* = \mathrm{det}M(-\mu^*). \tag{1.14}$$

This is the famous sign problem found in lattice formulations of quantum field theories[10] [36] and, as consequence, one cannot use Monte Carlo sampling because the probability measure would possess an imaginary part.

As expected, many people tried - and they are still trying - to circumvent this problem. One strategy that led to useful results is to Taylor expand the fermionic determinant in powers of μ/T (see, for instance, Ref. [78]). In this scheme, in the case of baryon chemical potential μ_B, the pressure can be reconstructed from the susceptibilities $\chi_n^B(T, \mu_B) \equiv \partial^n p/\partial\mu_B^n$, i.e.

$$p(T, \mu_B) = p(T, 0) + \sum_{n=1}^{\infty} \frac{1}{n!} \chi_n^B(T, 0)\mu_B^n. \tag{1.15}$$

The state-of-the-art lattice calculations in this regard go up to χ_8 [78], which means that one can probe regions where $\mu_B/T \lesssim 2.5$ in the (T, μ_B) plane. The drawback of this method is that it is very costly and, thus, it is unlikely that one can go much further in the phase diagram in this way. Also, it is interesting to notice that for purely imaginary chemical potential the determinant of $M(\mu)$ is always real and calculations can be directly performed [79]. The main issue in this method is how to translate the results to the real-valued chemical potentials. Such calculations provide another path that is currently being taken to circumvent the sign problem.

Therefore, without lattice results for a broad range of values of μ_B, the phase diagram of the strong interactions is vastly unknown and uncharted, with the experimental aspect being covered in the next section. In Fig. 1.3 there is a cartoon of the conjectured phase diagram. In this diagram there are only a few parts that we know for sure: the parts where perturbative QCD is applicable, i.e. where $T \gg \Lambda_{QCD}$ and/or $\mu_B \gg \Lambda_{QCD}$, and the part where $\mu_B \sim 0$ because lattice QCD gives unequivocally precise results in this

[10] This problem also pervades other systems as well. For instance, in a condensed matter context, the lattice formulation of strongly coupled models in the strange metal phase also suffers from this issue [77].

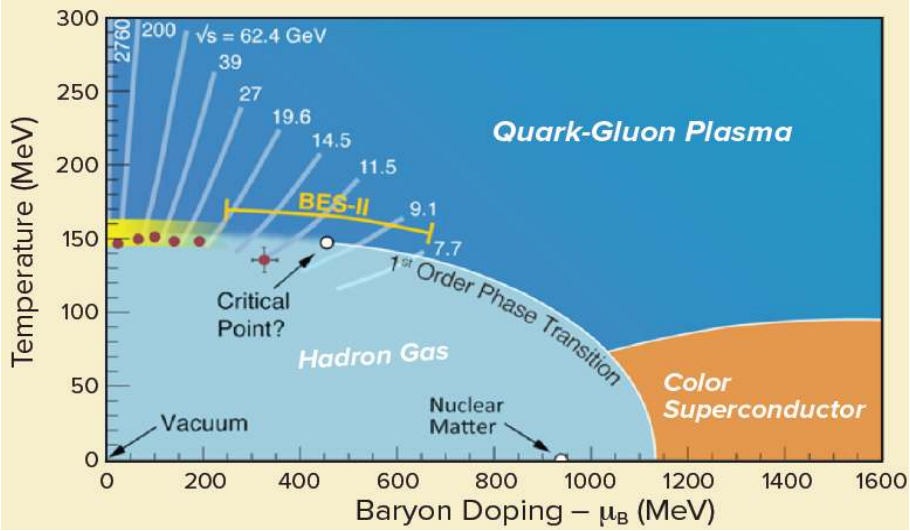

Figure 1.3: *Conjectured phase diagram of strong interactions. The critical point along with the 1st order phase transition line is the fruit of theoretical speculations. The yellow bands around the crossover are the regions probed so far in heavy ion collisions. The BES-II refers to the beam energy scan project developed at RHIC [80] to study the baryon rich QGP. For extremely large values of μ_B, where perturbative methods are applicable, there is an intriguing phase known as the* color superconducting phase *(CSC) [81]. Figure adapted from Ref. [82].*

region for $T \gtrsim 100$. Hence, the first order phase transition line along with its critical end point (CEP), which may appear as the baryon chemical potential increases, is still a conjecture. Indeed, it is possible that such structure does not exist, or even that there are multiple CEP's in the phase diagram [83]. In the meantime, theorists came up with a considerable number of models to extend our knowledge of the phase diagram, but we are still far from a consensus. For instance, two models that can reproduce lattice EoS for small chemical potential are the Cluster Expansion Model (CEM) of Ref. [84], and the holographic model of Ref. [70].

In the next section we shall see how one can probe the QGP and the QCD phase diagram in laboratory and see how complex this task might be.

1.2 Heavy ion collisions, relativistic (viscous) hydrodynamics, and the primordial liquid

The way to produce the QGP in laboratory is by colliding heavy ions against each other - see Refs. [42–44, 85] for reviews. In these collisions, two ultrarelativistic nuclei collide with an amount of energy more than sufficient to break the Coulomb barrier to allow hadrons to interact and create the QGP. As it is usual in particle physics, one does not measure the QGP directly, that is, one has to figure out how it behaves solely from

the final particles measured in detectors (e.g. protons, kaons, photons, etc.). Analogously, imagine that you have to guess how a wooden house was before a fire that completely destroyed it having access only to its ashes. Another complication is that the QGP created is out-of-equilibrium and it is not clear how that affects the idea to explore the phase diagram of the strong interactions.

The history of colliding heavy ions began in 1971 with the Bevalac, the first heavy ion collider at the Lawrence Berkeley National Laboratory (LBNL). The next experiment was designed in Europe with the Super Proton Synchrotron (SPS) at CERN in 1981 [86], and then again in the US with the Alternating Gradient Synchrotron Booster (AGS) at Brookhaven National Laboratory (BNL) in 1991 [87]. Currently, there are two operational facilities, the Relativistic Heavy Ion Collider (RHIC) at BNL, with energy capability of $7.7\,\text{GeV} \lesssim \sqrt{s_{NN}} \lesssim 200$ GeV, and the Large Hadron Collider (LHC) at the CERN, with energy capability in the TeV regime. It is interesting to notice that, to study the baryon rich QGP the collision energy must go down. Indeed, one of the objectives of RHIC is to perform a beam energy scan (BES) of the collisions [80]. For the future, besides updates on the LHC and RHIC programs, it is expected that new facilities to study the QGP phase diagram and the location of the CEP will become operational: the compressed baryonic matter (CBM) experiment at FAIR (GSI) [88, 89] and also the upcoming experiments at NICA [90].

As mentioned above, one does not create only the QGP in heavy ion collisions. On the contrary, the collision probes a very wide range of energy scales in QCD. In Fig. 1.4 it is shown schematically the different stages of the collision: initially, due to the immense speed of the nuclei, the initial phase is usually described by the so-called color-glass-condensate (CGC) formalism [91]; after the collision, for a very short period of time (~ 0.5 fm/c) an intermediate stage between the CGC and the QGP called glasma [92, 93] is formed. Eventually, the quarks and gluons thermalize and the QGP is formed. The QGP is described by relativistic viscous hydrodynamics, an effective theory for many-body problems valid at longwavelengths [50]. As the plasma expands and cools down, hadronization occurs and after the interaction between the hadrons cease (and after they decay) the final fragments of the collision are measured in the detectors.

Thus, although we have a good idea of what happens in a heavy ion collision, one of the main challenges lies in making connections between these different stages. For instance, the initial stage described by CGC is an effective theory derived from weakly coupled QCD, whilst the QGP seems to be strongly coupled; a smooth connection between the initial stages and the strongly coupled QGP is essential for a consistent description of heavy ion collisions.

The success of describing the QGP as a relativistic viscous fluid is remarkable. In

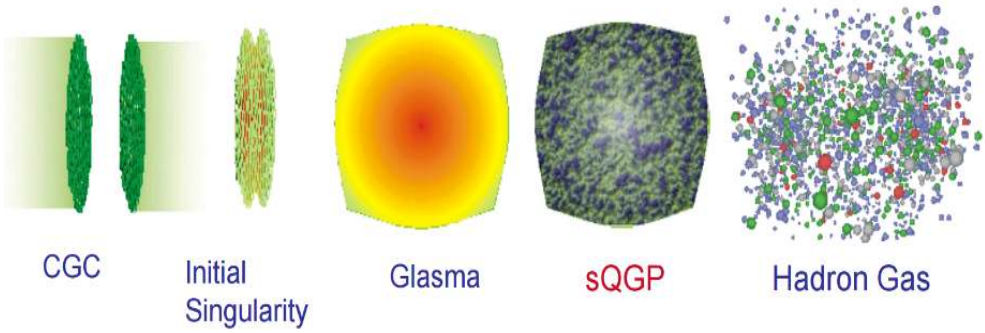

Figure 1.4: *A cartoon showing the main stages of heavy ion collisions. The scale of time in such an event is about* 10^{-23} *s. Typical lenghscales involved in this process are* $\lesssim 10$ *fm. This figure was adapted from [94].*

Fig. 1.5 it is presented some results that validate this description. Furthermore, in recent years, experimental results have suggested that one could have hydrodynamics even in smaller systems, such as in proton-nucleus and even in proton-proton collisions. Thus, the fact that hydrodynamics seems to be more effective than one previously imagined led theorists to pursue a more general formulation [95], where hydrodynamics works even when the system is not so close to equilibrium. Today, this is a rapidly developing topic of fundamental research in fluid dynamics [95–101].

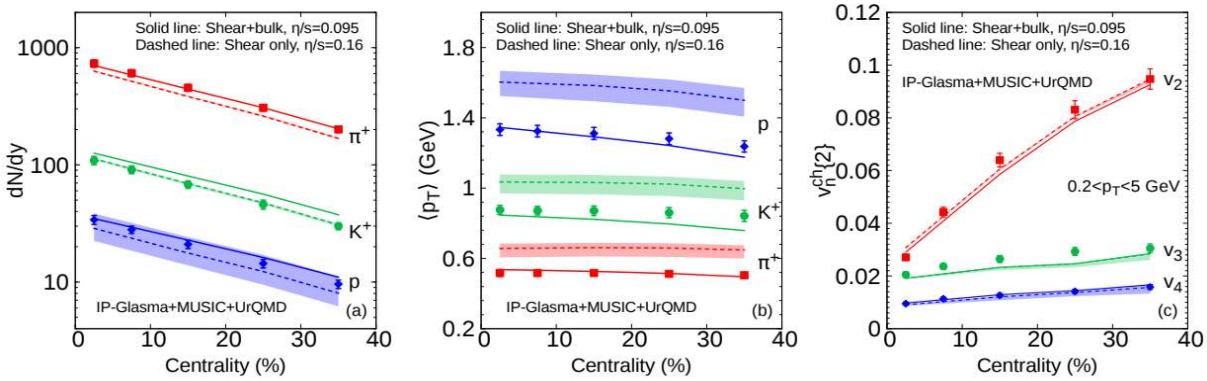

Figure 1.5: *The striking success in treating the QGP as a relativistic viscous fluid. The dots are experimental data, and the curves are results from hydrodynamic model [102]. Left: Multiplicity of charged hadrons as function of centrality. Center: Mean* p_T *as function of centrality. Right: Particle correlations as function of centrality. Figure adapted from [102].*

Now that while there is a general consensus that hydrodynamics is a reasonable description of the QGP formed in nucleus-nucleus collisions, one still has to compute the transport coefficients from the underlying microscopic theory. One way to compute these coefficients, such as the shear viscosity η, is using the so-called Kubo formulas [103]. This was done for the Effective Kinetic Theory (EKT) of QCD [45, 46] and for AdS/CFT [56]. The hydrodynamic model combined with experimental data favored the AdS/CFT result [102], which indicates the strongly coupled nature of the QGP created in heavy ion

collisions; indeed, the result displayed in Fig. 1.5 for the shear viscosity (in natural units) is in the ballpark of result (1.7). Fig. 1.6 is a cartoon that shows the abysmal difference between the QGP and other liquids when it comes to viscous effects. The viscosity of the QGP is believed to be in the vicinity of the AdS/CFT result[11]. A more phenomenological path to extract transport coefficients is using Bayesian analysis, in which, given a theory, one can calculate what is the most likely for the coefficients of the theory [105].

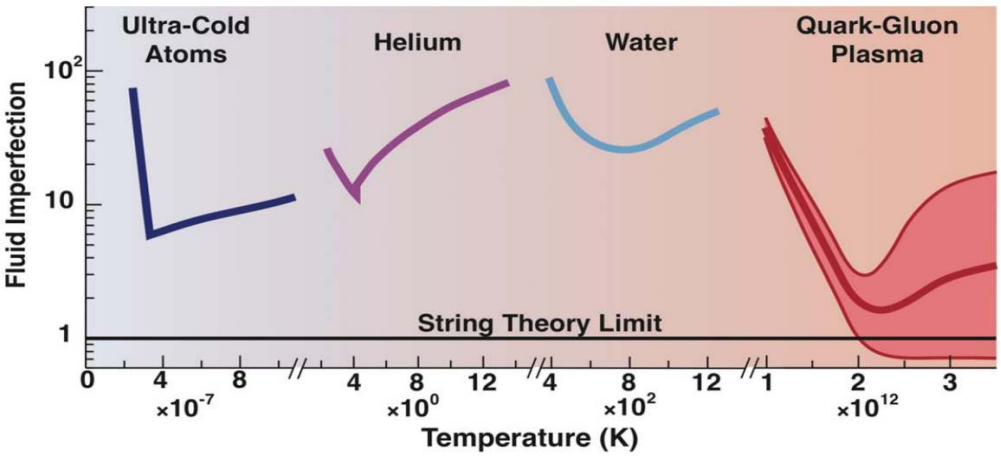

Figure 1.6: *A comparison between η/s in the QGP and other types of fluids (in units of $4\pi\hbar/k_B$), with the "String Theory Limit" being defined by Eq. (1.7). Notice also that the QGP viscosity is near unity, which suggests that quantum effects governs its behavior. The red band around the QGP viscosity expresses our ignorance about its details, and it is less wide for low temperatures because the HRG model [106, 107] gives us more reliable results than perturbative QCD for temperatures that are not so large. Figure adapted from [108].*

Although great progress have been made in the last years, several important points remain unanswered and here I give a sample of them: What is the general principle that can be used to derive far-from-equilibrium hydrodynamics? What is the value of the transport coefficients in the strongly coupled regime? And what about their values at finite baryon chemical potential? Indeed, Ref. [109] studied the baryon rich QGP using mixed values of transport coefficients provenient from AdS/CFT and kinetic theory, which are two very distinct approaches. Moreover, looking carefully at Fig. 1.5, one realizes that the bulk viscosity (absent in conformal theories) is very important to describe the QGP, which implies that more elaborated holographic models are needed for a quantitative description of the QGP.

Now, let us check in the next section in a more precise way how the AdS/CFT correspondence might help us to study properties of the QGP.

[11] It is interesting to point out that the AdS/CFT result for η/s is very close to a quantum limit derived in 1984 [104], where the authors used the uncertainty principle in a quasi-particle description of the plasma.

1.3 Dualities to the rescue

The idea that there may be a duality between gauge theories and string theory is somewhat old. In 1973 Gerard 't Hooft found an intriguing relation between large N_c theories and the perturbative expansion of string theories [110], although at the time this analogy was not very clear yet. Only in 1997, after Maldacena's seminal paper that introduced a duality between QFT's in flat space and string theory [54], that the connection between gauge theories and string theory became clear. To be more precise, the duality corresponds to the equivalence between the strongly coupled $\mathcal{N} = 4$ SYM and type IIB superstring theory[12] in $AdS_5 \times S^5$. Further technical details are given in Chapter 2.

Moreover, motivated by the fact that the entropy of a black hole grows with its area rather than its volume, 't Hooft tried in 1993 to connect gauge theories with gravity in higher dimensions by proposing that all information could be encoded on the boundary of the gravitational theory [111]. Later, Susskind defined this idea as the *Holographic Principle* [112]. In this case, the AdS/CFT correspondence is the first practical realization of the holographic principle in which there exists a bulk-to-boundary correspondence.

Soon after Maldacena's paper, Witten, Gubser, Polyakov, and Klebanov provided a holographic dictionary [113, 114]. Hence, the idea is to compute quantities on the easy side of the duality, namely classical gravity being described by general relativity, and then translate the result to the hard part, i.e., the strongly coupled field theory. Additionally, the original duality was extended to embrace thermal field theory [115], opening new ways to study strongly coupled plasmas such as the QGP. Next, around 2005, one of the most important papers in holography came out. In this paper, Son, Kovtun, and Starinets showed that the ratio between the shear viscosity and the entropy density is given by Eq. (1.7) for a broad range of holographic models [56][13]. This result for η/s, which is in the ballpark of the QGP created in heavy ion collisions, sparked great interest in the scientific community to study strongly coupled plasmas via AdS/CFT. Now, after many years of efforts, we have many interesting possibilities to pursue this goal: ability to study non-equilibrium physics [59]; development of more realistic phenomenological models that match lattice EoS with magnetic field or chemical potential [68,70,119–121]; developments in fluid dynamics [122]; study of hard probes and jets from a strongly coupled point of view [123–125]. The list goes on and on.

It is also challenging to study strongly coupled systems in condensed matter systems. For instance, one can find strongly interacting QFT's in ultracold fermi systems [126],

[12] The "super" in this case refers to the supersymmetry that is incorporated in these string theories.

[13] More precisely, this result holds for any holographic theory whose gravitational dual is isotropic and its Lagrangian has at most two derivatives of the metric. For instance, in Gauss-Bonnet gravity, where one includes corrections proportional to the square of the curvature (i.e. $\propto R^2$), the result (1.7) is no longer valid [116–118].

graphene [127], and high T_c superconductors [128]. Theoretical tools to investigate these phenomena are scarce, and AdS/CFT – or better AdS/CMT [129, 130] in this context – came to help theorists to devise models able to describe strongly interacting systems.

Today, it is fair to say that the majority of the original community of string theorists that worked on AdS/CFT now turned their eyes towards *quantum information theory* [131]. This interest was sparked by the seminal papers of Ryu and Takayanagi [132, 133], in which the authors calculated the entanglement entropy (EE) of a QFT via AdS/CFT. Additionally, the EE entropy is extremely hard to be computed in field theory and only CFT's in low dimensions have their EE known [134]. In hindsight, this led to efforts towards understanding classical gravity as an emergent phenomenon from quantum information theory [135].

The main goal of the work done in this thesis is to use the capacity of holography to compute non-equilibrium phenomena in strongly coupled plasmas with nonzero chemical potential. In this context, near equilibrium dynamics can be understood in terms of the *quasinormal modes* (QNM) [136]. On the other hand, far-from-equilibrium dynamics is harder to study and one needs a sophisticated scheme to solve the time dependent Einstein's equations. In holography, far-from-equilibrium dynamics started with Chesler and Yaffe in 2008, in a paper about the isotropization of strongly coupled $\mathcal{N} = 4$ SYM, where they found a "nested" way to organize the corresponding partial differential equations in the bulk. Soon after, several other papers followed this idea, helping define how first principles calculations in non-equilibrium phenomena may be done in strongly coupled plasmas. In other words, with this method one can study how the plasma thermalizes and acquires hydrodynamic behavior.

1.4 Structure of this thesis

In this section there is a detailed summary of the work done in this thesis.

- In Chapter 2 further explanations regarding the AdS/CFT duality are given. After an overview of the original conjecture proposed by Maldacena, it is explained how one can compute observables using the holographic dictionary. In particular, there is an emphasis in how one can compute one-point functions in the gauge theory using the correspondence. This procedure is fundamental to obtain the one-point functions ($\langle T_{\mu\nu}\rangle$, $\langle J_\mu\rangle$, $\langle O_\phi\rangle$ [137]) discussed in Chapters 3 and 4.

- Chapter 3, which is based on Ref. [137], starts the part of original work done in this thesis. There, it is presented in more details the holographic model 1-R charged black (1RCBH) [138–143], which possesses a critical point. This model is a rigorous

top-down model obtained from truncations of the superstring theory. The point of this Chapter is to perform the first study of the homogeneous isotropization near a critical point. Moreover, for this far-from-equilibrium calculation, several numerical details are given in this chapter as well.

- Chapter 4 is based on Ref. [144] and it deals with the holographic 1RCBH model undergoing Bjorken flow [145]. The goal here is to assess the influence of the critical point on the *hydrodynamization* process of a non-Abelian strongly coupled plasma. In other words, we investigate how hydrodynamics emerges near a critical point starting from initial conditions out-of-equilibrium.

- Chapter 5 ends the main body of this thesis with conclusions and outlook.

- Appendix A is an augmented version of Ref. [146] that incorporates the appendix of Ref. [137]. This appendix analyzes the near-equilibrium behavior of the 1RCBH via its QNM's. This is also interesting because the near-equilibrium behavior is captured by the final evolution of the plasma in the homogeneous isotropization process. More discussions about this can be found in Chapter 3.

1.4.1 Units and conventions used throughout this thesis

In this thesis we use natural units where $c = \hbar = k_B = 1$. For instance, in this convention ,Eq. (1.7) becomes $\eta/s = 1/(4\pi)$.

Capital Latin indices $\{M, N, \dots\}$ denote the coordinates $\{t, r, x, y, z\}$ of a five dimensional asymptotically AdS spacetime where the gravity theory is defined, whereas Greek indices $\{\mu, \nu, \dots\}$ represent the coordinates $\{t, x, y, z\}$ of the four dimensional boundary. Additionally, we use a mostly plus metric signature.

Given a line element of a generic pseudo-Riemannian manifold

$$ds^2 = g_{\mu\nu} dx^\mu dx^\nu \tag{1.16}$$

where $g_{\mu\nu}$ is the metric for a specific chart x^μ, the Riemann tensor will be given by the expression

$$R^\alpha{}_{\beta\mu\nu} = \partial_\mu \Gamma^\alpha_{\beta\nu} - \partial_\nu \Gamma^\alpha_{\beta\mu} + \Gamma^\alpha_{\mu\sigma}\Gamma^\sigma_{\beta\mu} - \Gamma^\alpha_{\nu\sigma}\Gamma^\sigma_{\beta\mu}, \tag{1.17}$$

with $\Gamma^\mu_{\alpha\beta}$ being the Christoffel symbol, defined as

$$\Gamma^\alpha_{\mu\nu} = \frac{1}{2} g^{\alpha\sigma} \left(\partial_\nu g_{\sigma\mu} + \partial_\mu g_{\sigma\nu} - \partial_\sigma g_{\mu\nu}\right). \tag{1.18}$$

Regarding the radial coordinate of the AdS_5 space, we use the letter r to represent it

when the boundary is located at infinity ($r_{bdry} \to \infty$), and we use the letter u when the boundary is at the origin ($u_{bdry} = 0$).

Chapter 2

The gauge/gravity duality

Now it is time to take a closer look at the gauge/gravity duality, which started a revolution in high energy physics by giving tools and recipes to study strongly coupled quantum field theories. Moreover, it is based on this framework that the whole work of this thesis is done.

In this work holography is introduced in a more or less chronological order, i.e. we first give the original argument presented by Maldacena[1], then we discuss the holographic dictionary derived by Gubser, Klebanov, Polyakov, and Witten [113, 114]. In the end of this chapter there is a thorough discussion of the holographic renormalization procedure under the light of modern algorithms.

Moreover, after twenty years of the AdS/CFT duality proposal, there is now plenty of good quality reviews [55, 147, 148] and books [130, 149, 150] available for further reading.

2.1 The original AdS/CFT correspondence conjecture

Before we present the decoupling argument that led Maldacena to establish the AdS/CFT duality, let us analyze first some arguments that give support to the correspondence.

Back in 1973, 't Hooft considered the large N_c limit of $SU(N_c)$ gauge theories [110] in an attempt to simplify the theory in the non-perturbative regime and solve it through an expansion in powers of $1/N_c$[2]. To follow his argument, we first have to understand what is the effective coupling of a gauge theory in terms of its original coupling g_{YM} and the

[1] Another way to introduce the AdS/CFT duality is via the renormalization group and how the radial coordinate of the AdS_5 space may be viewed as an energy scale of the theory [147].

[2] Notice also that in four dimensions the Lagrangian of a pure gauge theory does not have any dimensional parameter and the energy scale Λ of the theory arises from dimensional transmutation.

number of colors N_c. The beta function of a pure gauge theory is given by

$$\mu \frac{dg_{YM}}{d\mu} = -\frac{11}{3} N_c \frac{g_{YM}^3}{16\pi^2} + \mathcal{O}(g_{YM}^5), \tag{2.1}$$

where μ is the energy scale. Taking now the *'t Hooft limit* $N_c \to \infty$ while keeping the *'t Hooft coupling* $\lambda_t \equiv g_{YM}^2 N_c$ fixed (i.e. $g_{YM} \to 0$), the beta function (2.1) can be rearranged as

$$\mu \frac{d\lambda_t}{d\mu} = -\frac{11}{24\pi^2} \lambda_t^2 + \mathcal{O}(\lambda_t^3), \tag{2.2}$$

whose expression makes patent the asymptotic freedom character of the theory. Moreover, the perturbative expansion parameter of large N_c Yang-Mills theory is λ_t.

With the definition of λ_t at hand, it is time to organize the perturbative expansion of the Yang-Mills theory in terms of N_c and λ_t. To accomplish this, we take the $U(N_c)$ Yang-Mills Lagrangian

$$\mathcal{L} = -\frac{1}{g_{YM}^2} \mathrm{Tr} F_{\mu\nu} F^{\mu\nu}, \tag{2.3}$$

and redefine the gauge field in a way that the final Lagrangian reads

$$\mathcal{L} = -\frac{N_c}{\lambda_t} \mathrm{Tr} F_{\mu\nu} F^{\mu\nu}. \tag{2.4}$$

For the Feynman rules of large N_c theories that come from the Lagrangian (2.4), it is easier to work with the so-called double line formalism since it saves us from dealing with structure constants f_{abc}. The propagator of the gauge field, in the adjoint representation, is given by the product of a fundamental and anti-fundamental representations of the gauge field[3]

$$\langle A_b^a A_d^c \rangle \propto \delta_d^a \delta_c^b, \tag{2.5}$$

where A is the gluon field, and $a, b = 1, 2, \ldots, N_c$. The representation of this propagator in the double line formalism for the Feynman diagrams is shown in Fig 2.1. We also give in Fig. 2.1 the Feynman rules that are necessary to perform the power counting. For more examples and details about large N_c gauge theories we indicate Ref. [151].

Hence, a generic vacuum amplitude $\mathcal{A}$ with P propagators, V vertices and L loops has the following schematic form

$$\mathcal{M}(P, V, L) \propto \left(g_{YM}^2\right)^P \left(\frac{1}{g_{YM}^2}\right)^V (N_c)^L = N_c^{V-P+L} \lambda_t^{P-V}, \tag{2.6}$$

where in the last step we wrote the answer in terms of the 't Hooft coupling. Now, the

[3]For an $SU(N_c)$ theory there is also a mixing term proportional to $1/N_c\, (\delta_b^a \delta_d^c)$. However, as $N_c \to \infty$, this difference becomes negligible.

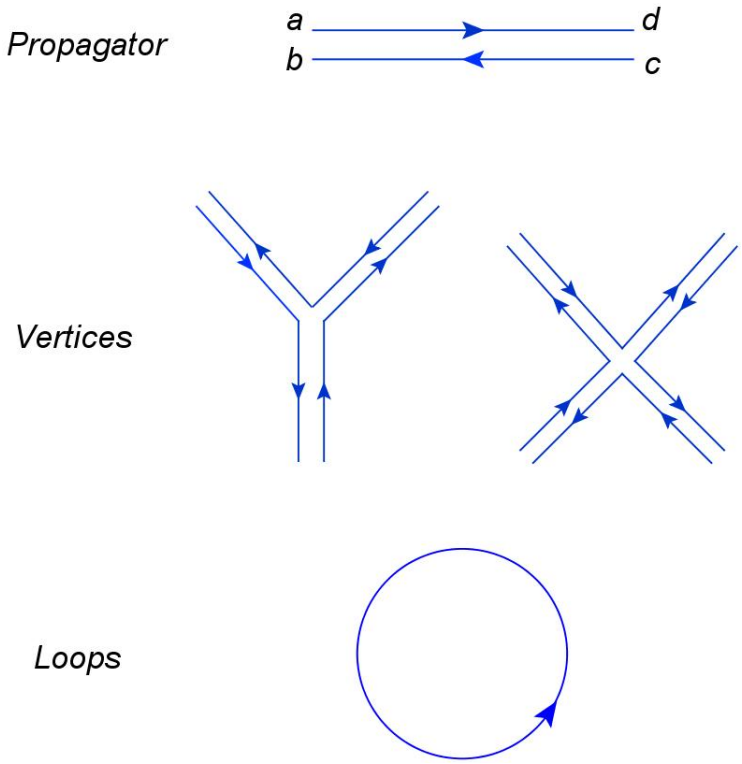

Figure 2.1: *Feynman rules for the gauge theory in the double line formalism in terms of N and g_{YM}. In the scattering amplitude, the propagator contributes with $g^2_{YM}\delta^d_a\delta^b_c$, the vertices contribute with $1/g^2_{YM}$, and the loops contribute with $\delta^a_a = N_c$.*

key observation to relate a gauge theory amplitude to the ones found in string theory is to evoke Euler's characteristic formula, i.e. [152, 153]

$$V - P + L = 2 + 2g, \tag{2.7}$$

where g is the genus number, that is, the number of "holes" in the topology of the Feynman diagram. In Fig. 2.2 there are two examples of Feynman diagrams with different topologies.

The final expansion form for the scattering amplitude becomes

$$\mathcal{M} = \sum_{g=0}^{\infty} N^{2-2g} f_g(\lambda_t). \tag{2.8}$$

Therefore, from the above expression it is evident that the *planar diagrams*, the ones with $g = 0$, will be the dominant ones in the perturbation expansion as $N_c \to \infty$. What is remarkable in Eq. (2.8) is that it has the same structure of vacuum-to-vacuum amplitudes of string theory. Moreover, since the argument of large N_c was rather general, one may conclude that different gauge theories will correspond to different truncations of the dual string theory, if it exists.

Now, let us analyze the argument that led to the AdS/CFT duality. The theoretical

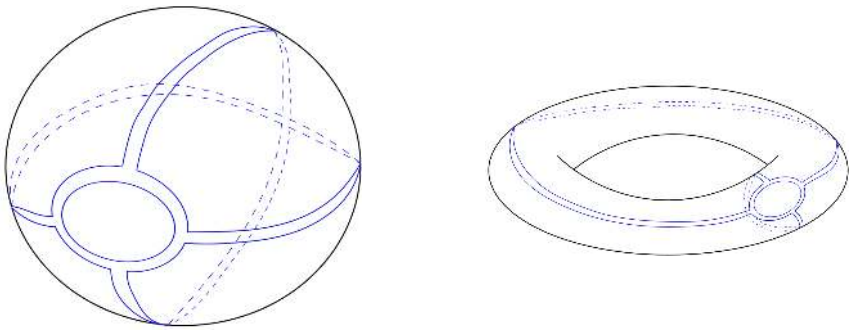

Figure 2.2: *Different topologies for scattering amplitudes in the double line formalism. According to Eq. (2.8), scattering amplitudes whose topology has higher genus-number are suppresed in the large N_c limit. Hence, the diagram on the right (torus) is suppressed when compared to the diagram on the left (sphere).*

background is superstring theory [152, 153], more specifically the 10-dimensional type IIB theory. This decoupling argument is based on two rather distinct views of the same physical situation: imagine that you have a stack of N_c coincident D3-branes[4] inserted in spacetime, then, you can proceed to describe this situation as follows:

(a) Due to the massless spectrum of open strings living at the brane, each D3-brane associated with type IIB theory carries a U(1) maximally symmetric gauge field in 3+1 dimensions. Hence, the stack of N_c coincident D3-branes will possess a field theory description in terms of $U(N_c)$ $\mathcal{N} = 4$ SYM theory. This is the open string point of view.

(b) If the number of D3-branes is large ($N_c \gg 1$) in a way that the energy density increases, it is expected that spacetime will curve and gravity must be included in order to describe the physics. Indeed, in the low energy limit ($\alpha' \to 0$), supergravity solutions were known since the beginning of the 90's [156, 157]. The supergravity solution corresponding the stack of D3-branes gives the famous $AdS_5 \times S^5$ space, which is valid when the AdS radius is large, i.e. when N_c is large. This is the closed string point of view.

Although different at first sight, the two descriptions above were derived from the same physics, hence, they are equivalent, i.e. $(a) = (b)$. This observation led one to conjecture [54]

$$\boxed{\mathcal{N} = 4 \; SU(N_c) \text{ SYM in four dimensions} = \text{type IIB string theory in } AdS_5 \times S^5.} \quad (2.9)$$

[4] Dp-branes are soliton-like extended objects with p dimensions where open strings can end [154]. Indeed, the name of this object is a direct reference to the Dirichlet boundary condition. Moreover, as showed by Witten in 1995 [155], D-branes are interesting objects because they incorporate gauge theories in their worldvolume.

To better understand the limits in which this duality is valid, we write the following relation

$$\frac{L^4}{l_s^4} = g_{YM}^2 N_c = \lambda_t, \tag{2.10}$$

where L is the AdS radius, and l_s is the string length. Therefore, if the AdS radius is large (supergravity solution is valid), then the 't Hooft coupling is also large, which means that there is a weak/strong duality at play here.

The basic consistency checks that one could perform is to compare the symmetries of each side of the duality. For instance, $AdS^5 \times S^5$ has 32 Killing spinors and $\mathcal{N} = 4$ SYM has 32 supercharges. Nowadays, after 20 years of the conjecture, we have many precise tests of the duality [158, 159].

2.2 Obtaining observables from the holographic dictionary

A duality is only useful if you can compute quantities on one side and translate the result to the other side. In the case of the AdS/CFT correspondence, we want to do some classical general relativity calculations in AdS, which is the "easy" side, and translate this result to the CFT side. Below, we shall see how to relate the partition function of the CFT side to the gravity action of the dual theory.

Given a generic field (Φ) with its source (Φ_0) and corresponding expectation value ($\mathcal{O}$), the "GKPW" rule states that [113, 114]

$$\left\langle \exp\left(\int_x \Phi_0 \mathcal{O}\right)\right\rangle_{CFT} = Z_{String}[\Phi], \tag{2.11}$$

where Z_{String} is the partition function of the IIB superstring theory. Additionally, the above expression is only meaningful if the procedure of holographic renormalization, which we explain in the next section, is performed.

In the classical approximation, the partition function of the string side is simplified to

$$Z_{String}[\Phi] \approx \exp\left(-S_{clas}[\Phi(u=0,x) = \Phi_0]\right), \tag{2.12}$$

where the on-shell action is assumed. In this supergravity approximation, the partition function is approximated by a steepest descent method in which the classical solution is the saddle point.

Moreover, to compute Eq. (2.11), one first need to know what is the field on the gravity side that is dual to the operator on the CFT side, i.e. the *field-operator map*. For instance, the dual field in the bulk corresponding to the stress-energy tensor operator ($T^{\mu\nu}$) is the

metric (g_{MN}) of the AdS space. Once the map between fields on the gravity side and operators of the CFT side has been identified, one uses the GKPW rule (2.11) to obtain the partition function.

In general, at least in Euclidean signature[5], any n-point functions can be obtained via functional derivatives of the partition function with respect to the source and then taking the limit where the source vanishes, i.e.

$$\langle \mathcal{O}_1(x_1)\dots\mathcal{O}_n(x_n)\rangle = \left.\frac{\delta^n Z_{string}[J]}{\delta J_1(x_1)\dots\delta J_n(x_n)}\right|_{J=0}, \tag{2.13}$$

where the source is the boundary value of the field, e.g. $\Phi_0(\vec{x}) = \Phi(u=0,\vec{x})$.

Furthermore, to introduce temperature in the dual field theory, one has to insert a black hole in the AdS space and then all the thermodynamic properties of the theory follows from the laws of black holes thermodynamic. For instance, the temperature is given by Hawking's temperature [162], whilst the entropy is calculated using the Bekenstein-Hawking prescription [163, 164].

2.3 Holographic renormalization

In this section it is given the details on how one may obtain the one-point functions $\langle T_{\mu\nu}\rangle$, $\langle J_\nu\rangle$, and $\langle \mathcal{O}_\phi\rangle$ of an Einstein-Maxwell-Dilaton (EMD) theory using the holographic renormalization procedure [165–167]. As remarked in Sec. 1.4, the one-point functions are the core observables probed throughout this thesis. The purpose of the holographic renormalization is to determine the counter-term action S_{ct} that removes the divergences of the theory when one calculates one-point functions.

The general EMD holographic model is characterized by the following five dimensional bulk gravitational Lagrangian[6],

$$S = \frac{1}{2\kappa_5^2}\int_{\mathcal{M}} d^5x\sqrt{-g}\left[R - \frac{f(\phi)}{4}F_{MN}F^{MN} - \frac{1}{2}(\partial_M\phi)^2 - V(\phi)\right], \tag{2.14}$$

where $\kappa_5^2 = 8\pi G_5$ with G_5 being the five dimensional Newton's constant, $F_{MN} = \partial_M A_N - \partial_N A_M$, with A_M being the Maxwell gauge field, and ϕ is the dilaton field. To perform the holographic renormalization, we do not need to specify the dilaton potential $V(\phi)$ and the coupling $f(\phi)$. The only thing that we need to specify is the mass (m) of the dilaton, i.e.

$$m^2L^2 = V''(0). \tag{2.15}$$

[5]The generalization to Minkowski signature is somewhat non-trivial [160, 161], especially for higher point functions [113].

[6]The Chern-Simon term is not included because it does not appear in the 1RCBH holographic model.

The reason for that is because the mass of the dilaton is related to its asymptotic behavior, i.e. $\phi(r \to \infty, x) \sim r^{\Delta-4}$, where $\Delta(\Delta - 4) = m^2L^2$ is the scaling dimension. Moreover, the scaling dimension of the dilaton reveals which kind of the deformation it induces in the original conformal field theory.

The possible deformations of the theory are

- $4 - \Delta > 0$: relevant operator.
- $4 - \Delta < 0$: irrelevant operator.
- $4 - \Delta = 0$: marginal operator.

In this thesis we are interested in a relevant operator, where the deformation is weak in the UV ($\phi(r \to \infty) \to 0$) and strong in the IR. Indeed, the 1RCBH has $\Delta = 2$ (c.f. Chap. 3), which means that the analysis done below will be valid for this deformation only. After this interlude about the EMD holographic model, whose details are given in Chap. 3, we can continue with the renormalization procedure.

In what follows, and as it is common in the treatment of holographic renormalization, we adopt the Fefferman-Graham (FG) coordinates in which there is an explicit relation between the renormalization group (RG) flow at the boundary QFT and the bulk radial coordinate

$$ds^2_{FG} = \frac{d\rho^2}{4\rho^2} + \gamma_{\mu\nu}(\rho, x)dx^\mu dx^\nu, \tag{2.16}$$

with the Greek indices running through the coordinates of the dual QFT, $x \in \{t, \vec{x}\}$, and ρ denoting the radial coordinate in the FG chart, where the boundary lies at $\rho = 0$.

The first step to renormalize the on-shell action is to identify, in a covariant manner, what are the divergent terms. This analysis is done by integrating out the ρ-direction in the on-shell action up to a near-boundary hypersuface $\rho = \epsilon$ that acts as a cutoff, defining then a regulated action, $S_{reg} = (S_{bulk} + S_{GHY})|_\epsilon$. Once the divergences of the regulated action are identified, the counterterm action S_{ct} is defined as follows [165–167]

$$S_{ct} = -(\text{divergent terms of } S_{reg}). \tag{2.17}$$

The subtracted action, S_{sub}, which is supposed to be evaluated at the cutoff $\rho = \epsilon$, is given by

$$S_{sub} = S_{reg} + S_{ct} = S_{bulk} + S_{GHY} + S_{ct}. \tag{2.18}$$

The renormalized on-shell action is obtained by taking the limit $\rho \to 0$ on the subtracted action, i.e.

$$S_{ren} = \lim_{\rho \to 0} S_{sub}. \tag{2.19}$$

Once the renormalized on-shell action (2.19) is found, we follow the holographic dictionary and take functional derivatives of the renormalized action with respect to the boundary values of the bulk fields to obtain the corresponding one-point functions in the dual QFT. In particular, for an EMD model, the important one-point functions are[7]

$$\langle T_{\mu\nu}\rangle = -\frac{2}{\sqrt{-g_{(0)}}}\frac{\delta S_{ren}}{\delta g^{\mu\nu}_{(0)}} = -\lim_{\rho\to 0}\frac{1}{\rho}\frac{2}{\sqrt{-\gamma}}\frac{\delta S_{sub}}{\delta \gamma^{\mu\nu}}, \tag{2.20}$$

$$\langle J^{\mu}\rangle = \frac{1}{\sqrt{-g_{(0)}}}\frac{\delta S_{ren}}{\delta A_{(0)\mu}} = \lim_{\rho\to 0}\frac{1}{\rho^2}\frac{1}{\sqrt{-\gamma}}\frac{\delta S_{sub}}{\delta A_{\mu}}, \tag{2.21}$$

$$\langle \mathcal{O}_{\phi}\rangle = \frac{1}{\sqrt{-g_{(0)}}}\frac{\delta S_{ren}}{\delta \phi_{(0)}} = \lim_{\rho\to 0}\frac{\ln\rho}{\rho}\frac{1}{\sqrt{-\gamma}}\frac{\delta S_{sub}}{\delta \phi}, \tag{2.22}$$

where $g_{\mu\nu} = \rho\,\gamma_{\mu\nu}$ is the metric of the boundary QFT, which we shall take to be Minkowski at the end of the calculations. The subscript (0) denotes that these fields are computed at the boundary of the asymptotically AdS space; we will give the precise meaning of it below when we expand the fields near the boundary.

2.3.1 Counterterm action

Counterterm action for $\Delta = 2$

The counterterm action for the 1RCBH model, which is an EMD model whose bulk scalar field has dimension $\Delta = 2$, is the same counterterm action for the Coulomb branch flow [167]

$$S_{ct} = \frac{1}{\kappa_5^2}\int_{\partial M} d^4x\sqrt{-\gamma}\left[-3 - \frac{1}{4}R[\gamma] + \frac{\ln\rho}{16}\left(R^{\mu\nu}[\gamma]R_{\mu\nu}[\gamma] - \frac{1}{3}R[\gamma]^2 + f(0)F_{\mu\nu}F^{\mu\nu}\right) + \frac{1}{2}\left(1+\frac{1}{\ln\rho}\right)\phi^2\right], \tag{2.23}$$

where $f(0) = f(\phi = 0)$, and $R[\gamma]$, $R_{\mu\nu}[\gamma]$, are the respective Ricci scalar and Ricci tensor of the induced metric at the boundary, $\gamma_{\mu\nu}$. From now on, though, in order to simplify the notation, we will suppress the explicit metric dependence γ of the curvature tensors evaluated at the boundary of the bulk space, e.g. $R \equiv R[\gamma]$. Also, from the term multiplying $\ln\rho$ one can already see what is the trace anomaly of the theory, which is zero for the case of the conformal 1RCBH model[8]. Regarding the derivation of the counterterm action, we refer the reader to Ref. [169] for very enlightening and clear discussions about

[7] Note that for a bulk scalar field with dimension $\Delta = 2$, as it is the case of the dilaton in the 1RCBH model, we need to introduce an extra $\ln\rho$ term to regularize the expectation value of its dual scalar operator in the boundary QFT.

[8] We remark that, although a chemical potential does not induce a trace anomaly, a magnetic field does induce a trace anomaly in the SYM plasma [168].

it. Also, one may find insightful discussions about the derivation of counterterm actions in the EMD context using the Hamiltonian approach in Ref. [170].

Moreover, it is important to know that, due to the fact that in the 1RCBH model the scalar field and the Abelian gauge field do not break the original conformal symmetry of the SYM plasma, one may add finite contributions to the counterterm action (2.23), which unveils the scheme dependence of the holographic renormalization procedure. The finite counterterms that one may add are

$$S_{ct}^{finite} = \frac{1}{\kappa_5^2}\int_{\partial M} d^4x\sqrt{-\gamma}\left[c_1 F_{\mu\nu}F^{\mu\nu} + c_2\phi^2\right], \tag{2.24}$$

where $\{c_1, c_2\} \in \mathbb{R}$. In short, to see why these terms are finite, one just needs to recall that, with the scaling dimensions of the EMD fields for the 1RCBH model, one obtains

$$\begin{aligned} &\sqrt{-\gamma} \sim \rho^{-2}, \quad F_{\mu\nu}F^{\mu\nu} \sim \rho^2, \quad \phi^2 \sim \rho^2, \\ &\Rightarrow \sqrt{-\gamma}F_{\mu\nu}F^{\mu\nu} \sim \text{constant}, \quad \text{and} \quad \sqrt{-\gamma}\phi^2 \sim \text{constant}. \end{aligned} \tag{2.25}$$

Consequently, one may try to simplify the final expressions for the one-point functions of the dual QFT by including some finite counterterms, i.e.

$$S_{ct} \to S_{ct} + S_{ct}^{finite}. \tag{2.26}$$

In this work, though, we will not resort to the addition of any extra finite term to the counterterm action (2.23).

2.3.2 One-point functions

One-point functions for $\Delta = 2$

With the counterterm action at hand, we now have the subtracted on-shell action (2.18), which means that we can proceed with the functional derivatives to extract the one-point functions given in Eqs. (2.20)—(2.22). The analysis for the scalar field carried out here is based on Appendix C of Ref. [169], whilst the vector field analysis is based on Ref. [171]. Nonetheless, the full analysis of the EMD holographic renormalization is done for the first time here, and its results are essential for the next chapters.

It is clear from Eqs. (2.20)—(2.22) that we need to expand the fields near the boundary.

Thus, we perform the FG expansion of the EMD fields[9]

$$\gamma_{\mu\nu}(\rho,x) = \frac{1}{\rho}\gamma_{(0)\mu\nu}(x) + \gamma_{(2)\mu\nu}(x) + \gamma_{(2,1)\mu\nu}(x)\ln\rho + \rho\left(\gamma_{(4)\mu\nu}(x) + \gamma_{(4,1)\mu\nu}(x)\ln\rho + \gamma_{(4,2)\mu\nu}(x)\ln^2\rho\right) + \mathcal{O}(\rho^2), \tag{2.27}$$

$$A_\mu(\rho,x) = A_{(0)\mu}(x) + \rho\left(A_{(2)\mu}(x) + A_{(2,1)\mu}(x)\ln\rho\right) + \mathcal{O}(\rho^2), \tag{2.28}$$

$$\phi(\rho,x) = \rho\left(\phi_{(0)}(x) + \phi_{(0,1)}(x)\ln\rho\right) + \mathcal{O}(\rho^2). \tag{2.29}$$

Note that in order to obtain the one-point functions, it suffices to expand the fields up to $\mathcal{O}(\rho)$ since the remaining terms vanish as $\rho \to 0$. The independent terms of the above expansions are $\{\phi_{(0)}, \phi_{(0,1)}, A_{(0)\mu}, A_{(2)\mu}, \gamma_{(0)\mu\nu}, \gamma_{(4)\mu\nu}\}$ and, thus, any other coefficient may be recast in terms of these independent ones. Furthermore, we are keeping here the analysis fairly general for any EMD model with $\Delta = 2$; we shall only specialize to the 1RCBH background at the end of the calculations.

Next, one substitutes the above near-boundary expansions for $\gamma_{\mu\nu}$, A_μ, and ϕ into Eqs. (2.20)—(2.22) to obtain the explicit formulas for the one-point functions. However, since the required algebra is not so simple, we give some further details below. First, let us provide the formulas for the variation of the regularized on-shell action with respect to the sources[10]

$$\frac{1}{\rho}\frac{2}{\sqrt{-\gamma}}\frac{\delta S_{sub}}{\delta\gamma^{\mu\nu}} = \frac{1}{\rho}\left(T^{reg}_{\mu\nu} + T^{ct}_{\mu\nu}\right), \tag{2.30}$$

$$\frac{1}{\rho^2}\frac{1}{\sqrt{-\gamma}}\frac{\delta S_{sub}}{\delta A_\mu} = \frac{1}{\rho^2}J^\mu, \tag{2.31}$$

$$\frac{\ln\rho}{\rho}\frac{1}{\sqrt{-\gamma}}\frac{\delta S_{sub}}{\delta\phi} = -\frac{1}{\kappa_5^2}\frac{\ln\rho}{\rho}\left(-\rho\partial_\rho\phi + \left(1 + \frac{1}{\ln\rho}\right)\phi\right), \tag{2.32}$$

where

$$T^{reg}_{\mu\nu} = \frac{2}{\sqrt{-\gamma}}\frac{\delta S_{reg}}{\delta\gamma^{\mu\nu}} = \frac{1}{\kappa_5^2}\left(K_{\mu\nu} - \gamma_{\mu\nu}K\right), \tag{2.33}$$

$$T^{ct}_{\mu\nu} = \frac{1}{\kappa_5^2}\left(-2Y_{\mu\nu} + \mathcal{L}_{ct}\gamma_{\mu\nu}\right), \tag{2.34}$$

$$J^\mu = \frac{1}{\kappa_5^2}\left(\rho f(\phi)\gamma^{\mu\nu}\partial_\rho A_\nu + \frac{f(\phi)}{4}\nabla_\nu F^{\mu\nu}\ln\rho\right), \tag{2.35}$$

[9]Note that in the subscripts (n,m) of the coefficients of these expansions, $n = 0$ denotes the leading order term in ρ (as it goes to zero) and m denotes the power of $\ln\rho$. This is reminiscent of the general form of these expansions presented in Eqs. (3.18)—(3.22).

[10]When we integrated the ρ coordinate by parts in the variation of the integrals we considered that the normal vector $n^M = (-2\rho, 0, 0, 0, 0)$ at the boundary of the manifold is "outward-pointing", i.e. $g_{MN}n^M n^M = 1$.

with $K_{\mu\nu} = \rho\partial_\rho\gamma_{\mu\nu}$ denoting the extrinsic curvature of the boundary and $K = \gamma^{\mu\nu}K_{\mu\nu}$ its trace. We also have defined the following objects

$$\mathcal{L}_{ct} = -3 - \frac{1}{4}R + \frac{1}{2}\left(1 + \frac{1}{\ln\rho}\right)\phi^2 + \frac{\ln\rho}{16}\left(R^{\mu\nu}R_{\mu\nu} - \frac{1}{3}R^2 + f(0)F_{\mu\nu}F^{\mu\nu}\right), \tag{2.36}$$

$$\begin{aligned} Y_{\mu\nu} &= \frac{\delta\mathcal{L}_{ct}}{\delta\gamma^{\mu\nu}} \\ &= \frac{1}{4}R_{\mu\nu} + \ln\rho\left[-\frac{f(0)}{8}F_{\mu\sigma}F_{\nu}{}^{\sigma} + \frac{f(0)}{32}F_{\sigma\lambda}F^{\sigma\lambda}\gamma_{\mu\nu} + \frac{1}{32}\gamma_{\mu\nu}R^{\sigma\lambda}R_{\sigma\lambda}\right. \\ &\left. + \frac{1}{24}R_{\mu\nu}R - \frac{1}{96}\gamma_{\mu\nu}R - \frac{1}{8}R^{\sigma\lambda}R_{\mu\sigma\nu\lambda} + \frac{1}{48}(\nabla_\mu\nabla_\nu R) - \frac{1}{16}\Box R_{\mu\nu} + \frac{1}{96}\gamma_{\mu\nu}\Box R\right]. \end{aligned} \tag{2.37}$$

Substituting Eq. (2.32) into Eq. (2.22), and performing the asymptotic expansion of the dilaton field (2.29), we obtain the expectation value of the dual scalar operator at the boundary QFT

$$\boxed{\langle\mathcal{O}_\phi\rangle = -\frac{1}{\kappa_5^2}\phi_{(0)}.} \tag{2.38}$$

By the same token, if we substitute Eq. (2.35) into Eq. (2.31), expand the resulting equation near the boundary and take the limit $\rho \to 0$, we obtain the renormalized expectation value of the $U(1)$ R-current,

$$\langle J^\mu\rangle = \frac{1}{\kappa_5^2}\left(A^\mu_{(2)} + A^\mu_{(2,1)}\right). \tag{2.39}$$

Moreover, the leading order solution of Maxwell's equations (3.9) under the expansion (2.27)—(2.29) give us a relation between $A_{(2,1)\mu}$ and $A_{(0)\mu}$, i.e.

$$A_{(2,1)\mu} = \frac{f(0)}{4}\nabla_\nu F_{(0)\mu}{}^{\nu}, \tag{2.40}$$

which leads us to the final form the $U(1)$ R-current,

$$\boxed{\langle J_\mu\rangle = \frac{1}{\kappa_5^2}\left(A_{(2)\mu} + \frac{f(0)}{4}\nabla_\nu F_{(0)\mu}{}^{\nu}\right).} \tag{2.41}$$

Notice, however, that the last term of the equation above is absent in the 1RCBH background since $\partial_\mu A_{(0)\nu} = 0$.

Regarding the one-point function $\langle T_{\mu\nu}\rangle$, the algebra is a little bit more complicated. Thus, in order to simplify the analysis, we will only focus on the finite contributions of

Eq. (2.30)[11]. The finite terms coming from $T^{reg}_{\mu\nu}$ are

$$-\frac{\kappa_5^2}{\rho}T^{reg}_{\mu\nu} = -5\gamma_{(4)\mu\nu} - \gamma_{(4,1)\mu\nu} + \gamma_{(2)\mu\nu}\gamma^{\ \sigma}_{(2)\sigma} + \gamma_{(0)\mu\nu}(2\gamma^{\ \sigma}_{(4)\sigma} + \gamma^{\ \sigma}_{(4,1)\sigma} - \gamma_{(2)\sigma\lambda}\gamma^{\sigma\lambda}_{(2)}) + \text{divergent terms} + \text{vanishing terms as } \rho \to 0. \tag{2.42}$$

On the other hand, $T^{ct}_{\mu\nu}$ also contributes to the finite part of the total stress-energy tensor, i.e.

$$\begin{aligned}-\frac{\kappa_5^2}{\rho}T^{ct}_{\mu\nu} = {} & 3\gamma_{(4)\mu\nu} + \frac{1}{4}\gamma_{(2)\mu\nu}R_{(0)} + \frac{1}{4}\gamma^{\mu\sigma}_{(2)}R_{(0)\mu\sigma\nu\lambda} + \frac{1}{4}\nabla_\nu\nabla_\mu\gamma^{\sigma}_{(2)\sigma} - \frac{1}{4}\nabla_\nu\nabla_\sigma\gamma^{\sigma}_{(2)\nu} \\ & - \frac{1}{4}\nabla_\sigma\nabla_\mu\gamma^{\sigma}_{(2)\nu} + \frac{1}{4}\Box_{(0)}\gamma_{(2)\mu\nu} + \frac{1}{4}\gamma_{(0)\mu\nu}\Big(-R^{\sigma\lambda}_{(0)}\gamma_{(2)\sigma\lambda} + 4\phi^2_{(0)} + 8\phi_{(0)}\phi_{(0,1)} \\ & + \nabla_\sigma\nabla_\lambda\gamma^{\sigma\lambda}_{(2)} - \Box_{(0)}\gamma^{\sigma}_{(2)\sigma}\Big) + \text{divergent terms} + \text{vanishing terms as } \rho \to 0.\end{aligned} \tag{2.43}$$

Hence, the counterterms impact the finite result for the one-point functions, even though their original purpose was to eliminate the divergences of the on-shell action.

Proceeding with the tensorial algebra to obtain the one-point function of the stress-energy tensor, the next step is to sum Eq. (2.42) with Eq. (2.43), i.e.

$$\begin{aligned}-\kappa_5^2\langle T_{\mu\nu}\rangle = {} & -2\gamma_{(4)\mu\nu} - \gamma_{(4,1)\mu\nu} + \gamma_{(2)\mu\nu}\gamma^{\ \sigma}_{(2)\sigma} + \frac{1}{4}\gamma_{(2)\mu\nu}R_{(0)} + \frac{1}{4}\gamma^{\mu\sigma}_{(2)}R_{(0)\mu\sigma\nu\lambda} \\ & + \frac{1}{4}\nabla_\nu\nabla_\mu\gamma^{\sigma}_{(2)\sigma} - \frac{1}{4}\nabla_\nu\nabla_\sigma\gamma^{\sigma}_{(2)\nu} - \frac{1}{4}\nabla_\sigma\nabla_\mu\gamma^{\sigma}_{(2)\nu} + \frac{1}{4}\Box_{(0)}\gamma_{(2)\mu\nu} \\ & + \frac{1}{4}\gamma_{(0)\mu\nu}\Big(8\gamma^{\ \sigma}_{(4)\sigma} + 4\gamma^{\ \sigma}_{(4,1)\sigma} - 4\gamma_{(2)\sigma\lambda}\gamma^{\sigma\lambda}_{(2)} - R^{\sigma\lambda}_{(0)}\gamma_{(2)\sigma\lambda} + 2\phi^2_{(0)} + 4\phi_{(0)}\phi_{(0,1)} \\ & + \nabla_\sigma\nabla_\lambda\gamma^{\sigma\lambda}_{(2)} - \Box_{(0)}\gamma^{\sigma}_{(2)\sigma}\Big).\end{aligned} \tag{2.44}$$

Now we are close to give the full expression for $\langle T_{\mu\nu}\rangle$. The final step consists in expressing the coefficients of the metric expansion, such as $\gamma_{(2)}$, in terms of the curvature tensors of the boundary metric $\gamma_{(0)\mu\nu}$. This step, though, requires more laborious algebra, and more definitions are needed in order to do it in an simple way.

A convenient way to expand the EMD equations of motion using the FG coordinates is to use the ADM decomposition of general relativity [172, 173] in which one considers spacelike foliations keeping $\rho =$ constant at each foliation. We suggest at this point Ref. [170] for a more complete discussion about this subject. Using the ADM decomposition, from where the Gauss-Codazzi equations are derived, the $(\mu\nu)$-components of Einstein's

[11] Since all the divergences are mutually canceled out by taking into account the counterterms.

equations become

$$0 = 2\rho^2\partial_\rho^2\gamma_{\mu\nu} + \rho^2\gamma^{\sigma\lambda}(\partial_\rho\gamma_{\mu\sigma})(\partial_\rho\gamma_{\nu\lambda}) - 2\rho^2\gamma^{\sigma\lambda}(\partial_\rho\gamma_{\sigma\lambda})(\partial_\rho\gamma_{\mu\nu}) - R_{\mu\nu} + \frac{1}{2}\partial_\mu\phi\partial_\nu\phi + \frac{1}{3}\gamma_{\mu\nu}V(\phi) + 2\rho^2 f(\phi)(\partial_\rho A_\mu)(\partial_\rho A_\nu) - \frac{1}{12}f(\phi)F_{\sigma\lambda}F^{\sigma\lambda}\gamma_{\mu\nu} + \frac{1}{2}f(\phi)F_{\mu\sigma}F_\nu{}^\sigma - \frac{2}{3}f(\phi)\gamma_{\mu\nu}\gamma^{\sigma\lambda}(\partial_\rho A_\sigma)(\partial_\rho A_\lambda). \tag{2.45}$$

One can now expand the above equation near the boundary using Eqs. (2.27)—(2.29), obtaining

$$\gamma_{(2)\mu\nu} = \frac{1}{12}\left(\gamma_{(0)\mu\nu}R_{(0)} - 6R_{(0)\mu\nu}\right), \tag{2.46}$$

$$\gamma_{(2,1)\mu\nu} = 0, \tag{2.47}$$

$$\gamma_{(4,2)\mu\nu} = -\frac{1}{12}\phi_{(0,1)}^2\gamma_{(0)\mu\nu}, \tag{2.48}$$

$$\gamma_{(4,1)\mu\nu} = -\frac{1}{8}f(0)F_{(0)\mu\sigma}F_{(0)\nu}{}^\sigma + \frac{1}{8}R_{(0)}^{\sigma\lambda}R_{(0)\mu\sigma\nu\lambda} - \frac{1}{24}R_{(0)\mu\nu}R_{(0)} + \frac{1}{16}\Box_{(0)}R_{(0)\mu\nu} - \frac{1}{48}\nabla_\mu\nabla_\nu R_{(0)} + \gamma_{(0)\mu\nu}\left[\frac{1}{32}f(0)F_{(0)\sigma\lambda}F_{(0)}^{\sigma\lambda} - \frac{1}{32}R_{(0)\sigma\lambda}R_{(0)}^{\sigma\lambda} + \frac{1}{96}R_{(0)}^2 - \frac{\phi_{(0)}\phi_{(0,1)}}{6} - \frac{1}{96}\Box_{(0)}R_{(0)}\right], \tag{2.49}$$

$$\gamma_{(4)\mu}^{\ \ \mu} = \frac{1}{48}f(0)F_{(0)\mu\nu}F_{(0)}^{\mu\nu} + \frac{1}{16}R_{(0)\mu\nu}R^{(0)\mu\nu} - \frac{R_{(0)}^2}{72} - \frac{2}{6}\phi_{(0)}^2 - \frac{1}{6}\phi_{(0,1)}^2. \tag{2.50}$$

Finally, by substituting Eqs. (2.46)—(2.50) into Eq. (2.44), we obtain the expectation value of the stress-energy tensor of the dual QFT

$$\kappa_5^2\langle T_{\mu\nu}\rangle = 2\gamma_{(4)\mu\nu} - \frac{1}{4}\left(R_{(0)\mu}^{\sigma}R_{(0)\sigma\nu} - \frac{3}{2}R_{(0)}^{\sigma\lambda}R_{(0)\mu\sigma\nu\lambda} + \frac{1}{4}\nabla_\mu\nabla_\nu R_{(0)} - \frac{3}{4}\Box_{(0)}R_{(0)\mu\nu}\right) + \frac{1}{8}f(0)F_{(0)\mu\sigma}F_{(0)\nu}{}^\sigma - \frac{\gamma_{(0)\mu\nu}}{2}\left(\frac{f(0)}{48}F_{(0)\sigma\lambda}F_{(0)}^{\sigma\lambda} - \frac{\phi_{(0)}^2}{3} + \phi_{(0)}\phi_{(0,1)} - \frac{2\phi_{(0,1)}^2}{3}\right) - \frac{1}{32}\gamma_{(0)\mu\nu}\left(R_{(0)\sigma\lambda}R_{(0)}^{\sigma\lambda} + \frac{1}{9}R_{(0)}^2 - \Box_{(0)}R_{(0)}\right), \tag{2.51}$$

which is valid for any five dimensional EMD theory with a bulk scalar field with dimension $\Delta = 2$ and for any kind of boundary.

Specializing the above results for the 1RCBH background will vastly simplify the expression for $\langle T_{\mu\nu}\rangle$. First, the conformal boundary of such theory is flat (i.e., Minkowski), which means that all the curvature tensors are identically zero. Second, if one takes the

trace of Eq. (2.51), the resulting expression reads

$$\kappa_5^2\langle T^{\mu}_{\ \mu}\rangle = -2\phi_{(0)}\phi_{(0,1)} + \phi_{(0,1)}^2 - \frac{1}{8}\left(R_{(0)\mu\nu}R^{\mu\nu}_{(0)} - \frac{1}{3}R^2_{(0)}\right) - \frac{f(0)}{8}F_{(0)\mu\nu}F^{\mu\nu}_{(0)}. \tag{2.52}$$

Hence, one arrives at a very important result: *in a conformal EMD model with* $\Delta = 2$ *the logarithmic terms on the near-boundary expansions of the bulk fields are absent.* This sentence justifies the assumption made in Sec. 3.2 when we set to zero the logarithmic terms of the near-boundary asymptotic expansions. Furthermore, we remark that the finite counterterm contribution (2.24) does not modify the trace anomaly of the theory.

From the previous discussion, the stress-energy tensor for the 1RCBH model reads,

$$\boxed{\langle T_{\mu\nu}\rangle = \frac{1}{\kappa_5^2}\left[2\gamma_{(4)\mu\nu} + \frac{1}{8}f(0)F_{(0)\mu\sigma}F_{(0)\nu}{}^{\sigma} - \gamma_{(0)\mu\nu}\left(\frac{f(0)}{96}F_{(0)\sigma\lambda}F^{\sigma\lambda}_{(0)} - \frac{\phi^2_{(0)}}{6}\right)\right],} \tag{2.53}$$

which is the one-point function adopted throughout this work. We remark once more that, due to the fact $\partial_\mu A_{(0)\nu} = 0$ in our setup, the Maxwell terms in Eq. (2.53) will vanish.

A minimal internal consistency check of the above results may be done by looking at the trace Ward Identity [170, 174], i.e.

$$\langle T^{\mu}_{\ \mu}\rangle - (4-\Delta)\phi_{(0,1)}\langle \mathcal{O}_\phi\rangle = \mathcal{A}, \tag{2.54}$$

where $\mathcal{A}$ denotes the trace anomaly of the theory. For the specific case of the EMD theory with $\Delta = 2$, the anomaly is given by

$$\mathcal{A} = \mathcal{A}_{gravity} + \mathcal{A}_{Maxwell} + \mathcal{A}_{dilaton}, \tag{2.55}$$

where,

$$\mathcal{A}_{gravity} = \frac{1}{8}\left(R_{(0)\mu\nu}R^{\mu\nu}_{(0)} - \frac{1}{3}R^2_{(0)}\right), \quad \mathcal{A}_{Maxwell} = -\frac{f(0)}{8}F_{(0)\mu\nu}F^{\mu\nu}_{(0)}, \quad \mathcal{A}_{dilaton} = \phi^2_{(0,1)}. \tag{2.56}$$

Chapter 3

Homogeneous isotropization and equilibration of a strongly coupled plasma with a critical point

This chapter initiates some novel applications of the gauge/gravity duality (see Chapter 2) in the calculation of observables in strongly coupled non-Abelian plasmas, such as the QGP described in Chapter 1. More specifically, this chapter is concerned with the homogeneous isotropization and equilibration of a strongly coupled plasma with a critical point. This chapter is based on Ref. [137].

.

With the advent of the holographic gauge/gravity duality [54, 113–115], it has become possible to study physical properties of some strongly coupled quantum systems using classical gravity in higher dimensions (for reviews see, e.g., [57, 147, 175]). Concerning strongly correlated quantum fluids, this framework has made it possible the investigation of several aspects of such systems, such as their thermodynamics and hydrodynamics [56, 176, 177], quasinormal modes [178–180], and also the far-from-equilibrium dynamics describing the relaxation of holographic fluids toward thermodynamic equilibrium in many different settings (see e.g. [59, 181] for recent reviews).

One of the main attractive features of holography is its unique ability to deal with the entire evolution of a strongly coupled fluid within a single framework, starting from far-from-equilibrium anisotropic initial states and dynamically evolving them passing through different stages comprising several kinds of characteristic "relaxation times" until reaching thermodynamic equilibrium. These different relaxation times characterize, for instance, the onset of applicability of hydrodynamics (known as the "hydrodynamization time", which also depends on the specific formulation of hydrodynamics considered), the onset of nearly isotropization of the system (when the longitudinal and transverse pressures

in a given flow are approximately equal), the onset of applicability of the equilibrium equation of state in nonconformal plasmas (known as the "EoSization time" [182]), and the onset of true thermalization (when all the physical observables of the theory have approximately relaxed to their equilibrium values). In fact, one of the main outcomes of holographic investigations of far-from-equilibrium strongly coupled quantum fluids was the conclusion that in some cases the system may hydrodynamize when the fluid is still significantly anisotropic and far-from-equilibrium [95,183–185]. This finding, together with recent calculations [180, 186–188] that showed that the gradient expansion diverges, have significantly changed our understanding of relativistic hydrodynamics (for a review see [97]).

The fast expanding fireball produced in ultrarelativistic heavy ion collisions at RHIC [38–41] and LHC [189] is probably the most remarkable example of a dynamical system actually realized in nature featuring a very rich and complex time evolution characterized by both hard (i.e., perturbative) and soft (nonperturbative) physics. Just before the heavy ions collide, the gluon density inside these large nuclei at very high energies is expected to saturate producing the so-called color glass condensate (CGC) [91, 190–192], which has become the starting point for the initial conditions in heavy ion collisions. Right after the collision the medium has an enormous amount of energy concentrated in a very small volume, which starts to rapidly expand passing through different stages. Before 1 fm/c after the collision the system is expected to be a highly dense coherent medium dominated by the dynamics of classical QCD fields called glasma [193]. As the system keeps expanding, the glasma decoheres towards a new state of QCD matter called the quark-gluon plasma (QGP) [85, 194, 195], whose relevant degrees of freedom correspond to deconfined quarks and gluons.

In practice, the QGP produced in heavy ion collisions is well described by viscous hydrodynamics with an equilibrium equation of state and transport coefficients which are compatible with soft physics expectations [102, 196–198], indicating that at this stage the system is strongly coupled, contrary to the scenario just after the collision where weak coupling physics plays a prominent role. As the QGP keeps expanding and cooling down it eventually enters in the crossover region [199, 200] and hadronizes, giving place to a hadron gas. Later stages of the temporal evolution of heavy ion collisions include the regions of chemical freeze-out[1] and the thermal or kinetic freeze-out[2]. After this stage, the produced hadrons are essentially free and the yields of their decays reach the detectors of the experimental apparatus providing a large amount of information about the evolution

[1]When inelastic collisions between the produced hadrons cease and the relative ratio between the different kinds of particles remains fixed.

[2]When the average distance between the hadrons is large enough to make the nuclear interaction between them effectively negligible, causing the momentum distribution of the particles to remain fixed.

of the system.

The full dynamical evolution of high energy heavy ion collisions outlined above cannot be completely described by the gauge/gravity duality since the former encompasses both hard and soft physics while the latter can only deal with strongly coupled systems. In fact, it is well-known that the asymptotically free ultraviolet regime of QCD cannot be described by the gauge/gravity duality given that holographic models are usually characterized by strongly coupled ultraviolet fixed points. On the other hand, even though a rigorous top-down construction of a gravity dual of the hydrodynamized and strongly coupled QGP is missing, there are phenomenological bottom-up EMD gauge/gravity constructions which have been shown to successfully describe in practice, not only on a qualitative level but also quantitatively, a plethora of thermodynamical and hydrodynamical observables characterizing the physics of the strongly coupled QGP under many different situations [68, 70, 119–122, 201–207]. Therefore, one striking question which is posed in face of the above considerations is the following: in which cases could one hope, at least in principle, to obtain possible useful insights (or even some quantitatively accurate results) for the far-from-equilibrium dynamics of heavy ion collisions using holographic techniques?

The answer to the question above is still unsettled but one may gauge the applicability of gauge/gravity models to the analysis of heavy ion collisions by looking at some recent results comparing lattice QCD calculations (which are performed in equilibrium) with heavy ion experimental data. This kind of comparison may help to identify under which conditions the expanding fireball would probe, through more stages, a strongly coupled regime of QCD.

For instance, in Ref. [198] it was shown that in central heavy ion collisions at RHIC and LHC the experimentally extracted ratio between the pressure and the internal energy density of the QGP, $(p/\epsilon)_{\rm exp}(T_{\rm eff}) = 0.21 \pm 0.10$, is in good agreement with the corresponding lattice QCD estimate, $(p/\epsilon)_{\rm lQCD}(T_{\rm eff}) \approx 0.23$, where $T_{\rm eff}$ is half-way between the effective temperatures associated with the collision energies $\sqrt{s} = 200$ GeV and $\sqrt{s} = 2.76$ TeV (at these high energies, the baryon chemical potential is negligible compared to the temperature of the medium). Moreover, in Ref. [197] a state-of-the-art Bayesian analysis was simultaneously applied to several physical observables while varying the free parameters of the model. The results in the space of parameters of the model which match combined heavy ion data measured at RHIC and LHC within the interval $\sqrt{s} = 200$ GeV — 2.76 TeV were also found to be consistent with results from lattice QCD simulations. These findings show that the QGP produced in these collisions at high energies is not only adequately described by hydrodynamics but also that the (equilibrium) QCD equation of state obtained in lattice simulations may be trustfully used in hydrodynamic simulations

of the spacetime evolution of the system at these high energies (i.e., $\sqrt{s} \gtrsim 200$ GeV).

Furthermore, it was also shown in Refs. [208, 209] that ratios between higher order susceptibilities of baryon and electric charges calculated in equilibrium on the lattice give a good description of experimentally measured ratios between moments of net-proton and net-electric charge multiplicity distributions for collision energies $\sqrt{s} \geq 39$ GeV; however, for $\sqrt{s} < 39$ GeV the compatibility observed at higher energies between the set of chemical freeze-out parameters extracted from the independent analysis performed in the baryon and electric charge sectors on the lattice is not warranted [209]. This suggests that at chemical freeze-out the system produced in heavy ion collisions is less close to equilibrium if the system has a higher chemical potential (corresponding to a lower collision energy).

Recently, using a phenomenological holographic EMD model which quantitatively reproduces lattice QCD thermodynamics at zero and nonzero baryon chemical potential [204, 207], it was found that an increase in the baryon chemical potential decreases the shear viscosity times temperature to enthalpy density ratio, $\eta T/(\epsilon + p)$, which gives a measure of the fluidity of the medium [210][3]. This indicates that the QGP at finite baryon density remains strongly coupled. From the above considerations, one may expect that the gauge/gravity duality is more likely to produce useful insights for the far-from-equilibrium dynamics of heavy ion collisions when the system is doped with a nonzero chemical potential[4]. This is exactly the scenario we are interested in analyzing in the present chapter.

The literature regarding out-of-equilibrium holographic dynamics is vast, and even if we restrict ourselves to works that deal with models endowed with a chemical potential there is a substantial amount of papers already available. For non-equilibrium aspects of some strongly coupled plasmas doped with a chemical potential which do not employ numerical relativity and probe the thermalization process using non-local observables (e.g. Wilson's loops), see e.g. Refs. [212–215]. In the far-from-equilibrium context, there is the study of Ref. [168] regarding homogeneous equilibration in a charged plasma without a critical point, while Ref. [211] considers a shock wave analysis with baryon charge, yet without a critical point. One can also study quantum critical points in the context of holographic quenches, as done in Refs. [216, 217]. Recent studies about holographic isotropization in the context of Gauss-Bonnet gravity can be found in Ref. [218].

[3] At zero density this ratio reduces to η/s.

[4] This is so because, as discussed before, there are indications that the baryon dense QGP experiences relevant far-from-equilibrium effects while remaining strongly coupled through more stages than in the case of higher energy collisions (where the chemical potential is negligible). In fact, this may provide a partial explanation for the findings of Ref. [211] where a qualitative agreement between the rapidity distribution of baryon charge in a holographic shock wave analysis at finite density and in heavy ion collisions at moderate and low energies was found to disappear at full RHIC or LHC energies (i.e., $\sqrt{s} \gtrsim 200$ GeV).

One of the main goals of the present chapter is to assess the impact of a critical point in the far-from-equilibrium dynamics of a relativistic strongly coupled plasma at finite density, which to the best of our knowledge is a question that has not been previously studied in the literature. In fact, this is the simplest problem one may consider that can lead to interesting insights into the strongly coupled dynamics of the QGP near a critical point at finite density, one of the focus of RHIC's Beam Energy Scan (BES) program. Even though the holographic model we consider here is very different from QCD, we believe such a study is important given that there are no other approaches that can be used to perform real-time, far-from-equilibrium calculations at strong coupling near a critical point.

More specifically, we shall investigate here the homogeneous equilibration dynamics of a far-from-equilibrium top-down holographic plasma at finite density known as the 1RCBH [138–143]. This model describes a strongly coupled conformal $\mathcal{N} = 4$ Super Yang-Mills (SYM) plasma charged under a $U(1)$ subgroup of the global $SU(4)$ R-symmetry and features a critical point (CP)[5] in its phase diagram. Our gravitational setup is different from the one considered in Ref. [168] where the authors studied the homogeneous equilibration of a strongly coupled SYM plasma with a nonzero charge density without a CP. Indeed, as we are going to see in a moment, the action of the 1RCBH model includes a dilaton field that considerably changes the dynamics of the theory and leads to a CP in its phase diagram.

In order to solve the corresponding numerical relativity problem, in this chapter we follow the pioneering work of Chesler and Yaffe [219] by employing the so-called characteristic formulation of general relativity [220], which is very convenient for asymptotically AdS spacetimes (see, e.g., Ref. [59] for a review). Alternatively, one may also use the ADM formulation [172, 173] of numerical relativity in asymptotically AdS spacetimes, as done in Refs. [221, 222].

An important remark must be done at this point. As it is well-known, the thermodynamics and the hydrodynamics of the SYM plasma are very different than what is observed in the QGP produced in heavy ion collisions (see, e.g., [223]). Thus, one should not expect to obtain, in general, quantitative insights for the early time dynamics of heavy ion collisions from the study of the far-from-equilibrium dynamics of the 1RCBH model. However, it may be that some qualitative properties derived in the far-from-equilibrium dynamics of this model are robust or "nearly universal", as it happens with the shear viscosity to entropy density ratio of holographic fluids where $\eta/s = 1/4\pi$ for a broad class of strongly coupled systems [56]. In order to look for possible signatures of this kind

[5]Since the 1RCBH does not have a first order phase transition line, we refer to the critical point of this model as CP instead of CEP.

of "universality", one should also consider the far-from-equilibrium dynamics in other holographic models at finite density endowed with a CP.

For instance, QNM oscillations of the 1RCBH model in the external scalar and vector diffusion channels were found in the Appendix A [146] to be damped as one increases the $U(1)$ R-charge chemical potential, as long as one is away from criticality. This finding is in qualitative accordance with the observation done in Ref. [204] that by increasing the baryon chemical potential far from the CP there is a damping in the QNM oscillations of the external scalar channel of a phenomenological bottom-up EMD model at finite baryon density that quantitatively describes QGP thermodynamics. This damping of the QNM oscillations caused by increasing the chemical potential away from criticality in two very different holographic models may be a signature of robustness or an indication of a general behavior for strongly coupled systems at finite density.

Therefore, even though the 1RCBH model (and the SYM plasma in general) is not a holographic setup suited for direct applications to heavy ion phenomenology, it may potentially contain some general properties displayed by strongly coupled fluids driven out-of-equilibrium. Moreover, one of the main conclusions of the present work will be the distinction of two characteristic equilibration times of the far-from-equilibrium system. Namely, by looking at the imaginary part of the lowest non-hydrodynamic QNM's of the model one may extract an upper bound for some characteristic "relaxation times" of the theory, according to the general reasoning first devised in Ref. [178]. The aforementioned behavior of the QNM's in the external scalar and vector diffusion channels would, therefore, suggest that the "equilibration time" of the 1RCBH model decreases with increasing chemical potential far from the CP, while close to the CP it would instead increase. As we shall see in this work, this is, in fact, the behavior found for the *isotropization* time of the system, which is dominated by the lowest non-hydrodynamic QNM of the external scalar channel of the theory.

On the other hand, even after (nearly) isotropization is reached, the scalar condensate dual to the bulk dilaton field may still be significantly far from its equilibrium value. Since in the present work the equilibration of the scalar condensate will always be the last equilibration time of the system, we shall associate it with the true thermalization time of the medium. Contrary to the isotropization time, in this model the thermalization time always increase with increasing chemical potential. As we are going to show, this is in consonance with the behavior of the lowest non-hydrodynamic QNM of the dilaton channel. Also, it would be interesting to extend the present analysis to consider the case of the QCD-like EMD model of Ref. [70], which provided a prediction for the location of the long-sought critical point of the QCD phase diagram in the plane of temperature and baryon chemical potential.

The outline of this chapter is as follows. In Sec. 3.1 we present the equations of motion for the 1RCBH model assuming a time-dependent and spatially homogeneous anisotropic Ansatz for the bulk fields. This gives a set of nonlinear partial differential equations (PDEs) to be solved numerically. We also discuss the relevant observables of the dual quantum field theory (QFT) that we need to compute to analyze the homogeneous isotropization and thermalization processes in this setup, namely, the one-point functions associated with the expectation value of the boundary stress-energy tensor, $\langle T_{\mu\nu}\rangle$, dual to the bulk metric field $g^{\mu\nu}$, the scalar condensate, $\langle \mathcal{O}_\phi\rangle$, dual to the bulk dilaton field ϕ, and the expectation value of the conserved $U(1)$ R-current, $\langle J_\mu\rangle$, dual to the bulk Maxwell field A^μ. The derivation of the general form of these one-point functions via holographic renormalization were presented in Sec. 2.3. In Sec. 3.2 we perform the near-boundary asymptotic expansion of the bulk fields in order to fix the boundary conditions for the set of PDEs. From this near-boundary analysis, we will be left with a couple of unknown time-dependent ultraviolet coefficients that shall be related with the one-point functions of the dual QFT. In Sec. 3.3, we briefly review the analytical equilibrium solutions of the 1RCBH model and its thermodynamics. In Sec. 3.4, we discuss some relevant technical issues related to the numerical time-dependent far-from-equilibrium solutions of the 1RCBH model, such as the choice of the initial conditions, and explain how we numerically solve the set of coupled nonlinear PDEs for the far-from-equilibrium system. Once the numerics is settled, we proceed in Sec. 3.5 to provide the main results of the homogeneous equilibration dynamics of the 1RCBH model. Moreover, in Subsection 3.5.7 we perform the match of the late time behavior of the pressure anisotropy and the scalar condensate with the lowest non-hydrodynamic QNM's of the external scalar and dilaton channels, respectively. The details regarding the QNM's are treated in the Appendix A. Finally, we close the work in Sec. 3.6 with an outlook of our main results and also point out future perspectives and ongoing investigations.

3.1 The holographic model and its equations of motion

The 1RCBH model [138–143] first appeared as a solution of the five dimensional $\mathcal{N}=8$ gauged supergravity action [139], which was later demonstrated to lie within a class of solutions equivalent to near-extremal spinning D3-branes in $AdS_5\times S^5$ [142]. The Kaluza-Klein compactification of the five sphere S^5 on the spinning D3-branes solutions leads to the $SU(4)$ R-symmetry and the three independent Cartan subgroups of the R-Symmetry $U(1)_a\times U(1)_b\times U(1)_c$ are associated with three distinct conserved charges (Q_a, Q_b, Q_c) of the black hole background [139]. The general solution is known as the STU model,

whilst the 1RCBH model is obtained by considering only one charge, i.e., $Q \equiv Q_a$ and $Q_b = Q_c = 0$. A thorough discussion of the matter content of the dual QFT at zero temperature may be found in Ref. [224]. For the thermal plasma at finite density, detailed discussions may be found in Refs. [146, 203]. For the sake of completeness, in the present chapter we briefly review the thermodynamics of the 1RCBH plasma in Sec. 3.3.1.

The gravitational action of the 1RCBH model is given by [138–143],

$$S = \frac{1}{2\kappa_5^2}\int_{\mathcal{M}} d^5x\sqrt{-g}\left[R - \frac{f(\phi)}{4}F_{MN}F^{MN} - \frac{1}{2}(\partial_M\phi)^2 - V(\phi)\right] + S_{GHY} + S_{ct}, \tag{3.1}$$

where

$$S_{GHY} = \frac{1}{\kappa_5^2}\int_{\partial\mathcal{M}} d^4x\sqrt{-\gamma}K \tag{3.2}$$

is the Gibbons-Hawking-York boundary action [225, 226] needed to provide a well-posed Dirichlet problem. In this term, $\gamma_{\mu\nu}$ denotes the induced metric at the boundary and K represents its extrinsic curvature. The last term in Eq. (3.1) is the boundary counterterm action needed to remove the divergences of the on-shell action. In Sec. 2.3 we gave the details regarding the boundary terms and showed how to obtain the desired one-point functions of the dual QFT.

The expressions for the dilaton potential $V(\phi)$ and the Maxwell-Dilaton coupling $f(\phi)$ in the action (3.1), which define the top-down construction corresponding to the 1RCBH model, are given by

$$V(\phi) = -\frac{1}{L^2}\left(8e^{\frac{\phi}{\sqrt{6}}} + 4e^{-\sqrt{\frac{2}{3}}\phi}\right), \quad f(\phi) = e^{-2\sqrt{\frac{2}{3}}\phi}, \tag{3.3}$$

with the AdS radius L being set to unity henceforth for simplicity. Moreover, by Taylor expanding the dilaton potential in powers of ϕ close to the boundary, we obtain

$$V(\phi) = -12 - 2\phi^2 + \mathcal{O}(\phi^4), \tag{3.4}$$

which tells us that the mass of the dilaton is given by $m^2 = -4$. Recalling that the relation between the mass of the dilaton and the scaling dimension of its dual operator in the boundary QFT is given by $m^2 = \Delta(\Delta - 4)$, one concludes that $\Delta = 2$ (as stated in Sec. 2.3). Note also that the dilaton field vanishes at the boundary such that the bulk geometry is asymptotically AdS_5.

Einstein's equations are obtained from the variation of the EMD action with respect to the metric,

$$R_{MN} - \frac{1}{2}g_{MN}R = \kappa_5^2 T_{MN}, \tag{3.5}$$

where,

$$T_{MN} = \frac{1}{\kappa_5^2}\left[\frac{1}{2}\partial_M\phi\partial_N\phi + \frac{f(\phi)}{2}F_{MP}F_N{}^P - \frac{g_{MN}}{2}\left(\frac{1}{2}(\partial_P\phi)^2 + V(\phi) + \frac{f(\phi)}{4}F_{PQ}F^{PQ}\right)\right], \tag{3.6}$$

is the stress-energy tensor of the matter fields A_μ and ϕ. It is usually simpler to work with the "trace-reversed" form of Einstein's equations.[6] This may be derived by noting that Eq. (3.5) implies that

$$R_{MN} = \kappa_5^2\left(T_{MN} - \frac{1}{2}g_{MN}T^Q_Q\right). \tag{3.7}$$

By substituting Eq. (3.6) into Eq. (3.7), one rewrites Einstein's equations as follows

$$R_{MN} - \frac{g_{MN}}{3}\left[V(\phi) - \frac{f(\phi)}{4}F_{PQ}F^{PQ}\right] - \frac{1}{2}\partial_M\phi\partial_N\phi - \frac{f(\phi)}{2}F_{MP}F_N{}^P = 0. \tag{3.8}$$

On the other hand, Maxwell's equations are obtained by varying the EMD action with respect to the Maxwell field

$$\nabla_M\left(f(\phi)F^{MN}\right) = 0. \tag{3.9}$$

The last equation that one needs to fully specify the dynamics of the model is the Klein-Gordon equation for the dilaton field

$$\nabla^2\phi - \frac{\partial V}{\partial\phi} - \frac{F_{PQ}F^{PQ}}{4}\frac{\partial f}{\partial\phi} = \frac{1}{\sqrt{-g}}\partial_M\left(\sqrt{-g}g^{MN}\partial_N\phi\right) - \partial_\phi V - \frac{F_{PQ}F^{PQ}}{4}\partial_\phi f = 0. \tag{3.10}$$

To explore the far-from-equilibrium solutions of the model, we adopt the well-known characteristic formulation for asymptotically AdS spacetimes [219]. We consider here a time-dependent and spatially homogeneous anisotropic Ansatz for the metric field, which is suited to study homogeneous isotropization dynamics, in which one starts with an anisotropic configuration and an energy density that is conserved as time evolves. We work with generalized infalling Eddington-Finkelstein (EF) coordinates, in terms of which one may write the Ansatz for the line element as follows [219],

$$ds^2 = 2dv\left[dr - A(v,r)dv\right] + \Sigma(v,r)^2\left[e^{B(v,r)}(dx^2+dy^2) + e^{-2B(v,r)}dz^2\right], \tag{3.11}$$

where v represents the EF time, which near the boundary is interpreted as the time of

[6] The tensorial algebra using a specific chart in this work is done with the help of the Mathematica package "Riemann Geometry and Tensor Calculus" (RGTC) [227].

the dual QFT. To see this, recall that the EF time is defined via

$$dv = dt + \sqrt{-\frac{g_{rr}}{g_{tt}}}dr, \tag{3.12}$$

where g_{rr} and g_{tt} are the radial and temporal diagonal components of an asymptotically AdS_5 metric. Thus, as one goes to the boundary located at $r \to \infty$, one obtains $v \to t$. We also remark that in these generalized infalling EF coordinates, infalling radial null geodesics satisfy $v =$ constant, while outgoing radial null geodesics satisfy $dr/dv = A(v,r)$ [219][7]. Furthermore, there is a residual diffeomorphism invariance in Eq. (3.11) corresponding to the radial shift $r \mapsto r + \lambda(v)$, where $\lambda(v)$ is an arbitrary function of the EF time [59].

With respect to the Maxwell and dilaton fields, the Ansätze are

$$A = \Phi(v,r)dv, \qquad \phi = \phi(v,r). \tag{3.13}$$

The $U(1)$ R-charge chemical potential is associated with the boundary value of the Maxwell field $\Phi(v,r)$ in equilibrium, while the dilaton field vanishes at the boundary, as mentioned above.

The resulting equations of motion for the EMD system, which are obtained by plugging the line element (3.11), the dilaton and gauge field profiles (3.13) into Eqs. (3.8)–(3.10), form a set of coupled nonlinear PDEs,

$$4\Sigma(d_+\phi)' + 6\phi' d_+\Sigma + 6\Sigma' d_+\phi + \Sigma\partial_\phi f\mathcal{E}^2 - 2\Sigma\partial_\phi V = 0, \tag{3.14a}$$

$$\frac{\partial_\phi f\phi'}{f} + \frac{3\Sigma'}{\Sigma} + \frac{\mathcal{E}'}{\mathcal{E}} = 0 \tag{3.14b}$$

$$A'' + \frac{1}{12}\left(18B' d_+B - \frac{72\Sigma' d_+\Sigma}{\Sigma^2} + 6\phi' d_+\phi - 7f\mathcal{E}^2 - 2V\right) = 0, \tag{3.14c}$$

$$(d_+\Sigma)' + \frac{2\Sigma'}{\Sigma}d_+\Sigma + \frac{1}{12}\Sigma\left(f\mathcal{E}^2 + 2V\right) = 0, \tag{3.14d}$$

$$\Sigma\,(d_+B)' + \frac{3\Sigma'}{2}d_+B + \frac{3d_+\Sigma}{2}B' = 0, \tag{3.14e}$$

$$\frac{1}{6}\Sigma\left(3\,(B')^2 + (\phi')^2\right) + \Sigma'' = 0, \tag{3.14f}$$

$$d_+(d_+\Sigma) - A'\,d_+\Sigma + A^2\Sigma'' + \frac{\Sigma}{6}\left(3A^2\,(B')^2 + A^2\,(\phi')^2 + 3(d_+B)^2 + (d_+\phi)^2\right) = 0, \tag{3.14g}$$

[7]Note that $A(v,r)$ here is half the corresponding metric function in the convention of Ref. [219].

where the prime denotes ∂_r, and

$$d_+ \equiv \partial_v + A(v,r)\partial_r, \tag{3.15}$$

defines the directional derivative along outgoing null vectors. Eq. (3.14a) is the dilaton equation, Eq. (3.14b) is the Maxwell equation, and Eqs. (3.14c)—(3.14g) are Einstein's equations[8]. As in Ref. [168], we also defined a bulk "electric field",

$$\mathcal{E} \equiv -\Phi'. \tag{3.16}$$

It is important to note that the Maxwell equation (3.14b) relates ϕ, Σ, and Φ', i.e.

$$\ln(\Sigma^3\mathcal{E}) - 2\sqrt{\frac{2}{3}}\phi = \text{constant}. \tag{3.17}$$

We will show in the next section how one can relate the above unknown constant to the $U(1)$ R-charge density ρ_c using results from holographic renormalization. Indeed, Eq. (3.17) expresses the existence of a Gauss charge coming from the Gauss law of classical electromagnetism.

We explain now the general algorithm to solve the system of PDEs (3.14a)—(3.14g):

1. Choose an initial profile for $B(v_0,r)$ and $\phi(v_0,r)$, where v_0 denotes the initial time;
2. Once $B(v_0,r)$ and $\phi(v_0,r)$ are given, one can solve Eq. (3.14f) to obtain $\Sigma(v_0,r)$. Using the constraint (3.17) we also determine $\mathcal{E}(v_0,r)$;
3. With $B(v_0,r)$, $\phi(v_0,r)$, $\Sigma(v_0,r)$, and $\mathcal{E}(v_0,r)$ at hand, we proceed to solve Eq. (3.14d) for $d_+\Sigma(v_0,r)$;
4. Next we solve Eq. (3.14e) for $d_+B(v_0,r)$;
5. Next we solve Eq. (3.14a) for $d_+\phi(v_0,r)$;
6. Next we solve Eq. (3.14c) for $A(v_0,r)$;
7. When $B(v_0,r)$, $d_+B(v_0,r)$, $\phi(v_0,r)$, $d_+\phi(v_0,r)$, and $A(v_0,r)$ are known, it is clear from the definition of d_+ in Eq. (3.15) that we also have $\partial_v B(v_0,r)$ and $\partial_v\phi(v_0,r)$. With $\{B(v_0,r),\partial_v B(v_0,r)\}$ and $\{\phi(v_0,r),\partial_v\phi(v_0,r)\}$ at hand we have now the initial conditions required to evolve in time $B(v_0)$ and $\phi(v_0,r)$ from v_0 to $v_0+\Delta v$;

[8]Eqs. (3.14f) and (3.14g) are constraints, whose derivatives are implied by the dynamical Eqs. (3.14c)—(3.14e). Therefore, there is in total five dynamical equations, (3.14a)—(3.14e), for five unknowns, $\{\phi,\Phi,A,\Sigma,B\}$.

8. Next we repeat the process to obtain the fields at the next instant $v_0 + \Delta v$.

9. The constraint (3.14g) is useful for checking the accuracy of the numerical solutions.

Before we delve into the numerics and solve the system of PDEs (3.14a)—(3.14g) following the above algorithm, there are still some technical details that we need to take into account. Some of these details are: the boundary conditions, the equilibrium solutions, and the initial data.

In order to fix the boundary conditions for the EMD fields we first need to perform a near-boundary expansion of the bulk fields. This expansion will reveal which ultraviolet coefficients need to be dynamically fixed. Such analysis is done in Sec. 3.2. The detailed knowledge of the equilibrium solutions, which are discussed in Sec. 3.3, is very important to determine the final state given some initial geometry. Moreover, it is only possible to predict the equilibrium state because in this homogeneous setup the energy and charge density are constant. Still in Sec. 3.3, using the formulas derived from holographic renormalization in Sec. 2.3, we provide holographic formulas to calculate the energy density and the pressure coming from $\langle T_{\mu\nu} \rangle$, the charge density that comes from the temporal component of $\langle J^\mu \rangle$, and the expectation value of the scalar operator dual to the dilaton field, $\langle \mathcal{O}_\phi \rangle$. In Sec. 3.4, we discuss different initial data and specify the numerical techniques that we shall employ to solve the equations of motion of the 1RCBH model. After that, we will be ready to present in Sec. 3.5 our results for the homogeneous isotropization and thermalization of the 1RCBH plasma, emphasizing in particular the dynamics near the critical point.

3.2 Near-boundary expansion of the bulk fields

In a five dimensional model where the dilaton field has scaling dimension $\Delta = 2$ the near-boundary expansions of the bulk fields are given by integer powers of the radial

coordinate plus logarithmic terms [167], i.e.

$$A(v,r) = \frac{1}{2}(r+\lambda(v))^2 - \partial_v\lambda(v) + \sum_{n=0,m=0,m<n}^{n,m=\infty} \frac{A_{n,m}(v)}{r^n}\ln^m r, \tag{3.18}$$

$$\Sigma(v,r) = r + \lambda(v) + \sum_{n=0,m=0,m<n}^{n,m=\infty} \frac{\Sigma_{n,m}(v)}{r^n}\ln^m r, \tag{3.19}$$

$$B(v,r) = \sum_{n=0,m=0,m<n}^{n,m=\infty} \frac{B_{n,m}(v)}{r^n}\ln^m r, \tag{3.20}$$

$$\phi(v,r) = \sum_{n=2,m=0,m<n}^{n,m=\infty} \frac{\phi_{n,m}(v)}{r^n}\ln^m r, \tag{3.21}$$

$$\Phi(v,r) = \sum_{n=0,m=0,m<n}^{n,m=\infty} \frac{\Phi_{n,m}(v)}{r^n}\ln^m r, \tag{3.22}$$

where $\lambda(v)$ is the radial shift function associated with the aforementioned residual diffeomorphism invariance of the bulk metric [59]. As we saw in Sec. 2.3, the logarithmic terms in the above expansions vanish due to three main facts: the conformal flatness of the boundary, the scaling dimension of the QFT scalar operator dual to the bulk dilaton field, and the conformal symmetry of the system. Therefore, we can already set the logarithmic corrections to zero. We adopt then the following notation

$$\{A_n,\, \Sigma_n,\, B_n,\, \phi_n,\, \Phi_n\} \equiv \{A_{n,0},\, \Sigma_{n,0},\, B_{n,0},\, \phi_{n,0},\, \Phi_{n,0}\}. \tag{3.23}$$

Substituting the expansions (3.18)—(3.22) into the equations of motion (3.14a)—(3.14g), setting the radial shift function $\lambda(v)$ to zero, and eliminating all possible coefficients in favor of the others, the ultraviolet asymptotic behavior of the EMD fields reads

$$A(v,r) = \frac{r^2}{2} + \frac{H - \phi_2(v)^2/18}{r^2} - \frac{\phi_2(v)\dot{\phi}_2(v)}{18r^3} + \mathcal{O}(r^{-4}) \tag{3.24}$$

$$\Sigma(v,r) = r - \frac{\phi_2(v)^2}{18r^3} - \frac{\phi_2(v)\dot{\phi}(v)}{10r^4} + \mathcal{O}(r^{-5}) \tag{3.25}$$

$$d_+\Sigma(v,r) = \frac{r^2}{2} + \frac{H + 1/36\,\phi_2(v)^2}{r^2} + \mathcal{O}(r^{-3}) \tag{3.26}$$

$$B(v,r) = \frac{B_4(v)}{r^4} + \frac{\dot{B}_4(v)}{r^5} + \mathcal{O}(r^{-6}) \tag{3.27}$$

$$\phi(v,r) = \frac{\phi_2(v)}{r^2} + \frac{\dot{\phi}_2(v)}{r^3} + \frac{\sqrt{6}\phi_2(v)^2 + 9\ddot{\phi}_2(v)}{12r^4} + \mathcal{O}(r^{-5}) \tag{3.28}$$

$$d_+\phi(v,r) = -\frac{\phi_2(v)}{r} + \mathcal{O}(r^{-2}) \tag{3.29}$$

$$\Phi(v,r) = \Phi_0(v) + \frac{\Phi_2(v)}{r^2} + \frac{\sqrt{\frac{2}{3}}\phi_2(v)\Phi_2(v)}{r^4} + \mathcal{O}(r^{-5}). \tag{3.30}$$

where the dot represents the time derivative ∂_v.

Furthermore, we find that this near-boundary analysis cannot determine five coefficients: $A_2(v)$ (or, equivalently, the coefficient H defined below), $B_4(v)$, $\phi_2(v)$, $\Phi_0(v)$, and $\Phi_2(v)$. With the exception of Φ_0, these coefficients are *dynamical*, i.e. we need the bulk solution to determine them. The coefficient $\Phi_0(v)$ is fixed by the Dirichlet boundary condition for the Maxwell field which imposes that its boundary value gives the chemical potential associated with the $U(1)$ R-symmetry[9]

$$\mu = \lim_{v\to\infty} \Phi_0(v). \tag{3.31}$$

The coefficient H is defined by

$$H \equiv 18A_2(v) + \phi_2(v)^2. \tag{3.32}$$

By working out the equations of motion up to $\mathcal{O}(r^{-3})$ in the near-boundary expansions of the bulk fields one concludes that H is a constant. Moreover, as we shall see in a moment, this coefficient H is, up to a numerical factor, the energy of the system which is conserved in this homogeneous setup. On the other hand, the coefficients $B_4(v)$ and $\phi_2(v)$ are time-dependent quantities related to the pressure anisotropy and the scalar condensate dual to the dilaton field, respectively.

Additionally, the coefficient $\Phi_2(v)$ is actually a constant. This can be shown by expanding the equations of motion near the boundary up to $\mathcal{O}(r^{-5})$. Moreover, by exploring relation (3.17) near the boundary using the expansions (3.24)—(3.30), one finds that,

$$\mathcal{E}(v,r) = 2\Phi_2\Sigma(v,r)^{-3}e^{2\sqrt{\frac{2}{3}}\phi(v,r)}. \tag{3.33}$$

We shall discuss how the charge density can be related to Φ_2 in Sec. 3.3.

3.3 Equilibrium solutions

Here we briefly review the main features of the equilibrium solution of the 1RCBH plasma and its thermodynamics [146, 203].

3.3.1 Thermodynamics

In equilibrium this model has the following analytical solution (written in a slightly different chart from Eq. (3.11), which we call the "modified EF" coordinates and denote

[9] The Dirichlet boundary condition for the metric field $g_{\mu\nu}$ has been already implemented when we imposed an asymptotically AdS_5 solution.

with a tilde),

$$ds^2 = dv\left[2e^{a(\tilde{r})+b(\tilde{r})}d\tilde{r} - e^{2a(\tilde{r})}h(\tilde{r})dv\right] + e^{2a(\tilde{r})}d\vec{x}^2 \tag{3.34}$$

$$a(\tilde{r}) = \ln\tilde{r} + \frac{1}{6}\ln\left(1+\frac{Q^2}{\tilde{r}^2}\right), \tag{3.35}$$

$$b(\tilde{r}) = -\ln\tilde{r} - \frac{1}{3}\ln\left(1+\frac{Q^2}{\tilde{r}^2}\right), \tag{3.36}$$

$$h(\tilde{r}) = 1 - \frac{M^2}{\tilde{r}^2(\tilde{r}^2+Q^2)}, \tag{3.37}$$

$$\phi(\tilde{r}) = -\sqrt{\frac{2}{3}}\ln\left(1+\frac{Q^2}{\tilde{r}^2}\right), \tag{3.38}$$

$$\Phi(\tilde{r}) = \left(-\frac{MQ}{\tilde{r}^2+Q^2} + \frac{MQ}{\tilde{r}_H^2+Q^2}\right), \tag{3.39}$$

where $\tilde{r}_h$ is the radius of the black hole's event horizon given by

$$\tilde{r}_h = \sqrt{\frac{\sqrt{Q^4+4M^2}-Q^2}{2}}. \tag{3.40}$$

As discussed in Refs. [146,203] this model is characterized by two non-negative parameters (Q, M) or, alternatively, $(Q, \tilde{r}_h)$. They are related to the Hawking temperature of the black hole

$$T = \frac{Q^2+2\tilde{r}_h^2}{2\pi\sqrt{Q^2+\tilde{r}_h^2}}, \tag{3.41}$$

and the $U(1)$ R-charge chemical potential

$$\mu = \lim_{\tilde{r}\to\infty}\Phi(\tilde{r}) = \frac{Q\tilde{r}_h}{\sqrt{Q^2+\tilde{r}_h^2}}. \tag{3.42}$$

In fact, standard algebraic manipulations show that

$$\frac{Q}{\tilde{r}_h} = \sqrt{2}\left(\frac{1\pm\sqrt{1-\left(\frac{\mu/T}{\pi/\sqrt{2}}\right)^2}}{\frac{\mu/T}{\pi/\sqrt{2}}}\right). \tag{3.43}$$

Since $Q/\tilde{r}_h$ is non-negative, Eq. (3.43) implies that $\mu/T \in \left[0, \pi/\sqrt{2}\right]$. It also follows from (3.43) that for every value of $\mu/T \in \left[0, \pi/\sqrt{2}\right)$ there are two different values of $Q/\tilde{r}_h$, which in turn parameterize two different branches of solutions. By analyzing the thermodynamics in Fig. 3.1, one can see the two branches merge at $\mu/T = \pi/\sqrt{2}$, which defines a critical point marking a 2nd order phase transition.

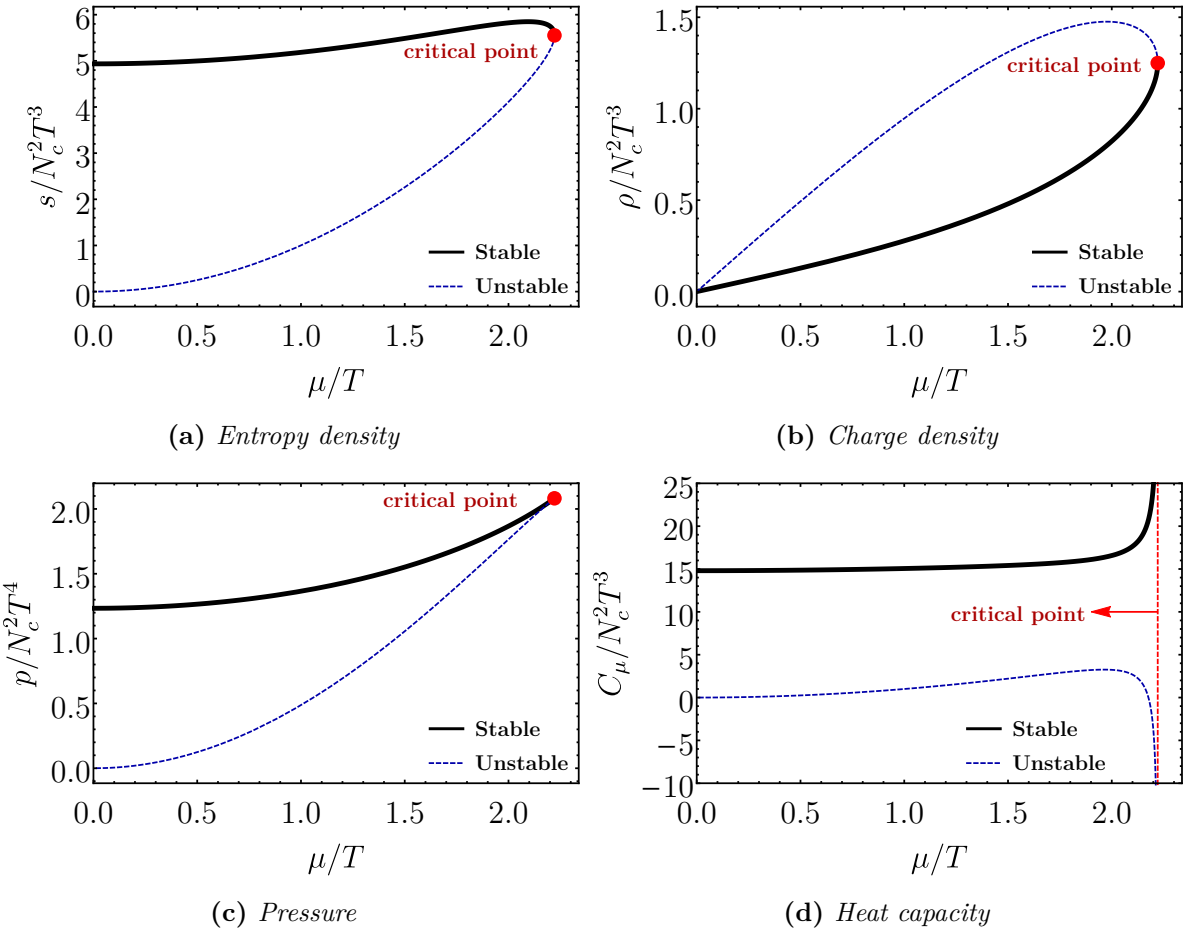

(a) *Entropy density* **(b)** *Charge density*

(c) *Pressure* **(d)** *Heat capacity*

Figure 3.1: *Thermodynamic quantities for the 1RCBH model. These figures are taken from Ref. [146].*

Since $\frac{1}{\kappa_5^2} = \frac{N_c^2}{4\pi^2}$ for a SYM plasma [228], the entropy density can be determined from Bekenstein-Hawking's relation [162, 163] as follows

$$\frac{s}{N_c^2T^3} = \frac{\pi^2}{16}\left(3 \pm \sqrt{1-\left(\frac{\mu/T}{\pi/\sqrt{2}}\right)^2}\right)^2\left(1 \mp \sqrt{1-\left(\frac{\mu/T}{\pi/\sqrt{2}}\right)^2}\right). \tag{3.44}$$

On the other hand, the $U(1)$ R-charge density, $\rho_c = \lim_{\tilde{r}\to\infty} \delta S/\delta\Phi'$, may be expressed as

$$\frac{\rho_c}{N_c^2T^3} = \frac{\mu/T}{16}\left(3 \pm \sqrt{1-\left(\frac{\mu/T}{\pi/\sqrt{2}}\right)^2}\right)^2, \tag{3.45}$$

where the stable/unstable branches correspond to lower/upper signs, as in Eq. (3.43).

Furthermore, standard thermodynamic relations give us the pressure

$$\frac{p}{N_c^2 T^4} = \frac{\pi^2}{128}\left(3 \pm \sqrt{1-\left(\frac{\mu/T}{\pi/\sqrt{2}}\right)^2}\right)^3 \left(1 \mp \sqrt{1-\left(\frac{\mu/T}{\pi/\sqrt{2}}\right)^2}\right). \tag{3.46}$$

which can be shown to be $p = \varepsilon/3$ with the internal energy density given by $\varepsilon = Ts - p + \mu\rho$. This is the expected result for a conformal field theory (CFT) in 4 spacetime dimensions.

3.3.2 Mapping between FG (2.16) and the modified EF (3.34) coordinates

Once the equilibrium solution is known, one may compute the one-point functions of the dual QFT by using Eqs. (2.38), (2.41), and (2.53) derived in Sec. 2.3. However, we note that these equations are written in the so-called Fefferman-Graham (FG) coordinates and, thus, we need to find a relation between these coordinates and the modified EF coordinates in order to calculate $\langle T_{\mu\nu}\rangle$, $\langle J^\mu\rangle$, and $\langle \mathcal{O}_\phi\rangle$ in equilibrium.

First we consider the diagonal form of the line element (3.34),

$$ds^2 = e^{2a(\tilde{r})}(-h(\tilde{r})dt^2 + d\vec{x}^2) + \frac{e^{b(\tilde{r})}}{h(\tilde{r})}d\tilde{r}^2. \tag{3.47}$$

The task now is to find a relation between $\tilde{r}$ and ρ (the radial coordinate of the FG chart discussed in Sec. 2.3). This can be achieved by evaluating the following integral

$$\int \frac{e^{b(\tilde{r})}}{\sqrt{h(\tilde{r})}}d\tilde{r} = -\frac{1}{2}\ln\rho. \tag{3.48}$$

This integral can be solved perturbatively in $\tilde{r}$ close to the boundary in order to determine $\tilde{r}(\rho)$ as a series expansion. Such expansion will enable us to expand the bulk fields near the boundary in the form of Eqs. (2.27)—(2.29), which is what we need to fix the ultraviolet coefficients $\gamma_{(4)\mu\nu}$, $A_{(0)\mu}$, and $\phi_{(0)}$ by comparing these expansions with the equilibrium solution. With these ultraviolet coefficients fixed, we may proceed to calculate $\langle T^{\mu\nu}\rangle$, $\langle J^\mu\rangle$ and $\langle \mathcal{O}_\phi\rangle$ using Eqs. (2.53), (2.41), and (2.38), respectively. Thus, by perturbatively evaluating the integral (3.48) close to the boundary using the equilibrium solution, we find that

$$\tilde{r} = \frac{1}{\sqrt{\rho}} - \frac{Q^2\sqrt{\rho}}{6} + \frac{1}{72}\left(9M^2 + Q^4\right)\rho^{3/2} + \mathcal{O}(\rho)^{5/2}. \tag{3.49}$$

The next step is to expand the bulk fields near the boundary and substitute $\tilde{r}$ by ρ

using Eq. (3.49). This gives the following asymptotic results,

$$\gamma_{tt}(\rho) = -\frac{1}{\rho} - \frac{\rho}{2}\left(\frac{5}{2}M^2 - \frac{Q^4}{9}\right) + \mathcal{O}(\rho^2), \tag{3.50}$$

$$\gamma_{xx}(\rho) = \frac{1}{\rho} + \frac{\rho}{2}\left(\frac{1}{2}M^2 - \frac{Q^4}{9}\right) + \mathcal{O}(\rho^2), \tag{3.51}$$

$$\Phi(\rho) = \frac{MQ}{Q^2 + \tilde{r}_h^2} - MQ\rho + \mathcal{O}(\rho^2), \tag{3.52}$$

$$\phi(\rho) = -\sqrt{\frac{2}{3}}Q^2\rho + \mathcal{O}(\rho^2). \tag{3.53}$$

By comparing the above expressions with Eqs. (2.27)—(2.29) (taking into account that all the logarithmic terms vanish for the 1RCBH model, as stated before), and then using Eqs. (2.53), (2.41), and (2.38), we find

$$\langle T_{tt}\rangle = \frac{1}{\kappa_5^2}\frac{3M^2}{2}, \tag{3.54}$$

$$\langle T_{xx}\rangle = \frac{1}{\kappa_5^2}\frac{M^2}{2}, \tag{3.55}$$

$$\langle J^t\rangle = \frac{1}{\kappa_5^2}MQ, \tag{3.56}$$

$$\langle \mathcal{O}_\phi\rangle = \frac{1}{\kappa_5^2}\sqrt{\frac{2}{3}}Q^2. \tag{3.57}$$

At this stage, it is useful to rewrite the energy density (ε), the equilibrium pressure (p), and the $U(1)$ R-charge density (ρ_c) as

$$\varepsilon \equiv \langle T_{tt}\rangle = \frac{N_c^2}{4\pi^2}\frac{3M^2}{2}, \quad p \equiv \langle T_{xx}\rangle = \frac{N_c^2}{4\pi^2}\frac{M^2}{2}, \quad \rho_c \equiv \langle J^t\rangle = \frac{N_c^2}{4\pi^2}MQ. \tag{3.58}$$

The above results hold for the 1RCBH plasma in equilibrium.

3.3.3 Mapping between modified EF (3.34) and the original EF (3.11) coordinates

The purpose of this subsection is to find relations between the coefficients of the non-equilibrium solution in the near-boundary expansions (3.24)—(3.30), and the parameters of the equilibrium solution for the 1RCBH plasma (3.34). Evidently, we can only match the equilibrium solution with the asymptotically late time behavior of the non-equilibrium solution when thermodynamic equilibrium is achieved by the system. For this reason, before we derive an expression for $r(\tilde{r})$, we define the equilibrium coefficients of the non-

equilibrium solution as follows,

$$X^{(eq)} \equiv \lim_{v\to\infty} X(v), \quad \text{with} \quad \partial_v X^{(eq)} = 0, \tag{3.59}$$

where $X(v) \in \{B_4(v), \phi_2(v), \Phi_0(v)\}$. Note that the coefficients H and Φ_2 are not included in this definition because they are constant, as stated before.

In order to find the relation between $\tilde{r}$ and r, we need to solve the following equation

$$e^{a(\tilde{r})+b(\tilde{r})} d\tilde{r} = dr. \tag{3.60}$$

The above expression renders an analytical relation between r and $\tilde{r}$,

$$r = \frac{3\tilde{r}^{4/3}\, {}_2F_1\left(\frac{1}{6}, \frac{2}{3}; \frac{5}{3}; -\frac{\tilde{r}^2}{Q^2}\right)}{4\sqrt[3]{Q}} + \xi, \tag{3.61}$$

where ${}_2F_1$ is the hypergeometric function and ξ is an integration constant which we choose to be

$$\xi = \frac{3\sqrt{\pi}\,\Gamma\left[\frac{5}{3}\right]}{2\,\Gamma\left[\frac{1}{6}\right]} Q, \tag{3.62}$$

in order to obtain $\lim_{\tilde{r}\to\infty} r(\tilde{r}) - \tilde{r} = 0$. Just as we did in Sec. 3.3.2 to relate $\tilde{r}$ with ρ, we expand the above relation in powers of $\tilde{r}$ close to the boundary

$$r(\tilde{r}) = \tilde{r} + \frac{Q^2}{6\tilde{r}} - \frac{7Q^4}{216\tilde{r}^3} + \frac{91Q^6}{6480\tilde{r}^5} + \mathcal{O}(\tilde{r}^{-7}). \tag{3.63}$$

Next, we substitute the above expression into Eqs. (3.24)—(3.30) and take the asymptotic equilibrium limit defined by Eq. (3.59). The result reads

$$g_{tt}(\tilde{r}) = -2A(\tilde{r}) = -\tilde{r}^2 - \frac{Q^2}{3} + \frac{Q^4 - 54H + 3(\phi_2^{(eq)})^2}{27\tilde{r}^2} + \mathcal{O}(\tilde{r}^{-4}), \tag{3.64a}$$

$$g_{xx}(\tilde{r}) = \Sigma(\tilde{r})^2 = \tilde{r}^2 + \frac{Q^2}{3} + \frac{-Q^4 - 3(\phi_2^{(eq)})^2}{27\tilde{r}^2} + \mathcal{O}(\tilde{r}^{-4}), \tag{3.64b}$$

$$\phi(\tilde{r}) = \frac{\phi_2^{(eq)}}{\tilde{r}^2} + \frac{-4Q^2\phi_2^{(eq)} + \sqrt{6}(\phi_2^{(eq)})^2}{12\tilde{r}^4} + \mathcal{O}(\tilde{r}^{-6}), \tag{3.64c}$$

$$\Phi(\tilde{r}) = \Phi_0^{(eq)} + \frac{\Phi_2}{r^2} - \frac{\left(Q^2 - \sqrt{6}\phi_2^{(eq)}\right)\Phi_2}{3r^4} + \mathcal{O}(\tilde{r}^{-6}). \tag{3.64d}$$

On the other hand, the near-boundary behavior of the analytical static solution of the

1RCBH model obtained from Eqs. (3.35)—(3.39) is

$$g_{tt}(\tilde{r}) = -\tilde{r}^2 - \frac{Q^2}{3} + \frac{M^2 + \frac{Q^4}{9}}{\tilde{r}^2} + \frac{-\frac{1}{3}\left(2M^2Q^2\right) - \frac{5Q^6}{81}}{\tilde{r}^4} + \frac{\frac{5M^2Q^4}{9} + \frac{10Q^8}{243}}{\tilde{r}^6} + \mathcal{O}(\tilde{r}^{-8}), \tag{3.65a}$$

$$g_{xx}(\tilde{r}) = \tilde{r}^2 + \frac{Q^2}{3} - \frac{Q^4}{9\tilde{r}^2} + \frac{5Q^6}{81\tilde{r}^4} - \frac{10Q^8}{243\tilde{r}^6} + \mathcal{O}(\tilde{r}^{-8}), \tag{3.65b}$$

$$\phi(\tilde{r}) = -\frac{\sqrt{\frac{2}{3}}Q^2}{\tilde{r}^2} + \frac{Q^4}{\sqrt{6}\tilde{r}^4} - \frac{\sqrt{\frac{2}{3}}Q^6}{3\tilde{r}^6} + \mathcal{O}(\tilde{r}^{-8}), \tag{3.65c}$$

$$\Phi(\tilde{r}) = \frac{MQ}{Q^2 + \tilde{r}_h^2} - \frac{MQ}{\tilde{r}^2} + \frac{MQ^3}{\tilde{r}^4} - \frac{MQ^5}{\tilde{r}^6} + \mathcal{O}(\tilde{r}^{-8}). \tag{3.65d}$$

Comparing Eqs. (3.64a)—(3.64d) and Eqs. (3.65a)—(3.65d), we find that

$$\phi_2^{(eq)} = -\sqrt{\frac{2}{3}}Q^2, \tag{3.66}$$

$$H = -\frac{M^2}{2}, \tag{3.67}$$

$$\Phi_0^{(eq)} = \frac{MQ}{Q^2 + \tilde{r}_h^2}, \tag{3.68}$$

$$\Phi_2 = -MQ. \tag{3.69}$$

3.3.4 Mapping between EF (3.11) and FG (2.16) coordinates

Now we want to relate the non-equilibrium metric in EF coordinates (3.11) with the expression for the metric in FG coordinates (2.16) in order to obtain expressions for the one-point functions $\langle T_{\mu\nu}\rangle$, $\langle J^\mu\rangle$, and $\langle \mathcal{O}_\phi\rangle$ far-from-equilibrium. To do so, we need to solve the integral below

$$\int \frac{dr}{\sqrt{2A(v,r)}} = -\frac{1}{2}\ln\rho, \tag{3.70}$$

which, again, may be solved perturbatively near the boundary with the help of Eq. (3.24). The result is,

$$r(\rho) = \frac{1}{\sqrt{\rho}} + \rho^{3/2}\left(-\frac{H}{4} + \frac{1}{72}\phi_2(v)^2\right) + \frac{1}{90}\rho^2\phi_2(v)\dot{\phi}_2(v) + \mathcal{O}(\rho^{5/2}). \tag{3.71}$$

Plugging $r(\rho)$ into Eqs. (3.24)—(3.30), one obtains

$$\gamma_{tt}(\rho) = -\frac{1}{\rho} + \frac{1}{12}\rho\left(-18H + \phi_2(v)^2\right) + \mathcal{O}(\rho^2), \tag{3.72a}$$

$$\gamma_{xx}(\rho) = \frac{1}{\rho} + \rho\left(-\frac{H}{2} + B_4(v) - \frac{1}{12}\phi_2(v)^2\right) + \mathcal{O}(\rho^2), \tag{3.72b}$$

$$\gamma_{zz}(\rho) = \frac{1}{\rho} + \rho\left(-\frac{H}{2} - 2B_4(v) - \frac{1}{12}\phi_2(v)^2\right) + \mathcal{O}(\rho^2), \tag{3.72c}$$

$$\phi(\rho) = \rho\phi_2(v) + \mathcal{O}(\rho^2), \tag{3.72d}$$

$$\Phi(\rho) = \Phi_0(v) + \rho\Phi_2(v) + \mathcal{O}(\rho^2). \tag{3.72e}$$

With the above set of equations at hand, we obtain $\langle T^{\mu\nu}\rangle$, $\langle J^\mu\rangle$, and $\langle \mathcal{O}_\phi\rangle$ from Eqs. (2.53), (2.41), and (2.38), respectively,

$$\langle T_{tt}\rangle = \frac{1}{\kappa_5^2}(-3H), \tag{3.73}$$

$$\langle T_{xx}\rangle = \frac{1}{\kappa_5^2}(-H + 2B_4(v)), \tag{3.74}$$

$$\langle T_{zz}\rangle = \frac{1}{\kappa_5^2}(-H - 4B_4(v)), \tag{3.75}$$

$$\langle J^t\rangle = -\frac{1}{\kappa_5^2}\Phi_2, \tag{3.76}$$

$$\langle \mathcal{O}_\phi\rangle = -\frac{1}{\kappa_5^2}\phi_2(v). \tag{3.77}$$

Analogously to what was done in Eqs. (3.58), one may recast the physical observables of the boundary QFT as follows

$$\varepsilon = \langle T_{tt}\rangle = \frac{N_c^2}{4\pi^2}(-3H), \tag{3.78a}$$

$$\Delta p(v) \equiv \langle T_{xx}\rangle - \langle T_{zz}\rangle = \frac{N_c^2}{4\pi^2}6B_4(v), \tag{3.78b}$$

$$\rho_c = \langle J^t\rangle = -\frac{N_c^2}{4\pi^2}\Phi_2, \tag{3.78c}$$

$$\langle \mathcal{O}_\phi\rangle(v) = -\frac{N_c^2}{4\pi^2}\phi_2(v), \tag{3.78d}$$

where $\Delta p(v)$ is the pressure anisotropy. The above expressions hold for the far-from-equilibrium 1RCBH plasma undergoing a spatially homogeneous equilibration process. Moreover, in terms of the charge density ρ_c, the bulk electric field defined in Eq. (3.33) is given by

$$\mathcal{E}(v,r) = -\frac{8\pi^2\rho_c}{N_c^2}\Sigma^{-3}(v,r)e^{2\sqrt{\frac{2}{3}}\phi(v,r)}. \tag{3.79}$$

Thus, we finish here the discussion of the quantities that we need to follow when solving the full nonlinear PDEs of the 1RCBH model far-from-equilibrium. Next, we discuss how to proceed with the numerics to obtain the time evolution of the 1RCBH plasma.

3.4 Far-from-equilibrium solutions

3.4.1 Field redefinitions

First, we express the system of PDEs in a form where the numerical analysis becomes as simple as possible, mapping the infinite radial domain to a finite one. This may be accomplished by redefining the radial coordinate as follows

$$u = \frac{1}{r}, \tag{3.80}$$

which means that the boundary now lies at $u = 0$. How far we go into the bulk in a numerical simulation is an issue which shall be discussed in Sec. 3.4.2. Moreover, since all the nontrivial dynamics of the system depends on the subleading terms of the near-boundary expansion of the bulk fields, as indicated in Eqs. (3.18)—(3.22), we define the following subtracted fields[10]

$$\begin{aligned} u^2 A_s = A - \frac{1}{2u^2}, \quad u^4 B_s = B, \quad u^2 \Sigma_s = \Sigma - \frac{1}{u}, \quad u^2 \phi_s = \phi, \quad \mathcal{E}_s = \mathcal{E}, \\ u^2 (d_+\Sigma)_s = d_+\Sigma - \frac{1}{2u^2}, \quad u^3 (d_+ B)_s = d_+ B, \quad u (d_+\phi)_s = d_+\phi. \end{aligned} \tag{3.81}$$

The equations of motion (3.14a)—(3.14f) rewritten in terms of these subtracted fields

[10] Our redefinitions are similar to the ones given in Ref. [181]. We also remark that $d_+(\Sigma_s) \neq (d_+\Sigma)_s$.

read

$$u^2\Sigma_s'' + 6u\Sigma_s' + \frac{\Sigma_s}{6}\left(36 + u^4\left(4\phi_s^2 + u\left(3u^3\left(4B_s + uB_s'\right)^2 + u(\phi_s')^2 + 4\phi_s'\phi_s\right)\right)\right)$$
$$+ \frac{1}{6}u\left(4\phi_s^2 + u\left(3u^3(4B_s + uB_s')^2 + u(\phi_s')^2 + 4\phi_s'\phi_s\right)\right) = 0, \tag{3.82a}$$

$$\mathcal{E} = \frac{2e^2\sqrt{\frac{2}{3}}u^2\phi_s u^3\Phi_2}{\left(1 + u^3\Sigma_s\right)^3}, \tag{3.82b}$$

$$-(1 + u^3\Sigma_s)(d_+\Sigma)_s' - 2u^2(3\Sigma_s + u\Sigma_s')(d_+\Sigma)_s$$
$$+ \frac{12\left(1 + \Sigma_s u^3\right) - 12\left(-1 + 2\Sigma_s u^3 + u^4\Sigma_s'\right) + \left(1 + \Sigma_s u^3\right)^2\left(\mathcal{E}^2 f\left(u^2\phi_s\right) + 2V\left(u^2\phi_s\right)\right)}{12u^5} = 0, \tag{3.82c}$$

$$-u\left(1 + \Sigma_s u^3\right)(d_+B)_s' - \frac{3}{2}\left(1 + 4\Sigma_s u^3 + u^4\Sigma_s'\right)(d_+B)_s$$
$$-\frac{3}{4}\left(1 + 2u^4(d_+\Sigma)_s\right)\left(4B_s + uB_s'\right) = 0, \tag{3.82d}$$

$$-4\left(u + u^4\Sigma_s\right)(d_+\phi)_s' + (2 - 2u^3(8\Sigma_s + 3u\Sigma_s'))(d_+\phi)_s$$
$$+ \frac{-3u^3\left(1 + 2u^4(d_+\Sigma)_s\right)\phi_s' - 6\left(u^2 + 2u^6(d_+\Sigma)_s\right)\phi_s}{u^2}$$
$$+ \frac{\left(1 + \Sigma_s u^3\right)\left(\mathcal{E}^2\partial_\phi f\left(u^2\phi_s\right) - 2\partial_\phi V\left(u^2\phi_s\right)\right)}{u^2} = 0, \tag{3.82e}$$

$$u^2\left(1 + u^3\Sigma_s\right)^2 A_s'' + 6u\left(1 + u^3\Sigma_s\right)^2 A_s' + 6\left(1 + u^3\Sigma_s\right)^2 A_s$$
$$- \frac{-\left(1 + u^3\Sigma_s\right)^2 - 3\left(1 + 2(d_+\Sigma)_s u^4\right)\left(-1 + 2u^3\Sigma_s + u^4\Sigma_s'\right)}{u^4}$$
$$- \frac{6(d_+B)_s u^8\left(1 + u^3\Sigma_s\right)^2\left(4B_s + uB_s'\right) + 2(d_+\phi)_s u^4\left(1 + u^3\Sigma_s\right)^2\left(u\phi_s' + 2\phi_s\right)}{4u^4}$$
$$+ \frac{7\left(1 + u^3\Sigma_s\right)^2\mathcal{E}^2 f\left(u^2\phi_s\right) + 2\left(1 + u^3\Sigma_s\right)^2 V\left(u^2\phi_s\right)}{12u^4} = 0, \tag{3.82f}$$

with the prime now representing ∂_u. The price we paid to remove the redundant information from the bulk fields is that the equations of motion for them are now longer. Moreover, to solve these equations we need to specify the boundary conditions which, in

light of Eqs. (3.24)—(3.30) and Eqs. (3.81), are given by

$$A_s(v,u) = H - \phi_2(v)^2/18 + \mathcal{O}(u), \tag{3.83}$$

$$\Sigma_s(v,u) = -\frac{\phi_2(v)^2}{18}u - \frac{\phi_2(v)\dot{\phi}(v)}{10}u^2 + \mathcal{O}(u^3), \tag{3.84}$$

$$(d_+\Sigma)_s(v,u) = H + 1/36\,\phi_2(v)^2 + \mathcal{O}(u), \tag{3.85}$$

$$B_s(v,u) = B_4(v) + \mathcal{O}(u), \tag{3.86}$$

$$(d_+B)_s(v,u) = -2B_4(v) + \mathcal{O}(u), \tag{3.87}$$

$$\phi_s(v,u) = \phi_2(v) + \dot{\phi}_2(v)u + \mathcal{O}(u^2), \tag{3.88}$$

$$(d_+\phi)_s(v,u) = -\phi_2(v) + \mathcal{O}(u). \tag{3.89}$$

The time evolution equations for B_s and ϕ_s, which are obtained from the definitions of d_+B and $d_+\phi$ using the redefined fields (3.81), are given by

$$\partial_v B_s = \frac{2B_s}{u} + \frac{(\mathrm{d}_+B)_s}{u} + 4A_sB_su^3 + \frac{B_s'}{2} + A_su^4B_s', \tag{3.90}$$

$$\partial_v \phi_s = \frac{(\mathrm{d}_+\phi)_s}{u} + \frac{\phi_s}{u} + 2u^3A_s\phi_s + \frac{1}{2}\phi_s' + u^4A_s\phi_s'. \tag{3.91}$$

We discuss in Sec. 3.4.4 the numerical scheme we use to evolve in time the EMD fields provided $\partial_v B_s$ and $\partial_v \phi_s$ are known.

3.4.2 Radial position of the black hole event horizon

A delicate aspect of the numerical solution of the far-from-equilibrium equations of motion is how deep into the bulk one should go when integrating the radial dependence of the PDEs. Since we are working with a finite temperature setup, there is a black hole inside the bulk and one needs to cover the entire portion of the bulk between the black hole's event horizon and the boundary of the asymptotically AdS_5 spacetime, since this is the region of the bulk geometry causally connected to the boundary QFT. In the case of time-dependent backgrounds, one main difficulty is that the radial position of the event horizon is unknown *a priori* since it depends on the time evolution of the system. If one cuts off the radial integration before reaching the horizon, then the obtained numerical solution will be inevitably inaccurate; on the other hand, if the radial integration proceeds too deep inside the horizon, the numerical simulation will probably break down due to possible singularities (caustics) associated with strong curvatures in this deep infrared region.

One possible way to deal with this issue is to use the radial shift function $\lambda(v)$ associated with the residual diffeomorphism invariance of the metric and regard it as an

auxiliary field to fix the (apparent) horizon position at a specific value of the radial coordinate [59]. However, we do not adopt this strategy here. Instead, as mentioned above Eq. (3.24) we set $\lambda(v) = 0$ and let the horizon position fluctuate in each simulation. We then follow the reasoning of Ref. [229] in which it is imposed that in equilibrium the radius of the black hole is located at $u_h = 1$, while the inner radial cutoff for numerical integration lies at $u \approx 1.01$. Moreover, since we are interested here in analyzing the equilibration dynamics of the system in terms of the dimensionless "time combination" vT for different values of μ/T, we choose to set the equilibrium temperature to $1/\pi$ for any value of μ/T. This gives the following relation between $\tilde{r}_h$ and Q coming from Eq. (3.41),

$$\frac{1}{\pi} = \frac{Q^2 + 2\tilde{r}_h^2}{2\pi\sqrt{Q^2 + \tilde{r}_h^2}}. \tag{3.92}$$

Therefore, given some value of μ/T we use Eqs. (3.43) and (3.92) to determine the corresponding values of $\tilde{r}_h$ and Q. In Fig. 3.2 we show the plots for $\tilde{r}_h$, Q, and u_h as functions of μ/T.[11] In particular, Fig. 3.2 (c) indicates that it is fine to adopt $u \approx 1.01$ as the inner radial cutoff for numerical integration since this prescription already works well at zero density and the horizon position in equilibrium gets closer to the boundary as the chemical potential is increased. Moreover, in Fig. 3.2 (d) we illustrate a typical case with the time evolution of the event horizon[12], showing that also for transient states our inner radial cutoff is always beyond the horizon.

3.4.3 Initial states

The last step required before we numerically simulate the far-from-equilibrium evolution of the 1RCBH plasma is to choose the initial data. In the context of the homogeneous equilibration of the 1RCBH model, we need to specify three inputs to start the numerical integration of the PDEs (3.82a)—(3.82f):

- The initial metric anisotropy function, $B_s(v_0, u)$;
- The initial profile for the dilaton, $\phi_s(v_0, u)$;
- The value of the equilibrium chemical potential, μ/T.

[11] In order to go from $\tilde{r}_h$ to r_h and then to u_h one must use Eqs. (3.61) and (3.80).

[12] To calculate the event horizon, one just needs to calculate a null geodesic

$$0 = 2dvdr - 2A(v,r)dv^2 \Rightarrow \frac{dr}{dv} = A(v, r(v)), \tag{3.93}$$

subjected to the boundary condition $r(v \to \infty) = r_h$.

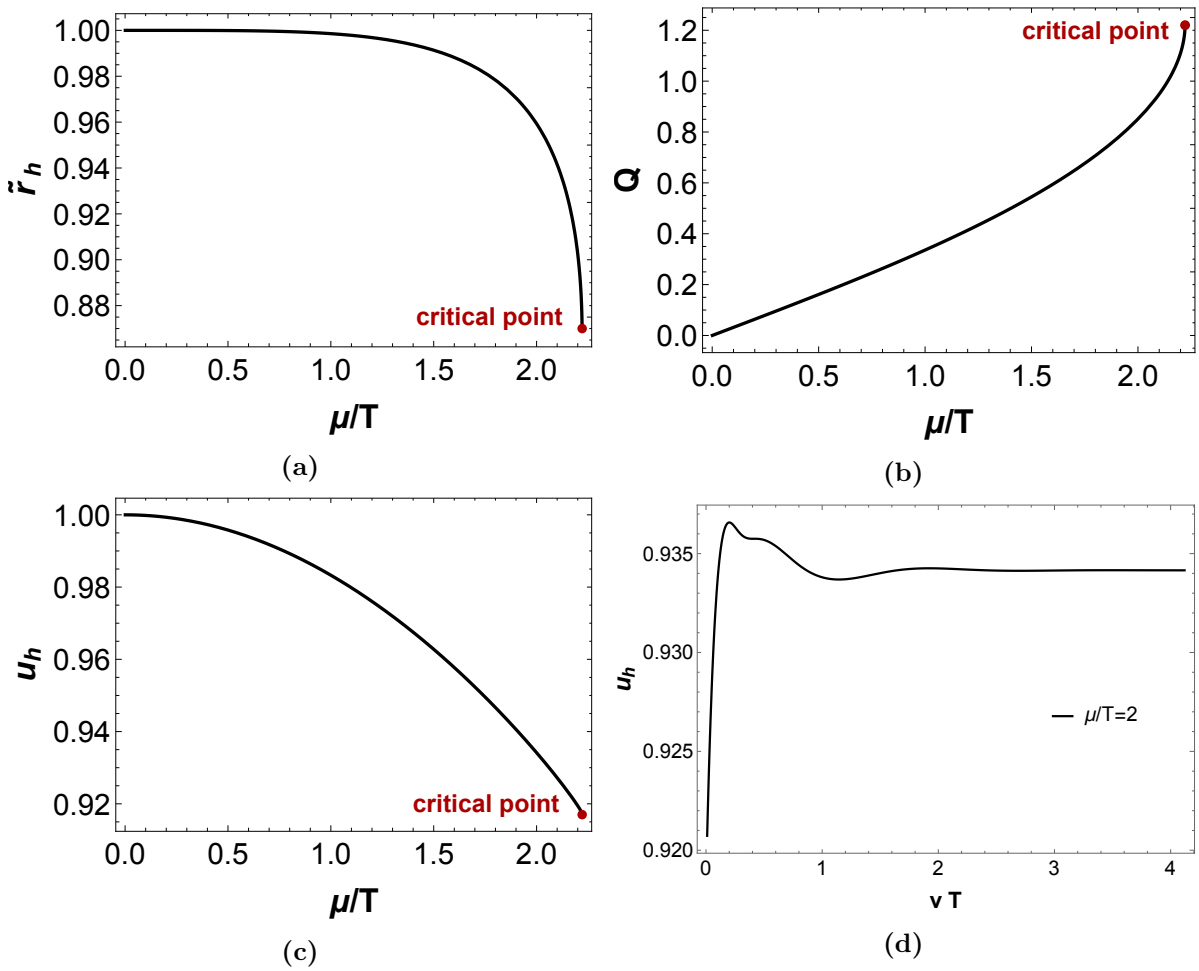

Figure 3.2: *(a) Radius of the equilibrium black hole expressed in the modified EF coordinates (3.34), (b) the parameter Q of the equilibrium solution, and (c) the radius of the equilibrium black hole expressed in the numerical radial coordinate (3.80), all of them plotted as functions of the chemical potential μ/T. (d) Time evolution of the radius of the far-from-equilibrium black hole solution obtained using constant profiles for the initial metric anisotropy and dilaton field at $\mu/T = 2$.*

The initial metric anisotropy will be assumed to have either the form of a "pulse" with a Gaussian parameterization [168], or simply a constant profile

$$(a) \quad B_s(v_0, u) = \mathcal{A}\, e^{\frac{1}{2}(u-u_0)^2/\sigma^2}, \tag{3.94}$$

$$(b) \quad B_s(v_0, u) = \mathcal{A}. \tag{3.95}$$

The parameter $\mathcal{A}$ controls the initial amplitude of the metric anisotropy whereas the parameters σ and u_0 are related to the width and how deep into the bulk the pulse is centered.

For the initial dilaton profile, we shall consider again the constant and Gaussian forms and, additionally, we will also consider the case where the initial dilaton profile is already

at its equilibrium solution, i.e.[13]

$$(a)\quad \phi_s(v_0,u) = -\kappa_5^2\langle\mathcal{O}_\phi\rangle = -\sqrt{\frac{2}{3}}Q^2, \tag{3.96}$$

$$(b)\quad \phi_s(v_0,u) = \mathcal{A}_\phi e^{\frac{1}{2}(u-u_0)^2/\sigma^2}, \tag{3.97}$$

$$(c)\quad \phi_s(v_0,u) = -\frac{1}{u^2}\sqrt{\frac{2}{3}}\ln\left(1+\tilde{u}(u)Q^2\right), \tag{3.98}$$

where $\tilde{u} = 1/\tilde{r}$, and Eq. (3.98) has this form to match the equilibrium solution (3.38). Note that for $B(v_0,u) = 0$ (corresponding to a pure thermalization process with no initial anisotropy), the use of the last initial condition for the dilaton field automatically gives the equilibrium solution for the 1RCBH plasma.

Finally, one needs to choose a value for the equilibrium chemical potential $\mu/T \in [0,\pi/\sqrt{2}]$. The value $\mu/T = 0$ corresponds to the standard $\mathcal{N} = 4$ SYM plasma whereas $\mu/T = \pi/\sqrt{2}$ corresponds to the critical point. Moreover, by fixing μ/T we also fix the values of Q and u_h as explained above in Eq. (3.92).

Regarding the initial energy density (and the pressure, since $\varepsilon = 3p$), one may find it using the expression obtained in Eq. (3.46) from the thermodynamics of the 1RCBH plasma, i.e.

$$\varepsilon = -3H = \frac{3\pi^2 N_c^2 T^4}{128}\left(3-\sqrt{1-\left(\frac{\mu/T}{\pi/\sqrt{2}}\right)^2}\right)^3\left(1+\sqrt{1-\left(\frac{\mu/T}{\pi/\sqrt{2}}\right)^2}\right), \tag{3.99}$$

where the temperature T is given by Eq. (3.41). Hence, far-from-equilibrium solutions with different values of μ/T will have different energy density and equilibrium pressure.

Furthermore, since the 1RCBH model is a conformal theory, one cannot use only v to measure the time evolution of the fields, i.e. one needs to compose this EF time with another quantity to produce a dimensionless time measure. Thus, since the temperature T will be the same for all the numerical simulations, as explained in Sec. 3.4.2, the dimensionless quantity that we use to measure the time flow is vT. A different approach, which we do not explore in this chapter, would be to fix the energy density for all the values of μ/T and let the temperature T vary among the solutions; in this case, one would use the dimensionless quantity $v\varepsilon^{1/4}$ to compare the time evolution between different values of μ/T. This is scheme will be explored in Sec. 4 and it is also done in Ref. [168].

[13]Note that these are initial profiles for the subtracted dilaton field defined in Eqs. (3.81). Therefore, the full initial dilaton profile $\phi(v_0,u) = u^2\phi_s(v_0,u)$ vanishes at the boundary $u = 0$ for all these initial data, as it should be.

3.4.4 Numerical techniques

In this work, in order to deal with the radial part of the system of PDEs (3.82a)—(3.82f) we developed a new numerical code that employs the so-called pseudospectral (or collocant) method [230–232], which is a widespread technique used to solve the equations of motion in the characteristic formulation of numerical relativity due to its accuracy and rapid convergence.

The main idea behind the pseudospectral method is to expand the numerical solution in terms of functions that form a complete basis, converge, and are easy to compute. One family of functions that accomplishes these demands are the Chebyshev polynomials of the first kind, $T_n(x)$. Indeed, for well-behaved functions, the convergence of the numerical solution is exponential with respect to the number of added polynomials [230,231]. A simple example where the solution is not so well-behaved occurs when there are logarithmic terms in the near-boundary expansion of the bulk fields; this situation led the authors of Ref. [233] to favor the Runge-Kutta method to solve the radial part of the PDEs.

Assuming that the domain of interest is $u \in [0,1]$, which is the case throughout this work, we write the numerical approximation $X_N(u)$ of a function $X(u)$ as,

$$X(u) \approx X_N(u) = \sum_{k=0}^{N-1} a_k T_k(2u-1), \tag{3.100}$$

where $\{a_k\}$ is the set of spectral coefficients. In the problem that we are interested to solve here, $X(u)$ represents the elements of the set $\{\Sigma_s, (d_+\Sigma)_s, \mathcal{E}, B_s, (d_+B)_s, \phi_s, (d_+\phi)_s, A_s\}$.

In the numerical calculation one needs to specify the set of grid points $\{u_i\}$ where the discretized equations of motion take place. For this work, we adopt the Chebyshev-Gauss-Lobatto grid, which is given by

$$u_k = \frac{1}{2}\left(1 + \cos\left(\frac{k\pi}{N-1}\right)\right), \quad k = 0, \ldots, N-1, \tag{3.101}$$

where N is the number of grid points, also known as the collocant points.

Another important representation of X_N is given in terms of the values it assumes at the grid points, i.e.

$$X_N(u_i) = \sum_{j=0}^{N-1} C_j(u_i) X_j, \tag{3.102}$$

where $C_i(u)$ is the cardinal function defined as

$$C_i(u) = \prod_{j=0, j\neq i}^{N-1} \frac{u-u_j}{u_i-u_j}, \tag{3.103}$$

which satisfies the condition,

$$C_j(u_i) = \delta_{ij}. \tag{3.104}$$

It is then evident that the set of coefficients $\{X_i\}$ are precisely the values of $X_N(u_i)$. Moreover, the description of the problem in terms of $\{X_i\}$ is completely equivalent to the description in terms of the spectral coefficients $\{a_i\}$, the choice between them being just a matter of convenience. In this work, in particular, we will solve the PDEs (3.82a)-(3.82f) using the cardinal basis representation (3.102) to get $\{X_i\}$.

The last element that we need to define before numerically solving the equations of motion is the pseudospectral differentiation matrix, D_{ij}, which provides the discrete version of $X'(u)$, i.e. $X'_i = D_{ij}X_j$. To obtain this matrix, one needs to go through the derivation of the cardinal functions. Here we just give the final form of the differentiation matrix [230]:[14]

$$D_{ij} = \left.\frac{dC_j}{du}\right|_{u=u_i} = \begin{cases} (1+2(N-1)^2)/6 & i=j=0, \\ -(1+2(N-1)^2)/6 & i=j=N-1, \\ -u_j/(2(1-u_j^2)) & i=j; 0<j<N-1, \\ (-1)^{i+j}p_i/(p_j(u_i-u_j)) & i\neq j, \end{cases} \tag{3.105}$$

where $p_0 = p_{N-1} = 2$ and $p_i = 1$ otherwise. A nice property of D_{ij} is that, to obtain higher order derivatives, one just needs to exponentiate this matrix

$$D^{(n)}_{ij} = (D^n)_{ij}, \tag{3.106}$$

where n is the order of the desired derivative. The discretized version of the differential equations acquire then the following generic form

$$Q_X \vec{X} = \vec{f}_X, \tag{3.107}$$

where Q_X is a $N \times N$ matrix and $\vec{f}_X$ is a vector with N components. Hence, we have transformed a continuum differential problem into a linear algebra problem, i.e. an inversion matrix problem since the solution of Eq. (3.107) is given by

$$\vec{X} = Q_X^{-1}\vec{f}_X. \tag{3.108}$$

We note that when going from Eq. (3.107) to Eq. (3.108) we assumed that Q_X is invertible.

[14] One can obtain the differentiation matrix in Mathematica using the command: `NDSolve‘FiniteDifferenceDerivative[1,ugrid,DifferenceOrder->N-1]["DifferentiationMatrix"]` where `ugrid` denotes the radial grid and `N` is the number of collocant points.

This is not always true. Indeed, in many cases one needs to add an initial/boundary condition to the original Eq. (3.107) to obtain an invertible matrix.

At this stage it is instructive to give a simple example to see what should be the form of Q_X and $\vec{f}_X$. For instance, the following second order differential equation

$$X''(u) = 2, \tag{3.109}$$

assumes a discretized version given by,

$$(D^2)_{ij} X_j = (2, \ldots, 2)_i, \tag{3.110}$$

which means that $Q_X = D^2$ and $\vec{f}_X = (2, \ldots, 2)^T$. Now the discussion regarding the solution of the radial part of the equations of motion is almost done, we only have to discuss the filtering process.

In our calculations, we have found the common "aliasing" (a.k.a. "spectral blocking") problem where high frequency modes have spurious growth and contaminate the numerical computation until it eventually breaks down. Such issue is typical in problems involving nonlinear equations [230,231]. To circumvent this problem, we need to access the spectral coefficients a_i and perform a "damping" on the higher modes. To go from $\{X_i\}$ to $\{a_i\}$ we use the Matrix Multiplication Transform (MMT) as defined in Ref. [230],

$$a_i = M_{ij} X_j, \tag{3.111}$$

where

$$M_{ij} = \frac{w(j)\, T_i(2u_{j+1} - 1)}{(T_i, T_i)}, \tag{3.112}$$

with

$$w(i) = \frac{\pi}{N-1}\left[1 - \frac{\delta_{i,0} + \delta_{i,N-1}}{2}\right], \tag{3.113}$$

denoting the Gaussian quadrature weight function and (T_i, T_i) denoting the scalar product,

$$(T_i, T_i) \equiv \begin{cases} \pi & i \in \{0, N-1\}, \\ \pi/2 & i \notin \{0, N-1\}. \end{cases} \tag{3.114}$$

Our damping process, in particular, is very efficient. For instance, if we take $N = 40$ as the number of radial grid points, setting the last three spectral coefficients to zero at each time step suffices to produce a well behaved numerical evolution. We illustrate this

process schematically below[15]

$$\{X_i\} \xrightarrow{M} \{a_i^{\text{aliased}}\} \xrightarrow{\text{damp}} \{a_i^{\text{anti-aliased}}\} \xrightarrow{M^{-1}} \{X_i^{\text{filtered}}\}. \tag{3.115}$$

For the time evolution we have used the Adams-Bashforth (AB) method, which is a well-known explicit multi-step method employed to solve ordinary differential equations. In particular, the third order AB formula is given by

$$\vec{X}_{n+1} = \vec{X}_n + \frac{\Delta t}{12}\left(23\vec{X}_n - 16\vec{X}_{n-1} + 5\vec{X}_{n-2}\right), \tag{3.116}$$

where the subscript n denotes the position of the variable at the nth time step and Δt is the time step value. Furthermore, since the AB method (3.116) requires the time derivative of several previous steps it needs to be initialized with another method. In this work we used the Euler method for the first three steps.

3.5 Equilibration dynamics: results for different initial data

After the detailed discussion carried out in the previous sections, we are finally in position to perform the full numerical evolution of the nonlinear PDEs of the 1RCBH model in their numerical form (3.82a)—(3.82f). Next, we present the results for the homogeneous equilibration of the 1RCBH plasma for different initial data given in Eqs. (3.94), (3.95) and Eqs. (3.96)—(3.98).

3.5.1 Constant metric anisotropy and dilaton profiles

We begin by discussing the results for the initial data specified in Eqs. (3.95) and (3.96), i.e. when the initial profiles for the metric anisotropy $B_s(v_0, u)$ and the dilaton field $\phi_s(v_0, u)$ are both constant with respect to the radial coordinate u. We are going to consider here the values

$$B_s(v_0, u) = 2 \quad \text{and} \quad \phi_s(v_0, u) = -\sqrt{\frac{2}{3}}Q^2, \tag{3.117}$$

which are similar to the first condition probed in Ref. [229].

In Fig. 3.3 we show a 3D plot with the time evolution of B_s and ϕ_s for $\mu/T = 2$. As discussed before, we choose the dimensionless quantity vT to represent the time flow in

[15] Another common way to do the filtering process is to use the Fast Fourier Transform (FFT). This is explained in the review [59] and it is also used, e.g., in Ref. [185].

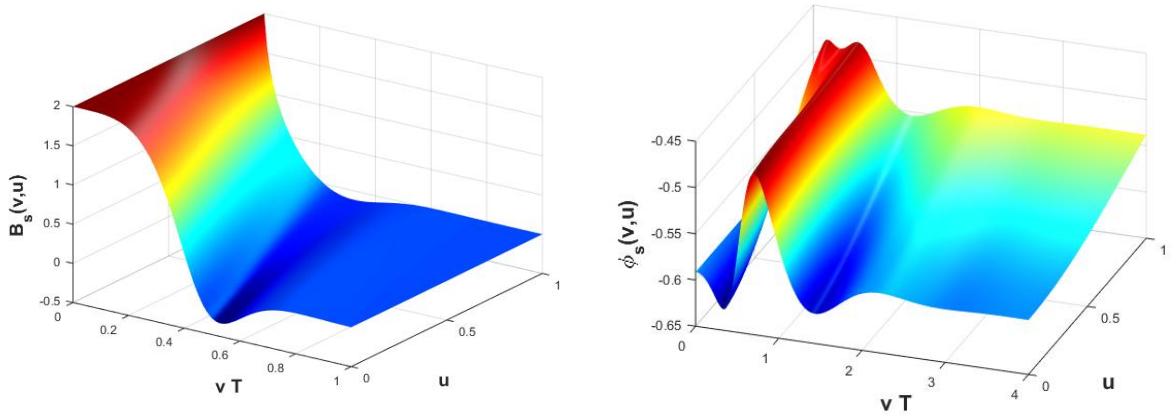

Figure 3.3: *Results for the time evolution of some fields involved in the 1RCBH setup for the initial condition* (3.117) *with* $\mu/T = 2$*: (a) the subtracted metric anisotropy function* $B_s(v,u)$*, and (b) the subtracted dilaton field* $\phi_s(v,u)$*.*

the CFT. With B_s and ϕ_s now fully determined, one may compute the time evolution of the pressure anisotropy Δp (3.78b) and the scalar condensate $\langle \mathcal{O}_\phi \rangle$ (3.78d).

The results for the isotropization process describing how the pressure anisotropy Δp goes to zero as the time evolves, taking into account the initial condition (3.117), are shown in Fig. 3.4. In Fig. 3.4 (a), where Δp is normalized by the (equilibrium) temperature to the fourth, one notes that at the earliest times the pressure anisotropy in insensitive to the value of the dimensionless chemical potential μ/T which, however, becomes relevant as the time evolves. In fact, as we shall discuss in Sec. 3.5.7, the isotropization time (which cannot be adequately resolved by eyeball in the scale of the plot shown in Fig. 3.4 (a)) has a non-monotonic dependence on the value of μ/T, which is a direct consequence of the presence of a critical point in the phase diagram of the 1RCBH model. Namely, as it will become clear in the analysis of Sec. 3.5.7, the isotropization time may decrease or increase for increasing values of μ/T depending on whether μ/T is far or close enough to the critical point, respectively. This is very different from what happens e.g. in the case of the AdS-Reissner-Nordstrom background investigated in Ref. [168], which does not feature a critical point in its phase diagram. It is also interesting to note that, as anticipated around Eq. (3.99), the equilibrium pressure (and energy density) depends on the chosen value of μ/T, which is clear from the curves shown in Fig. 3.4 (b), where Δp is normalized by the equilibrium pressure. Moreover, we have verified the effect on the isotropization time obtained by varying the value of the initial metric anisotropy and the effect was negligible. For instance, if one doubles the initial anisotropy, the only effect is to have a steeper downfall of Δp before it reaches the first minimum. The explanation for this is the surprising low nonlinearity of the system [229, 234], which is also quantitatively

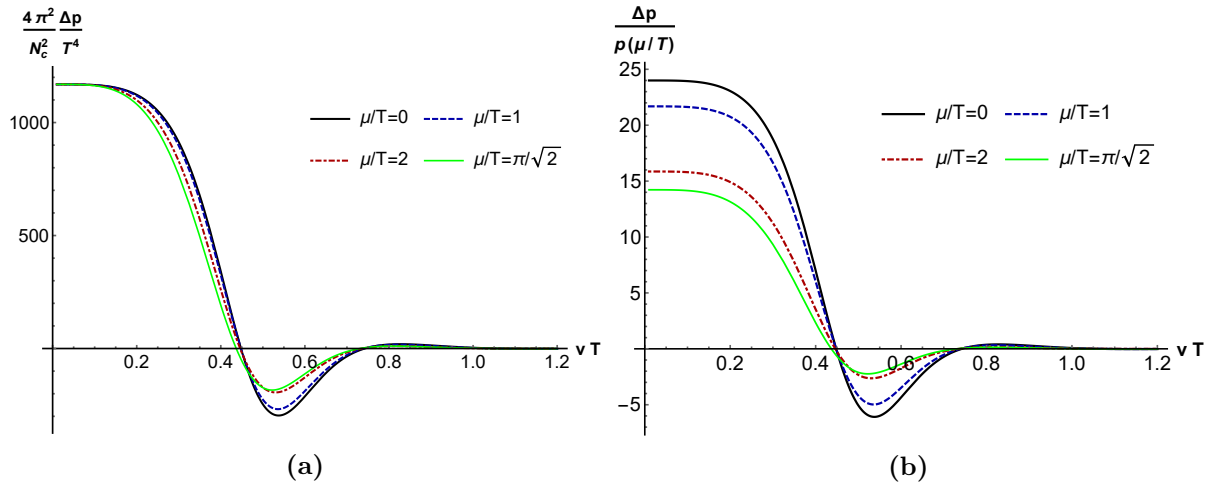

Figure 3.4: *Time evolution of the pressure anisotropy for several values of the chemical potential using the initial data (3.117): (a) Δp normalized by the (equilibrium) temperature to the fourth, and (b) Δp normalized by the equilibrium pressure.*

explored at length in Ref. [168].

The time evolution of the scalar condensate $\langle \mathcal{O}_\phi \rangle$ for different values of μ/T is presented in Fig. 3.5. The first remarkable feature of the time evolution of the scalar condensate is that it takes a much longer time to relax to equilibrium than the pressure anisotropy. This is the reason why we adopted the equilibration time associated with the relaxation of the scalar condensate toward equilibrium as the true thermalization time of the 1RCBH plasma. We also observe a qualitatively different behavior for the dependence of the thermalization time with μ/T when compared to the corresponding dependence of the isotropization time (note also that in the case of the AdS-Reisser-Nordstrom background studied in Ref. [168], spatially homogeneous isotropization corresponds already to the true thermalization of the system since there is no scalar condensate in that case). The thermalization time associated with the relaxation of the scalar condensate always increases with increasing μ/T. It is also interesting to note the qualitative similarity between the time evolution of $\langle \mathcal{O}_\phi \rangle$ and the thermalization process of confining theories studied in Ref. [233] using holographic quenches, even though the 1RCBH model is non-confining.

3.5.2 Constant metric anisotropy profile and Gaussian dilaton profile

In this subsection we study the time evolution of the system given the initial data:

$$B_s(v_0, u) = 2 \quad \text{and} \quad \phi_s(v_0, u) = 0.5\, e^{-100(u-0.3)^2}, \tag{3.118}$$

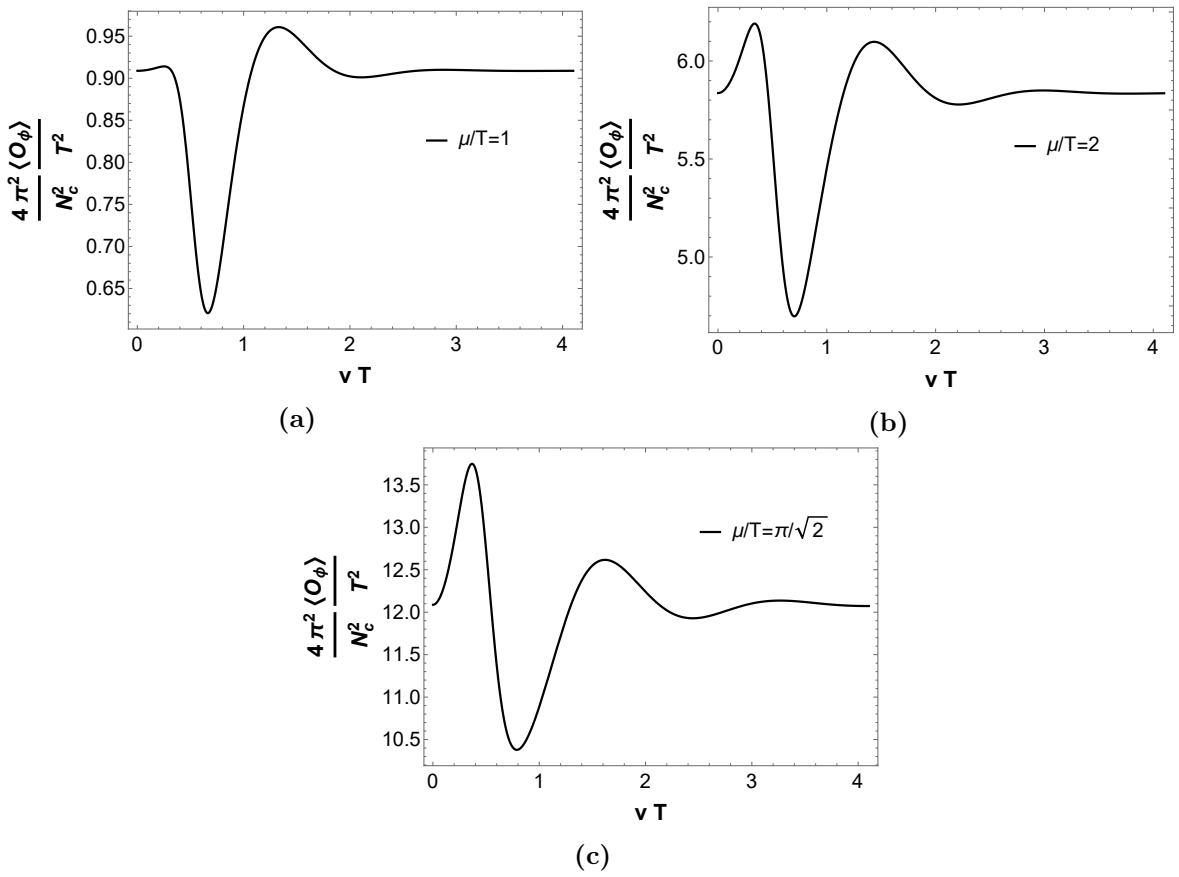

Figure 3.5: *Time evolution of the scalar condensate* $\langle \mathcal{O}_\phi \rangle$ *for different* μ/T *using the initial data* (3.117).

where we kept the same constant initial metric anisotropy as before but changed the initial condition for the dilaton field and considered now a Gaussian profile. This is a way to look for possible new features depending mostly on the choice for the initial dilaton profile.

In Fig. 3.6 we display a 3D plot with the time evolution of $B_s(v,u)$ and $\phi_s(v,u)$ for $\mu/T = 2$ and the initial conditions set by Eq. (3.118). By comparing with Fig. 3.3, one notes that the evolution of the metric anisotropy is not very sensitive to the variation of the initial profile for the dilaton field. On the other hand, as expected, the evolution of the dilaton field is significantly affected by the choice of its initial value. This seems to suggest that the backreaction produced on the metric anisotropy by varying the initial profile for the dilaton is small, which will be confirmed in the course of the next subsections.

In Fig. 3.7 we show our results for the time evolution of the pressure anisotropy Δp for different values of μ/T and the initial conditions given in Eq. (3.118). By comparing with the results obtained in the previous subsection, displayed in Fig. 3.4, one notes that the pressure anisotropy does not change much by varying the initial condition for the dilaton, if we keep fixed the constant initial metric anisotropy. This is a direct consequence of the

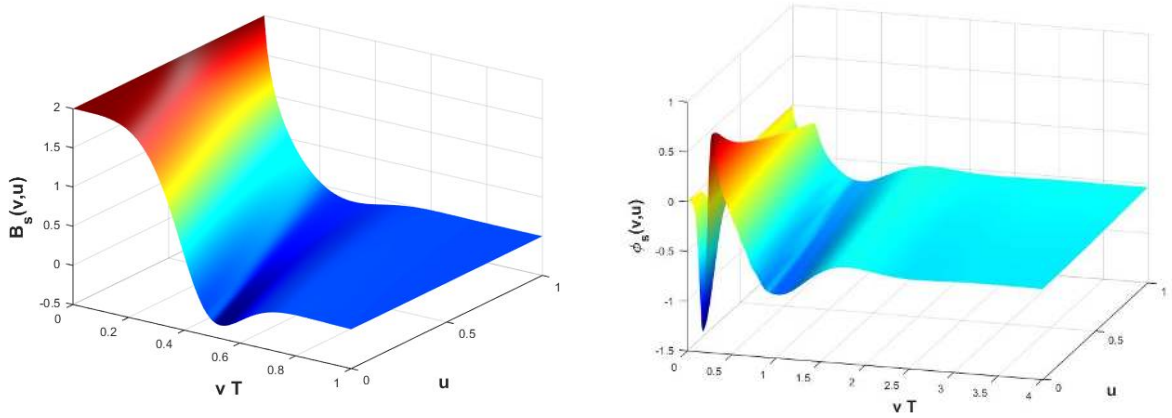

Figure 3.6: *Results for the time evolution of some fields involved in the 1RCBH setup for the initial condition* (3.118) *with* $\mu/T = 2$*: (a) the subtracted metric anisotropy function* $B_s(v,u)$*, and (b) the subtracted dilaton field* $\phi_s(v,u)$*.*

previously mentioned robustness of the metric anisotropy against variations of the initial dilaton profile. On the other hand, the early time dynamics of the scalar condensate $\langle \mathcal{O}_\phi \rangle$ displayed in Fig. 3.8 is very different from the result obtained in the previous subsection and shown in Fig. 3.5, while its late time dynamics is remarkably similar for the two different set of initial conditions given in Eqs. (3.118) and (3.117). Moreover, the same observations done in the previous subsection, that the thermalization time associated with the equilibration of the scalar condensate only happens significantly after the system has already relaxed to an (approximately) isotropic state, and that this thermalization time always increases with increasing μ/T, also hold for the initial conditions given in Eq. (3.118). As we are going to see in the next subsections, these qualitative trends hold for all the different initial conditions considered in the present work, suggesting that they are general features of the equilibration process of the 1RCBH plasma.

3.5.3 Constant metric anisotropy profile and equilibrium dilaton profile

In this subsection we study the time evolution of the system given the initial data:

$$B_s(v_0,u) = 2 \quad \text{and} \quad \phi_s(v_0,u) = -\frac{1}{u^2}\sqrt{\frac{2}{3}}\ln\left(1+\tilde{u}(u)Q^2\right), \tag{3.119}$$

where we kept the same constant initial metric anisotropy as in the two previous subsections but considered now the initial dilaton profile discussed in Eq. (3.98), corresponding to the equilibrium value of the dilaton field.

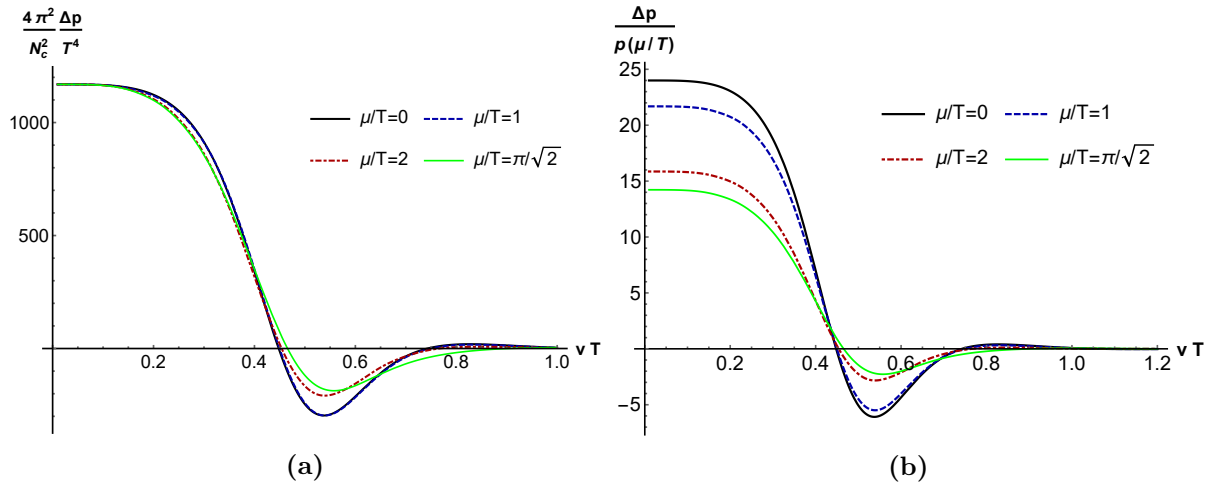

Figure 3.7: *Time evolution of the pressure anisotropy for several values of the chemical potential using the initial data (3.118): (a) Δp normalized by the (equilibrium) temperature to the fourth, and (b) Δp normalized by the equilibrium pressure.*

In Fig. 3.9 we display a 3D plot with the time evolution of $B_s(v,u)$ and $\phi_s(v,u)$ for $\mu/T = 2$ and the initial conditions set by Eq. (3.119). By comparing with the results in the two previous subsections, one confirms once again the robustness of the time evolution of the metric anisotropy against different choices for the initial dilaton profile.

In Fig. 3.10 we display our results for the time evolution of the pressure anisotropy, which are similar to what we have found in the two previous subsections. Regarding the time evolution of the scalar condensate shown in Fig. 3.11, we see that its early time dynamics is different from the previous cases considered here, although its late time dynamics is very similar to those found before. Furthermore, one also notes that in the present case where the initial condition for the dilaton is already its equilibrium value that the fluctuations in the value of the dilaton as time evolves are generally small. This is expected since in the present case the far-from-equilibrium dynamics of the system is being initially driven solely by the metric anisotropy.

3.5.4 Gaussian metric anisotropy profile and constant dilaton profile

Now we consider a different set of initial conditions to scan out possible new features in the equilibration dynamics of the 1RCBH plasma as a function of the chosen initial data. We change the initial metric anisotropy profile $B_s(v_0,u)$ but use the same constant initial profile for the dilaton field $\phi_s(v_0,u)$ as in subsection 3.5.1, which is a way to probe if there are some new features depending mostly on the chosen initial anisotropy. We present in this subsection the results for a Gaussian initial metric anisotropy (3.94), which is perhaps the most common initial condition chosen for this field, combined with a constant initial

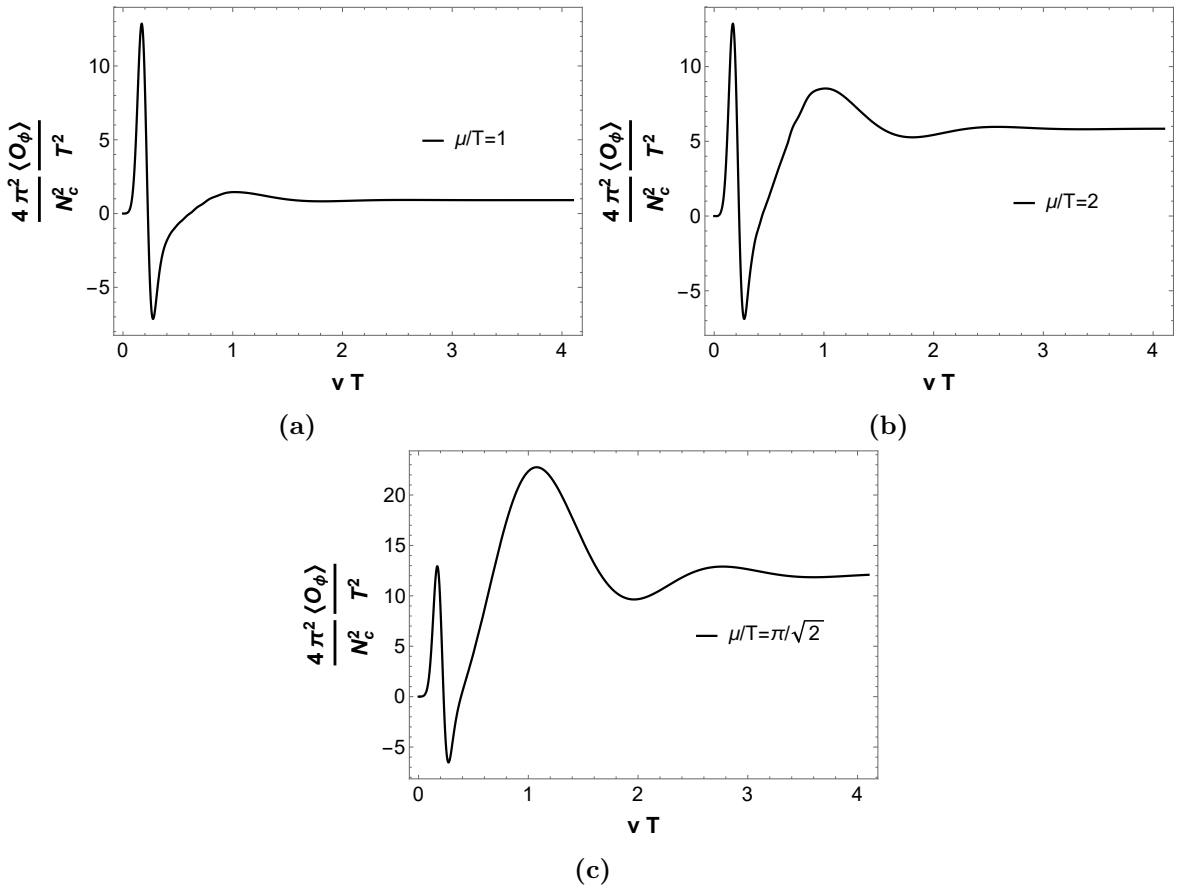

Figure 3.8: *Time evolution of the scalar condensate* $\langle \mathcal{O}_\phi \rangle$ *for different* μ/T *using the initial data* (3.118).

profile for the dilaton field (3.96)

$$B_s(v_0, u) = 0.5\, e^{-100(u-0.4)^2} \quad \text{and} \quad \phi_s(v_0, u) = -\sqrt{\frac{2}{3}} Q^2, \tag{3.120}$$

where the Gaussian initial anisotropy was chosen to be more or less half-way between the black hole horizon and the boundary.

In Fig. 3.12 we show a 3D plot with the time evolution of $B_s(v, u)$ and $\phi_s(v, u)$ using the initial condition given in Eq. (3.120) and $\mu/T = 2$. The shape of both functions are very different than the case considered in subsection 3.5.1, whose results are displayed in Fig. 3.3 and where the initial condition for the dilaton was the same as in Eq. (3.120) but the initial metric anisotropy was constant. This signalizes a strong backreaction induced on the dilaton field by changing the initial metric anisotropy, in contrast to the general trend observed in the previous subsections that the backreaction induced on the metric anisotropy by changing the initial dilaton profile is quite small. These general features of the far-from-equilibrium 1RCBH plasma will be further confirmed in subsections 3.5.5 and 3.5.6.

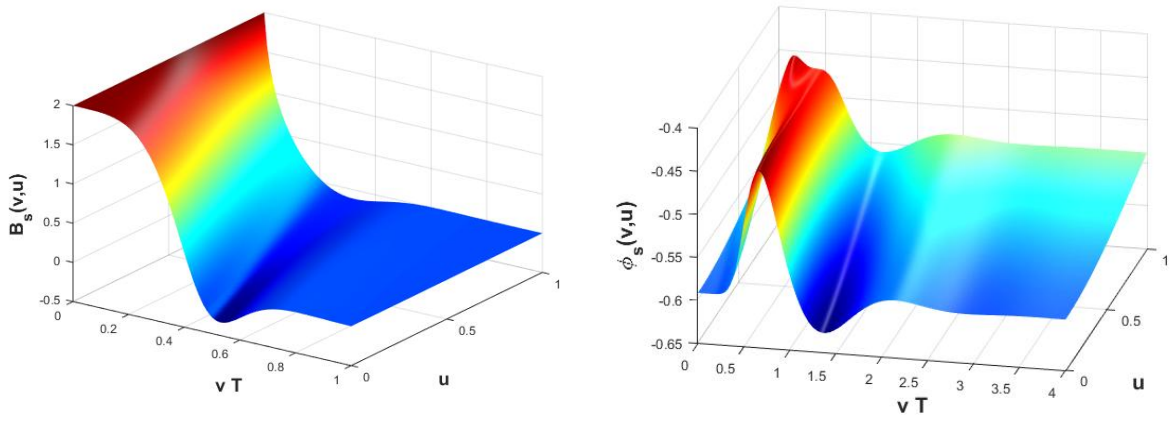

Figure 3.9: *Results for the time evolution of some fields involved in the 1RCBH setup for the initial condition* (3.119) *with* $\mu/T = 2$*: (a) the subtracted metric anisotropy function* $B_s(v,u)$*, and (b) the subtracted dilaton field* $\phi_s(v,u)$*.*

The time evolution of the pressure anisotropy Δp that we obtain from the boundary value of $B_s(v,u)$ in the present case is shown in Fig. 3.13. One can see that the early time dynamics of the pressure anisotropy in the case of the initial condition set in Eq. (3.120) is completely different than the one obtained in Fig. 3.4 by considering the initial condition given by Eq. (3.117). In particular, the isotropization time has significantly decreased by considering a Gaussian initial metric anisotropy when compared to the isotropization times associated with a constant initial metric anisotropy analyzed in the previous subsections.

The time evolution of the scalar condensate $\langle \mathcal{O}_\phi \rangle$ for the initial condition (3.120) is shown in Fig. 3.14. Compared with the result presented in Fig. 3.5 using a constant initial anisotropy (3.117), we note that the early time dynamics of $\langle \mathcal{O}_\phi \rangle$ is very different depending on the chosen initial data. However, the late time dynamics of the scalar condensate and the associated thermalization time are actually very similar for both sets of initial conditions. These observations are in agreement with the general trend observed in the previous subsections and will be further confirmed in the course of the next subsections.

3.5.5 Gaussian metric anisotropy and dilaton profiles

Now we change the initial dilaton profile $\phi_s(v_0,u)$ but maintain the prior parametrization for the initial metric anisotropy $B_s(v_0,u)$

$$B_s(v_0,u) = 0.5\, e^{-100(u-0.4)^2} \quad \text{and} \quad \phi_s(v_0,u) = 0.5\, e^{-100(u-0.3)^2}, \tag{3.121}$$

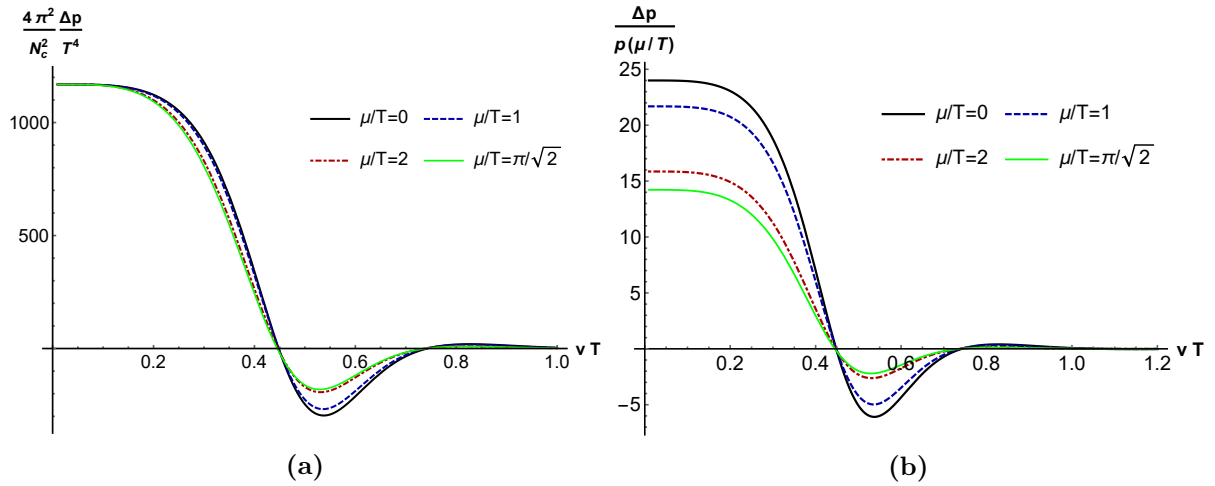

Figure 3.10: *Time evolution of the pressure anisotropy for several values of the chemical potential using the initial data (3.119): (a) Δp normalized by the (equilibrium) temperature to the fourth, and (b) Δp normalized by the equilibrium pressure.*

where $B_s(v_0, u)$ is kept the same as in the analysis of the previous subsection. Moreover, we also considered different values for $B_s(v_0, u)$ and $\phi_s(v_0, u)$ with the same functional forms provided in Eq. (3.121) and the results follow the same general behavior as the ones obtained with this equation.

The 3D plot with the time evolution of $B_s(v, u)$ and $\phi_s(v, u)$ is shown in Fig. 3.15 for the initial condition (3.121) and $\mu/T = 2$. From this plot, it is evident the similarity of the shape of the metric anisotropy $B_s(v, u)$ with the previous result shown in 3.12, i.e. a different parameterization for the initial dilaton profile $\phi_s(v_0, u)$ has essentially no effect on the time evolution of the metric anisotropy. On the other hand, one notes a very different time evolution for the dilaton $\phi_s(v, u)$, which is expected since we changed the initial parameterization of this field.

As a direct consequence of the features above, the time evolution of the pressure anisotropy Δp depicted in Fig. 3.16 is essentially the same as in the previous case shown in Fig. 3.13. The difference between them can be barely seen (what configures an even stronger test of robustness than observed before by considering initial conditions with a fixed constant initial metric anisotropy), indicating that the pressure anisotropy is remarkably robust against the addition of other fields in the gravitational action besides the metric. On the other hand, the early time dynamics of the scalar condensate $\langle \mathcal{O}_\phi \rangle$ presented in Fig. 3.17 is very different from the previous case shown in Fig. 3.14, although its late time dynamics and the associated thermalization time are very similar to the ones obtained in the previous subsections.

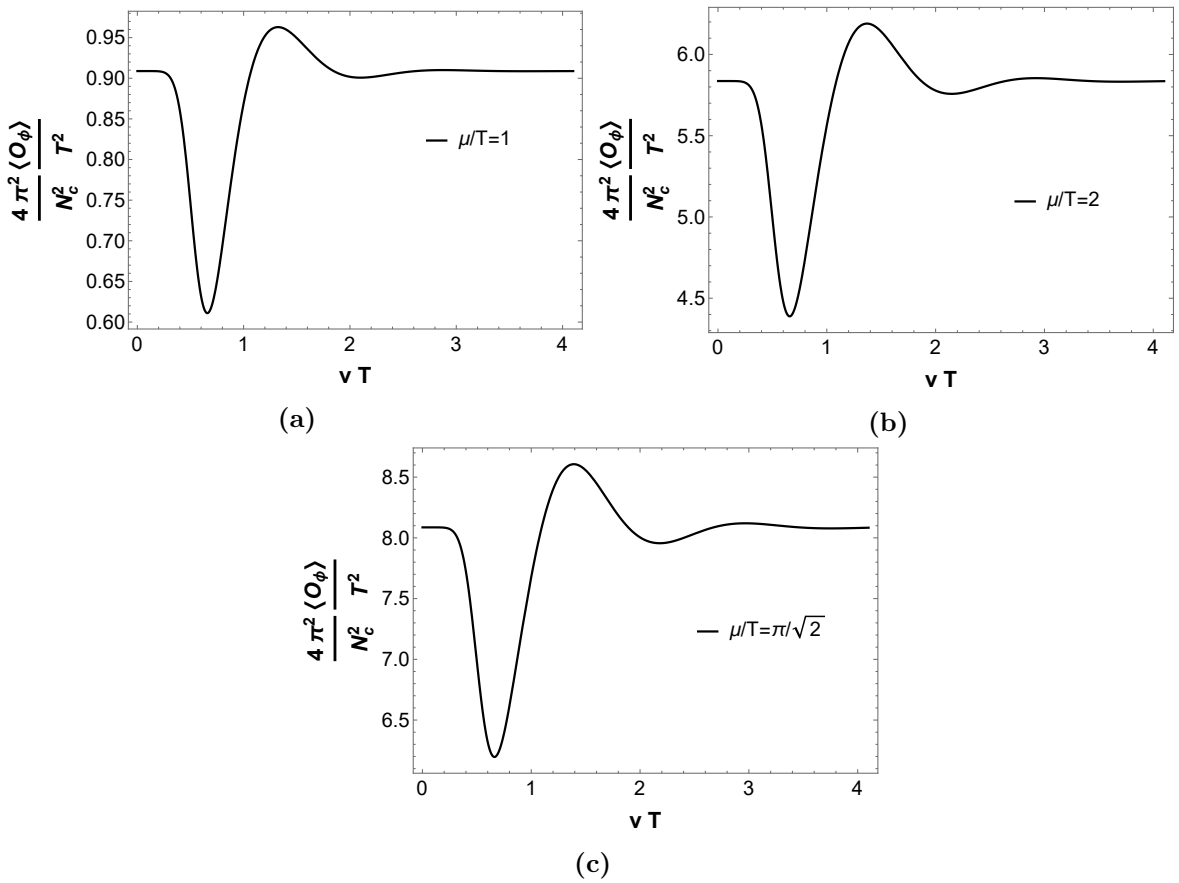

Figure 3.11: *Time evolution of the scalar condensate $\langle \mathcal{O}_\phi \rangle$ for different μ/T using the initial data (3.119).*

3.5.6 Gaussian metric anisotropy profile and equilibrium dilaton profile

Finally, the last case which remains to be analyzed corresponds to the initial condition with Gaussian initial metric anisotropy and an initial profile for the dilaton field equal to its equilibrium value

$$B_s(v_0,u) = 0.5\, e^{-100(u-0.4)^2} \quad \text{and} \quad \phi_s(v_0,u) = -\frac{1}{u^2}\sqrt{\frac{2}{3}}\ln\left(1+\tilde{u}(u)Q^2\right). \tag{3.122}$$

In Fig. 3.18 we present the 3D plot with the time evolution of $B_s(v,u)$ and $\phi_s(v,u)$ using the initial condition (3.122) and $\mu/T = 2$. As before, the metric anisotropy $B_s(v,u)$ is effectively unaffected by the change done in the initial condition for the dilaton field, while the dilaton profile $\phi_s(v,u)$ has only very small fluctuations in time, which is expected since we have already started the numerical simulations in the present case with an initial dilaton profile equal to its value in thermodynamic equilibrium. The pressure anisotropy evolves in time according to Fig. 3.19, which displays essentially the very same behavior

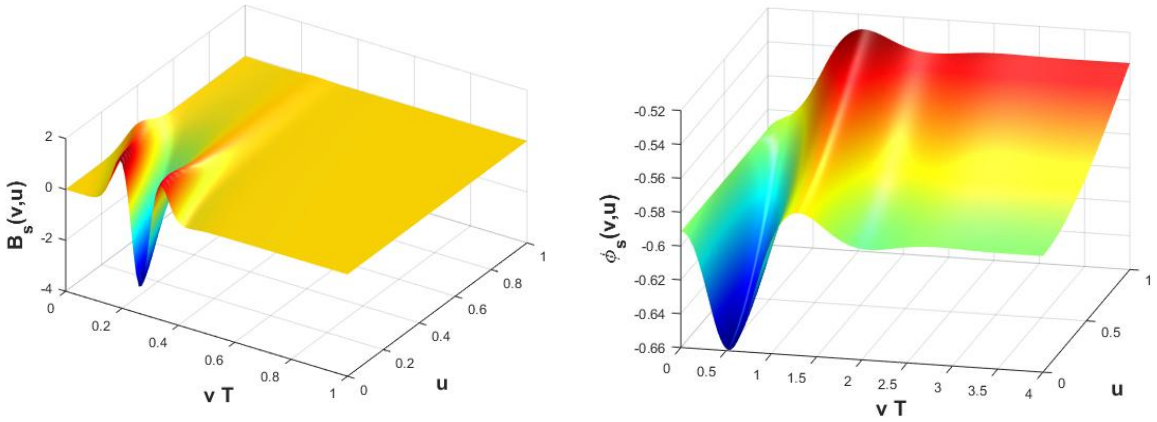

(a) (b)

Figure 3.12: *Results for the time evolution of some fields involved in the 1RCBH setup for the initial condition* (3.120) *with* $\mu/T = 2$*: (a) the subtracted metric anisotropy function* $B_s(v,u)$*, and (b) the subtracted dilaton field* $\phi_s(v,u)$*.*

found in the last two subsections. On the other hand, the early time dynamics of the scalar condensate depicted in Fig. 3.20 is different than what we have seen in the previous subsection, displaying only very small fluctuations in time. In any case, the thermalization time associated with the equilibration of the scalar condensate is found to be very similar to what has been observed in all the previous cases considered here.

Therefore, after we have exhausted the analysis of the selected sets of initial conditions, we may draw some general conclusions for the homogeneous equilibration dynamics of the 1RCBH plasma analyzed here:

1. The backreaction produced in the time evolution of the dilaton field by changing the initial metric anisotropy is extremely large, in contrast to what happens with the backreaction produced on the time evolution of the metric anisotropy by changing the initial dilaton profile, which is small. This implies that the pressure anisotropy is robust against the addition of other fields in the gravitational action besides the metric;

2. The isotropization (associated with the approximate vanishing of the pressure anisotropy Δp) always happen (well) before the true thermalization of the system (associated with the equilibration of the scalar condensate $\langle \mathcal{O}_\phi \rangle$);

3. Regarding the late time dynamics of the scalar condensate and the associated thermalization time, these are robust features of the medium which remain almost unchanged regardless of the initial conditions considered. In particular, the thermalization time always increases with increasing chemical potential. On the other hand,

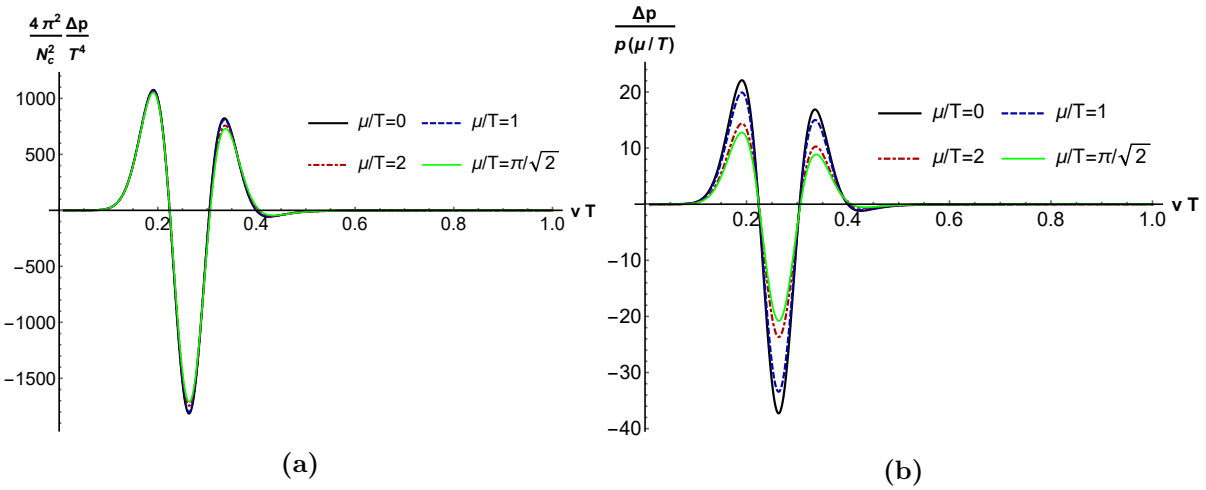

Figure 3.13: *Time evolution of the pressure anisotropy for several values of the chemical potential using the initial data (3.120): (a) Δp normalized by the (equilibrium) temperature to the fourth, and (b) Δp normalized by the equilibrium pressure.*

the early time dynamics of the scalar condensate is strongly dependent on the set of initial data chosen to seed the time evolution of the far-from-equilibrium 1RCBH plasma;

4. The time evolution of the pressure anisotropy and the associated isotropization time of the system strongly depend on the chosen initial condition for the metric anisotropy.

However, in the different cases considered above, due to the large scales plotted to cover the large amplitudes of oscillation observed in the time evolution of the pressure anisotropy, it was not possible yet to clearly reveal the crucial role played by the critical point in the isotropization of the system. We analyze this issue in detail in the next subsection, where we confront the late time dynamics of the pressure anisotropy with the lowest non-hydrodynamic QNM of the external scalar channel of the 1RCBH plasma obtained in Appendix A [146]. We also compare the late time behavior of the scalar condensate with the lowest non-hydrodynamic QNM of the dilaton channel, also derived in Appendix A.

3.5.7 Matching the quasinormal modes

In this section we compare the late time behavior of the full nonlinear evolution of the equations of motion with the quasinormal modes of the system, which describe exponentially damped collective excitations produced in response to disturbances of a black hole background (see e.g. [136, 235] for some recent reviews). The QNM spectra of the

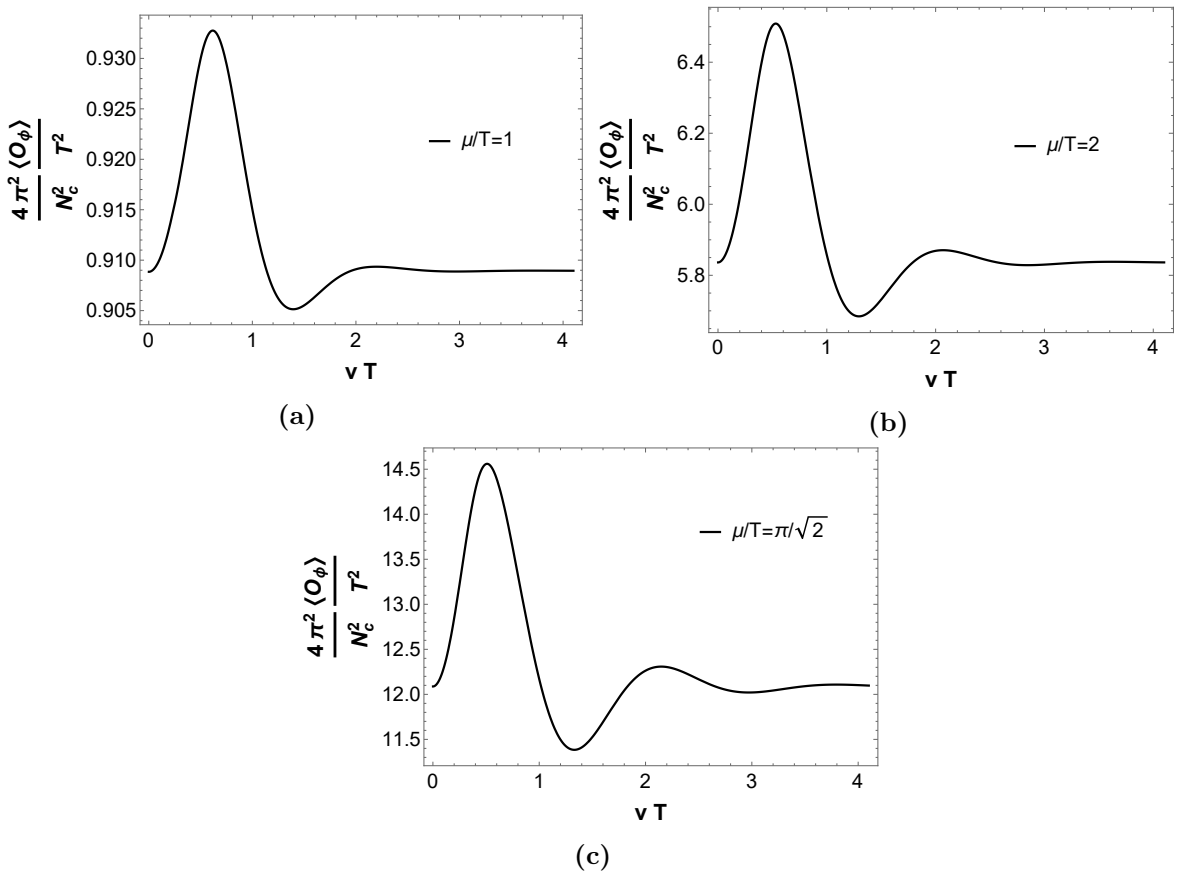

Figure 3.14: *Time evolution of the scalar condensate* $\langle \mathcal{O}_\phi \rangle$ *for different* μ/T *using the initial data* (3.120).

theory are responsible for the so-called "quasinormal ringdown" phenomenon describing the linear part of the decaying perturbations of a disturbed black hole at late times.

The purpose of this comparison is threefold: it can give a measure of the degree of nonlinearity of the full out-of-equilibrium solutions of the equations of motion[16]; it may be also used to provide an independent check of the accuracy of the numerical solutions at late times; finally, it can unveil some of the main differences between the early and the late time equilibration dynamics of the system.

By following the classification given in Ref. [203] for the gauge and diffeomorphism invariant perturbations of the EMD fields in the homogeneous zero wavenumber limit, in which case the system has a rotational $SO(3)$ symmetry, one has three different channels to analyze corresponding to the three lowest dimensional representations of $SO(3)$: the tensor/quintuplet channel, the vector/triplet channel, and the scalar/singlet channel. By working with the non-normalizable modes[17] of each channel, one obtains the associated

[16]Note that in the analysis of QNM's, by assuming small perturbations, one just considers quadratic fluctuations of the bulk fields in the disturbed action, which gives linearized equations of motion for these perturbations.

[17]These are the solutions of the linearized equations of motion for the perturbations with the conditions

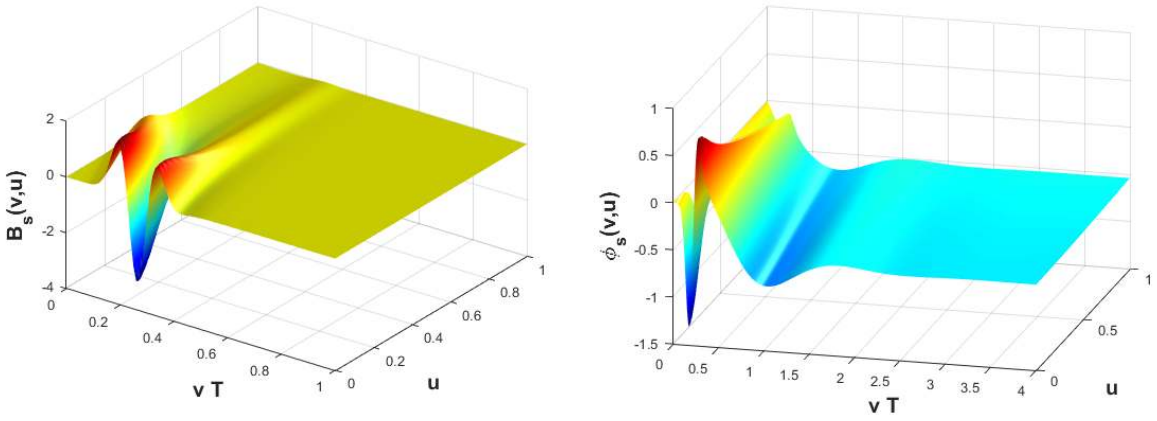

(a) **(b)**

Figure 3.15: *Results for the time evolution of some fields involved in the 1RCBH setup for the initial condition* (3.121) *with* $\mu/T = 2$*: (a) the subtracted metric anisotropy function* $B_s(v,u)$*, and (b) the subtracted dilaton field* $\phi_s(v,u)$*.*

transport coefficients through the use of Kubo formulas, namely, the shear viscosity from the $SO(3)$ quintuplet channel, the charge conductivity and diffusion from the $SO(3)$ triplet channel, and the bulk viscosity from the $SO(3)$ singlet channel [203]. On the other hand, by working with the normalizable modes[18], one obtains the QNM's of each channel. All the spectra of QNM's of the 1RCBH plasma are reviewed in the Appendix A.[19] The lowest non-hydrodynamic QNM's of the $SO(3)$ quintuplet and singlet channels will be compared in what follows with the late time dynamics of the pressure anisotropy and the scalar condensate, respectively.

In Fig. 3.21 we display our numerical results for the time evolution of the pressure anisotropy using the initial conditions set in Eq. (3.117) for different values of μ/T.[20] This time we plot the logarithmic of Δp which makes it possible to clearly resolve the late time exponential damp of the black hole oscillations. The inset displayed in Fig. 3.21 gives a zoom of the behavior of the pressure anisotropy in the far-from-equilibrium zone. To check whether the late time dynamics of the pressure anisotropy can be described by the lowest non-hydrodynamic QNM of the $SO(3)$ quintuple (external scalar) channel, we

that these perturbations are regular at the horizon and normalized to unity at the boundary.

[18]These are the solutions of the linearized equations of motions which are regular at the horizon and subjected to the Dirichlet condition that these perturbations vanish at the boundary.

[19]The $SO(3)$ quintuplet channel coincides with the perturbation for a massless external scalar field [146,203,204], while the $SO(3)$ singlet channel may be identified more generally with a so-called "dilaton channel", as we are going to explain in Appendix A.

[20]We remark that although the early time behavior of this plot changes significantly depending on the initial conditions considered, the qualitative behavior observed at late times is the same for the different initial conditions considered here.

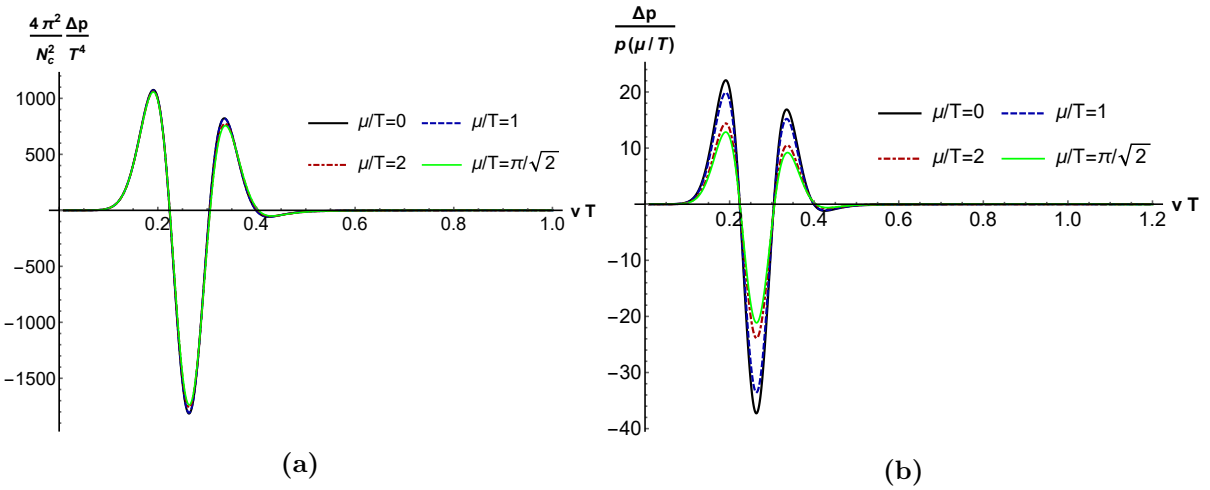

Figure 3.16: *Time evolution of the pressure anisotropy for several values of the chemical potential using the initial data (3.121): (a) Δp normalized by the (equilibrium) temperature to the fourth, and (b) Δp normalized by the equilibrium pressure.*

parametrize Δp using the following functional form

$$\frac{4\pi^2}{N_c^2}\frac{\Delta p}{T^4} = \mathsf{A}\, e^{\frac{\mathrm{Im}[\omega]}{T}\, vT} \cos\left(\frac{\mathrm{Re}[\omega]}{T}\, vT + \varphi\right), \tag{3.123}$$

where $\mathrm{Re}[\omega]/T$, $\mathrm{Im}[\omega]/T$, A, and φ are fixed by fitting the functional form (3.123) to the numerical result for the pressure anisotropy evaluated within the late time interval $vT \in [1.8, 4.1]$.[21] The relevant parameters extracted from this fitting procedure are $\mathrm{Re}[\omega]/T$ and $\mathrm{Im}[\omega]/T$, which may be then compared with the real and imaginary parts of the non-hydrodynamic QNM with lowest imaginary part (in magnitude), corresponding to the dominant, less damped mode in the external scalar channel.

Such comparison is done in Fig. 3.22, from which one notes a good agreement between the late time decay of the pressure anisotropy and the lowest non-hydrodynamic QNM of the external scalar channel obtained in Ref. [146]. Such agreement provides an independent check of the accuracy of our numerical routine at late times, as aforementioned. More importantly, we are now able to understand how the isotropization time depends on the presence of a critical point in the phase diagram of the 1RCBH plasma.

We note from Fig. 3.21 that the early time dynamics of the pressure anisotropy is qualitatively different from its late time dynamics. At early times, the pressure anisotropy is always damped as one increases μ/T, however, at late times the pressure anisotropy may decrease or increase with increasing chemical potential depending on whether the

[21] For the specific value of $\mu/T = \pi/\sqrt{2}$ (critical point), the fit interval used was $vT \in [5.0, 7.0]$, since the late time decay of the pressure anisotropy only converges to the critical behavior of the lowest non-hydrodynamic QNM of the external scalar channel at later times when compared to other values of μ/T.

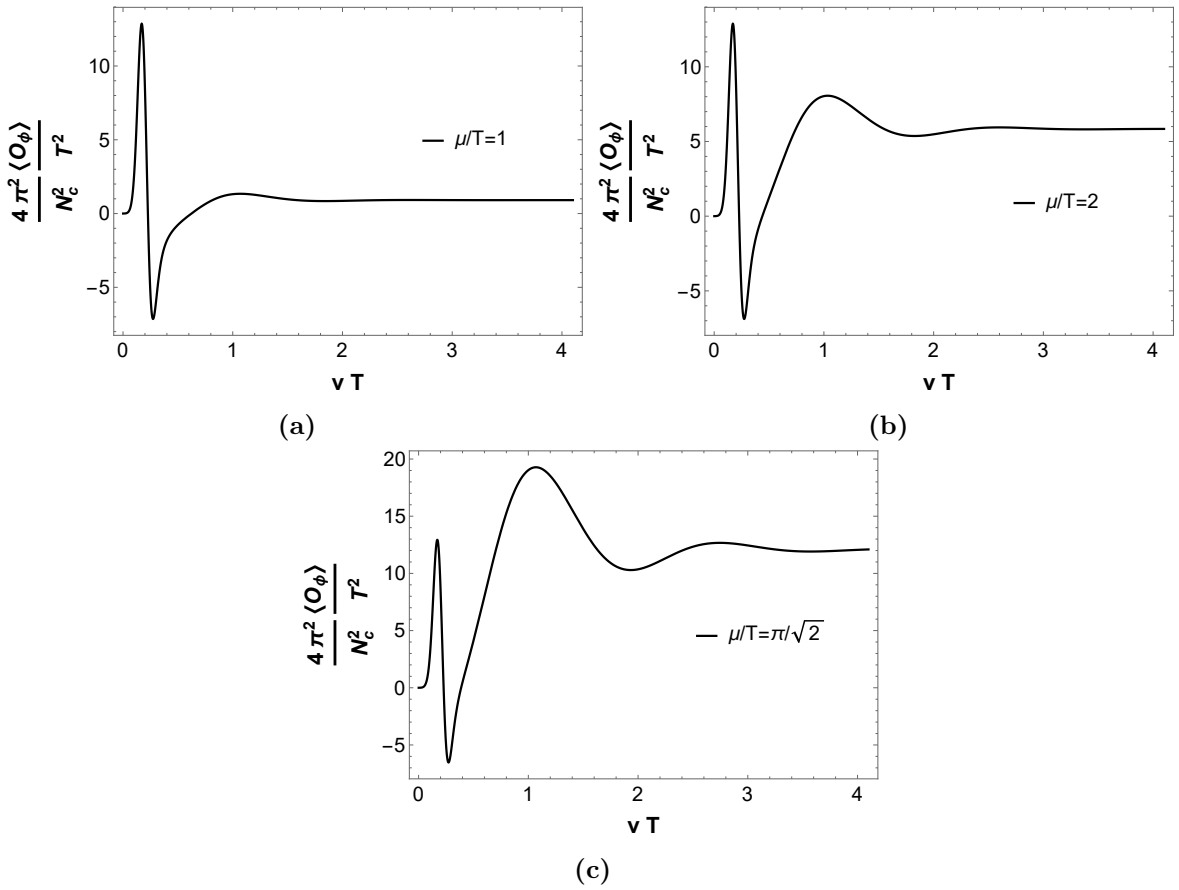

Figure 3.17: *Time evolution of the scalar condensate* $\langle \mathcal{O}_\phi \rangle$ *for different* μ/T *using the initial data* (3.121).

system is far or close enough to the critical point. Therefore, the isotropization time of the 1RCBH plasma is affected by the critical point in accordance with the behavior of the "relaxation time" extracted from the imaginary part of the lowest non-hydrodynamic QNM of the external scalar channel of the theory [146]. This is explained by the fact that, as shown in Fig. 3.22, the late time decay of the pressure anisotropy is in fact described by the lowest non-hydrodynamic QNM of the $SO(3)$ quintuplet channel.

This is qualitatively different from the thermalization time discussed before, which is associated with the equilibration of the scalar condensate. This process only sets in after a nearly isotropic state has been already achieved by the system and it always increase with increasing μ/T. In Fig. 3.23 we show our numerical results for the time evolution of the difference between the scalar condensate and its equilibrium value using the initial conditions set in Eq. (3.117) for different values of μ/T. To check whether the late time dynamics of this observable can be described by the lowest non-hydrodynamic QNM of the $SO(3)$ singlet (dilaton) channel, we parametrize it using once more the following

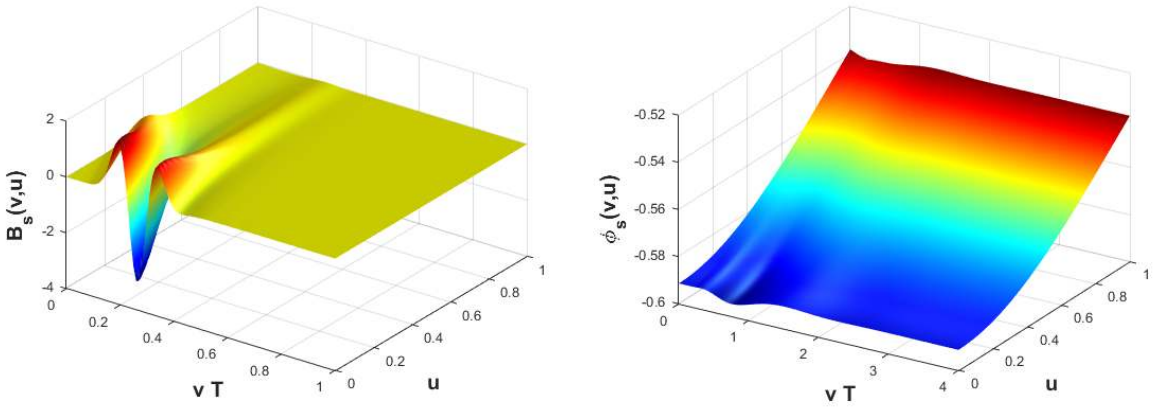

(a) **(b)**

Figure 3.18: *Results for the time evolution of some fields involved in the 1RCBH setup for the initial condition (3.122) with $\mu/T = 2$: (a) the subtracted metric anisotropy function $B_s(v,u)$, and (b) the subtracted dilaton field $\phi_s(v,u)$.*

functional form

$$\frac{4\pi^2}{N_c^2}\frac{(\langle\mathcal{O}_\phi\rangle - \langle\mathcal{O}_\phi\rangle_{\rm eq})}{T^2} = \mathsf{A}\, e^{\frac{{\rm Im}[\omega]}{T}\, vT} \cos\left(\frac{{\rm Re}[\omega]}{T}\, vT + \varphi\right), \tag{3.124}$$

where ${\rm Re}[\omega]/T$, ${\rm Im}[\omega]/T$, A, and φ are fixed by fitting the functional form (3.124) to the numerical result for the difference between the scalar condensate and its equilibrium value evaluated within the late time interval $vT \in [1.8, 4.1]$.[22]

The comparison between ${\rm Re}[\omega]/T$ and ${\rm Im}[\omega]/T$ extracted from these fits to the late time behavior of the full numerical solutions and the lowest non-hydrodynamic QNM of the dilaton channel is displayed in Fig. 3.24. One notes a good agreement between both results, which shows that the late dynamics of the scalar condensate is indeed dominated by the lowest non-hydrodynamic QNM of the dilaton channel. This also gives another independent check of the accuracy of our numerical routine at late times.

In summary, we see that the late time dynamics of the pressure anisotropy and the scalar condensate are dominated by the lowest non-hydrodynamic QNM's of the external scalar and dilaton channels, respectively. Consequently, the behavior of the isotropization and thermalization times of the 1RCBH plasma can be correctly inferred from the analysis of the QNM's of the system, even though the early time dynamics of these observables cannot be described by these linearized perturbations.

[22] At the critical point, however, we performed the fit starting from $vT = 2.2$.

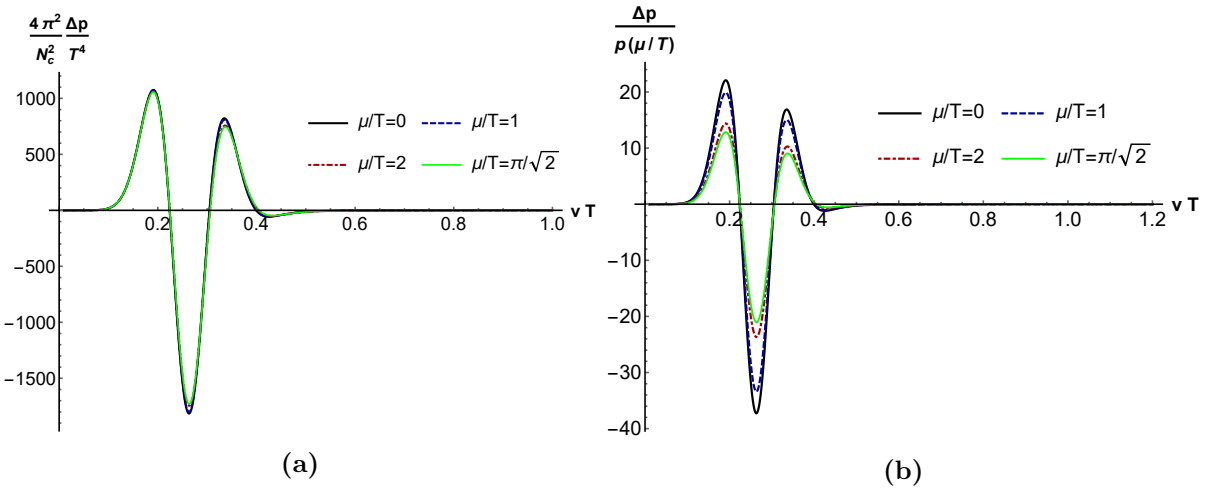

Figure 3.19: *Time evolution of the pressure anisotropy for several values of the chemical potential using the initial data (3.122): (a) Δp normalized by the (equilibrium) temperature to the fourth, and (b) Δp normalized by the equilibrium pressure.*

3.6 Conclusions of the chapter

Now we summarize the main findings of the present work concerning the spatially homogeneous equilibration dynamics of the 1RCBH plasma. The relevant one-point functions of the 1RCBH model correspond to the expectation value of the stress-energy tensor $\langle T^{\mu\nu}\rangle$ dual to the bulk metric $g_{\mu\nu}$, the scalar condensate $\langle \mathcal{O}_\phi\rangle$ dual to the bulk dilaton field ϕ, and the $U(1)$ R-charge density $\rho_c = \langle J^t\rangle$ associated with the bulk Maxwell field A_μ. The charge density is time-independent in this spatially homogeneous setup and it only depends on the value of the chemical potential of the medium. From $\langle T^{\mu\nu}\rangle$ one extracts the pressure anisotropy Δp which describes the isotropization of the system, while the approach of the scalar condensate toward its thermodynamic equilibrium value is associated with the true thermalization of the 1RCBH plasma. This is so because the scalar condensate was found here to always equilibrate only after the system has already reached a nearly isotropic state, being always the last equilibration time scale of the system. In other words, generally the isotropization time is shorter than the thermalization time of the 1RCBH plasma.

Moreover, while the thermalization time was found to always increase with increasing values of the $U(1)$ R-charge chemical potential, in agreement with the behavior of the lowest non-hydrodynamic QNM of the dilaton channel, the isotropization time shows a non-monotonic dependence on the chemical potential, namely, it decreases or increases with increasing chemical potential depending on how far or close to the critical point the system is, respectively. This behavior of the isotropization time is in consonance with the behavior of the lowest non-hydrodynamic QNM of the external scalar channel of the 1RCBH plasma [146]. These two observations are explained by the fact that the late

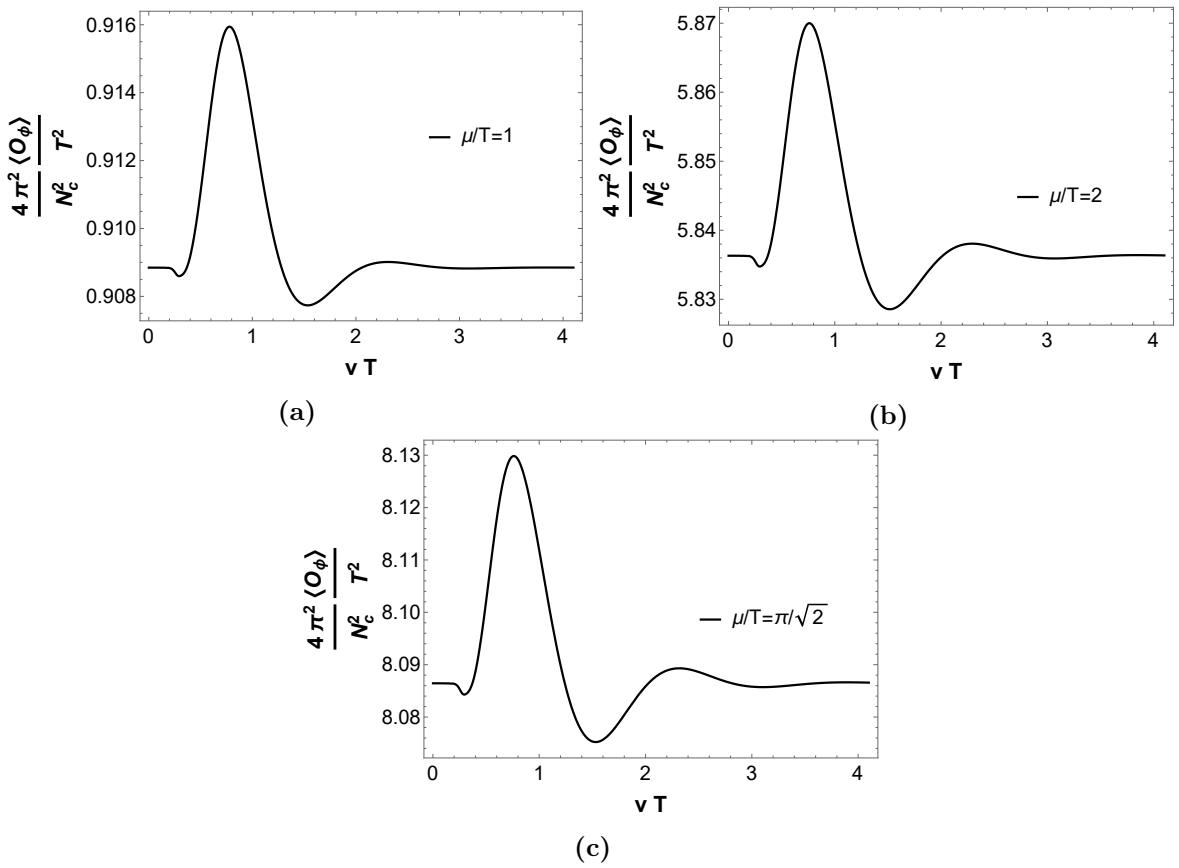

Figure 3.20: *Time evolution of the scalar condensate* $\langle \mathcal{O}_\phi \rangle$ *for different* μ/T *using the initial data* (3.122).

time dynamics of the pressure anisotropy and the scalar condensate are dominated by the lowest non-hydrodynamic QNM's of the external scalar and dilaton channels, respectively. These qualitative findings are robust for the 1RCBH model, in the sense that they hold for different initial conditions chosen to seed the time evolution of the far-from-equilibrium plasma.

On the other hand, the early time dynamics of the pressure anisotropy and the scalar condensate are strongly dependent on the chosen initial data. More specifically, the back-reaction produced in the time evolution of the dilaton field by changing the initial metric anisotropy was found to be very large, in contrast to what happens with the backreaction produced on the time evolution of the metric anisotropy by changing the initial dilaton profile, which was generally found to be small. This suggests that the pressure anisotropy is robust against the addition of other fields in the gravitational action besides the metric, being only significantly sensitive to the initial profile chosen for the metric anisotropy. In particular, the isotropization time may be significantly modified by changing the initial metric anisotropy. On the other hand, while the early time dynamics of the scalar condensate is strongly dependent on the set of initial data chosen to seed the time evolution of

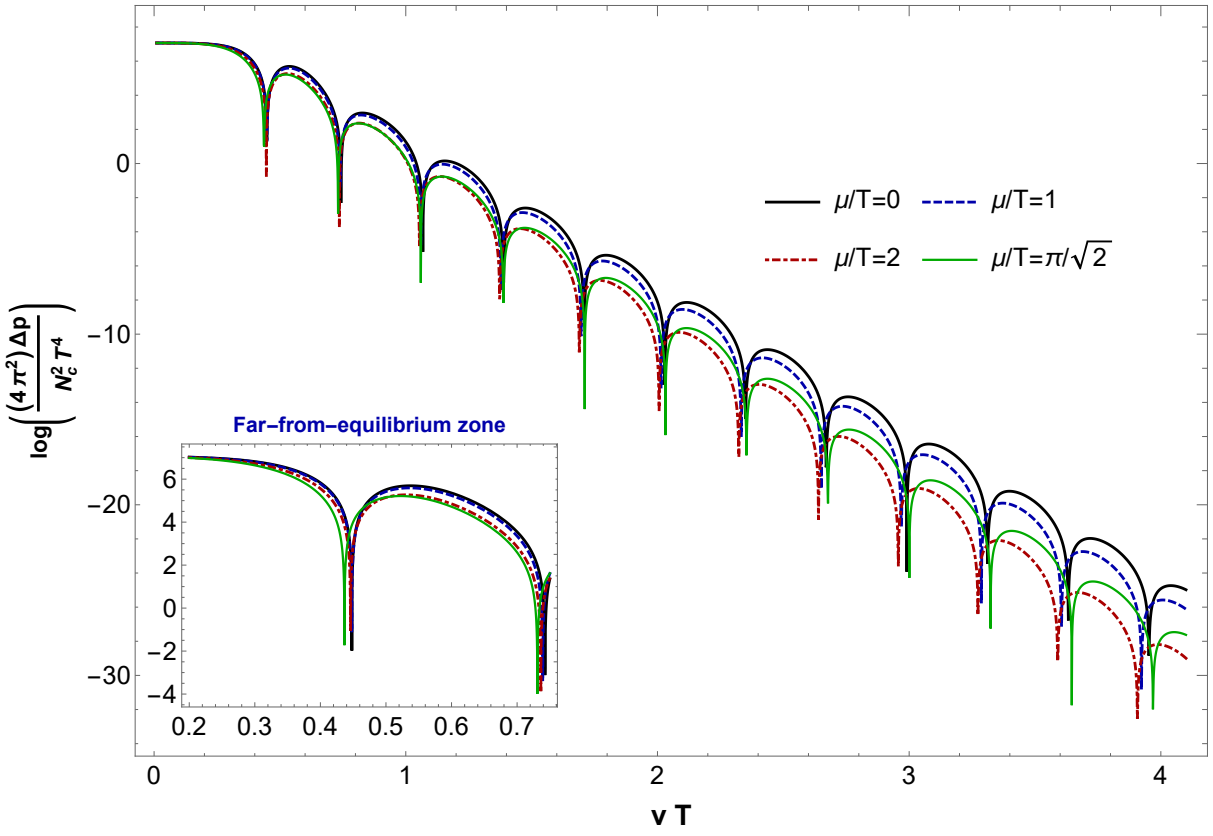

Figure 3.21: *Time evolution of the pressure anisotropy for different μ/T.*

the far-from-equilibrium 1RCBH plasma, its late time dynamics and the associated thermalization time of the medium were found to be remarkably similar for all the different initial conditions considered here.

Some follow-ups of the present work which will appear soon regard the generalization of the analysis of the spatially homogeneous equilibration dynamics of the 1RCBH plasma performed here to consider spatially dependent hydrodynamic flows, such as the Bjorken [145] and the Gubser [236, 237] flows. Indeed, the next chapter deals exactly with the Bjorken flow on top of the 1RCBH model [144]. Gubser flow is particulary interesting since the solution for the hydrodynamic Navier-Stokes approximation in this case displays general inconsistencies, such as regions in the fluid with negative temperature [236], which do not appear after resummation [53, 238]. We also intend to investigate the collisions of shock waves in the 1RCBH setup in the near future to study the interplay between critical phenomena and the rapid expansion developed by the system under these conditions.

As discussed at length in the introduction of this chapter, the 1RCBH plasma (as any conformal plasma) is not suited for direct applications in heavy ion phenomenology. Nonetheless, some of the qualitative features disclosed in the present analysis may be general enough and hold for other strongly coupled holographic fluids. Indeed, the fact

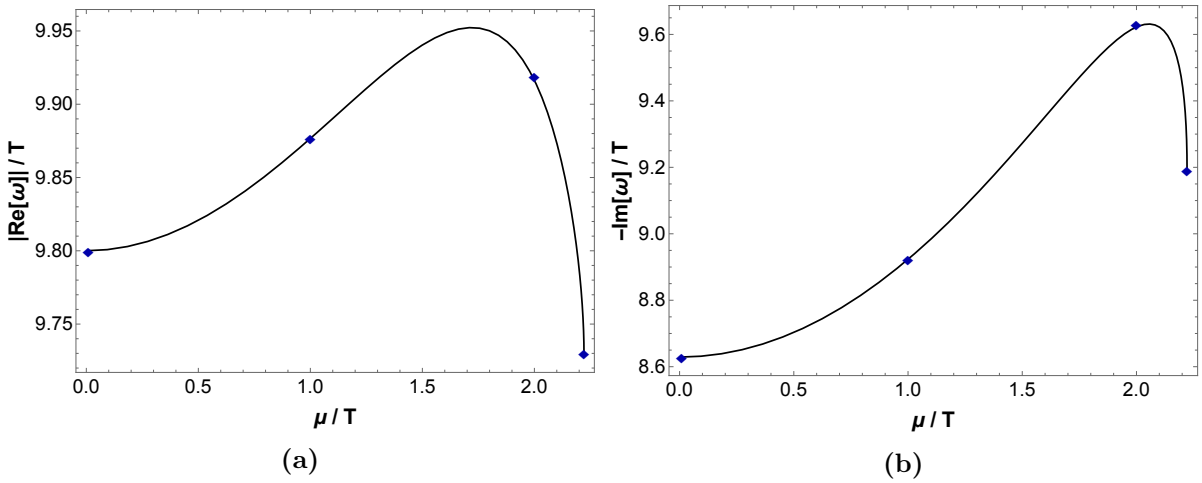

Figure 3.22: *(a) Real and (b) imaginary parts of the lowest non-hydrodynamic QNM of the $SO(3)$ quintuplet (external scalar) channel (curves) [146] compared with the late time decay of the pressure anisotropy (diamonds) described according to Eq.* (3.123).

that the thermalization time of the 1RCBH plasma increases with increasing chemical potential is in consonance with the suggested delayed equilibration of heavy ion collisions at lower energies or higher densities discussed in the introduction. In order to look for possible signatures of far-from-equilibrium universal dynamics of holographic systems, we also intend to generalize the analysis of the present work to the phenomenologically realistic EMD construction of Ref. [70], which provides a quantitative description of QCD thermodynamics at zero and finite baryon chemical potential.

Another perspective for future investigations consists in going beyond the calculation of one-point functions and study also higher order correlation functions [239–243] in far-from-equilibrium holographic settings. In particular, this kind of study may be of relevance for many different ongoing and future low energy heavy ion experiments, such as the BES program [80] being conducted at RHIC, the future fixed target (FXT) experiments [244, 245] also at RHIC, the ongoing HADES experiment [246] at GSI, the future Compressed Baryonic Matter (CBM) experiment at FAIR/GSI [88, 89], and also experiments in the future NICA facility [90].[23] This is so because, as recently discussed in Refs. [247, 248], the behavior of out-of-equilibrium critical cumulants in the QCD phase diagram may be very different from the equilibrium behavior of these real-time correlation functions [249–252]. Since ratios between some of these cumulants may be compared with ratios between moments of particle multiplicity distributions measured in heavy ion collisions, they are the main smoking gun used in experiments in order to try to identify clear experimental signatures of the QCD critical point in heavy ion collisions. Therefore, an

[23]The center of mass collision energies $\sqrt{s}$ (planned to be) reached in these experiments are the following: 7.7 — 200 GeV (BES), 3.0 — 7.7 GeV (FXT), 1.0 — 3.5 GeV (HADES), 2.7 — 4.9 GeV (CBM), and 4.0 — 11 GeV (NICA).

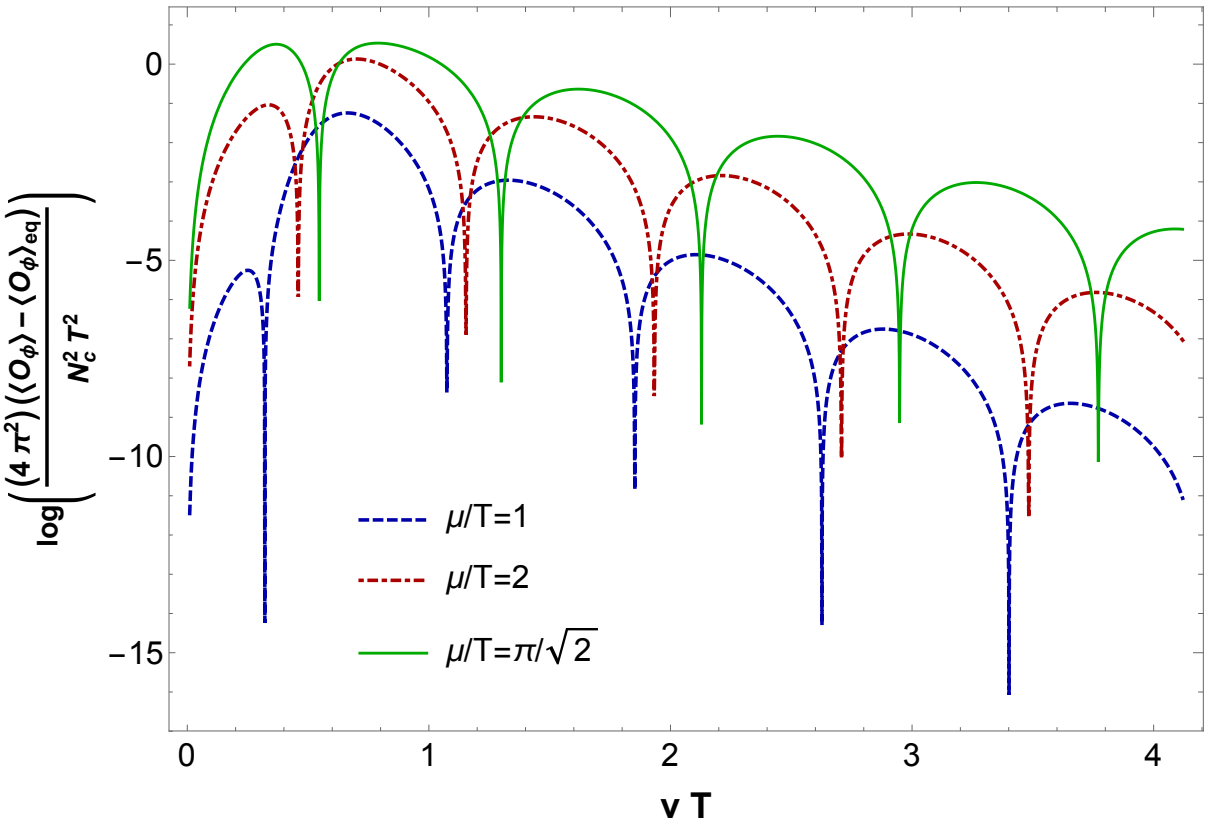

Figure 3.23: *Time evolution of the difference between the scalar condensate and its equilibrium value for different μ/T.*

understanding of the behavior of higher order correlation functions in out-of-equilibrium strongly coupled systems could disclose some fundamental insights which may potentially drive the experimental searches for the QCD critical point in the near future.

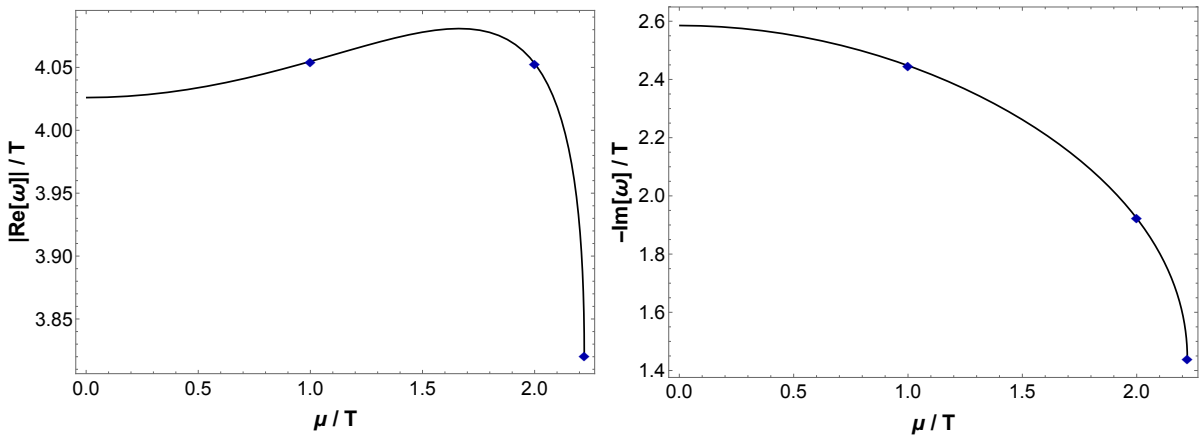

Figure 3.24: *(a) Real and (b) imaginary parts of the lowest non-hydrodynamic QNM of the $SO(3)$ singlet (dilaton) channel (curves) — see their derivation in Appendix A — compared with the late time decay of the difference between the scalar condensate and its equilibrium value (diamonds) described according to Eq. (3.124).*

Chapter 4

Holographic Bjorken flow of a hot and dense fluid in the vicinity of a critical point

In the last Chapter we presented a novel holographic study about the far-from-equilibrium dynamics of a strongly coupled plasma in the vicinity of a critical point. Nonetheless, the setup of the homogeneous isotropization that was employed does not have a description in terms of hydrodynamics since there is no flow, and, because heavy ion collisions produce the QGP which is described by relativistic viscous hydrodynamics, it is important to construct a holographic model which incorporates hydrodynamics. Hence, in this Chapter we will surpass this previous limitation of the mode, and go further in trying to answer some long-standing challenges in the field of high energy nuclear physics, which been the determination of the equilibrium and non-equilibrium properties of the QGP as a function of temperature T and baryon chemical potential μ_B [61].

In particular, a crucial question for the beam energy scan (BES) program conducted at RHIC [80], the future fixed target experiments at RHIC [244, 245], the CBM experiment at FAIR [88, 89], and also the upcoming experiments at NICA [90], is the location of the QCD CEP, which would mark the end of a first order phase transition line expected to exist in the QCD phase diagram at nonzero baryon density [249–252].

If the QCD CEP is within the reach of low energy heavy ion collisions, as predicted by a recent phenomenological holographic model [70] which is in quantitative agreement with state-of-the-art lattice QCD results [78, 253], the rapidly expanding medium formed in these collisions may generally pass close to this point when it is still far from thermal equilibrium being perhaps not even close to a hydrodynamical regime. Therefore, the investigation of how the presence of a critical point affects the far-from-equilibrium dynamics of the expanding medium, and its subsequent approach to hydrodynamics, is of fundamen-

tal importance. In the absence of first principle QCD calculations of the full dynamical evolution of the system, one must resort to effective models. Holographic shockwave-like simulations of a strongly coupled plasma at finite chemical potential (though without critical phenomena) were investigated in [211] while the spinodal instability in a first-order phase transition at strong coupling was studied in [254]. A way to extend hydrodynamics through the inclusion of parametric slowing down and critical fluctuations induced by a critical point has been recently proposed in [255]. Also, recently out-of-equilibrium effects have been shown to produce significant impact on the critical behavior of the cumulants of fluctuations of conserved charges, which has been investigated using the Fokker-Planck equation [247] and also the Kibble-Zurek formalism [248].

In this Chapter we employ the gauge/gravity correspondence [54, 113–115] to investigate the effects of a critical point on the hydrodynamization properties of a top-down holographic construction that stems from string theory known as the 1RCBH model [138–143]. This is the holographic dual of a $\mathcal{N} = 4$ SYM plasma at finite temperature and chemical potential featuring a critical point in its phase diagram. Although not directly related to QCD, the 1RCBH model is a very attractive setup for studying far-from-equilibrium phenomena at finite temperature and density in the presence of a critical point. This well-defined holographic construction allows one to investigate many different physical aspects of a strongly coupled relativistic fluid with chemical potential and critical behavior under well controlled theoretical conditions. As a matter of fact, in previous works the thermodynamics and hydrodynamics [203], the spectra of quasinormal modes [146] (Appendix A), and the homogeneous isotropization and thermalization dynamics [137] (Chap. 3) of the 1RCBH system have been analyzed in detail.

In this present Chapter we perform, for the first time in the literature, a *first principles holographic evaluation* of the full far-from-equilibrium evolution of a hot and dense relativistic fluid endowed with a critical point — the 1RCBH plasma —, undergoing a boost invariant expansion known as Bjorken flow [145]. The calculations done in the present work are all performed within a single theoretical framework, the gauge/gravity duality, and since the 1RCBH model is a top-down string theory construction, no auxiliary hypotheses or approximations are needed in order to investigate its physical properties. Such a simple and well controlled theoretical setting constitutes the ideal toy model for understanding general aspects of the influence of a critical point on the hydrodynamization dynamics of out-of-equilibrium strongly coupled media. As an example of a general insight coming from the holographic correspondence concerning hydrodynamics, the most robust result obtained from the duality is the nearly perfect fluidity of strongly coupled plasmas, which is encoded in a very small shear viscosity to entropy density ratio, $\eta/s = 1/4\pi$ [56, 256, 257]. This general feature of holographic models is remarkable close

to the results of the latest phenomenological simulations describing heavy ion data [105].

The properties of a SYM plasma undergoing Bjorken flow at zero chemical potential has been previously investigated using numerical general relativity techniques [183, 184, 258], which determined how long it takes for this system to hydrodynamize or, in other words, what is the relevant timescale that characterizes the emergence of hydrodynamic behavior. In the present work, we generalize these studies to the case of the 1RCBH model at finite chemical potential with a critical point. By numerically evolving the full nonlinear partial differential equations of motion of the system in the bulk using a large set of initial conditions that span different values of μ/T, we evaluate the pressure anisotropy, the charge density, the scalar condensate, and the hydrodynamization timescale. The latter describes the time after which a given far-from-equilibrium solution can be reasonably described in terms of the relativistic Navier-Stokes (NS) equations. As the main result of the present work, we show that the onset of hydrodynamics is considerably delayed as the chemical potential is increased towards its critical value.

However, before we go into the details of holographic calculations of the Bjorken flow near a critical point, let us review some of the basic features of dissipative relativistic hydrodynamics, and how the Bjorken flow appeared in the context of heavy ion collisions. For further details, we indicate Refs. [50, 259].

4.1 Relativistic viscous hydrodynamics

In the Introduction of this thesis, it was remarked that dissipative relativistic hydrodynamics is far from being an easy subject to study, being not completely understood albeit its tremendous success in describing heavy ion collisions. Hence, the purpose of this section is to review recent developments of this theory, which is also essential to cosmology [260] and astrophysics [261]. Moreover, the discussion performed here will be useful to define the Bjorken flow in subsection 4.1.1, and also to define later an extension that accommodates conserved charges in Sec. 4.3.

Hydrodynamics is a long-wavelength effective field theory[1] designed to describe few bulk macroscopic properties of the system such as energy density, pressure, and charge density. Textbooks definitions also include that hydrodynamics is valid only near local equilibrium, however, as we shall see in this Chapter, it is possible to be more flexible with this requirement and extend the validity of hydrodynamics to regions where the pressure anisotropy is not small.

[1]There are two main ingredients in the process of construction of an effective theory: the knowledge of the degrees of freedom that one tries to describe and the underlying symmetries of the theory. In a Lorentz invariant QFT, the symmetry to be considered is that of the diffeomorphism group, which means invariance under general coordinate transformations.

The fundamental ingredient to build a theory of fluid dynamics relies on (local) conservation laws. In the context of a quantum field theory in absence of conserved charges[2], the conservation law that we are interested in is energy and momentum conservation, i.e.

$$\nabla_\mu T^{\mu\nu} = 0, \tag{4.2}$$

where $T^{\mu\nu}$ is the stress-energy tensor of the theory. If one looks at the conventions defined in Sec. 1.4.1, one realizes that we tacitly assume a QFT in four dimensions. The discussion performed here can be easily extended to arbitrary dimensions, but we will stick with the four-dimensional case.

The modern construction of dissipative relativistic fluid dynamics is based on a series expansion of the stress-energy tensor relative to equilibrium. First, one begins considering the fluid in equilibrium with no fluctuations (dissipation) to construct the stress-energy tensor using the macroscopic degrees of freedom, namely, the energy density (ε), four-velocity (u^μ), and the space-time metric ($g_{\mu\nu}$). This process will give us the so-called ideal fluid dynamics. After ideal hydrodynamics is derived, one proceeds to include small departures from equilibrium of the fields, such as the velocity of the fluid, and a subsequent term on the stress-energy tensor must be considered. The consequence of these small gradients is the appearance of friction terms (viscosity) that break time reversal invariance and increase entropy[3] . The construction described here, which is based on a gradient expansion scheme, can be written as follows

$$T^{\mu\nu} = T^{\mu\nu}_{ideal} + T^{\mu\nu}_{(1)} + T^{\mu\nu}_{(2)} + \dots, \tag{4.3}$$

where $T^{\mu\nu}_{ideal}$ is the ideal hydrodynamic part, $T^{\mu\nu}_{(1)}$ is the first order correction, and $T^{\mu\nu}_{(2)}$ is the second order correction. The inclusion of all these terms gives rise to second order hydrodynamics[4]. Furthermore, the most accepted small parameter used to perform the gradient expansion (4.3) is the so-called Knudsen number (K_n), which is the ratio between the microscopic scale (ℓ) and the macroscopic scale (L), i.e. $K_n = \ell/L$. We will discuss more about K_n after we introduce the first order correction.

Let us then begin the discussion of ideal fluid dynamics, which is a well-defined theory,

[2]If the system has some global symmetry, i.e. a conserved charged associated with a four-current J^μ, then one has to consider also the current conservation equation

$$\nabla_\mu J^\mu = 0. \tag{4.1}$$

[3]Interestingly enough, according to Refs. [262, 263], there are some intriguing solutions of conformal dissipative relativistic hydrodynamics in which entropy is not increased.

[4]The third order correction was studied in Ref. [264], in which was found that 68 independent structures contributes to form the part $T^{\mu\nu}_{(3)}$ of the stress-energy tensor. However, since second order hydrodynamics is already very hard to work with in practice, we tend to neglect the third order correction.

free from the problems encountered in the dissipative formulation. The ideal part of the stress-energy tensor $T^{\mu\nu}_{ideal}$ can be written as

$$T^{\mu\nu}_{ideal} = \varepsilon u^\mu u^\nu + \Delta^{\mu\nu} p, \tag{4.4}$$

where $\Delta^{\mu\nu} = g^{\mu\nu} + u^\mu u^\mu$ is the orthogonal time-like projector of the four-velocity u^μ, and $p = p(\varepsilon)$ is the equilibrium pressure given by EoS. The projections of Eq. (4.2) parallel and orthogonal to the four-velocity, i.e. $u_\mu \nabla_\nu T^{\mu\nu}$ and $\Delta^\alpha_\nu \nabla_\mu T^{\mu\nu}$, give us the relativistic version of Euler's equations,

$$D\varepsilon + (\varepsilon + p)\nabla^\alpha_\perp u_\alpha = 0, \quad (\varepsilon + p) D u^\alpha + c_s^2 \nabla^\alpha_\perp \varepsilon = 0, \tag{4.5}$$

where $D = u^\mu \nabla_\mu$ is the comoving derivative, $\nabla^\alpha_\perp = \Delta^{\alpha\nu}\nabla_\nu$, and

$$c_s^2 = \frac{\partial p}{\partial \varepsilon} \tag{4.6}$$

is the speed of sound of the medium. The speed of sound is often recognized as the "zeroth order" transport coefficient that can be obtained once the EoS (i.e. $p = p(\varepsilon)$) is given. The relativistic Euler equations are mathematically well-defined, and can be easily extended to cases where one has magnetic field and/or conserved charges [265, 266]. Although ideal fluid dynamics can be a good starting point, it has limitations, since friction (viscosity) is absent and the domain of validity of ideal hydrodynamics is unknown *a priori*.

The first order correction to the stress-energy tensor, namely $T^{\mu\nu}_{(1)}$, produces the so-called relativistic Navier-Stokes (NS) theory where $\nabla_\mu \left[T^{\mu\nu}_{ideal} + T^{\mu\nu}_{(1)}\right] = 0$. Following the same idea of the non-relativistic case, it is interesting to split $T^{\mu\nu}_{(1)}$ into a traceless part ($\pi^{\mu\nu}$) and a part with trace (Π), i.e.

$$T^{\mu\nu}_{(1)} = \pi^{\mu\nu} + \Delta^{\mu\nu}\Pi, \tag{4.7}$$

where

$$\pi^{\mu\nu} = -\eta\sigma^{\mu\nu}, \quad \Pi = -\zeta\nabla^\lambda_\perp u_\lambda \tag{4.8}$$

with the shear tensor $\sigma_{\mu\nu}$ being defined as

$$\sigma^{\mu\nu} = 2\nabla^{\langle\mu} u^{\nu\rangle}, \tag{4.9}$$

where $A^{\langle\mu\nu\rangle} = \Delta^{\mu\nu\alpha\beta}A_{\alpha\beta}$ for a given tensor $A^{\mu\nu}$. The operator $\Delta^{\mu\nu\alpha\beta} = \frac{1}{2}\left(\Delta^{\mu\alpha}\Delta^{\nu\beta} + \Delta^{\mu\beta}\Delta^{\nu\alpha}\right) - \frac{1}{3}\Delta^{\mu\nu}\Delta^{\alpha\beta}$ is responsible to project the traceless part of a given tensor. Therefore, Eq. (4.8) defines the shear and bulk contributions to the dissipation of the fluid. Furthermore, the

scalars $\eta = \eta(\varepsilon)$ and $\zeta = \zeta(\varepsilon)$ are the shear and bulk viscosities, respectively. These coefficients are emergent properties from the underlying microscopic interactions of the theory.

The explicit form of the NS equations obtained from the projections $u_\mu \nabla_\nu T^{\mu\nu}$ and $\Delta^\alpha_\nu \nabla_\mu T^{\mu\nu}$ are, respectively

$$D\varepsilon + (\varepsilon + p + \Pi)\nabla^\perp_\mu u^\mu + \frac{1}{2}\pi_{\mu\nu}\sigma^{\mu\nu} = 0 \tag{4.10}$$

$$(\varepsilon + p + \Pi)Du^\mu + \nabla^\perp_\mu(p + \Pi) + \Delta^\mu_\nu \nabla_\alpha \pi^{\alpha\nu} = 0. \tag{4.11}$$

Moreover, with the first correction $T^{\mu\nu}_{(1)}$ at hand, it is possible to begin to infer the validity of the gradient expansion (4.3) using the Knudsen number defined above. For such a task, one can use the "size" of the gradient $\sigma_{\mu\nu}$ of the first correction to obtain the inverse value of the macroscopic scale L^{-1}, and use the transport coefficient of $T^{\mu\nu}_{(1)}$ to produce the small scale as follows

$$\frac{\eta}{\varepsilon + p} \equiv \ell = \lambda_{mfp}, \tag{4.12}$$

where λ_{mfp} can be considered to be like mean free path in a gas. For the gradient expansion (4.3) to be accurate, the mathematical reasoning requires that $\lambda_{mfp} \ll L$ [267], which means that

$$K_n \ll 1. \tag{4.13}$$

The above requirement would then set a limit of applicability for a theory of dissipative fluid dynamics. However, recent studies in the context of heavy ion collisions suggest that a good description of the system using hydrodynamics can be done even when the Knudsen number is close to unity [268, 269], which induces one to think that it is possible to extend the validity of fluid dynamics to regions not so close to the equilibrium [95]. A recent step towards a hydrodynamic formulation for systems that are not close to equilibrium, now in the context of the boost-invariant Bjorken flow, was the discovery of special solutions [96–101]. These solutions, dubbed as "attractors", indicate that different non-equilibrium solutions would coalesce first to these attractors rather than to other hydrodynamic solutions. This unreasonable success of hydrodynamics is a very active area of research [96–101].

Moving now to the second order correction, $T^{\mu\nu}_{(2)}$, Romatschke proposed in Ref. [270]

the following general form for the dissipative part of the stress-energy tensor

$$\begin{aligned}\pi^{\mu\nu} =& -\eta\sigma^{\mu\nu} + \eta\tau_\pi\left[D\sigma^{\langle\mu\nu\rangle} + \frac{\nabla_\perp^\lambda u_\lambda}{3}\sigma^{\mu\nu}\right] + \kappa\left[R^{\langle\mu\nu\rangle} - 2u_\lambda u_\rho R^{\lambda\langle\mu\nu\rangle\rho}\right] \\ &+ \lambda_1\sigma^{\langle\mu}{}_\lambda\sigma^{\nu\rangle\lambda} + \lambda_2\sigma^{\langle\mu}{}_\lambda\Omega^{\sigma\rangle\lambda} + \lambda_3\Omega^{\langle\mu}{}_\lambda\Omega^{\sigma\rangle\lambda} \\ &+ \kappa^\star 2u_\lambda u_\rho R^{\lambda\langle\mu\nu\rangle} + \eta\tau_\pi^\star\frac{\nabla_\perp^\lambda u_\lambda}{3}\sigma^{\mu\nu} + \lambda_4\nabla_\perp^{\langle\mu}\ln\varepsilon\nabla_\perp^{\nu\rangle}\ln\varepsilon, \qquad (4.14)\\ \Pi =& -\zeta\nabla_\perp^\lambda u_\lambda + \zeta\tau_\Pi D(\nabla_\perp^\lambda u_\lambda) + \xi_1\sigma^{\mu\nu}\sigma_{\mu\nu} + \xi_2(\nabla_\perp^\lambda u_\lambda)^2 \\ &+ \xi_3\Omega^{\mu\nu}\Omega_{\mu\nu} + \xi_4\nabla_\perp^\mu\ln\varepsilon\nabla_\mu^\perp\ln\varepsilon + \xi_5 R + \xi_6 u^\lambda u^\rho R_{\lambda\rho}, \qquad (4.15)\end{aligned}$$

where $\Omega = \frac{1}{2}\left(\nabla_\perp^\mu u^\nu - \nabla_\perp^\nu u^\mu\right)$ is the vorticity tensor. The coefficients τ_π, $\tau_\pi^\star$, τ_Π, κ, $\kappa^\star$, $\lambda_{1,2,3,4}$, and $\xi_{1,2,3,4,5,6}$, are second order transport coefficients.

Using Eq. (4.2) in the gradient expansion (4.3), i.e. $\nabla_\mu\left[T^{\mu\nu}_{ideal} + T^{\mu\nu}_{(1)} + T^{\mu\nu}_{(2)}\right] = 0$, one obtains the equations of motion for the second order dissipative relativstic hydrodynamics, also known as the non-conformal generalization of BRSSS theory (Baier-Romatschke-Son-Stephanov-Starinets) [177]. However, this theory solely based on a gradient expansion has problems with causality and stability [271,272]. Evidently, in a relativistic theory, causality is vital and it might even be the guiding principle to formulate a dissipative theory of fluid dynamics [53]. Hence, something must change in order to transform viscous fluid dynamics into a theory that respects causality and is stable. The standard way that this is currently done is to promote $\pi^{\mu\nu}$ and Π to independent dynamical variables, and then use relaxation-like equations for $\pi^{\mu\nu}$ and Π coupled to the old equations of motion obtained from Eq. (4.2).

From a historical perspective, Maxwell [273] and Cattaneo [274] were the first ones to introduce an *ad-hoc* modification of the structure of viscous fluid dynamics equations in a way where the final theory obeys causality at least in the linear regime. The model proposed by Cattaneo, generalized to the relativistic case, introduces a relaxation-like equation for the dissipative part of the stress-energy tensor, i.e. $\pi_{\mu\nu}$ and Π are now dynamical variables with the following equations of motion

$$\tau_\pi D\pi_{\mu\nu} + \pi_{\mu\nu} = -\eta\sigma_{\mu\nu}, \quad \tau_\Pi D\Pi + \Pi = -\zeta(\nabla_\perp^\lambda u_\lambda). \qquad (4.16)$$

After Cattaneo, it was time for Muller [275], Israel and Stewart [276,277], to formulate the so-called Muller-Israel-Stewart (MIS) theory, in which a linearly causal and stable theory is derived by imposing positiveness of the local entropy production. Interestingly enough, in the same spirit of Eqs. (4.16), the MIS theory also leads to relaxation-like equations for $\pi_{\mu\nu}$ and Π. More recently, an extension of the MIS theory was developed,

namely, the resummed BRSSS (rBRSSS)theory[5] [177]. Roughly speaking, the rBRSSS theory is obtained by considering the minimal substitutions $\sigma^{\mu\nu} \to -\pi^{\mu\nu}/\eta$ and $\nabla_\mu^\perp u^\mu \to -\Pi/\zeta$ to obtain a relaxation-like equation that is shown to be equivalent to a theory in which an infinite number of terms of the gradient expansion is resummed [177][6].

Furthermore, it is possible to derive dissipative relativistic fluid dynamics from a more fundamental microscopic theory. On the one hand, using relativistic kinetic theory, which is an approach valid for weakly coupled dilute systems, it is possible to derive a linearly causal theory of dissipative fluid dynamics in flat space-time known as DNMR (Denicol-Niemi-Molnar-Rischke) theory [278][7]. On the other hand, for strongly coupled systems, it is possible to use the AdS/CFT duality to formulate a fluid/gravity paradigm and then derive a theory for viscous fluids as shown in Ref. [176]. However, the drawback of the fluid/gravity paradigm is that it does not deliver a causal and stable theory yet since it leads to the BRSSS theory [280, 281].

In the absence of conserved charges such as baryon number, second order dissipative hydrodynamics has 17 transport coefficients as indicated by Eqs. (4.14) and (4.15). As remarked in the Introduction 1, one of the great open problems in QCD is to compute non-perburbatively these coefficients where a real-time formalism is needed [35]. In this dearth of trustful results for quantities that require real-time dynamics, AdS/CFT comes at the right time to offer some answers. Indeed, recently, a study in a bottom-up holographic model that emulates some properties of QCD thermodynamics computed the second order coefficients form Eqs. (4.14) and (4.15) [122][8]. Furthermore, in recent years, there has been an increasing effort towards a comprehensive Bayesian analysis of all the free parameters that are envolved in the theoretical description of a heavy ion collision to help constrain the transport properties of the QGP [105,196]; in this Bayesian approach, the values extracted for the shear and bulk viscosity generally agree with holographic calculations [207].

As a final remark on this conundrum concerning the compution of transport coefficients of the QGP, the situation seems even worse at finite chemical potential where all the transport coefficients must be functions of the pair (T, μ_B) [109]. Additionally, near the critical point one expects a small divergence of the shear viscosity [288], which would

[5] If one sets $\kappa = \kappa^\star = \tau_\pi^\star = \xi_{1,2,3,4,5,6} = \lambda_{1,3,4} = 0$ in Eqs. (4.14)-(4.15), then one recovers the MIS theory from the rBRSSS theory.

[6] One of the main criticisms that the rBRSSS theory receives, as remarked on footnote 38 of Ref. [122], is that their method is ambiguous since very different differential equations can lead to the same asymptotic behavior. Nonetheless, such "UV completion" problem might be irrelevant in the regime where hydrodynamics is applicable.

[7] Before the introduction of the method of moments in kinetic theory performed in Ref. [278], the so-called Chapman-Enskog gradient expansion [279] was used to derive the relativistic Burnett theory of fluid dynamics, which is acausal and unstable [122].

[8] In addition, if one breaks spatial symmetry and/or includes a magnetic field, more coefficients are needed to describe the plasma [121, 282–287].

indicate a need to formulate a hydrodynamic theory valid in that region [255]. Fortunately, the analysis done in this Chapter for the hydrodynamics near the critical point is not affected by divergences of the shear viscosity because the holographic model used here belongs to the dynamical universality class of type B [203].

Nowadays, perhaps the next challenge concerning relativistic viscous hydrodynamics is the proper modeling of binary neutron stars mergers [289]. Recent results concerning viscous hydrodynamics in the strong gravitational regime can be found in Ref. [290]. This is a very interesting area since several properties of neutron stars and QCD might be inferred from the detection of the signals of gravitational waves emitted from binary mergers that happened billions of years ago [291].

Now that we have reviewed some of the basics aspects of dissipative relativistic hydrodynamics, let us review Bjorken flow dynamics, the simplest approach to obtain a flow that emulates the situation encountered in heavy ion collisions.

4.1.1 Bjorken flow

Before we embark on the numerical calculations of the 1RCBH holographic model, we discuss some important aspects of Bjorken flow [145], which is the simplest analytic model for the fast expansion experienced by the QGP in heavy ion collisions. In the context of holography, we indicate Refs. [184, 292–296] for more discussions.

The Bjorken model can be considered the first approximation of a heavy ion collision in the sense that it is the simplest flow in which the fluid is expanding. The arguments needed to derive Bjorken flow, as well as any other relativistic analytic flow solution [236, 238, 297], rely on symmetry considerations. For the specific case at hand, the flow is assumed to be rotational invariant around the beam direction, translational invariant in the transverse plane of the collision, while possessing also boost invariance along the beam direction. Regarding boost invariance, which belongs to the isometry group $SO(1,1)$,it is a reasonable assumption around the mid rapidity region for very energetic collisions. The transverse invariance along the plane orthogonal do the beam direction, which leads to a Poincaré $ISO(2)$ symmetry, is also an oversimplification of the problem since it does not account for finite size effects and the transverse expansion as well. Altogether, Bjorken flow is characterized by the direct product of these three isometry groups, $SO(1,1) \times ISO(2) \times Z_2$, where Z_2 accounts for the parity symmetry of the spacetime rapidity[9].

The key observation that facilitates calculations in the context of a boost invariant flow is to switch from cartesian coordinates (t, x, y, z) to the so-called Milne coordinates

[9]It is possible to substitute the isometry group $ISO(2)$ by the $SO(3)$ isometry group in order to include a radial expansion as well. This solution is known as Gubser flow [236, 237], but it is valid only for conformal theories.

(τ, ξ, y, x), i.e.

$$t = \tau \cosh \xi, \quad \text{and} \quad z = \tau \sinh \xi, \tag{4.17}$$

where

$$\tau = \sqrt{t^2 - z^2}, \quad \text{and} \quad \xi = \tanh^{-1}\left(\frac{z}{t}\right) = \frac{1}{2}\ln\left(\frac{t+z}{t-z}\right), \tag{4.18}$$

and τ denotes the proper time, and ξ represents the spacetime rapidity. In Milne coordinates, the line element of the four dimensional Minkowski space becomes

$$ds^2 = -d\tau^2 + \tau^2 d\xi^2 + dx^2 + dy^2, \tag{4.19}$$

which covers only the future wedge of $\mathbf{R}^{1,3}$ as shown in Fig. 4.1. Although a change of coordinates does not alter the curvature of the space, i.e. we still have a flat spacetime, the non-triviality of the line element (4.19) produces non-zero Christoffel symbols,

$$\Gamma^{\tau}_{\xi\xi} = \tau, \quad \Gamma^{\xi}_{\xi\tau} = \frac{1}{\tau}. \tag{4.20}$$

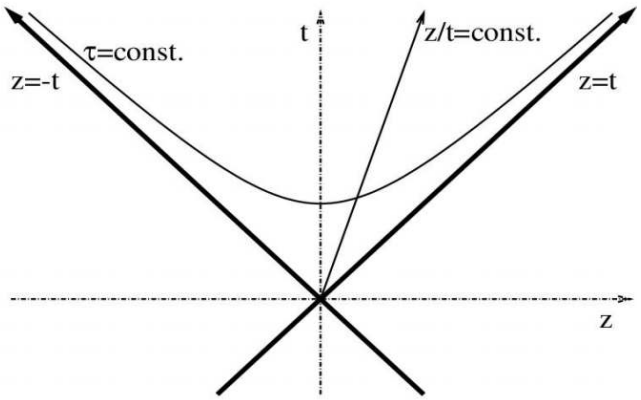

Figure 4.1: *Illustration of the coordinate transformation* (4.17)*, and how the line element* (4.19) *only comprises the future wedge of* $\boldsymbol{R}^{1,3}$*. The instant of the collision between the two nuclei is represented by the point* $(t, z) = (0, 0)$*.*

Boost invariance and reflection symmetry $\xi \to -\xi$ imply that the four-velocity u^μ in Milne coordinates is given by $u^\mu = (1, 0, 0, 0)$, with $u_\mu u^\mu = -1$. However, how exact is this boost invariance symmetry in heavy ion collisions? To answer this question, we show Fig. 4.2 in which one can see that the particle distribution is more or less independent of the rapidity in the mid-rapidity region.

Now, we want to show that the reconstruction of the stress-energy tensor of the Bjorken model in a conformal fluid depends only of a single variable [292]. To achieve this goal, one has to use the traceless condition $T^\mu_{\ \mu} = 0$ along with the conservation law $\nabla_\mu T^{\mu\nu} = 0$. The symmetries of the problem tell us that $T_{\mu\nu}$ is diagonal and has three different components,

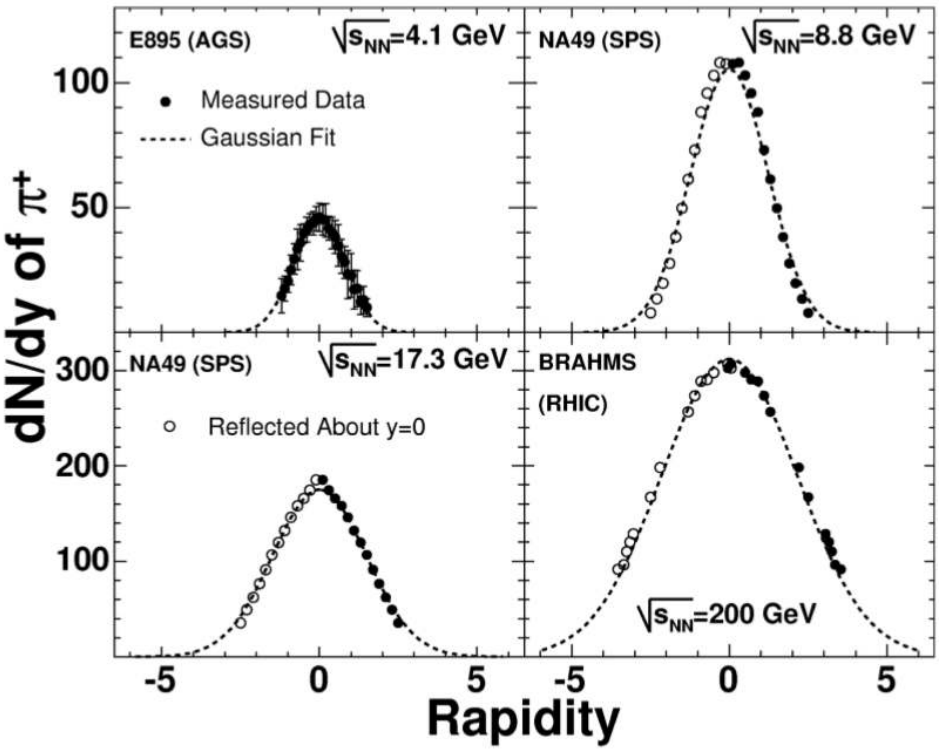

Figure 4.2: *Charged particle (pions) multiplicity distributions in heavy ion collisions for several energy setups as function of the spacetime rapidity. Figure adapted from Ref. [298].*

i.e.

$$T_{\mu\nu} = \mathrm{diag}\{T_{\tau\tau}, T_{xx}, T_{xx}, T_{\xi\xi}\} = \mathrm{diag}\{\varepsilon(\tau), p_T(\tau), p_T(\tau), \tau^2 p_L(\tau)\} \tag{4.21}$$

where p_T and p_L are the transverse and longitudinal pressures, respectively. Hence, the traceless condition for conformal theories and the energy-momentum conservation gives us the following set of equations

$$-T_{\tau\tau} + \frac{1}{\tau^2} T_{\xi\xi} + 2T_{xx} = 0 \tag{4.22}$$

$$\tau \frac{d}{d\tau} T_{\tau\tau} + T_{\tau\tau} + \frac{1}{\tau^2} T_{\xi\xi} = 0. \tag{4.23}$$

After some algebra, one arrives at the following expressions for both pressures

$$p_T(\tau) = -\varepsilon(\tau) - \tau \partial_\tau \varepsilon(\tau), \quad p_L(\tau) = \varepsilon(\tau) + \frac{1}{2} \tau \partial_\tau \varepsilon(\tau), \tag{4.24}$$

which are valid relations for any instant of time and for any type of hydrodynamic theory.

As an application, let us inspect what is the behavior of the energy density assuming ideal hydrodynamics. Notice that the symmetries of the Bjorken flow already fixed $u^\mu =$

$(1,0,0,0)$, thus, we only have to use the first equation in Eq. (4.5), which is reduced to

$$\partial_\tau \varepsilon + \frac{\varepsilon + p}{\tau} = 0. \tag{4.25}$$

The solution, if one assumes a relativistic gas with EoS $p = c_s^2 \varepsilon$, is given by

$$\frac{\varepsilon(\tau)}{\varepsilon(\tau_0)} = \left(\frac{\tau_0}{\tau}\right)^{1+c_s^2}, \tag{4.26}$$

where τ_0 is an integration constant. Additionally, if the quantum field theory is conformal, which is the case of the 1RCBH holographic model, one has $3p = \varepsilon$, i.e. $c_s^2 = 1/3$.

In Sec. 4.3 we will present the NS solution of the 1RCBH theory, while below, in Sec. 4.2, it is presented how the holographic Bjorken flow in the vicinity of a critical point can be constructed using the 1RCBH model.

4.2 Modeling the holographic Bjorken flow near a critical point

The gravitational EMD Lagrangian of the 1RCBH model was given in Sec. 3.1. Basically, the difference between the homogeneous isotropization explored in Chap. 3 and the Bjorken flow are the boundary conditions. Indeed, the Ansatz for the EMD fields in the holographic Bjorken flow, using in-falling Eddington-Finkelstein coordinates, is given by [183]

$$\begin{aligned} ds^2 &= 2d\tau\left[dr - A(\tau,r)d\tau\right] + \Sigma(\tau,r)^2\left[e^{-2B(\tau,r)}d\xi^2\right. \\ &\left. + e^{B(\tau,r)}(dx^2+dy^2)\right], \quad \phi = \phi(\tau,r), \quad A = \Phi(\tau,r)d\tau, \end{aligned} \tag{4.27}$$

where τ becomes the usual propertime of Bjorken flow at the boundary, r is the radial coordinate of the asymptotically AdS spacetime whose boundary is at $r \to \infty$, ξ denotes the spacetime rapidity, and (x, y) are the transverse spatial directions to the longitudinal flow direction.

The numerical solutions of the EMD equations accounting for the holographic Bjorken flow in the 1RCBH model are discussed in Sec. 4.4. From these solutions one can extract the energy density (ε), transverse pressure (p_T), longitudinal pressure (p_L), charge density (ρ), and the scalar condensate ($\langle \mathcal{O}_\phi \rangle$). Also, due to Bjorken symmetry, all of these quantities depend solely on the propertime τ. Because we have a conformal setup, it suffices to look at the energy density and its time derivative to probe the hydrodynamization

properties of the system since

$$\frac{\Delta p}{\varepsilon} \equiv \frac{p_T - p_L}{\varepsilon} = 2 + \frac{3}{2}\tau\frac{\partial_\tau \varepsilon}{\varepsilon}. \tag{4.28}$$

4.3 Viscous relativistic hydrodynamics with a chemical potential

Now we briefly review the hydrodynamics of a Bjorken expanding fluid with nonzero conserved charge [299, 300], which describes the late time behavior of our numerical gravity simulations. We restrict ourselves to first order hydrodynamics corresponding to the relativistic Navier-Stokes equations [261]. Higher order derivative corrections to hydrodynamics [177, 264] could be implemented once the corresponding transport coefficients (such as the shear viscosity relaxation time) become available for the system under consideration. The improvement in the hydrodynamic description of this system due to the inclusion of higher order gradient corrections, and the subsequent question about the convergence of the series at strong coupling [180, 186], is left to a future study.

Due to conformal invariance and the underlying symmetries of Bjorken flow, to first order in the gradient expansion the only contribution to the viscous evolution comes from the shear stress tensor of the system, $\pi^\mu_\nu = -\eta\sigma^\mu_\nu$, where the shear tensor is diagonal with $\sigma^\mu_\nu \sim 1/\tau$. Since the flow velocity is $u_\mu = (-1, 0, 0, 0)$ and π^μ_ν is given in terms of the hydrodynamic variables, the NS equations for Bjorken flow with a U(1) global charge reduce to a single equation for the energy density

$$\partial_\tau \varepsilon + \frac{4}{3}\frac{\varepsilon}{\tau} = \frac{4}{3}\frac{\eta}{\tau^2}, \tag{4.29}$$

while charge conservation imposes that the charge density associated with the R-charge of the black hole is $\rho(\tau) = \rho_0/\tau$; thus, the charge density is known once one specifies its initial value ρ_0.

Using that $\eta/s = 1/(4\pi)$ and the well-known thermodynamic relation for conformal theories, $4\varepsilon = Ts + \mu\rho$, Eq. (4.29) reduces to

$$\partial_\tau \varepsilon + \frac{4}{3}\frac{\varepsilon}{\tau} = \frac{1}{3\pi\tau^2}\left(\frac{4\varepsilon}{3T} - \frac{\mu\rho}{T}\right). \tag{4.30}$$

To proceed, we need the equilibrium equation of state of the 1RCBH model [137, 146,

203],

$$\varepsilon = \kappa_5^{-2} j(\mu/T) T^4 \Rightarrow T = \kappa_5^{1/2} j^{-1/4} \varepsilon^{1/4}, \tag{4.31}$$

$$\rho = \kappa_5^{-2} h(\mu/T) T^3 \Rightarrow \rho = \kappa_5^{-1/2} h j^{-3/4} \varepsilon^{3/4}, \tag{4.32}$$

where,

$$j(\mu/T) = \frac{3\pi^4}{32}\left(3 - \sqrt{1 - \left(\frac{\mu/T}{\pi/\sqrt{2}}\right)^2}\right)^3 \times \left(1 + \sqrt{1 - \left(\frac{\mu/T}{\pi/\sqrt{2}}\right)^2}\right), \tag{4.33}$$

$$h(\mu/T) = \frac{\pi^2}{4}\frac{\mu}{T}\left(3 - \sqrt{1 - \left(\frac{\mu/T}{\pi/\sqrt{2}}\right)^2}\right)^2. \tag{4.34}$$

Substituting the above results into Eq. (4.30), and keeping fixed the dimensionless ratio $\mu/T \equiv x$, it follows that

$$\partial_\tau \varepsilon + \frac{4}{3}\frac{\varepsilon}{\tau} = \frac{\varepsilon^{3/4}}{3\kappa_5^{1/2}\pi\tau^2}\left(\frac{4j^{1/4}}{3} - x\frac{h}{j^{3/4}}\right). \tag{4.35}$$

Using $\hat{\varepsilon} \equiv \kappa_5^2 \varepsilon$ and multiplying by $\tau/\hat{\varepsilon}$ one obtains

$$\tau\frac{\partial_\tau \hat{\varepsilon}}{\hat{\varepsilon}} = -\frac{4}{3} + \frac{4j - 3xh}{9j^{3/4}\pi w^{(\varepsilon)}}, \tag{4.36}$$

where we defined the dimensionless time flow $w^{(\varepsilon)} \equiv \hat{\varepsilon}^{1/4}\tau$. Eq. (4.36) is needed to evaluate the pressure anisotropy in the hydrodynamical regime, according to Eq. (4.28) (which holds also far-from-equilibrium).

Although the definition of w using the energy density seems more natural, as explained below in Sec. 4.4, it is possible to use another energy scale Λ, which is reminiscent from the asymptotic temperature $T_{\rm asym}(\tau) = \Lambda/(\Lambda\tau)^{1/3}$ [183], to compose another dimensionless time flow, i.e. $w^{(\Lambda)} \equiv T_{\rm asym}(\tau)\tau = (\Lambda\tau)^{2/3}$. In practice, we use the late time solution of Eq. (4.36) for the energy density to extract Λ for each solution, i.e.

$$\hat{\varepsilon}(\tau) = \frac{3\pi^4\Lambda^{8/3}}{2\tau^{4/3}} - \frac{\pi^2\Lambda^2(4j - 3xh)}{2^{7/4}\,3^{1/4}\,\tau^2 j^{3/4}}. \tag{4.37}$$

Hence, using also $w^{(\Lambda)}$ to probe the hydrodynamization time will give us confidence that our analysis is not a peculiarity associated to a particular choice for w.

The applicability of hydrodynamics in the late time dynamics of planar shockwave collisions in SYM was first investigated in [301] (see [181] for a comprehensive discussion of this problem). Recently, hydrodynamization was also studied in detail in non-conformal shockwave collisions in Ref. [185]. In the case of Bjorken flow, we follow the same convention of previous works [184, 258] and estimate the hydrodynamization time $w_{\text{hydro}}^{(\varepsilon/\Lambda)}$ as the timescale after which a given far-from-equilibrium numerical solution becomes well described by NS hydrodynamics, satisfying

$$\left|\left(\frac{\Delta p}{\varepsilon}\right)_{\text{numerical}} - \left(\frac{\Delta p}{\varepsilon}\right)_{\text{hydro}}\right| \leq tol \left(\frac{\Delta p}{\varepsilon}\right)_{\text{hydro}}, \tag{4.38}$$

where tol is the tolerance threshold for the difference in the above inequality. In particular, we choose $tol = 0.01$ and $tol = 0.1$ to verify how robust our results are.

4.4 Technical details

This section is devoted to clarify the details of the numerical procedure we employed to evaluate the Bjorken flow dynamics of the 1RCBH model. We stress that the steps followed here are similar to the ones described in Chapter 3 which considered the case of homogeneous isotropization [137]. The resulting EMD equations of motion for Bjorken flow constitute a set of coupled partial differential equations (PDE's) given by

$$\frac{1}{6}\Sigma\left(3\left(B'\right)^2 + \left(\phi'\right)^2\right) + \Sigma'' = 0, \tag{4.39a}$$

$$(d_+\Sigma)' + \frac{2\Sigma'}{\Sigma} d_+\Sigma + \frac{1}{12}\Sigma\left(f\mathcal{E}^2 + 2V\right) = 0, \tag{4.39b}$$

$$\Sigma\left(d_+B\right)' + \frac{3\Sigma'}{2} d_+B + \frac{3d_+\Sigma}{2} B' = 0, \tag{4.39c}$$

$$\begin{aligned} &4\Sigma(d_+\phi)' + 6\phi' d_+\Sigma \\ &+6\Sigma' d_+\phi + \Sigma\partial_\phi f\mathcal{E}^2 - 2\Sigma\partial_\phi V = 0, \end{aligned} \tag{4.39d}$$

$$\begin{aligned} A'' + \frac{1}{12}\Bigg(&18B' d_+B - \frac{72\Sigma' d_+\Sigma}{\Sigma^2} \\ &+6\phi' d_+\phi - 7f\mathcal{E}^2 - 2V\Bigg) = 0, \end{aligned} \tag{4.39e}$$

$$\frac{(\partial_\phi f)\phi'}{f} + \frac{3\Sigma'}{\Sigma} + \frac{\mathcal{E}'}{\mathcal{E}} = 0 \tag{4.39f}$$

where $' \equiv \partial_r$, $\mathcal{E} \equiv -\partial_r\Phi$, and $d_+ \equiv \partial_\tau + A(\tau, r)\partial_r$. From Eq. (3.14b), one obtains,

$$\mathcal{E}(\tau, r) = 2\Phi_2(\tau)\Sigma(\tau, r)^{-3} e^{2\sqrt{\frac{2}{3}}\phi(\tau,r)}, \tag{4.40}$$

where Φ_2 is a time-dependent coefficient following from the near-boundary expansion of Φ.

To perform the near-boundary expansion of the bulk EMD fields, which is needed to fix the boundary conditions corresponding to the Bjorken symmetry and obtain the one-point functions of the field theory undergoing Bjorken expansion at the boundary, we set as the boundary condition for the metric field the usual expression for the line element in Bjorken flow using Milne coordinates

$$ds^2 = -d\tau^2 + \tau^2 d\xi^2 + dx^2 + dy^2. \tag{4.41}$$

Hence, by imposing that at the boundary the bulk metric field in Eq. (4.27) is conformally equivalent to Eq. (4.41), while the dilaton vanishes and the Maxwell field reduces to the chemical potential of the field theory, one works out the following near-boundary expansions

$$A(\tau, r) = \frac{1}{2}(r + \lambda(\tau))^2 - \partial_\tau \lambda(\tau) + \sum_{n=2}^{\infty} \frac{a_n(\tau)}{r^n}, \tag{4.42a}$$

$$\Sigma(\tau, r) = \tau^{1/3} r + \frac{1 + 3\tau\lambda(\tau)}{3\tau^{2/3}} - \frac{1}{9r\tau^{5/3}} + \frac{5 + 9\tau\lambda(\tau)}{81 r^2 \tau^{8/3}} + \sum_{n=3}^{\infty} \frac{\sigma_n(\tau)}{r^n}, \tag{4.42b}$$

$$B(\tau, r) = -\frac{2}{3r\tau} - \frac{2\log(\tau)}{3} + \frac{1 + 2\tau\lambda(\tau)}{3r^2\tau^2} - \frac{2 + 6\tau\lambda(\tau) + 6\tau^2\lambda(\tau)^2}{9r^3\tau^3} + \sum_{n=4}^{\infty} \frac{b_n(\tau)}{r^n}, , \tag{4.42c}$$

$$\phi(\tau, r) = \sum_{n=2}^{\infty} \frac{\phi_n(\tau)}{r^n}, \tag{4.42d}$$

$$\Phi(\tau, r) = \Phi_0(\tau) + \sum_{n=2}^{\infty} \frac{\Phi_n(\tau)}{r^n}, \tag{4.42e}$$

where $\Phi_0(\tau \to \infty) = \mu$ is the gauge theory chemical potential and $\lambda(\tau)$ is an arbitrary function. This function is associated with the residual diffeomorphism invariance of the line element (4.27) under radial shifts of the form $r \to r + \lambda(\tau)$ [59].

The relevant observables used to probe the hydrodynamization properties of the system, i.e. the energy-momentum tensor $\langle T_{\mu\nu} \rangle$, the U(1) four-current $\langle J_\mu \rangle$, and the scalar condensate $\langle \mathcal{O}_\phi \rangle$ are obtained from the one-point functions via holographic renormaliza-

tion. Their formulas for the 1RCBH model are [137]

$$\kappa_5^2\langle T_{\tau\tau}\rangle = -3a_2 - \frac{1}{6}\phi_2^2, \tag{4.43}$$

$$\kappa_5^2\langle T_{xx}\rangle = -3a_2 - \frac{1}{6}\phi_2^2 - \frac{3}{2}\tau\partial_\tau a_2 - \frac{1}{6}\phi_2\partial_\tau\phi_2, \tag{4.44}$$

$$\tau^{-2}\kappa_5^2\langle T_{\xi\xi}\rangle = 3a_2 + \frac{1}{6}\phi_2^2 + \frac{3}{2}\tau\partial_\tau a_2 + \frac{1}{6}\phi_2\partial_\tau\phi_2, \tag{4.45}$$

$$\kappa_5^2\langle J^t\rangle = \Phi_2(\tau) = \frac{\rho_0}{\tau}, \tag{4.46}$$

$$\kappa_5^2\langle \mathcal{O}_\phi\rangle = \phi_2, \tag{4.47}$$

where ρ_0 is an input corresponding to the initial charge density. The near-boundary coefficients a_2 and ϕ_2 are dynamical quantities and they can be determined once the equations of motion are solved. The energy density, the parallel and longitudinal pressures, and the charge density are, respectively,

$$\varepsilon \equiv \langle T_{\tau\tau}\rangle, \quad p_T \equiv \langle T^x{}_x\rangle, \quad p_L \equiv \langle T^\xi{}_\xi\rangle, \quad \rho \equiv \langle J^t\rangle. \tag{4.48}$$

To solve numerically the PDE's (4.39a) — (4.39f), we first redefine the radial domain in such a way that the new domain is finite, i.e., $u \equiv 1/r$, which means that in this new radial coordinate the boundary lies at $u = 0$.

The next step is to define subtracted fields X_s by removing the trivial information encoded in the leading order terms of the near-boundary expansions of the bulk fields

X,[10]

$$u^2 A_s = A - \frac{1}{2}\left(\frac{1}{u} + \lambda\right)^2 + \partial_\tau \lambda, \tag{4.49}$$

$$u^3 \Sigma_s = \Sigma - \tau^{1/3}\frac{1}{u} - \frac{1+3\tau\lambda}{3\tau^{2/3}} + \frac{u}{9\tau^{5/3}} - \frac{5+9\tau\lambda}{81\tau^{8/3}}u^2, \tag{4.50}$$

$$u^4 B_s = B(\tau,u) + \frac{2u}{3\tau} + \frac{2\log(\tau)}{3} - \frac{1+2\tau\lambda}{3\tau^2}u^2 + \frac{2+6\tau\lambda+6\tau^2\lambda^2}{9\tau^3}u^3, \tag{4.51}$$

$$u^2 \phi_s = \phi, \tag{4.52}$$

$$u^3 \left(d_+ B\right)_s = d_+ B + \frac{1}{3\tau} - \frac{u}{3\tau^2} + \frac{u^2(\tau\lambda+1)}{3\tau^3}, \tag{4.53}$$

$$u^2 \left(d_+ \Sigma\right)_s = d_+\Sigma - \frac{10u}{81\tau^{8/3}} - \frac{\tau^{1/3}}{2u^2} - \frac{(1+\tau\lambda)(-1+3\tau\lambda)}{6\tau^{5/3}} - \frac{1+3\tau\lambda}{3u\tau^{2/3}}, \tag{4.54}$$

$$u\left(d_+\phi\right)_s = d_+\phi, \tag{4.55}$$

$$\mathcal{E}_s = \mathcal{E}. \tag{4.56}$$

We then rewrite Eqs. (4.39a) — (4.39f) in terms of the variables $\{A_s, \Sigma_s, B_s, \phi_s, (d_+B)_s, (d_+\Sigma)_s, (d_+\phi)_s, \mathcal{E}_s\}$. We do not write them explicitly here because the expressions are lengthy and not particularly enlightening.

Since we solve the radial problem using the pseudospectral method [230], the radial $u-$grid is given by the Chebyshev-Gauss-Lobatto grid

$$u_k = \frac{u_\star}{2}\left(1 + \cos\left(\frac{k\pi}{N-1}\right)\right), \quad k = 0, \ldots, N-1, \tag{4.57}$$

where N is the number of grid points, also known as collocant points. Here, $u_\star$ defines the infrared (IR) limit of the radial grid. The IR limit of the radial $u-$grid must be chosen in such a way that it covers the entire portion of the bulk geometry causally connected to the boundary, which means that the *locus* of the event horizon is a good place to set the IR limit. Commonly, this is done by tracking the apparent horizon u_h,

$$d_+\Sigma|_{u=u_h} = 0, \tag{4.58}$$

and then using $\lambda(\tau)$ to fix the position of u_h in the course of the simulation. In our

[10] Notice that $(d_+X)_s \neq d_+(X_s)$, where $X \in \{\Sigma, B, \phi\}$.

numerical algorithm, we approximated the above condition by using the following relation

$$d_+\Sigma|_{u=u_\star} = \delta, \tag{4.59}$$

where δ is a small negative number, typically of the order $\mathcal{O}(10^{-3})$. Since $d_+\Sigma$ is a monotonically decreasing function for increasing values of u, Eq. (4.59) tells us that $u_\star$ is a little bit behind the apparent horizon u_h; consequently, if the radial grid spans $u \in [0, u_\star]$, we ensure that it covers the whole portion of the bulk geometry causally connected to the boundary. For the initial conditions considered in this work, which are given at the end of this section, one can start with a radial grid $u \in [0, 1]$ with $\lambda(\tau_0) = 0$, where τ_0 is the initial time used in the simulation, and in all the cases we considered, the condition (4.59) could be found after the following steps: i) one starts with $d_+\Sigma(\tau, u = 1)$, which is generally equal to some negative number (and, therefore, we know that at this point we are behind the horizon, since at the apparent horizon Eq. (4.58) holds, and beyond it $d_+\Sigma > 0$); ii) as the simulation proceeds and we march towards the boundary, the value of $d_+\Sigma$ begins to increase and when the condition (4.59) is met, the corresponding value of $u_\star$ has been found; iii) in order to keep this value of $u_\star$ fixed through the numerical simulation for a given initial condition, we impose that $\partial u_\star/\partial\tau = 0$. Bearing this condition in mind, and manipulating the field equations (3.14f) — (3.14b) at $u = u_\star$, the following relation is found

$$A = 2\frac{\Sigma\left((3(d_+B)^2 + (d_+\phi)^2)\,\Sigma + 6u_\star^2 A'\delta\right)}{(2V + f\mathcal{E}^2)\Sigma^2 - 24u_\star^2\Sigma'\delta}, \tag{4.60}$$

where all the functions in this expression are assumed to be evaluated at $u = u_\star$. In the limit where $\delta \to 0$ we recover the usual expression for the stationary apparent horizon [59]. Expressing A in terms of the subtracted field A_s in the LHS of Eq. (4.60), one obtains the following expression for $\partial_\tau\lambda$

$$\begin{aligned}\partial_\tau\lambda = u_\star^2 A_s + \frac{\lambda^2}{2} + \frac{1}{2u_\star^2} + \frac{\lambda}{u_\star} \\ + 2\frac{\Sigma\left((3(d_+B)^2 + (d_+\phi)^2)\,\Sigma + 6u_\star^2 A'\delta\right)}{(2V + f\mathcal{E}^2)\Sigma^2 - 24u_\star^2\Sigma'\delta}.\end{aligned} \tag{4.61}$$

Thus, the condition $\partial u_\star/\partial\tau = 0$ provides an expression for $\partial_\tau\lambda$, which is used to update the value of $\lambda(\tau)$ through the simulation keeping fixed the position of the approximated apparent horizon $u_\star$.

To solve the radial problem using the pseudospectral method, one needs the boundary conditions that are derived using the near-boundary expansion of the subtracted bulk

fields

$$\Sigma(\tau, u=0)_s = 0, \tag{4.62}$$

$$(d_+\Sigma(\tau, u=0))_s = a_2\tau^{1/3} - \frac{5(6\lambda\tau+5)}{243\tau^{11/3}} + \frac{1}{12}\tau^{1/3}\phi_2^2, \tag{4.63}$$

$$(d_+B(\tau, u=0))_s = 2a_2 + \frac{3\tau\partial_\tau a_2}{2} + \frac{\lambda^2}{3\tau^2} + \frac{2\lambda}{3\tau^3} + \frac{1}{3\tau^4} \frac{\tau\phi_2\partial_\tau\phi_2}{6} + \frac{\phi_2^2}{9}, \tag{4.64}$$

$$(d_+\phi(\tau, u=0))_s = -\phi_2, \tag{4.65}$$

$$A(\tau, u=0)_s = a_2, \tag{4.66}$$

$$\partial_u A(\tau, u=0)_s = \frac{\partial_\tau a_2}{2} - 2\lambda a_2. \tag{4.67}$$

Thus, in order to solve the radial problem at a given time τ, one has to know[11] $\{B(\tau,u), \phi(\tau,u), a_2(\tau), \Phi_2(\tau), \lambda(\tau)\}$. Evidently, the initial state that we define must contemplate this set as well.

To perform the time evolution of the system one has to use $d_+ \equiv \partial_\tau + A(\tau,r)\partial_r$ to extract $\{\partial_\tau B_s, \partial_\tau\phi_s\}$ from $\{(d_+B)_s, (d_+\phi)_s\}$; $\partial_\tau a_2$ from the coefficient $b_4(\tau)$ of the expansion (3.20); and $\partial_\tau\lambda$ from Eq. (4.61). By doing so, one can evolve in time the fields necessary to start the cascade solution of the nested set of PDE's

$$B(\tau+\Delta\tau, u)_s = B(\tau,u)_s + \Delta\tau(\partial_\tau B_s), \tag{4.69}$$

$$\phi(\tau+\Delta\tau, u)_s = \phi(\tau,u)_s + \Delta\tau(\partial_\tau\phi_s), \tag{4.70}$$

$$a_2(\tau+\Delta\tau) = a_2(\tau) + \Delta\tau(\partial_\tau a_2), \tag{4.71}$$

$$\lambda(\tau+\Delta\tau) = \lambda(\tau) + \Delta\tau(\partial_\tau\lambda), \tag{4.72}$$

where $\Delta\tau$ is the time step. There are several ways to do the time evolution. In this work, we choose a fourth-order Adams-Bashforth method to evolve in time.

[11] If we know $B(\tau,u)$ and $a_2(\tau)$, then we know $\partial_\tau a_2$. This is because the term $b_4(\tau)$ is proportional to $a_2(\tau)$ and $\partial_\tau a_2$:

$$b_4(\tau) = a_2(\tau) + \frac{3}{4}\tau\partial_\tau a_2(\tau) - \frac{1}{6\tau^4} - \frac{2\lambda(\tau)}{3\tau^3} - \frac{\lambda(\tau)^2}{\tau^2} - \frac{2\lambda(\tau)^3}{3\tau} + \frac{1}{18}\phi_2(\tau)^2 + \frac{1}{12}\phi_2(\tau)\partial_\tau\phi_2(\tau). \tag{4.68}$$

Regarding the initial conditions used in the present work, they were chosen as follows

$$B(\tau_0,u)_s = f(u) + \frac{\alpha}{u^4}\left[-\frac{2}{3}\log\left(u+\tau_0\right) - \left(-\frac{2}{3}\log\left(\tau_0\right) - \frac{2u^3}{9\tau_0^3} + \frac{u^2}{3\tau_0^2} - \frac{2u}{3\tau_0}\right)\right], \tag{4.73}$$

$$a_2(\tau_0) = -20/3, \tag{4.74}$$

$$\phi(\tau_0,u)_s = 0, \tag{4.75}$$

$$\Phi_2(\tau_0) = \frac{\rho_0}{\tau_0}, \tag{4.76}$$

$$\lambda(\tau_0) = 0, \tag{4.77}$$

$$\tau_0 = 0.2, \tag{4.78}$$

where

$$f(u) = \sum_{i=0}^{5}\beta_i u^i. \tag{4.79}$$

Thus, different values for the set $\{\alpha,\beta_i,\rho_0\}$ will produce different evolutions and, consequently, different results for the hydrodynamization time (4.38). In particular, to generate the results presented in this work, we have randomly selected values for $\{\alpha,\beta_i,\rho_0\}$ in the range,

$$1 \leq \alpha \leq 1.05, \quad -0.5 \leq \beta_i \leq 0.5 \ \text{ and } \ 0 \leq \rho_0 \lesssim 3.7. \tag{4.80}$$

The fact that ρ_0 does not have a clear upper bound, i.e. $\rho_0 \lesssim 3.7$, is because some initial conditions do not have a well-behaved evolution for e.g. $\rho_0 = 3.7$. The reason is because some initial profiles tend to reach the vicinity of the critical point with a smaller value of ρ_0. Indeed, one cannot predict the final value of μ/T by just looking at the initial conditions since this is an equilibrium quantity which is only determined by the late time evolution of the system, constituting, therefore, *a posteriori* analysis of the numerical data.

Regarding our first definition of the dimensionless time flow, $w^{(\varepsilon)} \equiv \hat{\varepsilon}(\tau)^{1/4}\tau$, which was used to probe the hydrodynamization time and employed in the plots of the main text instead of an alternative definition such as $w \equiv T(\tau)\tau$, this is justified based on the following facts. First, the energy density is a physically well defined observable at all times along the evolution of the system while the temperature is a quantity which rigorously only makes sense in or at least close to thermal equilibrium. Therefore, one should track the far-from-equilibrium time evolution of the system by using an observable which is physically well defined regardless whether the system is in equilibrium or not and this is the case for the energy density, but not for the temperature. Second, if one insists in defining $w \equiv T(\tau)\tau$ in the present setup, one immediately finds an ambiguity in such definition. In

fact, by looking at the *equilibrium* equation of state given by Eqs. (4.31) and (4.32), one can extract the relations $T = j^{-1/4}\hat{\varepsilon}^{1/4}$ and $T = h^{-1/3}\hat{\rho}^{1/3}$, which agree with each other in equilibrium. By naively trying to define and "out-of-equilibrium temperature" $T(\tau)$ by extrapolating these equilibrium relations to the far-from-equilibrium regime, $T(\tau) = j^{-1/4}\hat{\varepsilon}^{1/4}(\tau)$ and $T(\tau) = h^{-1/3}\hat{\rho}^{1/3}(\tau)$, one is left with an ambiguity in the definition of such "out-of-equilibrium temperature", since these two expressions are generally different from each other and only agree in equilibrium. Such an ambiguity is a clear manifestation of the fact that one should not use equilibrium relations when the system is far-from-equilibrium. Nonetheless, the simulations do coalesce to a near equilibrium state and the ideal fluid limit is recovered for asymptotic times $\tau \to \infty$, in which the temperature has a well defined profile in the Bjorken flow $T_{\rm asym}(\tau) = \Lambda/\left(\Lambda\tau\right)^{1/3}$ [183], where Λ is an energy scale that depends on the initial conditions. Therefore, although it is not possible to define $T(\tau)$ throughout the whole evolution, one can analyze the near equilibrium stage of the evolution to define a second dimensionless time flow, i.e. $w^{(\Lambda)} \equiv T_{\rm asym}(\tau)\tau = \left(\Lambda\tau\right)^{2/3}$.

Furthermore, just as in the homogeneous isotropization case [137], we also had to use a filter to avoid spurious growth of hard modes [230]. This is done by accessing the spectral coefficients $\{a_i\}$ and damping the high frequency modes using an exponential map of the type $a_i \to e^{-(n_1/N)^{n_2}}a_i$. Typical values for the pair (n_1, n_2) used in our work are in the ballpark of $(16, 18)$.

To check the numerical consistency of our results, besides standard tests such as the variation of number of collocant points N and the size of the time step $\Delta\tau$, we have also analyzed the late time convergence of the numerical solutions to the analytical NS solution (4.36); we were also able to reproduce the results of Wilke van der Schee's code[12] valid for $\mu/T = 0$. Another non-trivial consistency check is the observation that the value of δ as defined in Eq. (4.59) does not change in the course of the simulation. Our code that solves the Bjorken expanding far-from-equilibrium 1RCBH model was initially developed in Mathematica, and later translated to C++ using the Eigen linear algebra package [302] and OpenMP to parallelize the code.

4.5 Results

After presenting all the technical details in the previous section, now we present our results for the far-from-equilibrium Bjorken flow in the holographic 1RCBH model. In Fig. 4.3 we show the time evolution of the relevant observables characterizing the Bjorken expansion for a sample of numerical solutions with many different initial conditions and four different equilibrium values of μ/T. Subfigures (a) and (b) are the most important

[12] https://sites.google.com/site/wilkevanderschee/ads-numerics.

ones, as they show the evolution of the pressure anisotropy along with the coalescence to hydrodynamics at late times, with the dashed lines indicating the analytical NS result associated with (4.36). It is clear from subfigures (a) and (b) that, as the value of μ/T increases and approaches the critical point, the numerical solution takes longer to coalesce to hydrodynamics. Subfigures (c) and (d) show the evolution of the charge density $\hat{\rho} \equiv \kappa_5^2 \rho$, whose asymptotic behavior is used to extract the equilibrium value of μ/T in each simulation. Finally, subfigures (e) and (f) show the evolution of the scalar condensate (4.47), which similarly to the equilibrium solution [137], increases with increasing values of the charge density.

Regarding the hydrodynamization time defined in Eq. (4.38), we plot in Fig. 4.4 the results for its relative variation (as a function of μ/T) with respect to the SYM result at vanishing chemical potential

$$\Delta w_{\text{hydro}}^{(\varepsilon/\Lambda)} \equiv \frac{w_{\text{hydro}}^{(\varepsilon/\Lambda)}(\mu/T) - w_{\text{hydro}}^{(\varepsilon/\Lambda)}(0)}{w_{\text{hydro}}^{(\varepsilon/\Lambda)}(0)}. \tag{4.81}$$

Fig. 4.4 emphasizes, in a very clear way, the main result of Fig. 4.3 and of this work: the onset of hydrodynamics is significantly delayed as the chemical potential is increased towards its value at the critical point of the phase diagram, with $\Delta w_{\text{hydro}}^{(\Lambda)}$ being even larger than $\Delta w_{\text{hydro}}^{(\varepsilon)}$. Furthermore, subfigures (a) and (b) show that this qualitative effect is also robust against variations of the tolerance *tol* in Eq. (4.38).

4.6 Conclusions of the chapter

In the present chapter we presented a *first principles holographic calculation* of the full nonlinear evolution of a hot and dense (i.e., $\mu \neq 0$) far-from-equilibrium strongly coupled relativistic fluid with a critical point. We investigated how the top-down holographic construction corresponding to the 1RCBH model, which describes a superconformal non-Abelian plasma with a chemical potential, evolves in space and time undergoing Bjorken flow. We found that increasing μ/T towards its critical value considerably delays the emergence of hydrodynamic behavior, as defined by the relativistic Navier-Stokes equations. This feature of the 1RCBH model, if also applicable to QCD, could imply in important differences for correlation functions calculated in and out of equilibrium, with direct impact on the experimental searches for the QCD critical point, since the main signatures of the critical point are usually considered to be the cumulants of fluctuations of conserved charges [247, 248, 252].

Regarding the far-from-equilibrium properties of the 1RCBH model, it would also be interesting to investigate the presence of hydrodynamic attractor behavior in Bjorken

flow [95–101] and understand how the critical point affects the properties of such an attractor. Previous studies in the case of SYM at $\mu = 0$ and Gauss-Bonnet holography were already done in [99] and [101], respectively.

We stress that the 1RCBH model has important differences with respect to the QGP. For instance, the 1RCBH model is conformal, while the QGP is highly non-conformal in the crossover region. Moreover, the dynamic universality classes [303] are different: while QCD is expected to be in the type H dynamic universality class [288], the 1RCBH system is of type B [203]. The fact that the dynamic universality class of the 1RCBH model is of type B is interesting because in this case η/s is finite at the critical point, which means that viscous hydrodynamics is, in principle, well defined everywhere in the phase diagram. Nonetheless, it is also important to stress that phenomenologically realistic non-conformal holographic settings at finite temperature and chemical potential with a critical point may be constructed using the class of bottom-up holographic models first proposed in Ref. [202], which was recently investigated in [70] and [304]. Therefore, the results presented here may be seen as the first steps towards a more realistic holographic description of the far-from-equilibrium hot and dense QGP produced in heavy ion collisions.

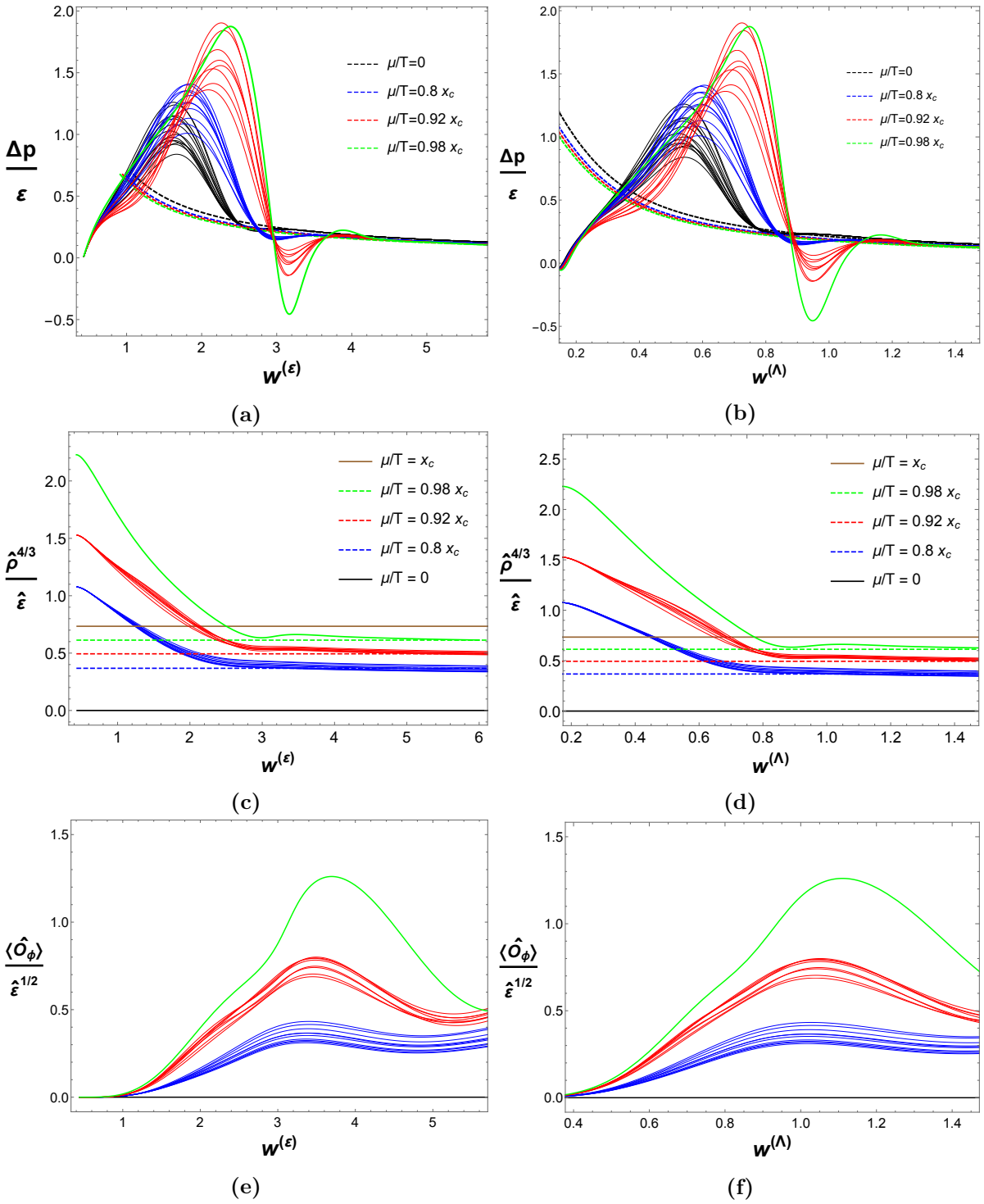

Figure 4.3: *Holographic results for the Bjorken flow evolution of far-from-equilibrium 1RCBH backgrounds as functions of $w^{(\varepsilon)}$ and $w^{(\Lambda)}$($x_c \equiv (\mu/T)_c = \pi/\sqrt{2}$ is the critical point [137, 146, 203]). (a)-(b) Pressure anisotropy divided by energy density (dashed curves are the corresponding Navier-Stokes results).(c)-(d) Charge density. (e)-(f) Scalar condensate.*

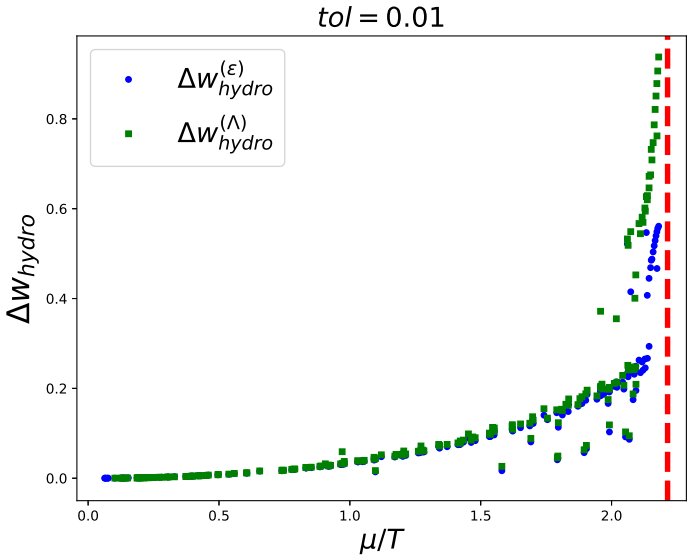

(a)

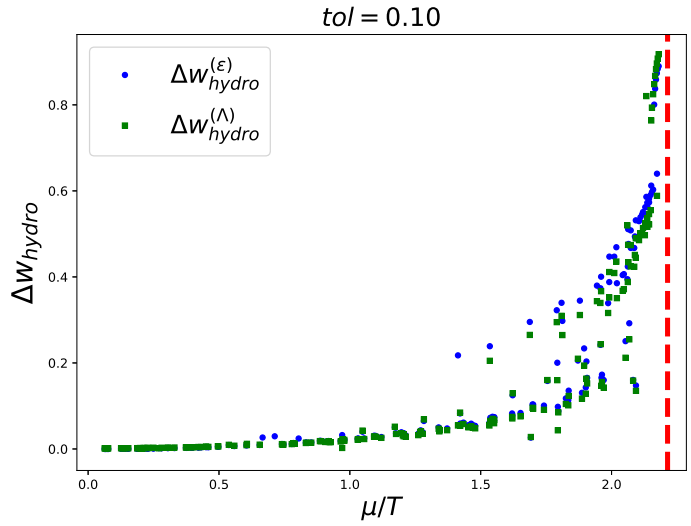

(b)

Figure 4.4: *Variation of the hydrodynamization time with respect to the vanishing chemical potential case, as defined in Eq. (4.81) (the vertical asymptote indicates the location of the critical point, $x_c \equiv (\mu/T)_c = \pi/\sqrt{2}$). Results using a tolerance tol of (a)* 1% *and (b)* 10% *in Eq. (4.38).*

Chapter 5

Conclusion and outlook

In this thesis, holography is employed to present for the first time first principle calculations of far-from-equilibrium dynamics of non-Abelian strongly coupled plasmas near a critical point. The motivation, as explained at length in the Introduction, is to unveil possible properties of the non-equilibrium QGP and eventually the QGP dopped with baryon charge that will be probed in future research programs [80, 88–90]. To be more specific, motivated by possible non-equilibrium effects probed in heavy ion collisions, we wanted to investigate the effects of the conjectured critical point in the properties of the far-from-equilibrium dynamics of the QGP.

In Chapter 2, after a brief revision of the original AdS/CFT conjecture, we introduced the holographic renormalization procedure that eliminates the divergences of the classical EMD holographic on-shell action [165–167]. This part is essential because it gave us the formulas for the one-point functions that were extensively used throughout Chapters 3 and 4.

In Chapter 3, once we reviewed the 1RCBH model, we started this enterprise by studying the homogeneous isotropization of a strongly coupled plasma near a critical point. In this homogeneous setup, where energy is conserved and there is no flow, we begin with anisotropic states far-from-equilibrium and evolve the system in time using numerical techniques of general relativity. The results, displayed in Sec. 3.5, show that the isotropization time that comes from pressure anisotropy always occurs before the true thermalization of the system, which is encompassed also by the relaxation of the scalar condensate. It is interesting to note also that the late time behavior of the time evolution is described by the QNM's extracted from a linear analysis, which were calculated in Appendix A. Moreover, the effect of the critical point in the dynamics is mild. The little sensitivity of the critical point might be a consequence that only non-hydrodynamic modes are probed in this system with the slow hydrodynamic modes being absent (as expected in a homogeneous isotropization problem).

Passing now to Chapter 4, we showed how to implement holographic Bjorken flow in the 1RCBH holographic model. This situation is more interesting than the previous homogeneous isotropization example because now there is nontrivial flow, i.e. hydrodynamics is applicable to late time solution. Accordingly, the purpose of the work done in that Chapter was to investigate the interplay between the critical point of the theory and the time that it takes for the system to display hydrodynamic behavior (hydrodynamization). The principal result, summarized in Fig. 4.4, tells us that the hydrodynamization time substantially increases near the critical point, a phenomenon similar to the critical slowing-down found in critical phenomena.

Altogether, the studies related above embody the very first steps towards understanding the *formation* of the QCD phase diagram that might be probed in future experiments of heavy ion collisons. Concomitant with holographic efforts, other research groups are also using different methods, such as the Functional Renormalization Group (FRG) approach [305, 306], to study non-equilibrium properties of the baryon rich QGP [307]. For instance, there is an interesting overlap of results obtained using different methods, e.g.: according to Ref. [307], time-dependent fluctuations have a peak on the thermalization scale near the critical point, wich is a result in consonance with what was found in Chapter 4 for the hydrodynamization time. For the future, one can expect further progress towards understanding the non-equlibrium dynamics of the QGP, either using only holography [308], or a mixture of holography and perturbative methods [309].

Appendix A

Quasinormal modes of the 1RCBH model

In this appendix we give a detailed analysis of the non-hydrodynamic QNM's of the 1RCBH. The introduction of this appendix, and Sections A.1 and A.2 are based on Ref. [146], whilst Sec. A.3 is based on the appendix of Ref. [137].

QNM's are exponentially damped collective excitations [310,311] that define the characteristic behavior of fluctuations of black holes and black branes (for reviews, see [136, 235,312,313]). The spectra of QNM's collectively describe the linear part of the decaying fluctuations of a disturbed black hole, a phenomenon known as "quasinormal ringing", which is analogous to the decaying sound emitted by a brass bell when struck by a mallet [314]. For this reason, QNM's are of great interest to astrophysical and cosmological observations since they describe the ringdown of possible black hole remnants of binary stars and black hole mergers, which were pivotal to the direct detection of gravitational waves earlier this year [315,316].

In the context of the holographic gauge/gravity duality [54,113–115], the QNM's of asymptotically AdS spacetimes carry wealthy information about the near equilibrium behavior of the dual strongly interacting QFT. In fact, the QNM's associated with the fluctuations of a given bulk field are related to the poles of the retarded Green's function of the dual operator in the QFT [179,317]. These poles describe hydrodynamic and non-hydrodynamic dispersion relations with which one can not only compute hydrodynamic transport coefficients but also derive upper bounds for characteristic equilibration times of the dual QFT plasma [178]. Additionally, non-hydrodynamic modes play an important role in determining the applicability of the hydrodynamic gradient series, as demonstrated by studies in holography [180,186] and also in kinetic theory [187,188,318].

Previous works [319–321] have dealt with QNM's in bottom-up Einstein-dilaton con-

structions [68, 69, 122, 201] exhibiting different kinds of phase transitions at zero chemical potential. Additionally, Ref. [322] investigated the QNM's associated with scalar operators in a top-down $\mathcal{N} = 2^*$ non-conformal plasma also at zero chemical potential. On the other hand, in [204] it was investigated how the QNM's of an external scalar perturbation and, in particular, the equilibration time associated with the imaginary part of the lowest non-hydrodynamical quasinormal frequency, depends on the temperature and baryon chemical potential in a bottom-up, QCD-like Einstein-Maxwell-dilaton model at finite baryon density [205]. In general, through the holographic correspondence, any question regarding the thermalization process in a given strongly coupled gauge theory necessarily involves a study of the QNM's of its gravity dual. These modes describe different timescales in the gauge theory and, close to a critical point, one may expect that the QNM's of the corresponding gravity dual display critical behavior.

Near a critical point, thermodynamical quantities typically display fast variations which enable the definition of critical exponents. Static properties such as single time correlation functions and linear response coefficients to time-independent perturbations display critical behavior which are determined by the underlying equilibrium distribution. However, anomalous behavior is also observed in many dynamical quantities such as the transport coefficients, which depend on the properties of multi-time correlations functions and are not determined by the information contained in the equilibrium distribution. In fact, while static thermodynamical properties of several different physical systems may be grouped into a few different (static) universality classes, dynamical properties associated with slowly varying hydrodynamical fluctuations of a system near criticality do not fit into this static classification scheme, as discussed in detail in [323] nearly 40 years ago. As a matter of fact, the dynamic universality classes reviewed in [323] require the study of hydrodynamic modes, i.e., collective excitations whose frequency vanishes in the case of homogeneous disturbances. While these modes dominate the long time behavior of the system (since they are associated with conserved currents) and can be used to study how transport coefficients (such as the shear viscosity) behave near a critical point, it is conceivable that there is more information about dynamical critical phenomena in multi-time correlation functions that cannot be obtained from their zero frequency limit.

In this Appendix, based on Ref. [146], we investigate the critical behavior displayed by non-hydrodynamic modes in strongly coupled gauge theories with gravity duals, i.e., QNM's corresponding to collective excitations in the dual plasma whose frequency does not vanish in the zero wavenumber limit. This novel type of critical phenomena determines the behavior of different characteristic equilibration times of the system at zero wavenumber and, since these QNM's are not directly associated with conserved currents, their behavior at criticality does not follow from the analysis made in Ref. [323]. As the

first study in this new arena, we compute QNM's for an external scalar perturbation and also for the diffusion channel associated with a vector perturbation in the so-called 1RCBH model [138–143] studied throughout this thesis. As mentioned in previous sections, this theory is conformal and its phase diagram is a function of a single dimensionless ratio μ/T, where μ and T are the $U(1)$ R-charge chemical potential and temperature of the black brane background, respectively. The model has a very simple phase diagram with a critical point at $\mu/T = \pi/\sqrt{2}$ and its static critical exponents were computed in [324] and [325]. Also, the fact that the R-charge conductivity remains finite at the critical point [324] shows that this model belongs to the type B dynamical universality class [323] and the anomalous static critical exponent was found to vanish in [325]. Thus, this model is of mean-field type [325], which was later argued [326] to be a general consequence of the underlying large N_c approximation. This simple model provides a useful arena for investigating dynamical phenomena in a strongly coupled plasma at finite temperature and density, even though it does not possess the full set of physical properties (such as chiral symmetry) displayed by the real world quark-gluon plasma (QGP) [223]. In fact, such a model may be useful for discovering new dynamical phenomena associated with critical endpoints in strongly coupled non-Abelian plasmas which could be further investigated in more realistic models of the QGP such as [204, 205] , with a view towards applications to the ongoing beam energy scan program at RHIC. Other studies of critical phenomena in holography include Refs. [202, 327–330].

As we are going to show in the next sections, the real and imaginary parts of non-hydrodynamical modes in the external scalar and vector diffusion channels display an infinite slope at the critical point of the phase diagram of the 1RCBH model. This holds true also for higher order QNM's, showing that high frequency modes are also sensitive to the presence of the critical point. In particular, from the imaginary part of the QNM's it is possible to extract the behavior of different characteristic equilibration times in the finite density plasma at criticality (at zero wavenumber) and define a dynamical critical exponent associated with their derivatives with respect to the dimensionless ratio μ/T. We find the same critical exponent $1/2$ for all the equilibration times investigated in the different channels. Except close to the critical point, we observe that by increasing the chemical potential one generally increases the damping of the quasinormal black brane oscillations which, consequently, leads to a reduction of the characteristic equilibration times of the dual plasma. However, as one approaches the critical point these equilibration times are enhanced (though they remain finite) and they acquire an infinite slope. We also find a purely imaginary, non-hydrodynamical mode in the vector diffusion channel at nonzero chemical potential and zero wavenumber which dictates the critical behavior of the equilibration time in this channel (this mode was also found in Ref. [331] in the

context of a $(4+1)$-dimensional Einstein-Maxwell model).

A.1 QNM's for an external scalar fluctuation

A.1.1 Equation of motion

We now analyze near-equilibrium properties of the system encoded in its quasinormal modes. In this section we calculate the QNM's for an external scalar perturbation φ on top of the 1RCBH backgrounds, which is described by the bulk action,

$$S = \frac{1}{2\kappa_5^2}\int d^5x\sqrt{-g}\left[-\frac{1}{2}(\partial\varphi)^2\right]. \tag{A.1}$$

The equation of motion following from this action is just the massless Klein-Gordon equation on top of the solution given by Eq. (3.34). We take a plane-wave Ansatz for the Fourier modes of the perturbation, $\varphi = \mathrm{e}^{-i\omega t+i\vec{k}\cdot\vec{x}}\tilde{\varphi}(\omega,\vec{k},r)$, which for brevity we write simply as $\tilde{\varphi}(\omega,\vec{k},r)\equiv\tilde{\varphi}(r)$. The resulting equation of motion then only depends on the frequency ω, the magnitude of the spatial 3-momentum $k\equiv|\vec{k}|$, and the background control parameter y given by

$$y^2+\left(\frac{\mu}{T}\right)^2=1,\quad y\in[-1,1]. \tag{A.2}$$

In what follows we employ the in-falling EF "time" coordinate defined by,

$$dv = dt+\sqrt{-\frac{g_{rr}}{g_{tt}}}dr = dt+\frac{\mathrm{e}^{B-A}}{h}dr, \tag{A.3}$$

in terms of which the metric (3.34) becomes

$$ds^2 = \mathrm{e}^{2A}\left(-hdv^2+d\vec{x}^2\right)+2\mathrm{e}^{A+B}dvdr. \tag{A.4}$$

One of the main advantages of the EF coordinates is that the in-falling wave condition at the horizon, which is associated with the retarded Green's function, becomes automatically satisfied by just requiring regularity of the solutions there. In these coordinates, the equation of motion for $\tilde{\varphi}$ becomes,

$$\tilde{\varphi}''+\left(4A'-B'+\frac{h'}{h}\right)\tilde{\varphi}'-i\omega\frac{\mathrm{e}^{B-A}}{h}(2\tilde{\varphi}'+3A'\tilde{\varphi})-k^2\frac{\mathrm{e}^{2(B-A)}}{h}\tilde{\varphi}=0. \tag{A.5}$$

We map the radial coordinate r, defined on the interval $r_H\le r<\infty$, to a new dimensionless radial coordinate $u=r_H/r$, defined on the interval $0\le u\le 1$, which is more suitable

to be used in the pseudospectral method [230]. In these new coordinates, the equation of motion for the external scalar perturbation becomes,

$$\tilde{\varphi}'' - \frac{\left(u^4(3-y)+2u^2(1-y)-3(1+y)\right)\tilde{\varphi}'}{u\left(1-u^2\right)\left(u^2(3-y)+1+y\right)} + \\ - \frac{2i(\omega/T)}{\pi\left(1-u^2\right)\sqrt{3-y}\left(u^2(3-y)+1+y\right)}\left(\frac{\left(4u^2(1-y)+3(y+1)\right)\tilde{\varphi}}{u\sqrt{2u^2(1-y)+1+y}} + \right. \\ \left. + 2\sqrt{2u^2(1-y)+1+y}\,\tilde{\varphi}'\right) - \frac{4(k/T)^2\tilde{\varphi}}{\pi^2\left(1-u^2\right)(3-y)\left(u^2(3-y)+1+y\right)} = 0, \qquad \text{(A.6)}$$

where the primes now denote derivatives with respect to the new radial coordinate u. From the discussion above, and from the definition of the background control parameter y in Eq. (A.2), one concludes that the dimensionless quasinormal eigenfrequencies, ω/T, will depend only on the dimensionless ratios μ/T and k/T.

To completely specify the eigenvalue problem to be solved in order to find the QNM spectra associated to this external scalar perturbation, we still need to impose a Dirichlet boundary condition. From the fact that $\tilde{\varphi}$ is a scalar field defined on an asymptotically AdS_5 background, it follows that asymptotically close to the boundary it may be written as $\tilde{\varphi}(u) = G(u) + u^4 F(u)$, with the leading, non-normalizable mode $G(u \to 0) = J(\omega, \vec{k})$ being the source for the QFT operator $\hat{O}$ dual to the (external) scalar field φ, and the subleading, normalizable mode $F(u \to 0) = \langle \hat{O}(\omega, \vec{k}) \rangle$ being its expectation value. According to the real time holographic dictionary [160], the retarded propagator of the QFT operator $\hat{O}$ is given the ratio between the normalizable and non-normalizable modes, $\mathcal{G}^R_{\hat{O}\hat{O}}(\omega, \vec{k}) = -\langle \hat{O}(\omega, \vec{k}) \rangle / J(\omega, \vec{k})$, therefore, if we impose as a Dirichlet boundary condition the selection of the normalizable mode by setting $G(0) = 0$ with $F(0) \neq 0$, we are left with an eigenvalue problem whose eigenfrequencies correspond to dispersion relations $\omega/T = \omega(k/T; \mu/T)/T$ describing the poles of $\mathcal{G}^R_{\hat{O}\hat{O}}$, which are the QNM's we are looking for. Then, we set $\tilde{\varphi}(u) = u^4 F(u)$, with $F(0) \neq 0$, from which it follows that,

$$16u\left(1 - \frac{2}{u^2(3-y)+1+y}\right)F + \left(u^2\left(9 - \frac{8}{u^2(3-y)+1+y}\right) - 5\right)F' + \\ - u\left(1-u^2\right)F'' + \frac{2i(\omega/T)}{\pi\sqrt{3-y}\left(u^2(3-y)+1+y\right)}\left(-\frac{\left(12u^2(1-y)+5(1+y)\right)F}{\sqrt{2u^2(1-y)+1+y}} + \right. \\ \left. + 2u\sqrt{2u^2(1-y)+1+y}\,F'\right) + \frac{4(k/T)^2 uF}{\pi^2(3-y)\left(u^2(3-y)+1+y\right)} = 0. \qquad \text{(A.7)}$$

We now have a Generalized Eigenvalue Problem (GEP) for the eigenfunction $F(u)$ and the quasinormal eigenfrequency ω/T, which may be solved as functions of k/T and μ/T.

In this work we use the pseudospectral method.

Note that Eq. (A.7) also reveals one of the greatest virtues of the EF coordinates, namely, the fact that it reduces the QNM eigenvalue problem from a Quadratic Eigenvalue Problem [332] in the standard set of spacetime coordinates to a GEP, which requires far less computational cost when numerically evaluating the QNM spectra.

A.1.2 QNM spectra and equilibration time

In Fig. A.1 we show the evolution of the external scalar QNM spectra for the first 26 poles as we evolve k/T from 0 to 100, both for the AdS_5-Schwarzschild background at $\mu/T = 0$ and the critical geometry at $\mu/T = \pi/\sqrt{2}$. We observe the usual non-hydrodynamical QNM structure for the external scalar channel with an infinite series of QNM pairs with $\mathrm{Im}\,\omega < 0$ and $\mathrm{Re}\,\omega \neq 0$ symmetrically distributed with respect to the imaginary axis [179]. When $k/T = 0$, by increasing the μ/T ratio one increases the magnitude of the imaginary part of the QNM's, which becomes more appreciable for higher order, faster varying modes. On the other hand, an increase in k/T enhances (suppresses) the magnitude of the real (imaginary) part of the poles. We see that by increasing the chemical potential one generally increases the damping of the quasinormal black hole oscillations, which qualitatively agrees with the result found previously in [204] for a non-conformal, QCD-like bottom-up EMD model describing the physics of the QGP at finite baryon density.

Also, we note that the non-hydrodynamic modes in Fig. A.1 remain finite when evaluated at the critical point, even when $k = 0$. Thus, one can see that the timescales contained in the non-hydrodynamic modes are different than the usual relaxation time quantity $\tau_{rel} \sim \xi^z$, where ξ is the correlation length (which diverges at the critical point) and z is the dynamical critical exponent, which becomes infinitely large at criticality describing the well-known phenomenon of critical slowing down. Nevertheless, in this strongly coupled model the microscopic scales defined by the non-hydrodynamic QNM's still display some critical behavior, as we show below.

In Figs. A.2 and A.3 we display the imaginary and real parts of the first 4 QNM's as functions of μ/T, for both stable and unstable branches, at $k/T = 0$ and $k/T = 1$. We see that at the critical point all the QNM's develop an infinite slope. Moreover, we also note that the effects on the non-hydrodynamic modes due to finite momentum are small for $k/T \sim 1$ (especially for the imaginary part), being more pronounced for the lowest QNM's, which seems to be a general holographic property of the dispersion relation of non-hydrodynamics QNM's known as "ultralocality" [333, 334].

Following [178], one may define an upper bound for the equilibration time of the plasma, τ_{eq}, using the inverse of minus the imaginary part of the lowest non-hydrodynamical

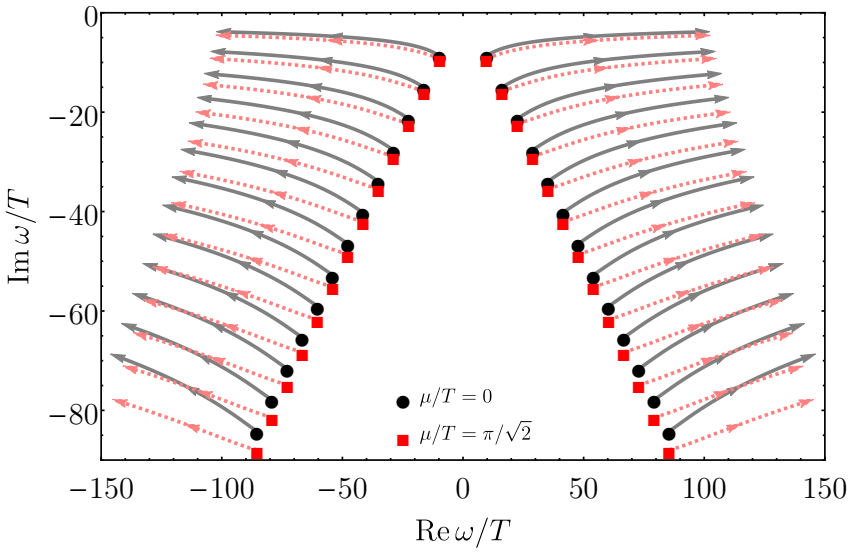

Figure A.1: *First 26 QNM's trajectories in the external scalar channel evolved within the interval* $0 \leq k/T \leq 100$ *for* $\mu/T = 0$ *(beginning with a black dot for* $k = 0$ *and evolving into solid gray lines for* $k > 0$*) and for the critical point* $\mu/T = \pi/\sqrt{2}$ *(beginning with a red square for* $k = 0$ *and evolving into dashed pink lines for* $k > 0$*).*

QNM evaluated at zero momentum. This is shown in Fig. A.4 (a), from which one can see that far from the critical point the equilibration time of the finite $U(1)$ R-charge density SYM plasma decreases with increasing chemical potential, again in qualitative agreement with what was previously found in [204] in the context of a phenomenologically realistic holographic model for the QGP at finite baryon chemical potential. However, for larger chemical potentials, as one approaches the critical point of the model, this behavior is modified and the equilibration time starts to increase, acquiring an infinite slope at the critical point.

We may associate a new critical exponent with the derivative of the equilibration time, $d(T\tau_{\rm eq})/d(\mu/T)$, since it diverges at the critical point, as shown in Fig. A.4 (b). Close to the critical point,

$$\frac{d(T\tau_{\rm eq})}{d\,(\mu/T)} \sim \left(\frac{\pi}{\sqrt{2}} - \frac{\mu}{T}\right)^{-\theta}, \tag{A.8}$$

where θ is the dynamical critical exponent which we want to calculate. We performed numerical fits of Eq. (A.8) to the data shown in Fig. A.4 (b) for different sets of intervals in μ/T increasingly closer to the critical point at $\mu/T = \pi/\sqrt{2}$. The final result gives a critical exponent compatible with $\theta = 1/2$.

More generally, one may consider different characteristic equilibration times of the medium associated with the different non-hydrodynamic QNM's, where equilibration times associated with higher order modes should be understood as estimates for how fast the system relaxes to equilibrium depending on how rapidly varying are the perturbations

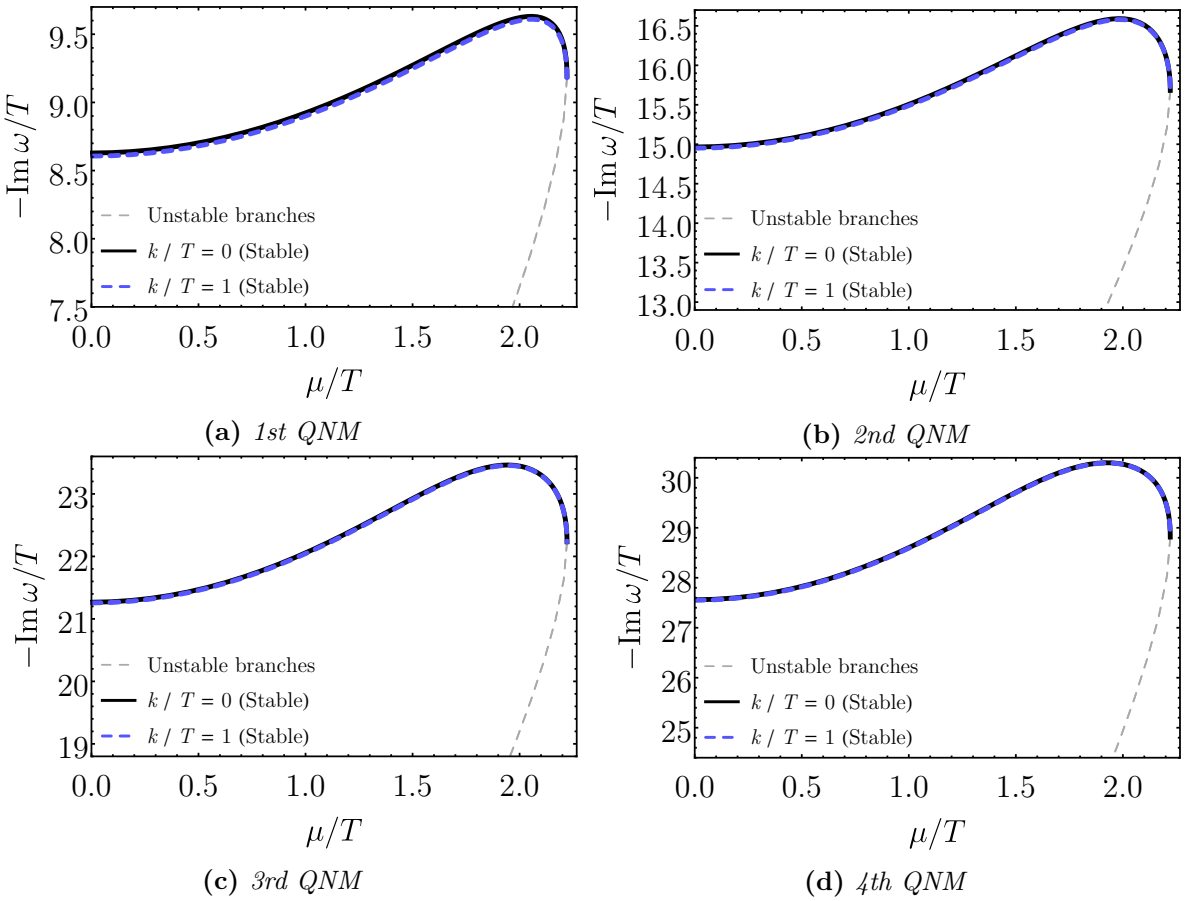

(a) *1st QNM* **(b)** *2nd QNM*

(c) *3rd QNM* **(d)** *4th QNM*

Figure A.2: *Imaginary part of the first 4 QNM's in the external scalar channel for* $k/T = 0$ *and* $k/T = 1$*, as a function* μ/T*, for both stable and unstable branches.*

to which it is subjected. Operationally, this amounts for computing the inverse of minus the imaginary part of the different non-hydrodynamic QNM's. By doing so, we obtain the same dynamical critical exponent $\theta = 1/2$ associated with all the different characteristic equilibration times of the plasma in the external scalar channel at zero wavenumber.

A.2 QNM's in the vector diffusion channel

A.2.1 Equation of motion

In this section we compute the QNM's of the vector diffusion channel in the long wavelength limit. Differently from what was done in the last section where we considered an external scalar perturbation on top of the 1RCBH background, now we need to consider fluctuations of the Maxwell field A_μ which is already nonzero in the background and, therefore, we also need to consider disturbances in the background metric $g_{\mu\nu}$ and dilaton field ϕ. At zero spatial momentum the different channels for these fluctuations, at the linearized level, are classified by different representations of the $SO(3)$ rotation group

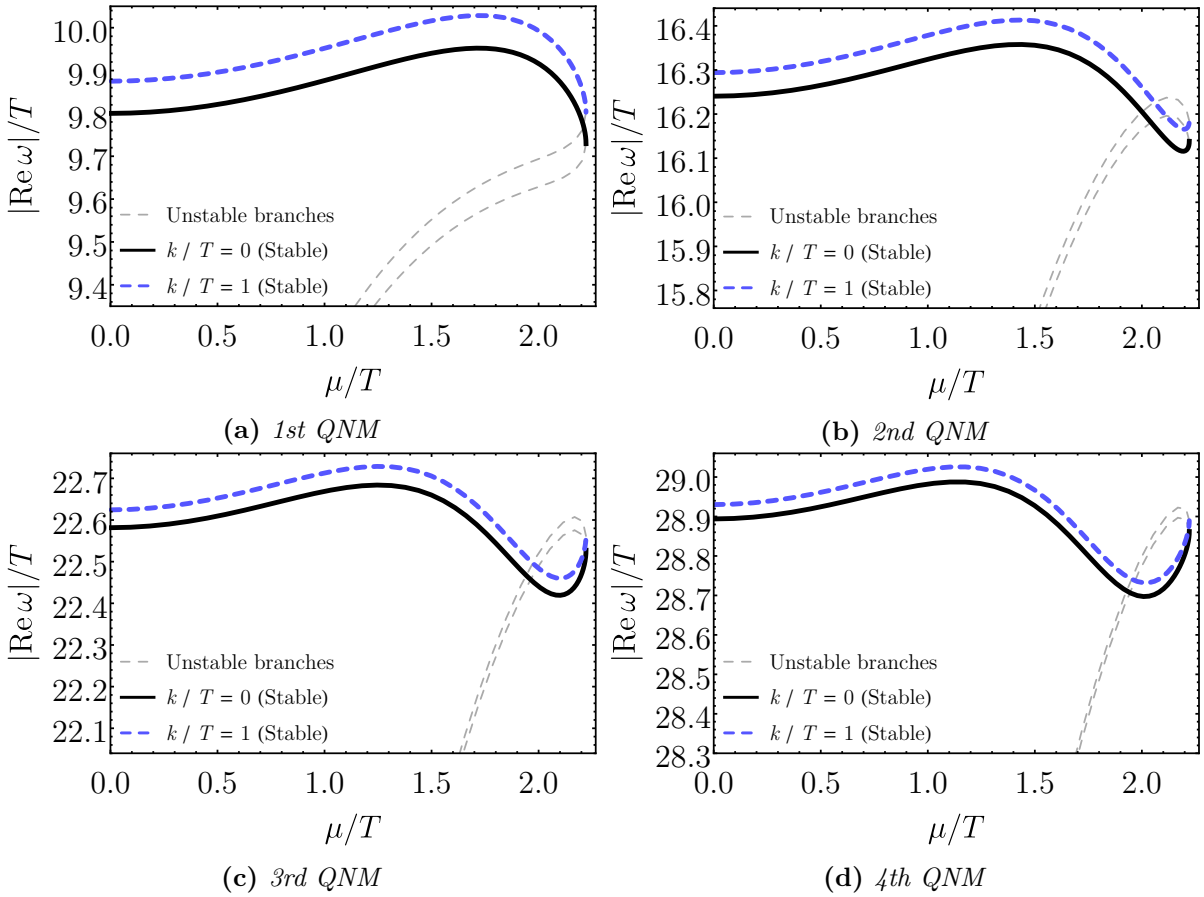

(a) *1st QNM* **(b)** *2nd QNM*

(c) *3rd QNM* **(d)** *4th QNM*

Figure A.3: *Absolute value of the real part of the first 4 QNM's in the external scalar channel for $k/T = 0$ and $k/T = 1$, as a function μ/T, for both stable and unstable branches.*

[203].[1] By taking the fluctuation of the gauge field along the z direction one finds that at the linearized level it only mixes with the fluctuation of g_t^z. Taking now the long wavelength limit, i.e. $k = 0$, we write down for the Fourier modes of these fluctuations,

$$\delta A_z = a(r)e^{-i\omega t}, \quad \delta g_t^z = s(r)e^{-i\omega t}. \tag{A.9}$$

[1] At nonzero k such classification is no longer valid and the corresponding fluctuations are organized in a more complicated way under a smaller $SO(2)$ symmetry group. We are not going to pursue the investigation of this more involved case in the present work.

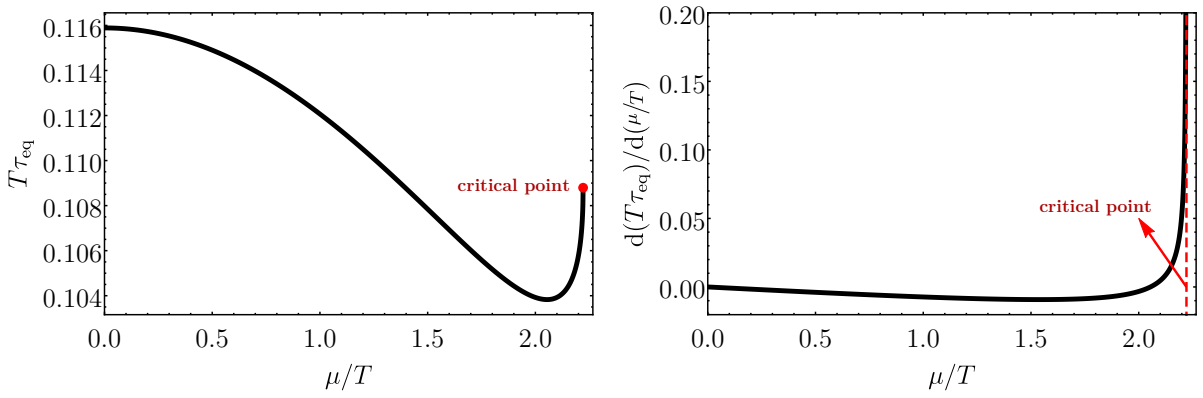

(a) **(b)**

Figure A.4: *Equilibration time (a) and its normalized derivative (b) in the external scalar channel as functions of μ/T at zero wavenumber.*

Then, the linearized Maxwell's equations, $\nabla_\mu\left(f(\phi)F^{\mu\nu}\right)=0$, expressed in Eddington-Finkelstein coordinates read,

$$-\Phi''+\left(-2A'+B'-\frac{f'(\phi)\phi'}{f(\phi)}\right)\Phi'=0, \tag{A.10}$$

$$a''+\left(2A'-B'+\frac{h'}{h}-2i\omega\frac{\mathrm{e}^{A-B}}{h}+\frac{f'(\phi)\phi'}{f(\phi)}\right)a'-i\omega\mathrm{e}^{B-A}\frac{f(\phi)A'+f'(\phi)\phi'}{f(\phi)h}a+ \\ +\frac{\Phi'}{2h'}s'+\left[\frac{f'(\phi)\phi'\Phi'+f(\phi)\Big((2A'-B')\Phi'+\Phi''\Big)}{2f(\phi)h}\right]s=0, \tag{A.11}$$

where the first equation is the equation of motion for the background Maxwell field, $\Phi(r)$, while the second equation is the equation of motion for the Maxwell perturbation, $a(r)$. We may decouple the perturbations $a(r)$ and $s(r)$ by using Einstein's equations for the metric field,

$$R_{\mu\nu}-\frac{g_{\mu\nu}}{3}\left(V(\phi)-\frac{f(\phi)}{4}F_{\alpha\beta}^2\right)-\frac{f(\phi)}{2}F_{\mu\alpha}F_{\nu}{}^{\alpha}-\frac{1}{2}\partial_\mu\phi\partial_\nu\phi=0. \tag{A.12}$$

By taking the vz-component minus the rz-component of the above equation of motion, one obtains the constraint,

$$s'=-f(\phi)\Phi'\mathrm{e}^{-2A}a. \tag{A.13}$$

By using the zeroth order Eq. (A.10) to eliminate the $s(r)$ term from Eq. (A.11) and substituting (A.13) into (A.11), one obtains a decoupled equation of motion for the radial profile of the vector field perturbation, which is associated with the diffusion of the $U(1)$

R-charge [179, 203],

$$a'' + \left[2A' - B' + \frac{h'}{h} + \frac{f'(\phi)\phi'}{f} - 2i\omega\frac{\mathrm{e}^{B-A}}{h}\right]a' + \\ -\frac{\mathrm{e}^{-2A}}{h}\left[i\omega\mathrm{e}^{A+B}\left(A' + \phi'\frac{f'(\phi)}{f(\phi)}\right) + f(\phi)\Phi'^2\right]a = 0. \tag{A.14}$$

Once again we apply the radial coordinate transformation $r \to r_H/u$, which yields,

$$a'' + \left(-\frac{10u^6(y-3)(y-1) - 3u^4(5(y-2)y+1) + 4u^2\left(y^2-1\right) + (y+1)^2}{u\left(u^2-1\right)\left(u^2(y-3) - y - 1\right)\left(-2u^2(y-1) + y + 1\right)^2} + \right. \\ \left. -\frac{4i(\omega/T)\sqrt{(3-y)\left(-2u^2(y-1)+y+1\right)}}{\pi\left(u^2-1\right)(y-3)\left(u^2(y-3)-y-1\right)}\right)a' + \\ + \left(-\frac{8u^4(y-3)(y-1)(y+1)}{\left(u^2-1\right)\left(u^2(y-3)-y-1\right)\left(-2u^2(y-1)+y+1\right)^2} + \right. \\ \left. -\frac{2i(\omega/T)\left(4u^2(y-1)+y+1\right)}{\pi\left(u^2-1\right)u\left(u^2(y-3)-y-1\right)\sqrt{(y-3)\left(2u^2(y-1)-y-1\right)}}\right)a = 0. \tag{A.15}$$

For the vector perturbation the normalizable mode at the boundary corresponds to set $a(u) = u^2F(u)$, with $F(0) \neq 0$, from which one finally obtains,

$$F'' + \left[-\frac{18u^6(y-3)(y-1) - 7u^4(5(y-2)y+1) + 20u^2\left(y^2-1\right) - 3(y+1)^2}{\left(u^2(y-3)-y-1\right)\left(-2u^2(y-1)+y+1\right)} + \right. \\ \left. -\frac{4iu(\omega/T)\sqrt{(3-y)\left(-2u^2(y-1)+y+1\right)}}{\pi(y-3)\left(u^2(y-3)-y-1\right)}\right]\frac{1}{u(u^2-1)}F' + \\ + \frac{1}{u(u^2-1)}\left[\frac{8u\left(6u^6(y-3)(y-1)^2 - 2u^4(y(7(y-3)y+9)+5)\right)}{\left(u^2(y-3)-y-1\right)\left(-2u^2(y-1)+y+1\right)^2}\right. \\ + \frac{8u\left(u^2(y+1)(3y-5)(3y-1) - 2(y-1)(y+1)^2\right)}{\left(u^2(y-3)-y-1\right)\left(-2u^2(y-1)+y+1\right)^2} \\ \left. -\frac{6i(\omega/T)\left(4u^2(y-1)-y-1\right)}{\pi\left(u^2(y-3)-y-1\right)\sqrt{(y-3)\left(2u^2(y-1)-y-1\right)}}\right]F = 0. \tag{A.16}$$

A.2.2 QNM spectra and equilibration time

With the QNM eigenvalue problem completely specified as discussed above, we can now apply the pseudospectral method to numerically solve it. In Fig. A.5 we display the QNM spectra for the first 30 symmetric poles in the vector diffusion channel in the limiting cases of $\mu/T = 0$ (AdS_5-Schwarzschild) and $\mu/T = \pi/\sqrt{2}$ (critical point). In Figs. A.6 and A.7 we show the imaginary and real parts of the first 4 complex QNM's as functions of μ/T, for both stable and unstable branches. We see that also in the vector

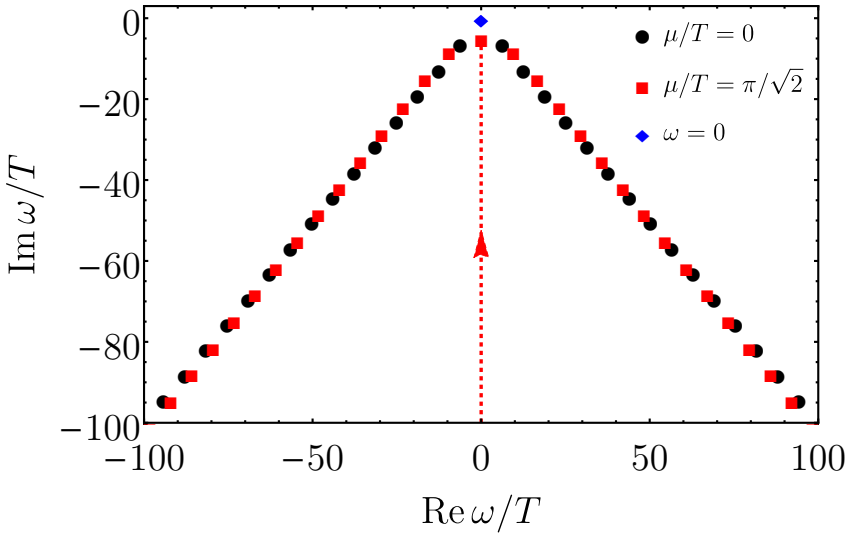

Figure A.5: *QNM spectra of the first 30 symmetric poles in the vector diffusion channel for* $\mu/T = 0$ *(black circles) and* $\mu/T = \pi/\sqrt{2}$ *(red squares) at* $k/T = 0$*. The hydrodynamical diffusive pole is depicted by the blue diamond. Note also the emergence of a new purely imaginary, non-hydrodynamical mode which comes from* $-i\infty$ *at* $\mu/T = 0$ *and remains at a finite distance from the origin at the critical point* $\mu/T = \pi/\sqrt{2}$*.*

diffusion channel both the real and imaginary parts of the QNM's develop an infinite slope at the critical point.

We remind the reader that at $k = \mu = 0$ the QNM spectra in the vector diffusion channel may be analytically calculated [179],

$$\frac{\omega}{T} = 2\pi n(1-i), \;\; n \in \mathbb{N} \;\; \text{at} \;\; \mu = 0. \tag{A.17}$$

Our numerical calculations at $\mu/T = 0$ agree with this analytical result. The standard hydrodynamical mode $\omega(k/T = 0)/T = 0$ is depicted by the blue diamond in Fig. A.5. Since this is a hydrodynamical pole, it does not evolve with the chemical potential if we keep $k = 0$. This mode determines the R-charge conductivity of the model and the zero frequency limit of this transport coefficient was found in [203] to remain finite at the critical point, as expected for a type B dynamic universality class. However, it was noticed in [203] that the derivative of this quantity near the critical point has infinite slope described by an exponent equal to 1/2, which matches the exponent found in the previous section in the study of non-hydrodynamic modes of different nature corresponding to external scalar perturbations.

On the other hand, the main effect of the chemical potential on the symmetric non-hydrodynamical modes is to increase the magnitude of both the imaginary and real parts of these poles. Therefore, also in the vector diffusion channel one sees that the inclusion of a chemical potential leads to additional damping for the quasinormal black hole oscillations.

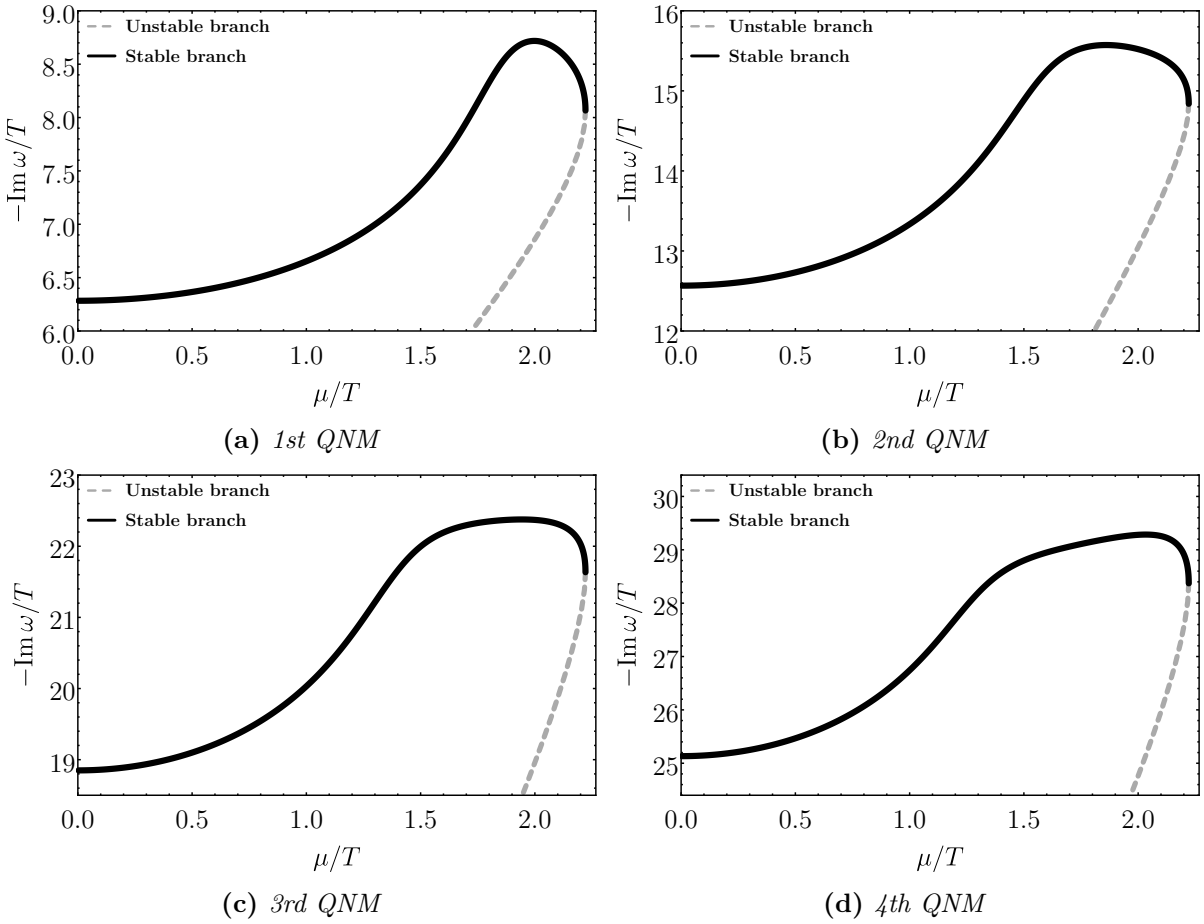

(a) *1st QNM* **(b)** *2nd QNM*

(c) *3rd QNM* **(d)** *4th QNM*

Figure A.6: *Imaginary part of the first 4 QNM's in the vector diffusion channel for $k/T = 0$, as a function of μ/T, for both stable and unstable branches.*

A novel feature we observe in Fig. A.5 is the emergence of a new purely imaginary, non-hydrodynamical pole at finite chemical potential, which comes from $\omega/T \to -i\infty$ at $\mu/T = 0$ and lies at $\omega/T \approx -7.315i$ at the critical point $\mu/T = \pi/\sqrt{2}$. For $\mu/T \gtrsim 2$, this new purely imaginary pole becomes the lowest non-hydrodynamical mode, while for lower values of the chemical potential the lowest non-hydrodynamical mode is given by any of the first two symmetric poles with respect to the imaginary axis. Therefore, this new non-hydrodynamical imaginary mode plays a crucial role in the description of the equilibration time of the system in the vector diffusion channel when the chemical potential is large, specially at criticality, when it dominates the physics of the slowest varying perturbations. The appearance of such a purely imaginary mode is an interesting feature of this model that shows that the distinction between transient phenomena at weak and strong coupling, currently understood in terms of their different pattern of non-hydrodynamic modes at zero wavenumber [335] (see also [336]) corresponding to fluctuations around global equilibrium, can become more complicated near a critical point.

We define the upper bound for the equilibration time of the system in the vector

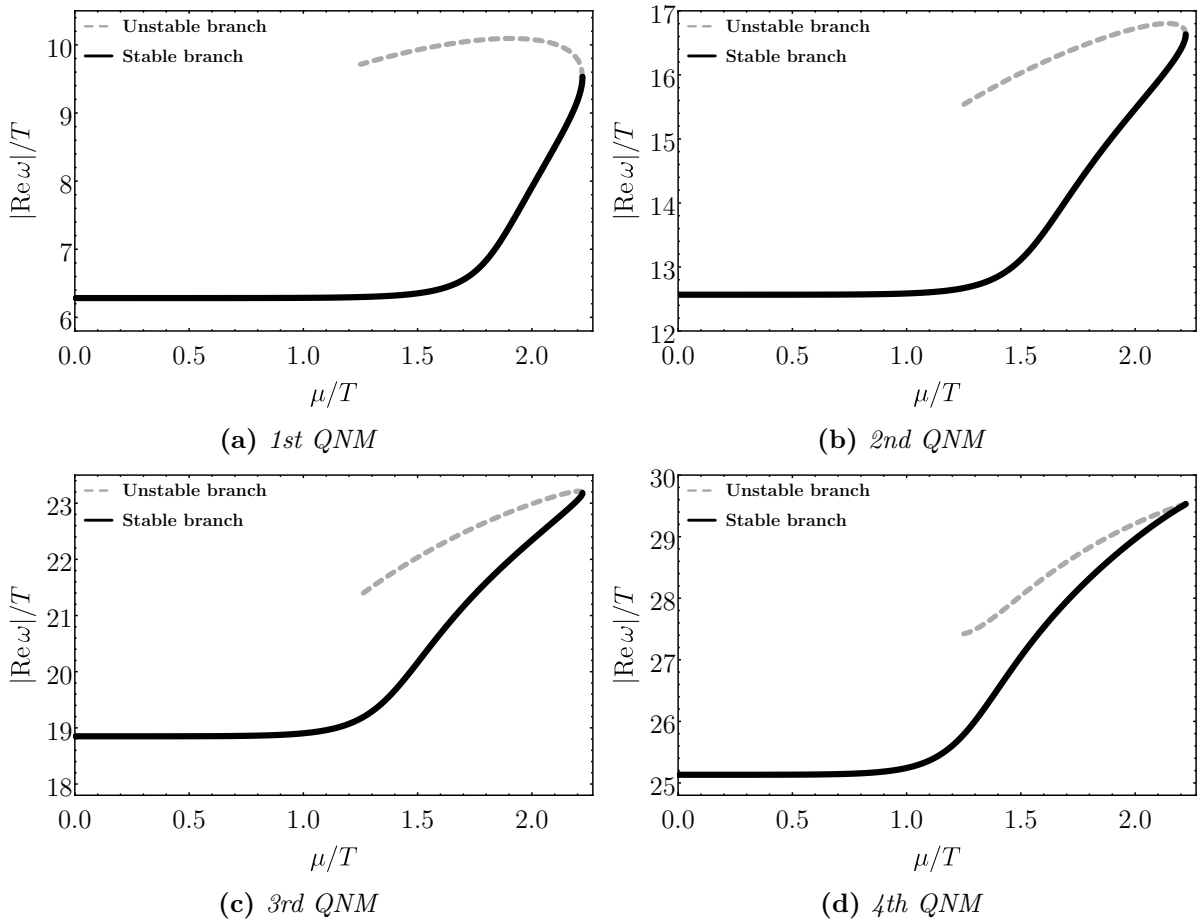

Figure A.7: *Absolute value of the real part of the first 4 QNM's in the vector diffusion channel for $k/T = 0$, as a function μ/T, for both stable and unstable branches.*

diffusion channel as before by taking the inverse of minus the imaginary part of the lowest non-hydrodynamical QNM. The result is shown in Fig. A.8 (a). The kink observed in the equilibration time at $\mu/T \approx 2$ is due to the shift from the regime dominated by the first symmetric poles to the regime dominated by the new purely imaginary mode. This also causes a discontinuity in the derivative of the equilibration time, as seen in Fig. A.8 (b). As before, one can calculate the critical exponent associated with this derivative at the critical point and the result is once again compatible with $\theta = 1/2$. This shows that in this model both the hydrodynamic and the non-hydrodynamic modes in this vector diffusion channel have the same critical exponents.

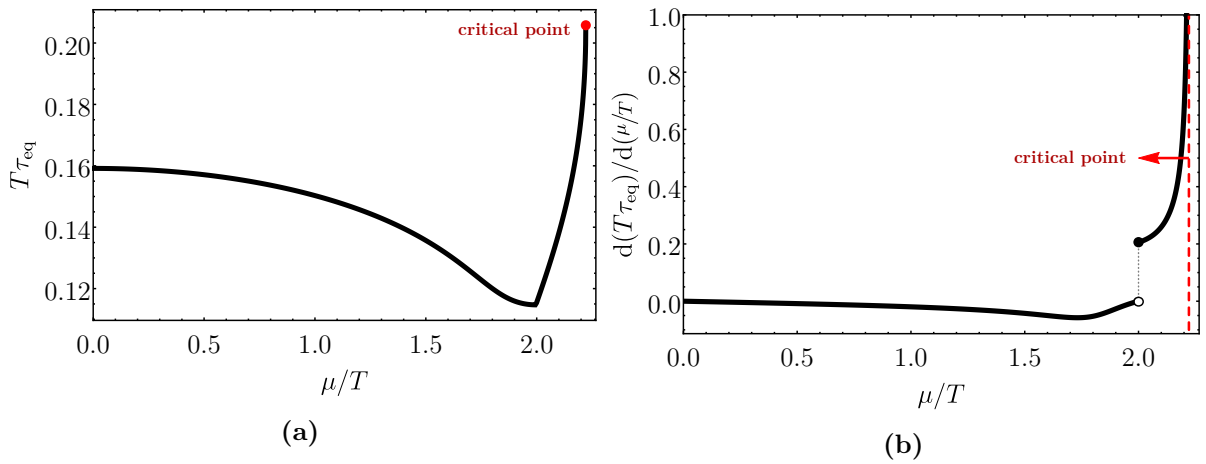

Figure A.8: *Equilibration time (a) and its normalized derivative (b) in the vector diffusion channel as functions of μ/T.*

A.3 QNM's for the dilaton channel

A.3.1 Equation of motion

Now, we obtain the QNMs of the 1RCBH model for the $SO(3)$ singlet (dilaton) channel in the homogeneous, zero wavenumber limit complementing the study carried out in Ref. [146] where the $SO(3)$ quintuplet (external scalar) and triplet (vector diffusion) channels have been analyzed in detail.

As discussed in Ref. [203], at zero wavenumber the EMD system features a rotational $SO(3)$ symmetry under which the gauge and diffeomorphism invariant perturbations of the system are organized into a quintuplet channel corresponding to the five traceless spatial components of the perturbation of the metric field h_{ij}, a triplet channel corresponding to the three spatial components of the perturbation of the Maxwell field a_i, and a singlet channel corresponding to a combination involving the dilaton perturbation φ and the trace of the spatial part of the perturbation of the metric field, namely,

$$\mathcal{S} = \varphi - \frac{\phi'}{2A'}\frac{1}{3}\left(h_{xx} + h_{yy} + h_{zz}\right), \tag{A.18}$$

where one sees that the background dilaton field ϕ couples the dilaton fluctuation with the spatial trace of the graviton. This $\mathcal{S}$-perturbation is analogous to the Z_2-mode of the so-called "non-conformal channel" discussed in Ref. [321].[2] This was called a non-conformal channel because this mode is intrinsically associated with the background dilaton field, which in the Einstein-dilaton models analyzed in Ref. [321] was responsible for breaking

[2]Note, however, that in Ref. [321] an $SO(2)$ group was associated with the residual rotational symmetry of the system in the spatial plane orthogonal to the direction of the nontrivial wavenumber of the perturbations.

conformal symmetry. However, the dilaton field may also preserve conformal symmetry when in the presence of other fields, as in the case of the 1RCBH model studied here. Therefore, more generally, one could say that this $\mathcal{S}$-perturbation defines the "dilaton channel". This nomenclature is also adequate due to the fact that this mode shares the same near-boundary asymptotics of the background dilaton field [203, 321].

The linearized equation of motion for the $\mathcal{S}$-perturbation derived in Ref. [203] translates as follows to the modified EF coordinates (3.34),[3]

$$S'' + \frac{\left(h\left(4A' - B'\right) - 2i\omega e^{B-A} + h'\right)}{h} S' + \frac{e^{-2A}}{18fh\left(A'\right)^2}\left(-18\left(A'\right)^2\left(\partial_\phi f\right)^2\left(\Phi'\right)^2 + f\left(3\left(A'\right)^2\left(-6e^{2(A+B)}\partial_\phi^2 V + 8e^{2A}h\left(\phi'\right)^2 + 3\partial_\phi^2 f\left(\Phi'\right)^2\right) + 6A'\phi'\left(e^{2A}\left(h'\phi' - 2e^{2B}\partial_\phi V\right) + \partial_\phi f\left(\Phi'\right)^2\right) - 54i\omega e^{A+B}\left(A'\right)^3 - e^{2A}h\left(\phi'\right)^4\right)\right) S = 0, \tag{A.19}$$

where ω is the frequency of the plane-wave Ansatz for the $\mathcal{S}$-perturbation, which shall give the QNM's of the dilaton channel under appropriate boundary conditions to be discussed below.

In order to solve the eigenvalue problem to be derived next for the quasinormal frequencies of the system we make use of the pseudospectral method as done in Ref. [146]. For this, we begin by mapping the radial coordinate $\tilde{r} \in [\tilde{r}_h, \infty)$ into a new radial coordinate $\tilde{r}_h/\tilde{r} =: \tilde{u} \in [0, 1]$. By doing so and substituting the equilibrium 1RCBH backgrounds (3.34) — (3.39) into the equation of motion (A.19), one is left with a linear differential equation for the perturbation $\mathcal{S}(\tilde{u})$ on top of the equilibrium 1RCBH backgrounds. In general, the near-boundary, ultraviolet asymptotic behavior of the $\mathcal{S}$-perturbation is given by, $\mathcal{S}(\tilde{u}) \sim \tilde{u}^{4-\Delta}G(\tilde{u}) + \tilde{u}^{\Delta}Y(\tilde{u}) + \cdots$, as $\tilde{u} \to 0$. Since in the 1RCBH model $\Delta = 2$, we have two degenerate exponents equal to two. As discussed in detail in Ref. [146], the correct eigenvalue problem for the QNM's is obtained by working with the subleading, normalizable mode of the relevant perturbation (in the dilaton channel considered here, the normalizable mode is associated with the expectation value of the boundary operator dual to the dilaton field, $\langle \mathcal{O}_\phi \rangle$), which in the present case corresponds to set the Dirichlet boundary condition $G(0) = 0$ with $Y(0) \neq 0$. Then, by substituting $\mathcal{S}(\tilde{u}) =: \tilde{u}^2 Y(\tilde{u})$ into the equation of motion for $\mathcal{S}(\tilde{u})$ and defining the dimensionless quasinormal frequency

[3] In order to go from the domain-wall coordinates used in Ref. [203] to the modified EF coordinates (3.34), one simply uses that $d/d\tilde{r} = (\partial v/\partial \tilde{r})\partial_v + \partial_{\tilde{r}}$ and $d/dt = (\partial v/\partial t)\partial_v$, where $\partial v/\partial \tilde{r} = \sqrt{-g_{\tilde{r}\tilde{r}}/g_{tt}} = e^{B-A}/h$ and $\partial v/\partial t = 1$.

$\bar{\omega} \equiv \omega/T$, one obtains the following differential equation for $Y(\tilde{u})$,

$$\tilde{u}\left(1-\tilde{u}^2\right)\left(Y''(\tilde{u})+Y'(\tilde{u})\left(-\frac{i\bar{\omega}\tilde{r}_h\left(2\tilde{r}_h^2+Q^2\right)\sqrt{\frac{Q^2\tilde{u}^2}{\tilde{r}_h^2}+1}}{\pi\left(\tilde{u}^2-1\right)\sqrt{\tilde{r}_h^2+Q^2}\left(\tilde{u}^2\left(\tilde{r}_h^2+Q^2\right)+\tilde{r}_h^2\right)}+\right.\right.$$
$$2\tilde{u}\left(\frac{\tilde{r}_h^2+Q^2}{\tilde{u}^2\left(\tilde{r}_h^2+Q^2\right)+\tilde{r}_h^2}+\frac{1}{\tilde{u}^2-1}\right)+\frac{1}{\tilde{u}}\Bigg)+$$
$$Y(\tilde{u})\left(\frac{4\left(4Q^4\left(\tilde{u}^4+6\tilde{u}^2-2\right)\tilde{u}^2\tilde{r}_h^2+3Q^2\left(8\tilde{u}^4+3\tilde{u}^2-2\right)\tilde{r}_h^4+9\tilde{u}^2\tilde{r}_h^6+4Q^6\tilde{u}^6\right)}{\left(\tilde{u}^2-1\right)\left(3\tilde{r}_h^2+2Q^2\tilde{u}^2\right)^2\left(\tilde{u}^2\left(\tilde{r}_h^2+Q^2\right)+\tilde{r}_h^2\right)}-\right.$$
$$\left.\left.\frac{i\bar{\omega}\left(2\tilde{r}_h^2+Q^2\right)\left(\tilde{r}_h^2+2Q^2\tilde{u}^2\right)}{2\pi\tilde{u}\left(\tilde{u}^2-1\right)\tilde{r}_h\sqrt{\tilde{r}_h^2+Q^2}\sqrt{\frac{Q^2\tilde{u}^2}{\tilde{r}_h^2}+1}\left(\tilde{u}^2\left(\tilde{r}_h^2+Q^2\right)+\tilde{r}_h^2\right)}\right)\right)=0, \tag{A.20}$$

which defines the relevant generalized eigenvalue problem (GEP) to be solved in order to find the QNM's $\bar{\omega}(\mu/T)$ of the dilaton channel of the 1RCBH model in the zero wavenumber limit.[4]

A.3.2 QNM spectra and equilibration time

The numerical routine used to solve the GEP equation (A.20) for the QNM's $\bar{\omega}(\mu/T)$ employed the pseudospectral method and it follows the same general steps discussed in Ref. [146] and we refer the interested reader to consult it for technical details. In Figs. A.9 and A.10 we show the behavior of the QNM's of the dilaton channel as a function of μ/T. In Fig. A.11 we show how the characteristic "equilibration time" associated with the inverse of minus the imaginary part of the lowest non-hydrodynamic QNM of the dilaton channel behaves as a function of μ/T. Remarkably, one notes that this characteristic equilibration time is qualitatively different from the equilibration times obtained in Ref. [146] for the external scalar and vector diffusion channels, since the latter are reduced as one increases μ/T far from the CP while increasing close to the CP. In the dilaton channel, however, the equilibration time always increases with increasing μ/T, in agreement with the late time behavior of the scalar condensate as we have discussed in Subsection 3.5.7.

[4]Note that in the EF coordinates the infalling wave condition at the horizon is imposed by just requiring regularity of the solutions there. This is one of the main reasons why the EF coordinates are very convenient to deal with the calculation of QNM's. Another reason is that in the domain-wall coordinates one would obtain instead of the GEP (A.20) a quadratic eigenvalue problem (QEP) for $\bar{\omega}$, which is far more demanding in terms of computational costs. Note also what the QNM's $\bar{\omega}$ are only functions of the dimensionless combination μ/T controlled by the background parameters $\tilde{r}_h$ and Q (here we restrict our analysis to the QNM's evaluated on the stable branch of black hole solutions).

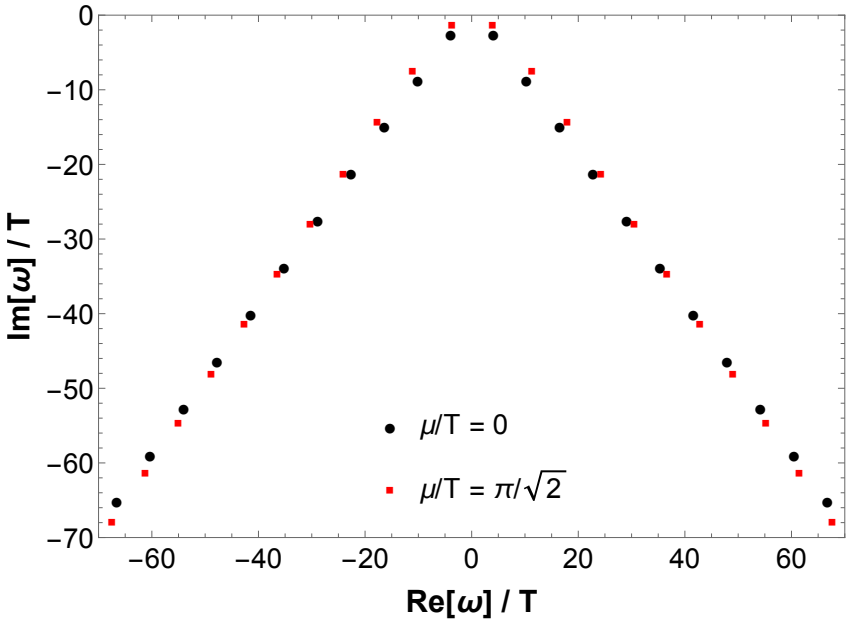

Figure A.9: *First 22 non-hydrodynamic QNM's of the dilaton channel evaluated at* $\mu/T = 0$ *and* $\mu/T = \pi/\sqrt{2}$ *(critical point).*

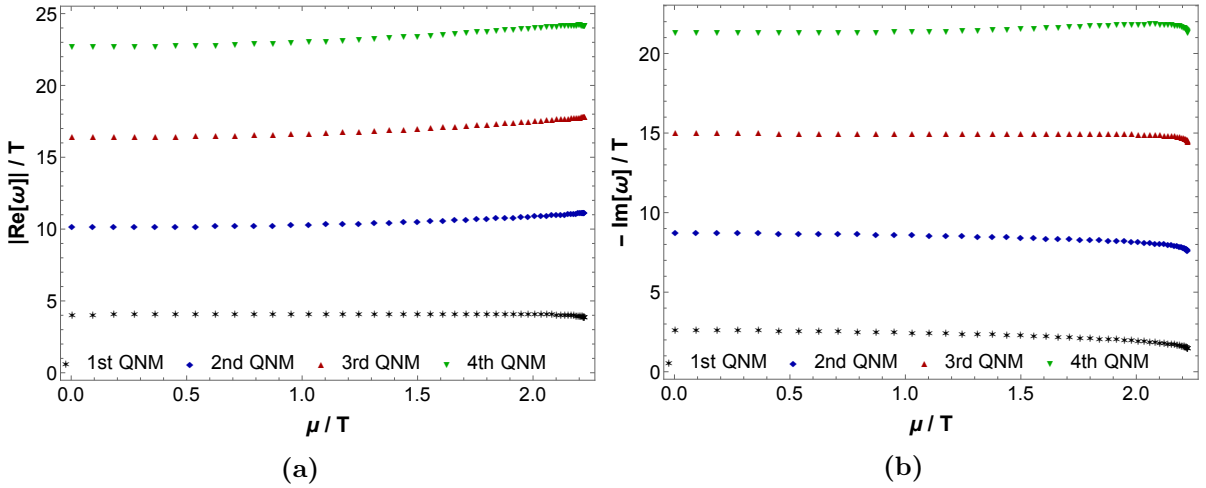

(a) **(b)**

Figure A.10: *(a) Real and (b) imaginary parts of the first four non-hydrodynamic QNM's of the dilaton channel as functions of* μ/T*.*

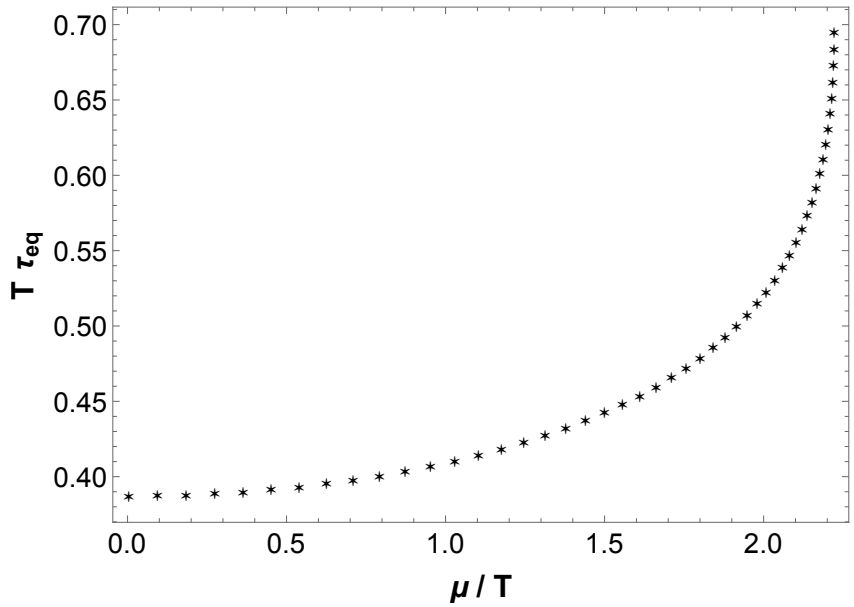

Figure A.11: *Characteristic "equilibration time" of the dilaton channel as a function of μ/T.*

Bibliography

[1] L. D. Landau and E. M. Lifshitz, *Course of Theoretical Physics, Volume 5, Statistical Physics - Part 1.* Butterworth-Heinemann, 3rd edition, 1980. 1

[2] L. D. Landau and E. M. Lifshitz, *Course of Theoretical Physics, Volume 10, Physical Kinetics.* Pergamon Press, 1981. 1

[3] P. L. Bhatnagar, E. P. Gross, and M. Krook, *A Model for Collision Processes in Gases. 1. Small Amplitude Processes in Charged and Neutral One-Component Systems*, *Phys. Rev.* **94** (1954) 511–525. 1

[4] C. Mouhot and C. Villani, *On Landau damping*, *Acta Math.* **207** (2011) 29–201, [arXiv:0904.2760]. 1

[5] https://www.quora.com/What-did-Cédric-Villani-prove-for-his-Fields-Medal. 1

[6] M. E. Peskin and D. V. Schroeder, *An Introduction to quantum field theory.* Addison-Wesley, Reading, USA, 1995. 1, 4

[7] M. L. Mangano and S. J. Parke, *Multiparton amplitudes in gauge theories*, *Phys. Rept.* **200** (1991) 301–367, [hep-th/0509223]. 2

[8] L. J. Dixon, *A brief introduction to modern amplitude methods*, in *Proceedings, 2012 European School of High-Energy Physics (ESHEP 2012): La Pommeraye, Anjou, France, June 06-19, 2012*, pp. 31–67, 2014. arXiv:1310.5353. 2

[9] H. Kawai, D. C. Lewellen, and S. H. H. Tye, *A Relation Between Tree Amplitudes of Closed and Open Strings*, *Nucl. Phys.* **B269** (1986) 1–23. 2

[10] Z. Bern, J. J. M. Carrasco, and H. Johansson, *Perturbative Quantum Gravity as a Double Copy of Gauge Theory*, *Phys. Rev. Lett.* **105** (2010) 061602, [arXiv:1004.0476]. 2

[11] R. Haag, *On quantum field theories*, *Kong. Dan. Vid. Sel. Mat. Fys. Med.* **29N12** (1955) 1–37. [Phil. Mag. Ser.746,376(1955)]. 2

[12] R. Haag, *Local quantum physics: Fields, particles, algebras.* 1992. 2

[13] T. Aoyama, M. Hayakawa, T. Kinoshita, and M. Nio, *Tenth-Order Electron Anomalous Magnetic Moment — Contribution of Diagrams without Closed Lepton Loops*, *Phys. Rev.* **D91** (2015), no. 3 033006, [arXiv:1412.8284]. [Erratum: Phys. Rev.D96,no.1,019901(2017)]. 2

[14] T. Aoyama, T. Kinoshita, and M. Nio, *Revised and Improved Value of the QED Tenth-Order Electron Anomalous Magnetic Moment*, *Phys. Rev.* **D97** (2018), no. 3 036001, [arXiv:1712.06060]. 2

[15] D. Hanneke, S. F. Hoogerheide, and G. Gabrielse, *Cavity Control of a Single-Electron Quantum Cyclotron: Measuring the Electron Magnetic Moment*, *Phys. Rev.* **A83** (2011) 052122, [arXiv:1009.4831]. 2

[16] D. B. Kaplan, *Five lectures on effective field theory*, 2005. nucl-th/0510023. 2

[17] M. Creutz, *Quarks, Gluons and Lattices*. Cambridge University Press, 1985. 2

[18] J. Greensite, *The Confinement problem in lattice gauge theory*, *Prog. Part. Nucl. Phys.* **51** (2003) 1, [hep-lat/0301023]. 2

[19] J. Polchinski, *Dualities of Fields and Strings*, *Stud. Hist. Philos. Mod. Phys.* **59** (2017) 6–20, [arXiv:1412.5704]. 2

[20] N. E. Hussey, *Phenomenology of the normal state in-plane transport properties of high- t c cuprates*, *Journal of Physics: Condensed Matter* **20** (2008), no. 12 123201. 3

[21] D. J. Gross and F. Wilczek, *Ultraviolet Behavior of Nonabelian Gauge Theories*, *Phys. Rev. Lett.* **30** (1973) 1343–1346. [,271(1973)]. 3, 4

[22] H. D. Politzer, *Reliable Perturbative Results for Strong Interactions?*, *Phys. Rev. Lett.* **30** (1973) 1346–1349. [,274(1973)]. 3, 4

[23] C. P. Burgess and G. D. Moore, *The standard model: A primer*. Cambridge University Press, 2006. 3

[24] S. Durr et al., *Ab-Initio Determination of Light Hadron Masses*, *Science* **322** (2008) 1224–1227, [arXiv:0906.3599]. 3, 5

[25] P. W. Anderson, *Plasmons, Gauge Invariance, and Mass*, *Phys. Rev.* **130** (1963) 439–442. [,153(1963)]. 3

[26] P. W. Higgs, *Broken symmetries, massless particles and gauge fields*, *Phys. Lett.* **12** (1964) 132–133. 3

[27] F. Englert and R. Brout, *Broken Symmetry and the Mass of Gauge Vector Mesons*, *Phys. Rev. Lett.* **13** (1964) 321–323. [,157(1964)]. 3

[28] M. Kamionkowski, *Dark Matter and Dark Energy*, in *Amazing Light: Visions for Discovery: An International Symposium in Honor of the 90th Birthday Years of Charles H. Townes Berkeley, California, October 6-8, 2005*, 2007. arXiv:0706.2986. 3

[29] **Particle Data Group** Collaboration, K. A. Olive et al., *Review of Particle Physics*, *Chin. Phys.* **C38** (2014) 090001. 4

[30] S. Bethke, *World Summary of α_s (2012)*, arXiv:1210.0325. [Nucl. Phys. Proc. Suppl.234,229(2013)]. x, 5

[31] M. A. Shifman, A. I. Vainshtein, and V. I. Zakharov, *QCD and Resonance Physics. Theoretical Foundations*, *Nucl. Phys.* **B147** (1979) 385–447. 5

[32] P. Colangelo and A. Khodjamirian, *QCD sum rules, a modern perspective*, hep-ph/0010175. 5

[33] K. G. Wilson, *Confinement of Quarks*, *Phys. Rev.* **D10** (1974) 2445–2459. [,319(1974)]. 5

[34] M. Creutz, *Monte Carlo Study of Quantized SU(2) Gauge Theory*, *Phys. Rev.* **D21** (1980) 2308–2315. 5

[35] H. B. Meyer, *Transport Properties of the Quark-Gluon Plasma: A Lattice QCD Perspective*, *Eur. Phys. J.* **A47** (2011) 86, [arXiv:1104.3708]. 5, 93

[36] M. Troyer and U.-J. Wiese, *Computational complexity and fundamental limitations to fermionic quantum Monte Carlo simulations*, *Phys. Rev. Lett.* **94** (2005) 170201, [cond-mat/0408370]. 5, 9, 10

[37] T. D. Lee and G. C. Wick, *Vacuum Stability and Vacuum Excitation in a Spin 0 Field Theory*, *Phys. Rev.* **D9** (1974) 2291–2316. 5

[38] **BRAHMS** Collaboration, I. Arsene et al., *Quark gluon plasma and color glass condensate at RHIC? The Perspective from the BRAHMS experiment*, *Nucl. Phys.* **A757** (2005) 1–27, [nucl-ex/0410020]. 5, 34

[39] **PHENIX** Collaboration, K. Adcox et al., *Formation of dense partonic matter in relativistic nucleus-nucleus collisions at RHIC: Experimental evaluation by the PHENIX collaboration*, *Nucl. Phys.* **A757** (2005) 184–283, [nucl-ex/0410003]. 5, 34

[40] B. B. Back et al., *The PHOBOS perspective on discoveries at RHIC*, *Nucl. Phys.* **A757** (2005) 28–101, [nucl-ex/0410022]. 5, 34

[41] **STAR** Collaboration, J. Adams et al., *Experimental and theoretical challenges in the search for the quark gluon plasma: The STAR Collaboration's critical assessment of the evidence from RHIC collisions*, *Nucl. Phys.* **A757** (2005) 102–183, [nucl-ex/0501009]. 5, 34

[42] E. V. Shuryak, *What RHIC experiments and theory tell us about properties of quark-gluon plasma?*, *Nucl. Phys.* **A750** (2005) 64–83, [hep-ph/0405066]. 5, 11

[43] T. Schaefer and D. Teaney, *Nearly Perfect Fluidity: From Cold Atomic Gases to Hot Quark Gluon Plasmas*, *Rept. Prog. Phys.* **72** (2009) 126001, [arXiv:0904.3107]. 5, 11

[44] T. Schaefer, *Fluid Dynamics and Viscosity in Strongly Correlated Fluids*, *Ann. Rev. Nucl. Part. Sci.* **64** (2014) 125–148, [arXiv:1403.0653]. 5, 11

[45] P. B. Arnold, G. D. Moore, and L. G. Yaffe, *Transport coefficients in high temperature gauge theories. 1. Leading log results*, *JHEP* **11** (2000) 001, [hep-ph/0010177]. 5, 13

[46] P. B. Arnold, G. D. Moore, and L. G. Yaffe, *Transport coefficients in high temperature gauge theories. 2. Beyond leading log*, *JHEP* **05** (2003) 051, [hep-ph/0302165]. 5, 13

[47] J.-P. Blaizot and E. Iancu, *The Quark gluon plasma: Collective dynamics and hard thermal loops*, *Phys. Rept.* **359** (2002) 355–528, [hep-ph/0101103]. 5, 8

[48] H. J. Bernstein and V. F. Weisskopf, *ABOUT LIQUIDS*, *Submitted to: Amer. J. Phys.* (1986). 6

[49] **STAR** Collaboration, L. Adamczyk et al., *Global Λ hyperon polarization in nuclear collisions: evidence for the most vortical fluid*, *Nature* **548** (2017) 62–65, [arXiv:1701.06657]. 6

[50] P. Romatschke and U. Romatschke, *Relativistic Fluid Dynamics In and Out of Equilibrium – Ten Years of Progress in Theory and Numerical Simulations of Nuclear Collisions*, arXiv:1712.05815. 6, 12, 88

[51] L. D. Landau and E. M. Lifshitz, *Course of Theoretical Physics, Volume 6, Fluid Mechanics*. Pergamon Press, 1982. 6

[52] C. Eckart, *The Thermodynamics of irreversible processes. 3.. Relativistic theory of the simple fluid*, *Phys. Rev.* **58** (1940) 919–924. 6

[53] F. S. Bemfica, M. M. Disconzi, and J. Noronha, *Causality and existence of solutions of relativistic viscous fluid dynamics with gravity*, arXiv:1708.06255. 6, 82, 92

[54] J. M. Maldacena, *The Large N limit of superconformal field theories and supergravity*, *Int. J. Theor. Phys.* **38** (1999) 1113–1133, [hep-th/9711200]. [Adv. Theor. Math. Phys.2,231(1998)]. 6, 15, 22, 33, 87, 114

[55] O. Aharony, S. S. Gubser, J. M. Maldacena, H. Ooguri, and Y. Oz, *Large N field theories, string theory and gravity*, *Phys. Rept.* **323** (2000) 183–386, [hep-th/9905111]. 6, 19

[56] P. Kovtun, D. T. Son, and A. O. Starinets, *Viscosity in strongly interacting quantum field theories from black hole physics*, *Phys. Rev. Lett.* **94** (2005) 111601, [hep-th/0405231]. 6, 13, 15, 33, 37, 87

[57] J. Casalderrey-Solana, H. Liu, D. Mateos, K. Rajagopal, and U. A. Wiedemann, *Gauge/String Duality, Hot QCD and Heavy Ion Collisions*, arXiv:1101.0618. 6, 33

[58] J. Berges, *Introduction to nonequilibrium quantum field theory*, *AIP Conf. Proc.* **739** (2005) 3–62, [hep-ph/0409233]. [,3(2004)]. 7

[59] P. M. Chesler and L. G. Yaffe, *Numerical solution of gravitational dynamics in asymptotically anti-de Sitter spacetimes*, *JHEP* **07** (2014) 086, [arXiv:1309.1439]. 7, 15, 33, 37, 42, 45, 57, 63, 101, 104

[60] J. I. Kapusta and C. Gale, *Finite-temperature field theory: Principles and applications*. Cambridge Monographs on Mathematical Physics. Cambridge University Press, 2011. 7

[61] O. Philipsen, *The QCD equation of state from the lattice*, *Prog. Part. Nucl. Phys.* **70** (2013) 55–107, [arXiv:1207.5999]. 7, 86

[62] N. Su, *A brief overview of hard-thermal-loop perturbation theory*, *Commun. Theor. Phys.* **57** (2012) 409, [arXiv:1204.0260]. 8

[63] R. D. Pisarski and F. Wilczek, *Remarks on the Chiral Phase Transition in Chromodynamics*, *Phys. Rev.* **D29** (1984) 338–341. 8

[64] E. Laermann and O. Philipsen, *The Status of lattice QCD at finite temperature*, *Ann. Rev. Nucl. Part. Sci.* **53** (2003) 163–198, [hep-ph/0303042]. 8

[65] B. Lucini and M. Panero, *SU(N) gauge theories at large N*, *Phys. Rept.* **526** (2013) 93–163, [arXiv:1210.4997]. 9

[66] R. Hagedorn, *How We Got to QCD Matter from the Hadron Side: 1984*, *Lect. Notes Phys.* **221** (1985) 53–76. [,287(2016)]. 9

[67] **HotQCD** Collaboration, A. Bazavov et al., *Equation of state in (2+1)-flavor QCD*, *Phys. Rev.* **D90** (2014) 094503, [arXiv:1407.6387]. x, 9

[68] S. S. Gubser and A. Nellore, *Mimicking the QCD equation of state with a dual black hole*, *Phys. Rev.* **D78** (2008) 086007, [arXiv:0804.0434]. 9, 15, 35, 115

[69] U. Gursoy, E. Kiritsis, L. Mazzanti, G. Michalogiorgakis, and F. Nitti, *Improved Holographic QCD*, *Lect. Notes Phys.* **828** (2011) 79–146, [arXiv:1006.5461]. 9, 115

[70] R. Critelli, J. Noronha, J. Noronha-Hostler, I. Portillo, C. Ratti, and R. Rougemont, *Critical point in the phase diagram of primordial quark-gluon matter from black hole physics*, *Phys. Rev.* **D96** (2017), no. 9 096026, [arXiv:1706.00455]. 9, 11, 15, 35, 38, 83, 86, 109

[71] Y. Nambu and G. Jona-Lasinio, *Dynamical Model of Elementary Particles Based on an Analogy with Superconductivity. 1.*, *Phys. Rev.* **122** (1961) 345–358. [,127(1961)]. 9

[72] Y. Nambu and G. Jona-Lasinio, *DYNAMICAL MODEL OF ELEMENTARY PARTICLES BASED ON AN ANALOGY WITH SUPERCONDUCTIVITY. II*, *Phys. Rev.* **124** (1961) 246–254. [,141(1961)]. 9

[73] K. Fukushima, *Phase diagrams in the three-flavor Nambu-Jona-Lasinio model with the Polyakov loop*, *Phys. Rev.* **D77** (2008) 114028, [arXiv:0803.3318]. [Erratum: Phys. Rev.D78,039902(2008)]. 9

[74] Z. Fodor and S. D. Katz, *The Phase diagram of quantum chromodynamics*, arXiv:0908.3341. 9

[75] O. Philipsen, *Lattice QCD at non-zero temperature and baryon density*, in *Modern perspectives in lattice QCD: Quantum field theory and high performance computing. Proceedings, International School, 93rd Session, Les Houches, France, August 3-28, 2009*, pp. 273–330, 2010. arXiv:1009.4089. 10

[76] G. Aarts, *Introductory lectures on lattice QCD at nonzero baryon number*, *J. Phys. Conf. Ser.* **706** (2016), no. 2 022004, [arXiv:1512.05145]. 10

[77] J. Zaanen, *Quantum critical electron systems: The uncharted sign worlds*, *Science* **319** (2008), no. 5867 1205–1207, [http://science.sciencemag.org/content/319/5867/1205.full.pdf]. 10

[78] A. Bazavov et al., *The QCD Equation of State to $\mathcal{O}(\mu_B^6)$ from Lattice QCD*, *Phys. Rev.* **D95** (2017), no. 5 054504, [arXiv:1701.04325]. 10, 86

[79] M. D'Elia and M.-P. Lombardo, *Finite density QCD via imaginary chemical potential*, *Phys. Rev.* **D67** (2003) 014505, [hep-lat/0209146]. 10

[80] **STAR** Collaboration, M. M. Aggarwal et al., *An Experimental Exploration of the QCD Phase Diagram: The Search for the Critical Point and the Onset of De-confinement*, arXiv:1007.2613. x, 11, 12, 83, 86, 112

[81] M. G. Alford, A. Schmitt, K. Rajagopal, and T. SchÃ¤fer, *Color superconductivity in dense quark matter*, *Rev. Mod. Phys.* **80** (2008) 1455–1515, [arXiv:0709.4635]. x, 11

[82] http://science.energy.gov/~/media/np/nsac/pdf/2015LRP/2015_LRPNS_091815. x, 11

[83] N. Sogabe and N. Yamamoto, *New dynamic critical phenomena in nuclear and quark superfluids*, *Phys. Rev.* **D95** (2017), no. 3 034028, [arXiv:1609.09214]. 11

[84] V. Vovchenko, J. Steinheimer, O. Philipsen, and H. Stoecker, *Cluster Expansion Model for QCD Baryon Number Fluctuations: No Phase Transition at $\mu_B/T < \pi$*, *Phys. Rev.* **D97** (2018), no. 11 114030, [arXiv:1711.01261]. 11

[85] U. Heinz and R. Snellings, *Collective flow and viscosity in relativistic heavy-ion collisions*, *Ann. Rev. Nucl. Part. Sci.* **63** (2013) 123–151, [arXiv:1301.2826]. 11, 34

[86] H. Satz, *The SPS heavy ion programme*, *Phys. Rept.* **403-404** (2004) 33–50, [hep-ph/0405051]. 12

[87] J. W. Harris and B. Muller, *The Search for the quark - gluon plasma*, *Ann. Rev. Nucl. Part. Sci.* **46** (1996) 71–107, [hep-ph/9602235]. 12

[88] **CBM** Collaboration, P. Staszel, *CBM experiment at FAIR*, *Acta Phys. Polon.* **B41** (2010) 341–350. 12, 83, 86, 112

[89] **CBM** Collaboration, T. Ablyazimov et al., *Challenges in QCD matter physics –The scientific programme of the Compressed Baryonic Matter experiment at FAIR*, *Eur. Phys. J.* **A53** (2017), no. 3 60, [arXiv:1607.01487]. 12, 83, 86, 112

[90] theor.jinr.ru/twiki-cgi/view/NICA/NICAWhitePaper. 12, 83, 86, 112

[91] F. Gelis, E. Iancu, J. Jalilian-Marian, and R. Venugopalan, *The Color Glass Condensate*, *Ann. Rev. Nucl. Part. Sci.* **60** (2010) 463–489, [arXiv:1002.0333]. 12, 34

[92] A. Kovner, L. D. McLerran, and H. Weigert, *Gluon production at high transverse momentum in the McLerran-Venugopalan model of nuclear structure functions*, *Phys. Rev.* **D52** (1995) 3809–3814, [hep-ph/9505320]. 12

[93] A. Krasnitz and R. Venugopalan, *The Initial energy density of gluons produced in very high-energy nuclear collisions*, *Phys. Rev. Lett.* **84** (2000) 4309–4312, [hep-ph/9909203]. 12

[94] L. McLerran, *The CGC and the Glasma: Two Lectures at the Yukawa Insitute*, *Prog. Theor. Phys. Suppl.* **187** (2011) 17–30, [arXiv:1011.3204]. x, 13

[95] P. Romatschke, *Relativistic Fluid Dynamics Far From Local Equilibrium*, *Phys. Rev. Lett.* **120** (2018), no. 1 012301, [arXiv:1704.08699]. 13, 34, 91, 109

[96] M. P. Heller and M. Spalinski, *Hydrodynamics Beyond the Gradient Expansion: Resurgence and Resummation*, *Phys. Rev. Lett.* **115** (2015), no. 7 072501, [arXiv:1503.07514]. 13, 91, 109

[97] W. Florkowski, M. P. Heller, and M. Spalinski, *New theories of relativistic hydrodynamics in the LHC era*, *Rept. Prog. Phys.* **81** (2018), no. 4 046001, [arXiv:1707.02282]. 13, 34, 91, 109

[98] M. Strickland, J. Noronha, and G. Denicol, *Anisotropic nonequilibrium hydrodynamic attractor*, *Phys. Rev.* **D97** (2018), no. 3 036020, [arXiv:1709.06644]. 13, 91, 109

[99] M. Spalinski, *On the hydrodynamic attractor of Yang-Mills plasma*, *Phys. Lett.* **B776** (2018) 468–472, [arXiv:1708.01921]. 13, 91, 109

[100] G. S. Denicol and J. Noronha, *Analytical attractor and the divergence of the slow-roll expansion in relativistic hydrodynamics*, *Phys. Rev.* **D97** (2018), no. 5 056021, [arXiv:1711.01657]. 13, 91, 109

[101] J. Casalderrey-Solana, N. I. Gushterov, and B. Meiring, *Resurgence and Hydrodynamic Attractors in Gauss-Bonnet Holography*, arXiv:1712.02772. 13, 91, 109

[102] S. Ryu, J. F. Paquet, C. Shen, G. S. Denicol, B. Schenke, S. Jeon, and C. Gale, *Importance of the Bulk Viscosity of QCD in Ultrarelativistic Heavy-Ion Collisions*, *Phys. Rev. Lett.* **115** (2015), no. 13 132301, [arXiv:1502.01675]. x, 13, 34

[103] D. T. Son and A. O. Starinets, *Viscosity, Black Holes, and Quantum Field Theory*, *Ann. Rev. Nucl. Part. Sci.* **57** (2007) 95–118, [arXiv:0704.0240]. 13

[104] P. Danielewicz and M. Gyulassy, *Dissipative Phenomena in Quark Gluon Plasmas*, *Phys. Rev.* **D31** (1985) 53–62. 14

[105] J. E. Bernhard, *Bayesian parameter estimation for relativistic heavy-ion collisions*. PhD thesis, Duke U., 2018-04-19. arXiv:1804.06469. 14, 88, 93

[106] L. P. Csernai, J. Kapusta, and L. D. McLerran, *On the Strongly-Interacting Low-Viscosity Matter Created in Relativistic Nuclear Collisions*, *Phys. Rev. Lett.* **97** (2006) 152303, [nucl-th/0604032]. x, 14

[107] J. Noronha-Hostler, J. Noronha, and C. Greiner, *Transport Coefficients of Hadronic Matter near T(c)*, *Phys. Rev. Lett.* **103** (2009) 172302, [arXiv:0811.1571]. x, 14

[108] https://science.energy.gov/~/media/np/nsac/pdf/20130201/2013_NSAC_Implementing_the_2007_Long_Range_Plan.pdf. x, 14

[109] G. S. Denicol, C. Gale, S. Jeon, A. Monnai, B. Schenke, and C. Shen, *Net baryon diffusion in fluid dynamic simulations of relativistic heavy-ion collisions*, arXiv:1804.10557. 14, 93

[110] G. 't Hooft, *A Planar Diagram Theory for Strong Interactions*, *Nucl. Phys.* **B72** (1974) 461. [,337(1973)]. 15, 19

[111] G. 't Hooft, *Dimensional reduction in quantum gravity*, *Conf. Proc.* **C930308** (1993) 284–296, [gr-qc/9310026]. 15

[112] L. Susskind, *The World as a hologram*, *J. Math. Phys.* **36** (1995) 6377–6396, [hep-th/9409089]. 15

[113] E. Witten, *Anti-de Sitter space and holography*, *Adv. Theor. Math. Phys.* **2** (1998) 253–291, [hep-th/9802150]. 15, 19, 23, 24, 33, 87, 114

[114] S. S. Gubser, I. R. Klebanov, and A. M. Polyakov, *Gauge theory correlators from noncritical string theory*, *Phys. Lett.* **B428** (1998) 105–114, [hep-th/9802109]. 15, 19, 23, 33, 87, 114

[115] E. Witten, *Anti-de Sitter space, thermal phase transition, and confinement in gauge theories*, *Adv. Theor. Math. Phys.* **2** (1998) 505–532, [hep-th/9803131]. 15, 33, 87, 114

[116] Y. Kats and P. Petrov, *Effect of curvature squared corrections in AdS on the viscosity of the dual gauge theory*, *JHEP* **01** (2009) 044, [arXiv:0712.0743]. 15

[117] M. Brigante, H. Liu, R. C. Myers, S. Shenker, and S. Yaida, *Viscosity Bound Violation in Higher Derivative Gravity*, *Phys. Rev.* **D77** (2008) 126006, [arXiv:0712.0805]. 15

[118] M. Brigante, H. Liu, R. C. Myers, S. Shenker, and S. Yaida, *The Viscosity Bound and Causality Violation*, *Phys. Rev. Lett.* **100** (2008) 191601, [arXiv:0802.3318]. 15

[119] R. Critelli, R. Rougemont, S. I. Finazzo, and J. Noronha, *Polyakov loop and heavy quark entropy in strong magnetic fields from holographic black hole engineering*, *Phys. Rev.* **D94** (2016), no. 12 125019, [arXiv:1606.09484]. 15, 35

[120] R. Rougemont, R. Critelli, and J. Noronha, *Holographic calculation of the QCD crossover temperature in a magnetic field*, *Phys. Rev.* **D93** (2016), no. 4 045013, [arXiv:1505.07894]. 15, 35

[121] S. I. Finazzo, R. Critelli, R. Rougemont, and J. Noronha, *Momentum transport in strongly coupled anisotropic plasmas in the presence of strong magnetic fields*, *Phys. Rev.* **D94** (2016), no. 5 054020, [arXiv:1605.06061]. [Erratum: Phys. Rev.D96,no.1,019903(2017)]. 15, 35, 93

[122] S. I. Finazzo, R. Rougemont, H. Marrochio, and J. Noronha, *Hydrodynamic transport coefficients for the non-conformal quark-gluon plasma from holography*, *JHEP* **02** (2015) 051, [arXiv:1412.2968]. 15, 35, 93, 115

[123] S. S. Gubser, *Drag force in AdS/CFT*, *Phys. Rev.* **D74** (2006) 126005, [hep-th/0605182]. 15

[124] H. Liu, K. Rajagopal, and U. A. Wiedemann, *Calculating the jet quenching parameter from AdS/CFT*, *Phys. Rev. Lett.* **97** (2006) 182301, [hep-ph/0605178]. 15

[125] H. Liu, K. Rajagopal, and U. A. Wiedemann, *Wilson loops in heavy ion collisions and their calculation in AdS/CFT*, *JHEP* **03** (2007) 066, [hep-ph/0612168]. 15

[126] M. Randeria and E. Taylor, *BCS-BEC Crossover and the Unitary Fermi Gas*, *Ann. Rev. Condensed Matter Phys.* **5** (2014) 209–232, [arXiv:1306.5785]. 15

[127] M. Müller, J. Schmalian, and L. Fritz, *Graphene: A nearly perfect fluid*, *Phys. Rev. Lett.* **103** (Jul, 2009) 025301. 16

[128] J. D. Rameau, T. J. Reber, H. B. Yang, S. Akhanjee, G. D. Gu, P. D. Johnson, and S. Campbell, *Nearly Perfect Fluidity in a High Temperature Superconductor*, *Phys. Rev.* **B90** (2014), no. 13 134509, [arXiv:1409.5820]. 16

[129] H. Nastase, *String Theory Methods for Condensed Matter Physics*. Cambridge University Press, 2017. 16

[130] J. Zaanen, Y.-W. Sun, Y. Liu, and K. Schalm, *Holographic Duality in Condensed Matter Physics*. Cambridge Univ. Press, 2015. 16, 19

[131] E. Witten, *A Mini-Introduction To Information Theory*, arXiv:1805.11965. 16

[132] S. Ryu and T. Takayanagi, *Holographic derivation of entanglement entropy from AdS/CFT*, *Phys. Rev. Lett.* **96** (2006) 181602, [hep-th/0603001]. 16

[133] S. Ryu and T. Takayanagi, *Aspects of Holographic Entanglement Entropy*, *JHEP* **08** (2006) 045, [hep-th/0605073]. 16

[134] P. Calabrese and J. L. Cardy, *Entanglement entropy and quantum field theory*, *J. Stat. Mech.* **0406** (2004) P06002, [hep-th/0405152]. 16

[135] D. Harlow, *TASI Lectures on the Emergence of the Bulk in AdS/CFT*, arXiv:1802.01040. 16

[136] E. Berti, V. Cardoso, and A. O. Starinets, *Quasinormal modes of black holes and black branes*, *Class. Quant. Grav.* **26** (2009) 163001, [arXiv:0905.2975]. 16, 74, 114

[137] R. Critelli, R. Rougemont, and J. Noronha, *Homogeneous isotropization and equilibration of a strongly coupled plasma with a critical point*, *JHEP* **12** (2017) 029, [arXiv:1709.03131]. xiii, 16, 17, 33, 87, 98, 100, 102, 107, 108, 110, 114

[138] S. S. Gubser, *Thermodynamics of spinning D3-branes*, *Nucl. Phys.* **B551** (1999) 667–684, [hep-th/9810225]. 16, 37, 39, 40, 87, 116

[139] K. Behrndt, M. Cvetic, and W. A. Sabra, *Nonextreme black holes of five-dimensional N=2 AdS supergravity*, *Nucl. Phys.* **B553** (1999) 317–332, [hep-th/9810227]. 16, 37, 39, 40, 87, 116

[140] P. Kraus, F. Larsen, and S. P. Trivedi, *The Coulomb branch of gauge theory from rotating branes*, *JHEP* **03** (1999) 003, [hep-th/9811120]. 16, 37, 39, 40, 87, 116

[141] R.-G. Cai and K.-S. Soh, *Critical behavior in the rotating D-branes*, *Mod. Phys. Lett.* **A14** (1999) 1895–1908, [hep-th/9812121]. 16, 37, 39, 40, 87, 116

[142] M. Cvetic and S. S. Gubser, *Phases of R charged black holes, spinning branes and strongly coupled gauge theories*, *JHEP* **04** (1999) 024, [hep-th/9902195]. 16, 37, 39, 40, 87, 116

[143] M. Cvetic and S. S. Gubser, *Thermodynamic stability and phases of general spinning branes*, *JHEP* **07** (1999) 010, [hep-th/9903132]. 16, 37, 39, 40, 87, 116

[144] R. Critelli, R. Rougemont, and J. Noronha, *Holographic Bjorken flow of a hot and dense fluid in the vicinity of a critical point*, arXiv:1805.00882. 17, 82

[145] J. D. Bjorken, *Highly Relativistic Nucleus-Nucleus Collisions: The Central Rapidity Region*, *Phys. Rev.* **D27** (1983) 140–151. 17, 82, 87, 94

[146] S. I. Finazzo, R. Rougemont, M. Zaniboni, R. Critelli, and J. Noronha, *Critical behavior of non-hydrodynamic quasinormal modes in a strongly coupled plasma*, *JHEP* **01** (2017) 137, [arXiv:1610.01519]. xi, xiii, 17, 38, 40, 46, 47, 48, 74, 76, 77, 78, 80, 83, 87, 98, 110, 114, 115, 128, 129, 130

[147] A. Adams, L. D. Carr, T. Schaefer, P. Steinberg, and J. E. Thomas, *Strongly Correlated Quantum Fluids: Ultracold Quantum Gases, Quantum Chromodynamic Plasmas, and Holographic Duality*, *New J. Phys.* **14** (2012) 115009, [arXiv:1205.5180]. 19, 33

[148] A. V. Ramallo, *Introduction to the AdS/CFT correspondence*, *Springer Proc. Phys.* **161** (2015) 411–474, [arXiv:1310.4319]. 19

[149] H. Nastase, *Introduction to the ADS/CFT Correspondence*. Cambridge University Press, 2015. 19

[150] M. Ammon and J. Erdmenger, *Gauge/gravity duality*. Cambridge University Press, Cambridge, 2015. 19

[151] A. V. Manohar, *Large N QCD*, in *Probing the standard model of particle interactions. Proceedings, Summer School in Theoretical Physics, NATO Advanced Study Institute, 68th session, Les Houches, France, July 28-September 5, 1997. Pt. 1, 2*, pp. 1091–1169, 1998. hep-ph/9802419. 20

[152] J. Polchinski, *String theory. Vol. 1: An introduction to the bosonic string*. Cambridge Monographs on Mathematical Physics. Cambridge University Press, 2007. 21, 22

[153] J. Polchinski, *String theory. Vol. 2: Superstring theory and beyond*. Cambridge Monographs on Mathematical Physics. Cambridge University Press, 2007. 21, 22

[154] J. Polchinski, *Dirichlet Branes and Ramond-Ramond charges*, *Phys. Rev. Lett.* **75** (1995) 4724–4727, [hep-th/9510017]. 22

[155] E. Witten, *Bound states of strings and p-branes*, *Nucl. Phys.* **B460** (1996) 335–350, [hep-th/9510135]. 22

[156] G. T. Horowitz and A. Strominger, *Black strings and P-branes*, *Nucl. Phys.* **B360** (1991) 197–209. 22

[157] M. J. Duff and J. X. Lu, *The Selfdual type IIB superthreebrane*, *Phys. Lett.* **B273** (1991) 409–414. 22

[158] N. Drukker and D. J. Gross, *An Exact prediction of N=4 SUSYM theory for string theory*, *J. Math. Phys.* **42** (2001) 2896–2914, [hep-th/0010274]. 23

[159] M. Hanada, Y. Hyakutake, G. Ishiki, and J. Nishimura, *Numerical tests of the gauge/gravity duality conjecture for D0-branes at finite temperature and finite N*, *Phys. Rev.* **D94** (2016), no. 8 086010, [arXiv:1603.00538]. 23

[160] D. T. Son and A. O. Starinets, *Minkowski space correlators in AdS / CFT correspondence: Recipe and applications*, *JHEP* **09** (2002) 042, [hep-th/0205051]. 24, 118

[161] C. P. Herzog and D. T. Son, *Schwinger-Keldysh propagators from AdS/CFT correspondence*, *JHEP* **03** (2003) 046, [hep-th/0212072]. 24

[162] S. W. Hawking, *Particle Creation by Black Holes*, *Commun. Math. Phys.* **43** (1975) 199–220. [,167(1975)]. 24, 48

[163] J. D. Bekenstein, *Black holes and entropy*, *Phys. Rev.* **D7** (1973) 2333–2346. 24, 48

[164] S. W. Hawking, *Black hole explosions*, *Nature* **248** (1974) 30–31. 24

[165] K. Skenderis, *Lecture notes on holographic renormalization*, *Class. Quant. Grav.* **19** (2002) 5849–5876, [hep-th/0209067]. 24, 25, 112

[166] S. de Haro, S. N. Solodukhin, and K. Skenderis, *Holographic reconstruction of space-time and renormalization in the AdS / CFT correspondence*, *Commun. Math. Phys.* **217** (2001) 595–622, [hep-th/0002230]. 24, 25, 112

[167] M. Bianchi, D. Z. Freedman, and K. Skenderis, *Holographic renormalization*, *Nucl. Phys.* **B631** (2002) 159–194, [hep-th/0112119]. 24, 25, 26, 45, 112

[168] J. F. Fuini and L. G. Yaffe, *Far-from-equilibrium dynamics of a strongly coupled non-Abelian plasma with non-zero charge density or external magnetic field*, *JHEP* **07** (2015) 116, [arXiv:1503.07148]. 26, 36, 37, 43, 58, 59, 64, 65

[169] H. Elvang and M. Hadjiantonis, *A Practical Approach to the Hamilton-Jacobi Formulation of Holographic Renormalization*, *JHEP* **06** (2016) 046, [arXiv:1603.04485]. 26, 27

[170] J. Lindgren, I. Papadimitriou, A. Taliotis, and J. Vanhoof, *Holographic Hall conductivities from dyonic backgrounds*, *JHEP* **07** (2015) 094, [arXiv:1505.04131]. 27, 30, 32

[171] B. Sahoo and H.-U. Yee, *Electrified plasma in AdS/CFT correspondence*, *JHEP* **11** (2010) 095, [arXiv:1004.3541]. 27

[172] R. L. Arnowitt, S. Deser, and C. W. Misner, *Dynamical Structure and Definition of Energy in General Relativity*, *Phys. Rev.* **116** (1959) 1322–1330. 30, 37

[173] R. L. Arnowitt, S. Deser, and C. W. Misner, *Canonical variables for general relativity*, *Phys. Rev.* **117** (1960) 1595–1602. 30, 37

[174] I. Papadimitriou and K. Skenderis, *AdS / CFT correspondence and geometry*, *IRMA Lect. Math. Theor. Phys.* **8** (2005) 73–101, [hep-th/0404176]. 32

[175] J. McGreevy, *Holographic duality with a view toward many-body physics*, *Adv. High Energy Phys.* **2010** (2010) 723105, [arXiv:0909.0518]. 33

[176] S. Bhattacharyya, V. E. Hubeny, S. Minwalla, and M. Rangamani, *Nonlinear Fluid Dynamics from Gravity*, *JHEP* **02** (2008) 045, [arXiv:0712.2456]. 33, 93

[177] R. Baier, P. Romatschke, D. T. Son, A. O. Starinets, and M. A. Stephanov, *Relativistic viscous hydrodynamics, conformal invariance, and holography*, *JHEP* **04** (2008) 100, [arXiv:0712.2451]. 33, 92, 93, 98

[178] G. T. Horowitz and V. E. Hubeny, *Quasinormal modes of AdS black holes and the approach to thermal equilibrium*, *Phys. Rev.* **D62** (2000) 024027, [hep-th/9909056]. 33, 38, 114, 119

[179] P. K. Kovtun and A. O. Starinets, *Quasinormal modes and holography*, *Phys. Rev.* **D72** (2005) 086009, [hep-th/0506184]. 33, 114, 119, 124, 125

[180] M. P. Heller, R. A. Janik, and P. Witaszczyk, *Hydrodynamic Gradient Expansion in Gauge Theory Plasmas*, *Phys. Rev. Lett.* **110** (2013), no. 21 211602, [arXiv:1302.0697]. 33, 34, 98, 114

[181] W. van der Schee, *Gravitational collisions and the quark-gluon plasma*. PhD thesis, Utrecht U., 2014. arXiv:1407.1849. 33, 54, 100

[182] M. Attems, J. Casalderrey-Solana, D. Mateos, I. Papadimitriou, D. Santos-OlivÃ¡n, C. F. Sopuerta, M. Triana, and M. ZilhÃ£o, *Thermodynamics, transport and relaxation in non-conformal theories*, *JHEP* **10** (2016) 155, [arXiv:1603.01254]. 34

[183] P. M. Chesler and L. G. Yaffe, *Boost invariant flow, black hole formation, and far-from-equilibrium dynamics in $N = 4$ supersymmetric Yang-Mills theory*, *Phys. Rev.* **D82** (2010) 026006, [arXiv:0906.4426]. 34, 88, 97, 99, 107

[184] M. P. Heller, R. A. Janik, and P. Witaszczyk, *The characteristics of thermalization of boost-invariant plasma from holography*, *Phys. Rev. Lett.* **108** (2012) 201602, [arXiv:1103.3452]. 34, 88, 94, 100

[185] M. Attems, J. Casalderrey-Solana, D. Mateos, D. Santos-Olivan, C. F. Sopuerta, M. Triana, and M. ZilhÃ£o, *Paths to equilibrium in non-conformal collisions*, *JHEP* **06** (2017) 154, [arXiv:1703.09681]. 34, 63, 100

[186] A. Buchel, M. P. Heller, and J. Noronha, *Entropy Production, Hydrodynamics, and Resurgence in the Primordial Quark-Gluon Plasma from Holography*, *Phys. Rev.* **D94** (2016), no. 10 106011, [arXiv:1603.05344]. 34, 98, 114

[187] G. S. Denicol and J. Noronha, *Divergence of the Chapman-Enskog expansion in relativistic kinetic theory*, arXiv:1608.07869. 34, 114

[188] M. P. Heller, A. Kurkela, and M. Spalinski, *Hydrodynamization and transient modes of expanding plasma in kinetic theory*, arXiv:1609.04803. 34, 114

[189] **ATLAS** Collaboration, G. Aad et al., *Measurement of the distributions of event-by-event flow harmonics in lead-lead collisions at = 2.76 TeV with the ATLAS detector at the LHC*, *JHEP* **11** (2013) 183, [arXiv:1305.2942]. 34

[190] L. D. McLerran, *The Color glass condensate and small x physics: Four lectures*, *Lect. Notes Phys.* **583** (2002) 291–334, [hep-ph/0104285]. 34

[191] E. Iancu and R. Venugopalan, *The Color glass condensate and high-energy scattering in QCD*, in *In *Hwa, R.C. (ed.) et al.: Quark gluon plasma* 249-3363*. 2003. hep-ph/0303204. 34

[192] H. Weigert, *Evolution at small x(bj): The Color glass condensate*, *Prog. Part. Nucl. Phys.* **55** (2005) 461–565, [hep-ph/0501087]. 34

[193] F. Gelis, *Color Glass Condensate and Glasma*, *Int. J. Mod. Phys.* **A28** (2013) 1330001, [arXiv:1211.3327]. 34

[194] M. Gyulassy and L. McLerran, *New forms of QCD matter discovered at RHIC*, *Nucl. Phys.* **A750** (2005) 30–63, [nucl-th/0405013]. 34

[195] E. Shuryak, *Strongly coupled quark-gluon plasma in heavy ion collisions*, *Rev. Mod. Phys.* **89** (2017) 035001, [arXiv:1412.8393]. 34

[196] J. E. Bernhard, J. S. Moreland, S. A. Bass, J. Liu, and U. Heinz, *Applying Bayesian parameter estimation to relativistic heavy-ion collisions: simultaneous characterization of the initial state and quark-gluon plasma medium*, *Phys. Rev.* **C94** (2016), no. 2 024907, [arXiv:1605.03954]. 34, 93

[197] S. Pratt, E. Sangaline, P. Sorensen, and H. Wang, *Constraining the Eq. of State of Super-Hadronic Matter from Heavy-Ion Collisions*, *Phys. Rev. Lett.* **114** (2015) 202301, [arXiv:1501.04042]. 34, 35

[198] A. Monnai and J.-Y. Ollitrault, *Constraining the equation of state with identified particle spectra*, arXiv:1707.08466. 34, 35

[199] Y. Aoki, G. Endrodi, Z. Fodor, S. D. Katz, and K. K. Szabo, *The Order of the quantum chromodynamics transition predicted by the standard model of particle physics*, *Nature* **443** (2006) 675–678, [hep-lat/0611014]. 34

[200] S. Borsanyi et al., *Calculation of the axion mass based on high-temperature lattice quantum chromodynamics*, *Nature* **539** (2016), no. 7627 69–71, [arXiv:1606.07494]. 34

[201] S. S. Gubser, A. Nellore, S. S. Pufu, and F. D. Rocha, *Thermodynamics and bulk viscosity of approximate black hole duals to finite temperature quantum chromodynamics*, *Phys. Rev. Lett.* **101** (2008) 131601, [arXiv:0804.1950]. 35, 115

[202] O. DeWolfe, S. S. Gubser, and C. Rosen, *A holographic critical point*, *Phys. Rev.* **D83** (2011) 086005, [arXiv:1012.1864]. 35, 109, 116

[203] O. DeWolfe, S. S. Gubser, and C. Rosen, *Dynamic critical phenomena at a holographic critical point*, *Phys. Rev.* **D84** (2011) 126014, [arXiv:1108.2029]. xiii, 35, 40, 46, 47, 75, 76, 87, 94, 98, 109, 110, 122, 124, 125, 128, 129

[204] R. Rougemont, A. Ficnar, S. Finazzo, and J. Noronha, *Energy loss, equilibration, and thermodynamics of a baryon rich strongly coupled quark-gluon plasma*, *JHEP* **04** (2016) 102, [arXiv:1507.06556]. 35, 36, 38, 76, 115, 116, 119, 120

[205] R. Rougemont, J. Noronha, and J. Noronha-Hostler, *Suppression of baryon diffusion and transport in a baryon rich strongly coupled quark-gluon plasma*, *Phys. Rev. Lett.* **115** (2015), no. 20 202301, [arXiv:1507.06972]. 35, 115, 116

[206] S. I. Finazzo and R. Rougemont, *Thermal photon, dilepton production, and electric charge transport in a baryon rich strongly coupled QGP from holography*, *Phys. Rev.* **D93** (2016), no. 3 034017, [arXiv:1510.03321]. 35

[207] R. Rougemont, R. Critelli, J. Noronha-Hostler, J. Noronha, and C. Ratti, *Dynamical versus equilibrium properties of the QCD phase transition: A holographic perspective*, *Phys. Rev.* **D96** (2017), no. 1 014032, [arXiv:1704.05558]. 35, 36, 93

[208] S. Borsanyi, Z. Fodor, S. D. Katz, S. Krieg, C. Ratti, and K. K. Szabo, *Freeze-out parameters: lattice meets experiment*, *Phys. Rev. Lett.* **111** (2013) 062005, [arXiv:1305.5161]. 36

[209] S. Borsanyi, Z. Fodor, S. D. Katz, S. Krieg, C. Ratti, and K. K. Szabo, *Freeze-out parameters from electric charge and baryon number fluctuations: is there consistency?*, *Phys. Rev. Lett.* **113** (2014) 052301, [arXiv:1403.4576]. 36

[210] J. Liao and V. Koch, *On the Fluidity and Super-Criticality of the QCD matter at RHIC*, *Phys. Rev.* **C81** (2010) 014902, [arXiv:0909.3105]. 36

[211] J. Casalderrey-Solana, D. Mateos, W. van der Schee, and M. Triana, *Holographic heavy ion collisions with baryon charge*, *JHEP* **09** (2016) 108, [arXiv:1607.05273]. 36, 87

[212] E. Caceres and A. Kundu, *Holographic Thermalization with Chemical Potential*, *JHEP* **09** (2012) 055, [arXiv:1205.2354]. 36

[213] A. Giordano, N. E. Grandi, and G. A. Silva, *Holographic thermalization of charged operators*, *JHEP* **05** (2015) 016, [arXiv:1412.7953]. 36

[214] E. Caceres, A. Kundu, J. F. Pedraza, and D.-L. Yang, *Weak Field Collapse in AdS: Introducing a Charge Density*, *JHEP* **06** (2015) 111, [arXiv:1411.1744]. 36

[215] G. Camilo, B. Cuadros-Melgar, and E. Abdalla, *Holographic thermalization with a chemical potential from Born-Infeld electrodynamics*, *JHEP* **02** (2015) 103, [arXiv:1412.3878]. 36

[216] P. Basu and S. R. Das, *Quantum Quench across a Holographic Critical Point*, *JHEP* **01** (2012) 103, [arXiv:1109.3909]. 36

[217] P. Basu, D. Das, S. R. Das, and T. Nishioka, *Quantum Quench Across a Zero Temperature Holographic Superfluid Transition*, *JHEP* **03** (2013) 146, [arXiv:1211.7076]. 36

[218] T. Andrade, J. Casalderrey-Solana, and A. Ficnar, *Holographic Isotropisation in Gauss-Bonnet Gravity*, *JHEP* **02** (2017) 016, [arXiv:1610.08987]. 36

[219] P. M. Chesler and L. G. Yaffe, *Horizon formation and far-from-equilibrium isotropization in supersymmetric Yang-Mills plasma*, *Phys. Rev. Lett.* **102** (2009) 211601, [arXiv:0812.2053]. 37, 41, 42

[220] L. Lehner, *Numerical relativity: A Review*, *Class. Quant. Grav.* **18** (2001) R25–R86, [gr-qc/0106072]. 37

[221] H. Bantilan, F. Pretorius, and S. S. Gubser, *Simulation of Asymptotically AdS5 Spacetimes with a Generalized Harmonic Evolution Scheme*, *Phys. Rev.* **D85** (2012) 084038, [arXiv:1201.2132]. 37

[222] M. P. Heller, R. A. Janik, and P. Witaszczyk, *A numerical relativity approach to the initial value problem in asymptotically Anti-de Sitter spacetime for plasma thermalization - an ADM formulation*, *Phys. Rev.* **D85** (2012) 126002, [arXiv:1203.0755]. 37

[223] R. Rougemont, *Holographic black hole engineering at finite baryon chemical potential*, *J. Phys. Conf. Ser.* **832** (2017), no. 1 012048, [arXiv:1610.06124]. 37, 116

[224] O. DeWolfe, S. S. Gubser, and C. Rosen, *Fermi surfaces in N=4 Super-Yang-Mills theory*, *Phys. Rev.* **D86** (2012) 106002, [arXiv:1207.3352]. 40

[225] J. W. York, Jr., *Role of conformal three geometry in the dynamics of gravitation*, *Phys. Rev. Lett.* **28** (1972) 1082–1085. 40

[226] G. W. Gibbons and S. W. Hawking, *Action Integrals and Partition Functions in Quantum Gravity*, *Phys. Rev.* **D15** (1977) 2752–2756. 40

[227] S. Bonanos, "*Mathematica's RGTC package*." http://www.inp.demokritos.gr/~sbonano/RGTC, 2013. 41

[228] S. S. Gubser, I. R. Klebanov, and A. W. Peet, *Entropy and temperature of black 3-branes*, *Phys. Rev.* **D54** (1996) 3915–3919, [hep-th/9602135]. 48

[229] M. P. Heller, D. Mateos, W. van der Schee, and M. Triana, *Holographic isotropization linearized*, *JHEP* **09** (2013) 026, [arXiv:1304.5172]. 57, 63, 64

[230] J. P. Boyd, *Chebyshev and Fourier Spectral Methods*. Dover Books on Mathematics. Dover Publications, Mineola, NY, second ed., 2001. 60, 61, 62, 103, 107, 118

[231] B. Fornberg, *A Practical Guide to Pseudospectral Methods*. Cambridge Monographs on Applied and Computational Mathematics. Cambridge University Press, first ed., 1998. 60, 62

[232] L. N. Trefethen, *Spectral Methods in MATLAB*. Software, Environments, Tools (Book 10). SIAM: Society for Industrial and Applied Mathematics, first ed., 2001. 60

[233] T. Ishii, E. Kiritsis, and C. Rosen, *Thermalization in a Holographic Confining Gauge Theory*, *JHEP* **08** (2015) 008, [arXiv:1503.07766]. 60, 65

[234] M. P. Heller, D. Mateos, W. van der Schee, and D. Trancanelli, *Strong Coupling Isotropization of Non-Abelian Plasmas Simplified*, *Phys. Rev. Lett.* **108** (2012) 191601, [arXiv:1202.0981]. 64

[235] R. A. Konoplya and A. Zhidenko, *Quasinormal modes of black holes: From astrophysics to string theory*, *Rev. Mod. Phys.* **83** (2011) 793–836, [arXiv:1102.4014]. 74, 114

[236] S. S. Gubser, *Symmetry constraints on generalizations of Bjorken flow*, *Phys. Rev.* **D82** (2010) 085027, [arXiv:1006.0006]. 82, 94

[237] S. S. Gubser and A. Yarom, *Conformal hydrodynamics in Minkowski and de Sitter spacetimes*, *Nucl. Phys.* **B846** (2011) 469–511, [arXiv:1012.1314]. 82, 94

[238] H. Marrochio, J. Noronha, G. S. Denicol, M. Luzum, S. Jeon, and C. Gale, *Solutions of Conformal Israel-Stewart Relativistic Viscous Fluid Dynamics*, *Phys. Rev.* **C91** (2015), no. 1 014903, [arXiv:1307.6130]. 82, 94

[239] T. Banks, M. R. Douglas, G. T. Horowitz, and E. J. Martinec, *AdS dynamics from conformal field theory*, hep-th/9808016. 83

[240] K. Skenderis and B. C. van Rees, *Real-time gauge/gravity duality*, *Phys. Rev. Lett.* **101** (2008) 081601, [arXiv:0805.0150]. 83

[241] K. Skenderis and B. C. van Rees, *Real-time gauge/gravity duality: Prescription, Renormalization and Examples*, *JHEP* **05** (2009) 085, [arXiv:0812.2909]. 83

[242] V. Keranen and P. Kleinert, *Non-equilibrium scalar two point functions in AdS/CFT*, *JHEP* **04** (2015) 119, [arXiv:1412.2806]. 83

[243] S. Banerjee, T. Ishii, L. K. Joshi, A. Mukhopadhyay, and P. Ramadevi, *Time-dependence of the holographic spectral function: Diverse routes to thermalisation*, *JHEP* **08** (2016) 048, [arXiv:1603.06935]. 83

[244] **STAR** Collaboration, K. C. Meehan, *Fixed Target Collisions at STAR*, *Nucl. Phys.* **A956** (2016) 878–881. 83, 86

[245] **for the STAR** Collaboration, K. Meehan, *STAR Results from Au + Au Fixed-Target Collisions at* $\sqrt{(s_{NN})} = 4.5$ *GeV*, 2017. arXiv:1704.06342. 83, 86

[246] **HADES** Collaboration, G. Agakishiev et al., *Statistical model analysis of hadron yields in proton-nucleus and heavy-ion collisions at SIS 18 energiesStatistical hadronization model analysis of hadron yields in p + Nb and Ar + KCl at SIS18 energies*, *Eur. Phys. J.* **A52** (2016), no. 6 178, [arXiv:1512.07070]. 83

[247] S. Mukherjee, R. Venugopalan, and Y. Yin, *Real time evolution of non-Gaussian cumulants in the QCD critical regime*, *Phys. Rev.* **C92** (2015), no. 3 034912, [arXiv:1506.00645]. 83, 87, 108

[248] S. Mukherjee, R. Venugopalan, and Y. Yin, *Universal off-equilibrium scaling of critical cumulants in the QCD phase diagram*, *Phys. Rev. Lett.* **117** (2016), no. 22 222301, [arXiv:1605.09341]. 83, 87, 108

[249] M. A. Stephanov, K. Rajagopal, and E. V. Shuryak, *Signatures of the tricritical point in QCD*, *Phys. Rev. Lett.* **81** (1998) 4816–4819, [hep-ph/9806219]. 83, 86

[250] M. A. Stephanov, K. Rajagopal, and E. V. Shuryak, *Event-by-event fluctuations in heavy ion collisions and the QCD critical point*, *Phys. Rev.* **D60** (1999) 114028, [hep-ph/9903292]. 83, 86

[251] D. H. Rischke, *The Quark gluon plasma in equilibrium*, *Prog. Part. Nucl. Phys.* **52** (2004) 197–296, [nucl-th/0305030]. 83, 86

[252] M. A. Stephanov, *On the sign of kurtosis near the QCD critical point*, *Phys. Rev. Lett.* **107** (2011) 052301, [arXiv:1104.1627]. 83, 86, 108

[253] R. Bellwied, S. Borsanyi, Z. Fodor, S. D. Katz, A. Pasztor, C. Ratti, and K. K. Szabo, *Fluctuations and correlations in high temperature QCD*, *Phys. Rev.* **D92** (2015), no. 11 114505, [arXiv:1507.04627]. 86

[254] M. Attems, Y. Bea, J. Casalderrey-Solana, D. Mateos, M. Triana, and M. Zilhao, *Phase Transitions, Inhomogeneous Horizons and Second-Order Hydrodynamics*, *JHEP* **06** (2017) 129, [arXiv:1703.02948]. 87

[255] M. Stephanov and Y. Yin, *Hydrodynamics with parametric slowing down and fluctuations near the critical point*, *Phys. Rev.* **D98** (2018), no. 3 036006, [arXiv:1712.10305]. 87, 94

[256] G. Policastro, D. T. Son, and A. O. Starinets, *The Shear viscosity of strongly coupled N=4 supersymmetric Yang-Mills plasma*, *Phys. Rev. Lett.* **87** (2001) 081601, [hep-th/0104066]. 87

[257] A. Buchel and J. T. Liu, *Universality of the shear viscosity in supergravity*, *Phys. Rev. Lett.* **93** (2004) 090602, [hep-th/0311175]. 87

[258] J. Jankowski, G. Plewa, and M. Spalinski, *Statistics of thermalization in Bjorken Flow*, *JHEP* **12** (2014) 105, [arXiv:1411.1969]. 88, 100

[259] S. Jeon and U. Heinz, *Introduction to Hydrodynamics*, in *Quark-Gluon Plasma 5* (X.-N. Wang, ed.), pp. 131–187. 2016. 88

[260] S. Weinberg, *Cosmology*. 2008. 88

[261] L. Rezzolla and O. Zanotti, *Relativistic hydrodynamics*. Oxford University Press, New York, 2013. 88, 98

[262] Y. Hatta, J. Noronha, and B.-W. Xiao, *Exact analytical solutions of second-order conformal hydrodynamics*, *Phys. Rev.* **D89** (2014), no. 5 051702, [arXiv:1401.6248]. 89

[263] Y. Hatta, J. Noronha, and B.-W. Xiao, *A systematic study of exact solutions in second-order conformal hydrodynamics*, *Phys. Rev.* **D89** (2014), no. 11 114011, [arXiv:1403.7693]. 89

[264] S. Grozdanov and N. Kaplis, *Constructing higher-order hydrodynamics: The third order*, *Phys. Rev.* **D93** (2016), no. 6 066012, [arXiv:1507.02461]. 89, 98

[265] V. Roy, S. Pu, L. Rezzolla, and D. Rischke, *Analytic Bjorken flow in one-dimensional relativistic magnetohydrodynamics*, *Phys. Lett.* **B750** (2015) 45–52, [arXiv:1506.06620]. 90

[266] S. Pu, V. Roy, L. Rezzolla, and D. H. Rischke, *Bjorken flow in one-dimensional relativistic magnetohydrodynamics with magnetization*, *Phys. Rev.* **D93** (2016), no. 7 074022, [arXiv:1602.04953]. 90

[267] S. Z. Belenkij and L. D. Landau, *Hydrodynamic theory of multiple production of particles*, *Nuovo Cim. Suppl.* **3S10** (1956) 15. [Usp. Fiz. Nauk56,309(1955)]. 91

[268] H. Niemi and G. S. Denicol, *How large is the Knudsen number reached in fluid dynamical simulations of ultrarelativistic heavy ion collisions?*, arXiv:1404.7327. 91

[269] J. Noronha-Hostler, J. Noronha, and M. Gyulassy, *Sensitivity of flow harmonics to subnucleon scale fluctuations in heavy ion collisions*, *Phys. Rev.* **C93** (2016), no. 2 024909, [arXiv:1508.02455]. 91

[270] P. Romatschke, *Relativistic Viscous Fluid Dynamics and Non-Equilibrium Entropy*, *Class. Quant. Grav.* **27** (2010) 025006, [arXiv:0906.4787]. 91

[271] W. A. Hiscock and L. Lindblom, *Stability and causality in dissipative relativistic fluids*, *Annals Phys.* **151** (1983) 466–496. 92

[272] W. A. Hiscock and L. Lindblom, *Generic instabilities in first-order dissipative relativistic fluid theories*, *Phys. Rev.* **D31** (1985) 725–733. 92

[273] J. C. Maxwell. On the Dynamical Theory of Gases. *Phil. Trans. R. Soc.*, 157:49, 1867. 92

[274] C. Cattaneo. Sulla conduzione del calore. *Atti Sem. Mat. Fis. Univ. Modena*, 3:3, 1948. 92

[275] I. Muller, *Zum Paradoxon der Warmeleitungstheorie*, *Z. Phys.* **198** (1967) 329–344. 92

[276] W. Israel, *Nonstationary irreversible thermodynamics: A Causal relativistic theory*, *Annals Phys.* **100** (1976) 310–331. 92

[277] W. Israel and J. M. Stewart, *Transient relativistic thermodynamics and kinetic theory*, *Annals Phys.* **118** (1979) 341–372. 92

[278] G. S. Denicol, H. Niemi, E. Molnar, and D. H. Rischke, *Derivation of transient relativistic fluid dynamics from the Boltzmann equation*, *Phys. Rev.* **D85** (2012) 114047, [arXiv:1202.4551]. [Erratum: Phys. Rev.D91,no.3,039902(2015)]. 93

[279] S. Chapman, T. Cowling, D. Burnett, and C. Cercignani, *The Mathematical Theory of Non-uniform Gases: An Account of the Kinetic Theory of Viscosity, Thermal Conduction and Diffusion in Gases*. Cambridge Mathematical Library. Cambridge University Press, 1990. 93

[280] M. Rangamani, *Gravity and Hydrodynamics: Lectures on the fluid-gravity correspondence*, *Class. Quant. Grav.* **26** (2009) 224003, [arXiv:0905.4352]. 93

[281] V. E. Hubeny, S. Minwalla, and M. Rangamani, *The fluid/gravity correspondence*, in *Black holes in higher dimensions*, pp. 348–383, 2012. arXiv:1107.5780. [,817(2011)]. 93

[282] A. Rebhan and D. Steineder, *Violation of the Holographic Viscosity Bound in a Strongly Coupled Anisotropic Plasma*, *Phys. Rev. Lett.* **108** (2012) 021601, [arXiv:1110.6825]. 93

[283] R. Critelli, S. I. Finazzo, M. Zaniboni, and J. Noronha, *Anisotropic shear viscosity of a strongly coupled non-Abelian plasma from magnetic branes*, *Phys. Rev.* **D90** (2014), no. 6 066006, [arXiv:1406.6019]. 93

[284] R. A. J. Critelli, *Strongly coupled non-Abelian plasmas in a magnetic field*, Master's thesis, Sao Paulo U., 2016. 93

[285] J. Erdmenger, P. Kerner, and H. Zeller, *Transport in Anisotropic Superfluids: A Holographic Description*, *JHEP* **01** (2012) 059, [arXiv:1110.0007]. 93

[286] S. A. Hartnoll, D. M. Ramirez, and J. E. Santos, *Entropy production, viscosity bounds and bumpy black holes*, *JHEP* **03** (2016) 170, [arXiv:1601.02757]. 93

[287] J. Hernandez and P. Kovtun, *Relativistic magnetohydrodynamics*, *JHEP* **05** (2017) 001, [arXiv:1703.08757]. 93

[288] D. T. Son and M. A. Stephanov, *Dynamic universality class of the QCD critical point*, *Phys. Rev.* **D70** (2004) 056001, [hep-ph/0401052]. 93, 109

[289] M. G. Alford, L. Bovard, M. Hanauske, L. Rezzolla, and K. Schwenzer, *Viscous Dissipation and Heat Conduction in Binary Neutron-Star Mergers*, *Phys. Rev. Lett.* **120** (2018), no. 4 041101, [arXiv:1707.09475]. 94

[290] F. S. Bemfica, M. M. Disconzi, and J. Noronha, *Causality of the Einstein-Israel-Stewart Theory with Bulk Viscosity*, arXiv:1901.06701. 94

[291] L. Baiotti and L. Rezzolla, *Binary neutron star mergers: a review of Einstein richest laboratory*, *Rept. Prog. Phys.* **80** (2017), no. 9 096901, [arXiv:1607.03540]. 94

[292] R. A. Janik and R. B. Peschanski, *Asymptotic perfect fluid dynamics as a consequence of Ads/CFT*, *Phys. Rev.* **D73** (2006) 045013, [hep-th/0512162]. 94, 95

[293] R. A. Janik and R. B. Peschanski, *Gauge/gravity duality and thermalization of a boost-invariant perfect fluid*, *Phys. Rev.* **D74** (2006) 046007, [hep-th/0606149]. 94

[294] S. Kinoshita, S. Mukohyama, S. Nakamura, and K.-y. Oda, *A Holographic Dual of Bjorken Flow*, *Prog. Theor. Phys.* **121** (2009) 121–164, [arXiv:0807.3797]. 94

[295] M. P. Heller, P. Surowka, R. Loganayagam, M. Spalinski, and S. E. Vazquez, *Consistent Holographic Description of Boost-Invariant Plasma*, *Phys. Rev. Lett.* **102** (2009) 041601, [arXiv:0805.3774]. 94

[296] G. Beuf, M. P. Heller, R. A. Janik, and R. Peschanski, *Boost-invariant early time dynamics from AdS/CFT*, *JHEP* **10** (2009) 043, [arXiv:0906.4423]. 94

[297] G. S. Denicol, U. W. Heinz, M. Martinez, J. Noronha, and M. Strickland, *New Exact Solution of the Relativistic Boltzmann Equation and its Hydrodynamic Limit*, *Phys. Rev. Lett.* **113** (2014), no. 20 202301, [arXiv:1408.5646]. 94

[298] P. Romatschke, *New Developments in Relativistic Viscous Hydrodynamics*, *Int. J. Mod. Phys.* **E19** (2010) 1–53, [arXiv:0902.3663]. xiii, 96

[299] J. Erdmenger, M. Haack, M. Kaminski, and A. Yarom, *Fluid dynamics of R-charged black holes*, *JHEP* **01** (2009) 055, [arXiv:0809.2488]. 98

[300] N. Banerjee, J. Bhattacharya, S. Bhattacharyya, S. Dutta, R. Loganayagam, and P. Surowka, *Hydrodynamics from charged black branes*, *JHEP* **01** (2011) 094, [arXiv:0809.2596]. 98

[301] P. M. Chesler and L. G. Yaffe, *Holography and colliding gravitational shock waves in asymptotically AdS5 spacetime*, *Phys. Rev. Lett.* **106** (2011) 021601, [arXiv:1011.3562]. 100

[302] http://eigen.tuxfamily.org/index.php?title=Main_Page. 107

[303] P. C. Hohenberg and B. I. Halperin, *Theory of Dynamic Critical Phenomena*, *Rev. Mod. Phys.* **49** (1977) 435–479. 109

[304] J. Knaute, R. Yaresko, and B. Kampfer, *Holographic QCD phase diagram with critical point from Einstein-Maxwell-dilaton dynamics*, *Phys. Lett.* **B778** (2018) 419–425, [arXiv:1702.06731]. 109

[305] B.-J. Schaefer, J. M. Pawlowski, and J. Wambach, *The Phase Structure of the Polyakov–Quark-Meson Model*, *Phys. Rev.* **D76** (2007) 074023, [arXiv:0704.3234]. 113

[306] A. K. Cyrol, M. Mitter, J. M. Pawlowski, and N. Strodthoff, *Nonperturbative quark, gluon, and meson correlators of unquenched QCD*, *Phys. Rev.* **D97** (2018), no. 5 054006, [arXiv:1706.06326]. 113

[307] M. Bluhm, Y. Jiang, M. Nahrgang, J. M. Pawlowski, F. Rennecke, and N. Wink, *Time-evolution of fluctuations as signal of the phase transition dynamics in a QCD-assisted transport approach*, in *27th International Conference on Ultrarelativistic Nucleus-Nucleus Collisions (Quark Matter 2018) Venice, Italy, May 14-19, 2018*, 2018. arXiv:1808.01377. 113

[308] M. Attems, Y. Bea, J. Casalderrey-Solana, D. Mateos, M. Triana, and M. Zilhao, *Holographic Collisions across a Phase Transition*, arXiv:1807.05175. 113

[309] J. Brewer, A. Sadofyev, and W. van der Schee, *Jet shape modifications in holographic dijet systems*, arXiv:1809.10695. 113

[310] C. V. Vishveshwara, *Scattering of Gravitational Radiation by a Schwarzschild Black-hole*, *Nature* **227** (1970) 936–938. 114

[311] M. Davis, R. Ruffini, W. H. Press, and R. H. Price, *Gravitational radiation from a particle falling radially into a schwarzschild black hole*, *Phys. Rev. Lett.* **27** (1971) 1466–1469. 114

[312] H.-P. Nollert, *TOPICAL REVIEW: Quasinormal modes: the characteristic 'sound' of black holes and neutron stars*, *Class. Quant. Grav.* **16** (1999) R159–R216. 114

[313] K. D. Kokkotas and B. G. Schmidt, *Quasinormal modes of stars and black holes*, *Living Rev. Rel.* **2** (1999) 2, [gr-qc/9909058]. 114

[314] M. Kac, *Can one hear the shape of a drum?*, *Am. Math. Mon.* **73** (1966) 1–23. 114

[315] **Virgo, LIGO Scientific** Collaboration, B. P. Abbott et al., *Observation of Gravitational Waves from a Binary Black Hole Merger*, *Phys. Rev. Lett.* **116** (2016), no. 6 061102, [arXiv:1602.03837]. 114

[316] **Virgo, LIGO Scientific** Collaboration, B. P. Abbott et al., *GW151226: Observation of Gravitational Waves from a 22-Solar-Mass Binary Black Hole Coalescence*, *Phys. Rev. Lett.* **116** (2016), no. 24 241103, [arXiv:1606.04855]. 114

[317] A. O. Starinets, *Quasinormal modes of near extremal black branes*, *Phys. Rev.* **D66** (2002) 124013, [hep-th/0207133]. 114

[318] W. Florkowski, R. Ryblewski, and M. Spalinski, *Gradient expansion for anisotropic hydrodynamics*, arXiv:1608.07558. 114

[319] J. Alanen, T. Alho, K. Kajantie, and K. Tuominen, *Mass spectrum and thermodynamics of quasi-conformal gauge theories from gauge/gravity duality*, *Phys. Rev.* **D84** (2011) 086007, [arXiv:1107.3362]. 114

[320] R. A. Janik, J. Jankowski, and H. Soltanpanahi, *Non-equilibrium dynamics and phase transitions*, *Phys. Rev. Lett.* **117** (2016), no. 9 091603, [arXiv:1512.06871]. 114

[321] R. A. Janik, J. Jankowski, and H. Soltanpanahi, *Quasinormal modes and the phase structure of strongly coupled matter*, *JHEP* **06** (2016) 047, [arXiv:1603.05950]. 114, 128, 129

[322] A. Buchel, M. P. Heller, and R. C. Myers, *Equilibration rates in a strongly coupled nonconformal quark-gluon plasma*, *Phys. Rev. Lett.* **114** (2015), no. 25 251601, [arXiv:1503.07114]. 115

[323] P. C. Hohenberg and B. I. Halperin, *Theory of dynamic critical phenomena*, *Rev. Mod. Phys.* **49** (Jul, 1977) 435–479. 115, 116

[324] K. Maeda, M. Natsuume, and T. Okamura, *Dynamic critical phenomena in the AdS/CFT duality*, *Phys. Rev.* **D78** (2008) 106007, [arXiv:0809.4074]. 116

[325] A. Buchel, *Critical phenomena in N=4 SYM plasma*, *Nucl. Phys.* **B841** (2010) 59–99, [arXiv:1005.0819]. 116

[326] M. Natsuume and T. Okamura, *Dynamic universality class of large-N gauge theories*, *Phys. Rev.* **D83** (2011) 046008, [arXiv:1012.0575]. 116

[327] A. Buchel, *Relaxation time of non-conformal plasma*, *Phys. Lett.* **B681** (2009) 200–203, [arXiv:0908.0108]. 116

[328] A. Buchel and C. Pagnutti, *Transport at criticality*, *Nucl. Phys.* **B834** (2010) 222–236, [arXiv:0912.3212]. 116

[329] A. Buchel and C. Pagnutti, *Critical phenomena in N=2* plasma*, *Phys. Rev.* **D83** (2011) 046004, [arXiv:1010.3359]. 116

[330] R.-G. Cai, S. He, and D. Li, *A hQCD model and its phase diagram in Einstein-Maxwell-Dilaton system*, *JHEP* **03** (2012) 033, [arXiv:1201.0820]. 116

[331] S. Janiszewski and M. Kaminski, *Quasinormal modes of magnetic and electric black branes versus far from equilibrium anisotropic fluids*, *Phys. Rev.* **D93** (2016), no. 2 025006, [arXiv:1508.06993]. 116

[332] F. Tisseur and K. Meerbergen, *The Quadratic Eigenvalue Problem*, *SIAM Rev.* **43(2)** (2001) 235–286. 119

[333] M. P. Heller, R. A. Janik, M. Spalinski, and P. Witaszczyk, *Coupling hydrodynamics to nonequilibrium degrees of freedom in strongly interacting quark-gluon plasma*, *Phys. Rev. Lett.* **113** (2014), no. 26 261601, [arXiv:1409.5087]. 119

[334] R. A. Janik, G. Plewa, H. Soltanpanahi, and M. Spalinski, *Linearized nonequilibrium dynamics in nonconformal plasma*, *Phys. Rev.* **D91** (2015), no. 12 126013, [arXiv:1503.07149]. 119

[335] G. S. Denicol, J. Noronha, H. Niemi, and D. H. Rischke, *Origin of the Relaxation Time in Dissipative Fluid Dynamics*, *Phys. Rev.* **D83** (2011) 074019, [arXiv:1102.4780]. 126

[336] J. Noronha and G. S. Denicol, *Transient Fluid Dynamics of the Quark-Gluon Plasma According to AdS/CFT*, arXiv:1104.2415. 126